A PRESCRIBED WAKE MODEL FOR VERTICAL AXIS WIND TURBINES

by

Bambang Basuno, B.Sc.

Dissertation submitted to the Faculty of Engineering, University of Glasgow, for the Degree of Doctor of Philosophy

February, 1992

CONTENTS

ACKNOWLEDGEMENTS

I would like to express my sincere thanks to Dr. Rodderick Galbraith for his supervision and encouragement in this work and also for the provision of the excellent research facilities in the Department of Aerospace Engineering.

I am greatly indebted to Dr. Frank N. Coton for his close supervision and constant encouragement throughout the work described in this dissertation. His patient advice and help in preparing this dissertation is also gratefully acknowledged.

I wish to acknowledge the Indonesian Government for the financial support during my period of study and also The British Council who administered all financial aspects.

It is also my pleasure to express many thanks to Dr. J. Dachun, Mr. D. Clark , Mr. R.D. Gordon, Mrs. E. Leitch and Mrs. E. Garman for much help in this work.

Finally, I would like to express my sincere thanks to Prof. O. Diran for his moral support and for the opening up the way to this further study in the field of aerodynamics. Many thanks also to my wife, Tati Rosyati, who allowed me to do this work and to be away from her for a few years. Moral support from my parents and my Indonesian fellows who study in Scotland is also acknowledged.

DECLARATION

The Author expresses that the work presented in this Dissertation was carried out at the Department of Aerospace Engineering, University of Glasgow, between October 1987, and December 1991. It is original in content except where indicated.

February, 1992

[Bambang Basuno]

SUMMARY

The development of a Prescribed Wake model for the prediction of the aerodynamic performance of a vertical axis wind turbine is described in this dissertation. Initially, current and projected trends in world energy demand are examined and the requirement for extensive exploitation of renewable energy resources is identified. The potential for wind energy is then discussed and the configurations of appropriate energy conversion devices are described. The particular aerodynamic features of the vertical axis wind turbine are then highlighted and possible modelling techniques assessed. The Free Wake vortex model is identified as the most comprehensive technique currently available for the analysis of such flows. This technique, together with momentum theory, is then used as the basis for the development of a Prescribed Wake model for straight bladed vertical axis wind turbines. The evolution of the Prescribed Wake model is described and the sensitivity of the resulting scheme to numerical inputs is then assessed. Finally, the method is applied to the Darrieus wind turbine and is found to agree well with field data. It is concluded that the Prescribed Wake model can accurately reproduce the results of the Free Wake method at a fraction of the computation time but that the result obtained is particularly sensitive to the vortex wake structure and the blade section aerofoil data used.

NOMENCLATURE

a	:	Axial interference factor
a_u	:	Upstream interference factor
a_d	:	Down stream interference factor
A	:	Actuator disk area
A_f	:	Frontal area
A_r	:	Aspect ratio
C_d	:	Drag force coefficient
C_l	:	Lift lift coefficient
C_n	:	Normal force coefficient
C_t	:	Tangential force coefficient
C_{te}	:	Torque coefficient
c_r	:	local chord
Cp	:	Power coefficient
$\mathbf{ds}$	:	differential length of vortex filament
F	:	Axial force
H_r	:	Blade height
$(\mathbf{i},\mathbf{j},\mathbf{k})$	:	unit vector in Cartesian coordinates
L	:	blade span
m	:	rate of mass
NB	:	Number of blades
NBE	:	Number of elements
NR	:	Number of rotational calculations
NTI	:	Number of time steps
P	:	Power
r	:	Local blade radius
R	:	Maximum blade radius
R_c	:	Radius cut off for the vortex filament
t	:	time
T_e	:	Torque
$U_\sim$	:	Free stream velocity
U_b	:	Axial velocity on the blade
U_{bu}	:	Axial velocity on the upwind blade
U_{bd}	:	Axial velocity on the down wind blade
U_{dd}	:	Down stream disk velocity
Udu	:	Upstream disk velocity
U_r	:	Velocity resultant relative to the blade

U_t	:	Rotational blade velocity
U_{wu}	:	The wake velocity of upstream disk actuator
U_{wd}	:	The wake velocity of down stream disk actuator
V_i	:	Inflow velocity
W_x	:	Component induced velocity in x-direction
W_y	:	Component induced velocity in y-direction
W_z	:	Component induced velocity in z-direction
(x,y,z)	:	Notation of Cartesian coordinates

Greek notation

α	:	angle of attack
Δ	:	differential operator
Γ_b	:	strength of bound vortex
Γ_s	:	strength of shed vortex
Γ_t	:	strength of trailing vortex
λ	:	tip speed ratio
θ	:	blade azimuth position in polar coordinate (r,θ)
ρ	:	air density
σ	:	solidity number
Ω	:	angular velocity

CHAPTER - ONE : INTRODUCTION.

1.1 The World Energy : Demand and Resources

The rapid growth of world population and increasing world income per capita usually promotes increasing demands for energy. The world population was already estimated to exceed 5 billion in July 1987 and, by the end of the century, current United Nations projections suggest that the population will have grown to 6.122 billion [1].

The calculation of total current world energy consumption and the forecasting of the future need for energy are quite complex. Data on total energy consumption are difficult to obtain and inaccurate in terms of domestic or non commercial consumption . This is , especially, true for data from the majority of underdeveloped and developing countries [Third World countries]. It is also noted in Ref. 2, that the United Nations, which represents the main source of information concerning statistical data on world energy consumption, generally ignores fuel quality and the effect of differencing end-use efficiency. This contributes to the difficulty in forecasting the future world energy demand .

In general, accurate data on energy consumption are only available in developed countries. Thus it is possible to estimate the future need for energy for a particular developed country. However a difficulty still exists, due to the close relationship between energy requirement and social and economic development internally and externally as part of the world economic system .

The Bottom-up approach combined with a social-economic scenario represents an example of a prediction method which has been adapted for estimating the need for energy in the U.K. [3,4]. The Bottom-up approach here means that the starting point of analysis is derived from the detailed picture of types and quantities of

energy consumed at the point of use for many different tasks. This requires around 5000 types of energy consumption to be considered. The social-economic scenario represents the description of how future events unfold.

In line with the Bottom-up approach, there are two scenarios that have been adopted. They are namely , Technical Fix Scenario and Conserver Society Scenario. The first is based on the assumption that the economic growth rates in the U.K. and the rest of the world are slightly less than the 4.5 % achieved in the year of cheap oil. In fact, this assumption seems inappropriate since the rate of world output during 1981-90 was around 2.8% [5]. The second scenario is based upon the UK's rate of economic growth being lower in the future than the past, while at the same time, the rate of world economic growth is modest. Unfortunately, for such important assumptions in both scenarios, Ref. 3 does not quantify the figures for economic growth. Therefore, it is difficult to assess that the estimates will be in line with the progress of world economics from now until the end of the century. However, the Technical Fix and Conserver society scenarios estimate that U.K. energy consumption, in the face of vigorous technological change, will amount to around 74% and 55% of 1976's energy consumption level [202 MTOE : Million Tonnes of Oil Equivalent], respectively. Hence, the forecasts agree that U.K. energy demand will drop by the end of the century.

The energy demand for the future, especially, towards the end of the century, within a larger community involving the 10 European Economic Community countries [E.E.C.], excluding Spain and Portugal, has been fully described in Ref. 6. This reference concluded that the rate of energy demand for these 10 countries, until the end of this century, will average 0.7 % per annum. In 1990, the demand for energy was 714 Million Tonnes of Oil Equivalence [MTOE]. It is estimated that, at the end of the century [2000], it will be 762 MTOE (both excluding bunkers).

To complete this description, the total energy consumption by the 12 countries of the E.E.C. in the years 1980 and 1987, in terms of energy demand by sector, fuel and also the overall usage of final primary fuel is shown in Table 1.1 [5]. The

main features are that the oil consumption dropped around 13.4% from 551 to 477 MTOE, whilst the nuclear contribution increased rapidly by more than 200 % from 46 to 139 MTOE.

In the case of a particular country, for example Denmark , fluctuations in energy consumption due to changing world economics are possible. In recent years this has happened twice. The first [1973] and second oil shock [1979] made Denmark's energy consumption decrease in the periods 1973 to 1975 and 1979 to 1983 [7]. However, for the large scale, namely the level of world demand, the continually increasing population overcame the decreasing economic situation. Thus , in recent times, world energy consumption has increased from year to year with the only exception between 1980 and 1981, when it dropped around -0.6% [8], as shown in Table 1.2. The world energy consumption data presented in this table also include the projected world energy consumption at the end of the century according to Hedly [8]. In the early nineteen seventies [1972] the world energy consumption was around 5630.7 MTOE and had risen to 8346 MTOE by 1990. By the end of the century , the projected figure is 10761 MTOE. This prediction of energy demand for the end of the century is close to an E.E.C. study which estimated that the world energy consumption will be around 10822 MTOE [5]

Until the present time, energy demand has been fulfilled by 5 types of energy resource. They are, oil, natural gas, coal, hydroelectric and nuclear. The first three of these resources are the main contributors although an effort to increase the supply of energy from the last two has been apparent. These types of resource, often referred to as fossil energy resources, will continue to be dominant and contribute nearly 80% of the total world energy demand between now and the end of the century , as shown in Table 1.3. This table illustrates the contribution of each type of energy resource at selected years from 1972 - 2000 according to Hedly [8]. In his estimation for the near future, he assumed that there is no significant additional effort to explore other alternative energy sources. This is in contrast with other estimates provided by Guilmot J.F et. al. [6], which are based

on the assumption that new technologies, which make more efficient use of energy, will penetrate into the consumer market. These estimates also include a contribution from the successful use of renewable energy in developing countries. This gives a map of required energy by type of fuel at the end of the century, as shown in Table 1.4. The difference between the two estimates is quite significant. For example, Hedly estimated the need for oil is 3333.0 MTOE(30.9%), while in Guilmot's estimation the requirement is 3436 MTOE(31.75%).

In addition, another forecast by Redetzki [9] provides a lower estimate of oil demand at 2634.42 MTOE, and indicates that this will be around 40% of the total energy demand. The last estimate seems inappropriate, since, if it is true, the total energy demand at the end of century will be only 6586.05 MTOE or, in other words, approximately the same as the energy consumption in the year 1978 when the population was around 4 Billion.

Oil, coal and natural gas have limited availability and, at some point in the near future, will disappear. Of these, oil is likely to be exhausted first. Oil reserves in 1987 amounted to 96000 MTOE [10] and, if the rate of oil production remains at the 1990 level of 3150 MTOE [11] , reserves will diminish within the next 30 years. Hence, efforts to find and to develop other alternative energy resources, are an immediate necessity.

It is interesting to note that significant time is needed to make new technologies fully operational . For instance, experience with the diesel engine showed that the time needed from scientific demonstration to the first commercial unit was approximately 60 years and then the time required to capture a significant percentage of the market was around 30-50 years [12]. Other examples of the required time for other types of pertinent technologies are shown in Table 1.5. It is , therefore, clear that an effort to explore extensively other alternative energy sources, as early as possible, is required before all the fossil energy resources disappear. This need is heightened by the increasing international pressure on fossil

fuel reserves, especially, due to the economic improvement of third world countries.

In addition, although accurate figures of energy consumption by the developing countries are not available, their need for energy was quoted to be of the order of 15% of total world energy consumption. Unfortunately, this energy is, generally, obtained from wood and agriculture crops with very low thermal efficiency. This has resulted in massive deforestation, removal of essential soil structure and nutrients, a rapid increase in soil erosion and the potential for almost global destruction of the world's tropical forests if present trends are not soon changed [35] .

These five energy resources mentioned above are often called Primary energy resources. The last two, hydraulic and nuclear power may last for a longer period compared to the first three resources. Hydraulic energy may represent the most environmentally acceptable energy resource but , unfortunately, it is limited by quantity of energy that can be produced. This energy is non polluting and continually renewable and represents an indirect form of solar energy from the hydrological cycle. The technology for capturing the hydraulic energy in the form of electricity, via water turbine generators, can be said to be already mature. The water turbine generator with efficiency levels near 95 % is already available on the market [13]. Unfortunately, this type of energy is very dependent on site, i,e. only in certain regions of the earth are such energy resources available. Some countries in North Africa as well as in the Middle East have poor hydraulic energy potential, while other countries like Norway and Canada are abundant with this type of energy.

An estimate of the potential for hydraulic energy, given by Ellis [13] suggested that, in the year 2020, nearly 80% of the total possible sites for hydraulic power will have been exploited, provided adequate financing averaging $ 33 billions per year is available. However, in that year, this resource will only contribute 16% of the total energy demand. Such a percentage may not be achieved due to

environmental concerns or political considerations [certain rivers belong to several countries for instance : Nile or Tigris river].

In some respects nuclear power may offer unlimited energy resources, since this energy can be derived from transforming mass into energy via fission or fusion. The equivalence between mass and energy according to Einstein's formula follows $e= mc^2$, where e is energy, m is mass and c is the velocity of light. This conversion allows very small amounts of mass to produce large amounts of energy. For instance, a 1000 gram mass can theoretically be converted to $8.918x10^{16}$ Joules which is equivalent to $2.497x10^{10}$ Kilowatt-hour (Kwh). This amount of energy can power a 100 watt light bulb for over 28.5 million years [14].

Several countries like the United Kingdom, U.S.A., Japan, France, etc. have already used this energy for producing electricity and, in total, there were 417 nuclear powered reactors worldwide at the end of 1987 with 120 additional units under construction [15]. Although, the number of France's nuclear power stations is less than the USA,they contribute a higher percentage of the nation's power. France, currently, has the highest proportional contribution from nuclear power in the world with approximately 75% of their total electricity coming from it [15]. France has a considerable lead in promoting the use of this energy. Ten years ago, nuclear power in this country provided 105.3 Twh [17] This figure had risen to 289.0 Twh in 1990 [16].

Since the Chernobyl accident in April 1987, it seems that the effort to utilise nuclear power more extensively has experienced a setback. For instance, Belgium, Italy, Finland and the Netherlands are postponing all new orders for nuclear plants at least for a few years [18]. The Chernobyl disaster has created pressure for environmental reasons and, in turn, has placed a demand on increasing standards of safety . In addition to these problems, there are also hypothetical risks, which were sometimes raised in public inquiries, of a power

station being hit by an aeroplane or earthquake. Concern also exists over the various aspects of cooling and steam generation. Such considerations have made the installation of nuclear power plants costly. The cost of a typical electricity power plant has risen significantly from the early 1970s, when it cost around $300/Kw(e), to around $4000 /Kw(e) in recent years. [19].

In this context, the comparison of the average cost of electricity generation for various power plants was as shown in Table 1.6, for the year 1984. The table showed that the average cost of electricity from a nuclear power plant was slightly below that from an oil or coal plant. Now , it is likely that the current figure will be proportionately higher.

To conclude the discussion on the correspondence between world energy demand and resources of primary energy, Table 1.7 shows a compilation of data on their rate of production and their reserves.

The many restrictions on primary energy resources must be considered against the fact that world energy consumption is increasing . Hence, the need to exploit other alternative resources is important , especially renewable energy resources. Renewable resources are defined as energy resources which have an infinite time availability, as opposed to the fossil fuels which are classified as nonrenewable energy resources. Renewable energy resources can provide an output energy which is nearly constant over a span of a million years. They include, direct sunlight, wind, wave, wave tidal current, biomass, geothermal and hydraulic energy. Basically, all types of renewable energy are derived from the radiation of the sun. The internal heat of the earth, the gravitational force of the moon and sun, and the rotation of the earth also play a role in creating many of these renewable energy resources.

The flux of the sun's radiated energy reaching the earth is enormous around : 1.7×10^{14} Kilowatts [20]. This amount is equivalent to 20000 times the world's

consumption of energy [21]. The earth's atmosphere acts as an absorbing and reflecting medium and the breakdown of radiation energy, combined with gravitational effects and the rotational motion of the earth, creates many forms of renewable energy resources [22-24].

Generally speaking, all renewable energy resources have common characteristics. They are intermittent and abundant but distributed unequally over a large area, thus making their energy intensity low. For example , solar energy not only varies from region to region but also from hour to hour, seasonally and depending on the weather conditions. In a favourable location, the maximum peak solar density could reach 1 kilowatt/m^2 and the maximum average power density about 250 Watt/m^2 [global isolation] at sea level [25]. Inland regions, namely the tropics and desert areas can be said to represent the most promising locations for the exploitation of solar energy. In these regions, the average intensity of solar energy is many times that of other parts of the earth. Typically , the average intensity in these areas is around 210-250 w/m^2 , while for less sunny regions , such as Northern Europe, this intensity drops to an average around 80-130 w/m^2 [21]. However, due to the low intensity and the range of present technology , a large area would be required to make solar energy contribute significantly to the world energy supply. For instance, to satisfy the energy demand of the USA in 1987 would have needed a collector of 12000 km^2 placed in a desert region [21].

Strictly speaking, the radiation energy which emanates from the sun is transformed into two forms of energy : direct and indirect solar energy. The first presents itself immediately in the form of heat and light, whilst the second [indirect solar energy] produces various forms of energy such as wind, wave and hydro power.

Heat and light, can be collected with or without concentration and stored or redistributed to provide space heating, cooling, process heat or to generate

electricity. Light itself, makes the plants grow and so makes possible the production of a whole range of biofuels. Besides that, the light from the sun can also be used directly to generate electricity through photo voltaic reactions.

The capture of solar energy, with or with out certain conversion devices, has introduced new definitions, namely passive and active solar energy. The first is concerned with the way a building should be built, in order to allow all rooms to be day lit, or for the maintenance of acceptable internal temperature in winter with less dependence on a conventional heating system. The second theme, active solar energy, corresponds to the use of devices which allow heat or light to be transformed into a useful form of energy. In this field, there are two methods that have been developed for capturing solar energy, they are, thermal excitation and the photo voltaic cell. The first of these may take the form of a solar collector in which a flat surface is arranged to absorb radiant energy from sun light, or, alternatively, it may take form of a curved mirror used to concentrate the direct radiant energy from the sun onto something capable of absorbing it.

The photo voltaic cell is the most promising method for converting solar radiation directly into electricity, even compared to other well known methods such as thermionic cells and thermoelectric generators [12]. However , since the main component of the photo voltaic cell is a very expensive material [silicon], the capital cost of such a device is ten times the capital cost of a fossil power station per Kw installed, This method is, therefore, not at present viable except in special circumstances.

Naturally, solar energy promotes chemical reactions through the photosynthesis process when interacting with plants. This leads to the possible creation of biofuels which, in effect, represents an indirect form of capturing solar energy. This process directly produces food and wood and offers the possibility of cultivation of appropriate plants exclusively for the purpose of generating power. There are, however, many disadvantages with this energy resource. The efficiency of plants in

transforming solar energy into useful energy is just around 5-6% [21]. Therefore, the creation of reasonable amounts of energy needs large quantities of plants. Consequently, a large land area would be required and the transportation problem to bring it to the consumers could not be avoided.

An assessment of geothermal potential is given in detail in Ref.26 , which indicates that this resource is a truly international resource. In other words, almost all countries have such a resource. However, to exploit it as a useful form of energy requires appropriate geological structures. Countries like Japan, Hungary, Iceland and USSR represent the largest direct users of geothermal energy. In these countries, the temperature T of the resource is in the range $20^{o}C < T < 150^{o}C$, and it can be easily exploited. [28].

Attempts have been made to use geothermal resources since ancient times, in the form of geothermal water for recreation and therapeutic purposes. The first efforts to use such resources for electrical power production began in 1904 in Italy. In 1981, there were 115 electric power station units derived from geothermal resources worldwide with installed capacity around 2538 Mw [27]. By 1988 this had risen to 182 units with 4818 Mw capacity [28].

Another way of producing energy in a useful form is from the sea . There are , currently, three ways of extracting energy from the sea : (1) wave, (2)based on the temperature gradients between the surface and depths of the ocean, or (3) ocean tides. The first form of energy [wave] results from friction between wind and the surface of the water. The available global wave power is estimated to be between 2000 and 2.700 Gigawatt[21]. In certain regions, the local availability of wave power has been studied. For instance, in the northeast of Scotland, the annual power in the waves is estimated to be around 91 Kw / m . If this power could be captured with an efficiency 20%, around $2x10^{4}$ Kwh of electricity could be provided by converters covering 1 Km of coast line [21].

The big temperature difference between warm surface water [heated by absorption of solar energy] and colder, deep water allows for the generation of power. In the tropical ocean region, the minimum temperature difference of 15 Celsius needed for a practical system is available [12]. However, implementation of this idea in practice faces enormous problems, since the energy contained in ocean thermal gradients is very low in density. As a result , ocean energy conversion plants would have to be of enormous size to generate relatively small amounts of power.

The ocean tides which are produced by the rotation of the earth and gravitational pull of the moon and sun have been used as a source of power since the Middle Ages [21]. The rise and fall in the ocean level is accompanied by lateral movements of the water. When this movement is obstructed by the land masses , many local variations in tide ranges and currents are produced. The largest tidal ranges are to be found in such areas as Canada's Bay of Fundy (16 meters), the U.K's. Severn Estuary (13-14 meters) and France's Rance Estuary (12 meters). At the present time there are two tidal power plants in operation, they are namely a 400 Kw plant in Kislaya Bay in the Soviet Union and a 240 - Mw plant on the Rance River on the north coast of France [25]. In the U.K., the tidal energy option has been considered as one of the most promising renewable energy prospects for large scale electricity generation [29]. A recent study undertaken by the U.K's. Department of Energy estimated that a tidal power installation on the Severn Estuary could provide an installed capacity of 8640 Megawatts (Mw) at a cost of around $ 8 billion [30].

Attempts to use wind energy as an energy resource have been recognised as early as 250 B.C when the Persians built the first known windmills [31]. This practice spread throughout the Islamic world after the Arab conquest of Iran. The windmill entered European society in the 11th century and by the 17th century the Netherlands had become the world's most industrialised nation through the extensive use of wind power. However, with the introduction of the steam engine during the Industrial revolution, the use of wind power started to decline. In this respect Man's

understanding of the importance of the potential of wind energy as a pertinent energy resource has been limited. When, however, the era of cheap oil was finished, greater attention was given back to the use of wind power in many countries around the world. Further discussion of the prospects for wind power will be given in the next section.

It has not been possible to review all possible energy resources in this dissertation. However, further details concerning current progress in various types of renewable energy can be obtained in Refs. 33 & 34. Table 1.8 provides a comparison of basic capital cost, overall efficiency and the generation cost per Kilowatt-hour if renewable energy resources are used for electricity generation.

1.2 Prospects for Wind Energy.

Wind and ocean wave energy resources have some common characteristics. Their existence is truly unpredictable from time to time. However, from measurement of wind velocity over a long period, it is possible to determine the average annual wind velocity from which the availability of wind power can be deduced.

A review of the availability of world wind energy has been conducted by Dr. Marvin Gustafon of the Lawrence Livermore Laboratories [38]. He indicated that about 2% of the total solar flux, on average about 7 w/m^2, will be dissipated in the form of wind energy. Of this, it is estimated that about 35% is extracted near the surface of the earth through surface friction and turbulence.

If 10% of the available wind power near the earth's surface could be captured by wind machines, it would produce around 4000 quads which is equivalent to 12 times the world energy consumption in the year 2000. It is , therefore, clear that wind

power can offer enough energy to supply world energy demand at present or in the future. However, there is a shortcoming associated with this type of energy, its availability is intermittent and so does not always coincide with the time that energy is needed. For a small scale energy requirement, say for a rural area, this limitation can be anticipated by providing a storage system. This , in turn, becomes a problem for the large scale, since wind power becomes uneconomical.

The enormous amount of wind energy and the fact that it is a non polluting source of energy has made it an attractive option in many countries around the world. A recent worldwide survey of the market for wind turbines during the 5 years from 1981-1986 conducted by Jaras [39], found that there were 75000 wind turbine shipments involving 90 countries. The proportion of the total energy requirement of a given country supplied by wind energy varies depending on the evaluation of its wind energy potential. The regions which enjoy the highest winds : like the U.K., Eire, Iceland, Newfoundland, New Zealand, Argentina, Chile, Greenland and the State of California consider that wind energy represents one of the most promising renewable energy sources.

The estimated pattern of global wind power potential, using a specific output (kilowatt hours/kilowatt rating), from wind power machines rated at a wind speed of 11.2 m/s , adopted from Ref. 40, is shown in Fig. 1.1.

Like other types of renewable energy resource, the availability of wind power is dependent on site. If the site wind characteristics are favourable, the key factor which will decide the implementation of a wind machine is the price comparison with other energy resources.

Recognising the wind power availability for a specific site is the first step in establishing a wind generation facility. An appropriate assessment might follow Lipman's suggestion [41], where he indicated that there are twenty types of data which should be available for the optimum wind power exploitation. Amongst these,

the most important data are the distribution of hourly mean wind speed and the associated direction data . An error such as an overestimated wind energy availability may result in an actual output from wind energy devices far less than expected. This has been experienced by The U.S. wind power industry in California which achieved an output of half that projected [42].

Although the distribution of hourly mean wind speed is not yet available in most parts of the world, the annual mean wind speed is commonly available from any wind speed monitoring site, such as weather stations and airports. As a general indicator, Table 1.9 provides a relationship between annual mean wind speed and the potential value of the wind energy resource in qualitative terms, as given by Scheffler et al. [43]. Quantitatively, for a given diameter d of any wind machine located at sites with annual wind speed V_a, McVeigh [44] estimated the energy production E_a per annum to be :

$$E_a = 3.2289\, d\, V_a \text{ Kilowatt-hour} \qquad 1\text{-}1$$

An extensive study to collect wind data has been conducted within The E.E.C. and this has been reported in Ref.45. This study produced wind map data for ten countries including the U.K., Belgium /Luxembourg, France, The Netherlands, Denmark, West Germany, Greece, Ireland and Italy. The assessment of the wind power potential for these ten countries showed an encouraging result. Although five classes of restrictions, legal, political, technical, environmental and economical constraints, had been imposed, a large number of possible sites for placing Wind Energy Conversion [WEC] devices were identified . For small WECs within coastal zones with wind speed above 4 m/s, there are 14 000 sites, while for large WECs (diameter > 100 m) in offshore locations up to 10 m water depth and on land, there are 417 000 possible sites. All these sites, if in use, would provide an electricity potential of more than 4000 Terawatthour [Twh] per year [46]. Such an amount of electricity is equal to two times the electricity production of Western Europe in the year 1985 which was around 1968 Twh [10].

Experience gained from aeroplane technologies, which were already well developed , has helped in developing wind machine technology. Hence it can be expected that , as an alternative energy resource, wind energy may offer a substantial contribution which can be realised in a short time.

1.3 The Physical Configuration of Wind Machines

The first wind energy conversion devices appeared as early as about 200 B.C for grinding grain in Persia [38] . The spread of these devices followed the spread of the Islamic world and was introduced into the European Community in the 11th century by returning Crusaders. From that century many European countries, like the Netherlands, Denmark, Russia and others, made significant progress in utilising wind energy resources by using windmills. The era of wind milling started to decline during the industrial revolution when steam engines were invented. Outside Europe, the United States had the highest number of wind turbines, but they reduced dramatically due to government policy. Before 1930, The U.S. had around six million wind turbines until the Rural Electrification Administration dictated that this number should reduce to around 150 000 wind turbines [47]. However, this number increased again when the U.S. government gave incentives to use wind energy by introducing tax relief in 1979 for the use of renewable energy. Thus , the U.S. represents the largest country in the world currently using wind energy. The main centre for this activity is the State of California where the wind turbine market in terms of total installed capacity is around 200 Mw. per year [39]. A survey on the wind turbine market activities during the years 1981-1986 by Jaras[39], showed that there were more than 75 000 wind turbine shipments involving 563 wind turbine models from 234 manufacturers.

Wind turbines are commonly classified in terms of their axis of rotation relative to the

wind stream. Further classification can be derived from the way in which the wind energy is extracted, namely lift or drag type devices. However, other types not covered by the above classifications may exist since there are many possible ways to capture wind energy. The three main types of wind turbine are :

1. Horizontal axis wind turbine
   (This device has its axis of rotation parallel to the direction of the wind stream)
2. Vertical Axis Wind turbine
   (In this device, the axis of rotation is perpendicular to both the earth and the wind stream.)
3. Cross wind horizontal axis wind turbine .
   (This device has its axis of rotation horizontal with respect to the earth surface and perpendicular to the wind stream.)

Each of the wind turbines mentioned above have variations due to the number of blades and the shape of the blades.

Horizontal axis wind turbines can be further classified according to the rotor placement, i.e. upwind or downwind configuration. In both cases, the generator is generally mounted on the top of the tower. If , however, the end use of this device is to pump water, the pump is usually mounted at ground level and driven by a long shaft or connecting rod [48]. In addition, large scale horizontal-axis wind turbines of the upwind type require a positive yaw drive system with associated controls to achieve orientation into the wind. The downwind type only needs a positive yaw control whenever the yaw error cannot be kept within acceptable limits [43].

Sometimes wind machines are classified without consideration of the physical configuration, but based on their rated output, namely as small, medium or large scale machines. Following the classification scheme adopted in Ref. 49, the small scale is defined as a machine with rated output in the range less then 100 kw, while

the medium scale represents the range between 100 to 300 kw. Above 300 Kw is called large scale.

Rotors for horizontal axis wind turbines have been built with various numbers of blades ranging from one to more than 20 blades. Large numbers of blades result in a high solidity (i.e. the ratio of blade frontal area to the rotor swept area) which provides a high starting torque. This is useful , for instance, for water pumping purposes, where turbines have typically about 24 blades [50]. Another main feature of the horizontal axis wind turbine, is that the device is usually self starting if the blade pitch angle is large enough to generate a torque sufficient to overcome the friction and inertia force present in the drive train and end-use device.

The first attempt to built multi-megawatt horizontal axis wind machines was in 1941 in the U.S.A., with the Smith-Putnam machine [48]. This machine , however, which had a rated output of 1.25 Megawatts, was in operation only a few months when the blade was broken due to over stressing. There was no further attempt to rebuild the machine due to lack of financial support. Now, there are several wind machines in this class in operation in six countries [39]. The Boeing MOD-1 wind machine [2 Mw] was erected in 1979 and was the first multi-megawatt machine after Smith-Putnam's era [51].

Moving on from horizontal axis wind turbines, the second class of wind machine, as mentioned above, is the vertical axis wind turbine. Since this configuration corresponds to the subject of study in the present work, it will be discussed in detail in the next section.

The third class of wind turbine,the cross wind turbine, has not been very effective due to the technical difficulty of turning the device into the wind as the wind direction changes. As indicated by Eldrige [38] , the use of this type of device is not widespread .

1.4 Special Case : Vertical Axis Wind Turbines

The vertical axis wind turbine has been recognised since the year 200 B.C. In recent times, however, the horizontal wind turbine has been more prominent than its counterpart. Until recently, the advantages to the aerodynamic characteristics of the turbine, due to blade sections in the form of airfoils, were not fully understood. As a result, the development of vertical axis wind turbines came rather late. The first viable example was the Darrieus wind turbine which was patented in 1924.

In some respects, vertical axis devices offer advantages over horizontal devices. These advantages are [50,52,53, 54] :

1. They do not need yaw control due to their vertical symmetry,
2. The tower support, may be simpler, thus reducing construction cost and design difficulties
3. Because of simplicity of the blade design and because the blades are relatively thin, blade fabrication costs are reduced.
4. They require no pitch control for synchronous application .
5. The absence of cyclic gravitational force on the rotor
6. Simple symmetric blade shape
7. A safer design in that the blade is held at two points instead of one (Darrieus)
8. Minimal vortex and shadow problem from mast or tower.

In addition to the advantages mentioned above, one can notice that shaft power output is at the ground level. Hence, such equipment as the speed increasing gearbox, the electrical generator, the brake and control electronics, etc can all be located close to the ground level. This, facilitates installation and also subsequent inspection and maintenance are easier. There are, however, some disadvantages for this configuration, i.e. [52,54] :

1. These devices do not usually self-start, though for application in parallel

with an existing power source [e.g.a utility grid system] this is unimportant, since power to start the wind turbine can be taken from the parallel supply

2. It is known that most vertical axis wind turbines have curved blades in order to minimise bending stress due to centrifugal loads. This makes blade pitch control impracticable.
3. Greater parasitic drag
4. Less well understood dynamic conditions
5. Reversing aerodynamic loads.

The Various types of wind machine belonging to this class might be further categorised as :

1. Savonius rotor.
2. Darrieus-Rotor
3. Straight bladed rotor
4. V-type rotor.

All the types of rotor mentioned above will be described elsewhere, however, for simplicity , Figure 1.2 shows their schematic configurations.

1.4.1 The Savonius Rotor.

This type of device was invented and used in the 1920s and 1930s in Finland, [55]. The Savonius type rotors generally employ a minimum of 2 curved blades in the shape of an S with up-to-date designs being multi bladed. This type of rotor is primarily a drag device. It works on essentially the same principle as a cup anemometer . That is, torque is produced by the pressure difference between the concave and convex surfaces and also by the recirculation effect on the convex surface moving upwind. The Savonius design is fairly inefficient. The maximum power

coefficient , which is one of the most important parameters to indicate the device performance, obtained from wind tunnel tests, shows a scatter largely in the range of 0.14 to 0.33 [56]. This scatter has been identified as being due to the wind tunnel blockage effect. Their low speed and efficiency compared to horizontal wind turbines or other types of vertical axis wind turbine, has resulted in the Savonius rotor not being widely developed. However , as the utilisation of natural energy has become more important, the Savonius rotor has been finding its application in, for example, pumping water for irrigation, agitating for aeration of ponds and starting up Darrieus rotors [57].

Theoretical studies on the Savonius rotor are not numerous. This is due to the complexity of the flow pattern about the rotor and, in particular , to the separation of the flow from the blade surface and the associated vortex - shedding creating an unsteady flow through the rotor [58,57]. Thus, Savonius designs are mostly derived from experimental observation. Extensive experimental work prior to the design of optimum Savonius rotors had been conducted by Ushiyama [57]. In this study, all the main design configuration factors including aspect ratio, overlap ratio, separation gap ratio, profile of bucket cross section, number of buckets, bucket end plates and bucket stacking were examined.

The most promising theoretical approach is the discrete vortex method first purposed by Ogawa [59] and then extended by Aldos and Obeidat[58] and Aldos and Kotb [60] .

1.4.2 The Darrieus Rotor

Georges Darrieus of Paris filed a U.S. patent in 1926 for a vertical axis rotor. However ,it appears that this type of device was not given the same attention as horizontal wind machines until the mid-1960's when South and Rangi of the

National Research Council of Canada in Ottawa started to reinvestigate the machine's performance. Since the work of South and Rangi, this type of configuration has received considerable attention diverted toward the development and understanding of the device's structural and aerodynamical characteristics. Numerous pieces of experimental work have been conducted in many research institutions throughout the world [61]. Wind tunnel data for such machines can be obtained in a series of reports, for instance, LTR-LA-74, March 71, LTR-LA-105, Sept. 72 , etc which were published in Canada.

From the aerodynamic point of view, the flow past a wind turbine, as seen by a rotor blade element, is quite complex. The atmospheric environment and operating conditions of a wind turbine are inevitably unsteady, and the blades may experience wind shear, tower shadow, yawed operation,rotation across the flow, gusting and turbulence. Such flow conditions, when transformed into a mathematical model, present a significant modelling problem.

Experience gained from the experimental work combined with improved performance prediction methods has made the development of larger scale machines possible. In the mid 1970's Blackwell [61] noted that the most common Darrieus turbine was in the 2-5 meters diameter range. By the mid 1980s, machines in the 15-25 meters diameter range with rated output 150-500 Kw were commercially available. An exceptional machine was the Flowind - F 19, with rated output of 300 Kw, which was manufactured in USA. More than 100 of these machines were built [39].

1.4.3 The Straight Bladed Rotor.

This machine represents the most simple configuration compared to other vertical

axis wind turbines. Unlike the Darrieus rotor with its curved blade and the S-shaped blade of the Savonius rotor, the straight bladed rotor utilises a simple straight blade. It is possible to classify the turbine type further by consideration of the change in orientation of the blade chord with respect to the span and the variation in blade inclination angle whilst the turbine is in operation. If there is a variation in blade pitch with respect to the cross arm during operation, the configuration is termed as straight bladed with variable pitch. A configuration which allows a variation in angle between the blade spanwise direction and the cross arm is known as a Variable Geometry Vertical Axis Wind Turbine (VGVAWT) [62]

Wind tunnel tests on a straight bladed variable pitch model have been conducted by Grylls et .al.[63]. In these tests, the pitch angle was varied sinusoidally and a study of possible ways of regulating the speed and power output of the rotor, above a rated wind speed, was conducted. The results showed that an amplitude of pitch below 3^{o} could provide better power coefficients for a range of tip speed ratio than fixed zero pitch. Above 3^{o} the power coefficients obtained were lower.

The VGVAWT was first purposed by Musgrove [64]. This model was developed to eliminate the disadvantages of the Darrieus Wind Turbine whilst retaining the advantages of the vertical type. The complex blades of the Darrieus machine were replaced by straight, untapered and untwisted blades, which reduced the capital costs of the turbine. The variable geometry was used as a means of shedding excess power at high wind speeds. At low speeds, the blades remained upright, giving a maximum efficiency when it was most needed. At high speeds, when the prime concern is to avoid structural failure, the blades on this turbine were adjusted to incline inwards, thus reducing the aerodynamic loading. The blade inclination was progressively increased with increasing wind speed.

Theoretical studies and experimental results for the VGVAWT are presented in Refs. 64 and 65 respectively. The most significant feature of these results was that the straight bladed machine could provide Cps above 0.3 at a moderate tip speed ratio

($\lambda \sim 4$).

Initially, the first VGVAWT prototype had a diameter of 3 meters, blade length of 2 m and a blade chord of 15 cms [66]. The advantages of this machine attracted commercial interest and a 4.5 meter diameter prototype of a commercial version was developed. Another machine of 6 metres diameter was built at Rutherford Appleton Laboratory for research purposes. This machine produced favourable results as described in Ref. 67.

Experiences with these two versions brought further development of a larger scale VGVAWT with diameter 25 meters and power rated at 130 kw. This machine was built in 1986 at Camarthen Bay [68]. The results from nearly 2000 running hours has been reported in Ref. 69, which concluded that the availability of this prototype had been very high, with no major component failure. In addition, experimental results agreed well with theoretical calculations in all areas of interest.

The use of a variable geometry configuration to allow self starting and a self governing straight bladed vertical axis wind turbine has been purposed by Sutton-Vanne [54]. However, at this early stage of the work, the results so far are not encouraging.

1.4.4 V-Type Rotor

All advantages already mentioned for vertical axis wind turbines are also valid for "V" type vertical axis devices. The configuration of a V-type is shown in Fig. 1.2d. Sharpe et. al.[70] indicated that such a configuration could lead to lower transportation, installation and maintenance costs. These additional advantages are due to a shorter tower required for any size of wind turbine, straight blades without cross arms and blades hinged at their roots for ease of installation,

inspection, and replacement.

The V-Type has not yet attracted further investigation and so, information on its performance at this time is poor. The experimental results for this rotor configuration with blade span 5.5 meters and 8.8 meters overall diameter, conducted by Sharpe et. al.[70] , indicated that the maximum power coefficient was less than 0.2. This value is well below that of horizontal wind turbines or equivalent straight bladed vertical axis wind turbines.

1.5 The Aim of the Study

The development of a theoretical approach which is a reliable and well proven method represents one of the main objectives in many research activities. In wind turbine design, as well as any other engineering design activity , many parameters must be assessed in order to obtain an optimum solution. The blade curvature shape, blade span, blade radius and aerofoil section represent a few examples of parameters which might determine the overall machine's performance.

For the vertical axis wind machine, it has been recognised that the prediction of the performance of such devices is inherently more difficult than in the case of horizontal axis, or propeller type, wind turbines. This is due to the unsteady nature of the aerodynamics associated with the blades and the lack of axial symmetry [71]. The local incidence of the blade is constantly varying and, furthermore, the blades must pass through their own wake on the down stream half of the rotation. There are several performance prediction methods that have been developed. Reviews of these prediction methods have been given by Simhan [72] and Strickland [73].

General speaking, Strickland [73] classified prediction methods into two groups :

momentum based models and vortex models. The first includes single and double disk representations of single or multiple stream tube models. The vortex models includes the Free Wake method, and the fixed wake method. The momentum based models, especially , the double disk multiple stream tube, have been widely used and extensively developed as described by Paraschivoiu [74].

These momentum type approaches require less computation time than vortex methods. They have, however, several shortcomings, as noticed by Wilson R.E. et. al [75]. The agreement of stream tube predictions with wind tunnel tests warrants some caution. An example of this lies in the results presented by Hirsch and Mandal [76]. When they applied their method to the case of a Darrieus wind turbine, a good agreement with experimental results was obtained. However, when used for the case of a straight bladed machine , it gave a poor comparison.

The results of the fixed wake method when compared to experimental tests showed good agreement, as presented in Ref. 77 for a single test case of a Darrieus wind turbine. Further results from this method have not been published , and so it is difficult to asses the reliability of this approach

The Free Wake method has been identified as the most complex and accurate method of the above techniques [77]. Unfortunately, this approach is time consuming and, therefore, seems inappropriate as a design tool. It has been identified that the long computation time is due to the wake part of the solution. The wake shape is developed in a step by step manner until a steady solution is reached. If the wake shape could be identified first , then, placing it in the algorithm as an input would reduce computation time. This approach has been used for several years in the case of helicopter rotors and is known as a Prescribed Wake method [78] . Recently Graham et.al [79] applied this approach for the case of a horizontal-axis wind turbine.

The aim of this research was to develop an algorithm using the Prescribed Wake concept, but applied to the case of a vertical axis wind turbine. Since the algorithm

would be similar in some respects to the Free Wake method, the main features of the Free Wake method have been retained.

The detailed algorithm will be presented in Chapter 3 and in the following chapter where the development process leading to a final form of the algorithm is discussed.

The results from the new method showed good agreement with the Free Wake method. The associated computation time is of the order of one hundredth of that required for the Free Wake method. The work also confirmed that the airfoil data play a significant role in determining the level of agreement between the solution and experimental results.

1.6 The Thesis Arrangement.

Wind energy is a source of energy which appears to follow a life cycle. In past centuries, it was part of society with more than one million wind energy devices spread throughout the world. Then, with the industrial revolution in the early nineteen hundreds, it almost disappeared. After the era of cheap oil and with the awareness that all fossil fuel will diminish in the near future, wind energy may again represent a solution to future energy problems.

This thesis has been written in 6 chapters. The first chapter contains the description of world energy demand including the availability of primary energy resources. Recognising such a situation is important, since this represents the driving force for further development of alternative energy resources. The prospects for wind energy including wind turbine technology, are also discussed in this first chapter. The second chapter presents a literature survey starting from the general field of computational fluid dynamics then narrowing to the numerical approaches commonly applied for the case of vertical axis wind turbine configurations.

The basic concept of the Prescribed Wake method is presented in Chapter 3, whilst the following chapter (4) discusses the numerical strategy involved in implementing the concept for vertical axis wind turbines.

The numerical parameter effects apparent in the Prescribed Wake method were investigated. These, together with the effect of airfoil data , are presented in Chapter 5. Application of the method to the case of the Darrieus wind turbine is also presented in this chapter. The last chapter (6) presents the conclusions and future work suggestions.

CHAPTER - TWO : AERODYNAMIC PREDICTION METHODS

2.1 Aerodynamic Prediction Methods in Fluid Dynamics : General View

The governing equations of fluid motion, i.e the Navier - Stokes equations , have been recognised since the first half of the nineteenth century [80]. At first, M. Navier and G . Stokes, who derived these equations independently, presented the equations for compressible unsteady viscous laminar flow . It is, however, possible to extend them easily for turbulent flow, by introducing variables as instantaneous quantities which consist of mean and fluctuation values. If no simplifying assumption is applied to the Navier stokes equations, they represent a system of highly non linear partial differential equations which has five equations with eight unknowns and so is difficult to solve.

The five equations mentioned above can be provided by the conservation of mass law , the momentum and energy equations. Since there are eight unknowns, three other equations are needed to make a closed system. Additional equations are, usually, provided by one equation of state and two equations for fluid properties. Detailed formulation of the Navier Stokes equations can be obtained in Ref. 80 [Anderson, 1985] or in Ref. 81 [Schlicting, 1979].

The difficulties in solving the Navier Stokes equations for practical engineering problems has promoted various other approaches in the field of fluid mechanics. However, for aerodynamic problems , Anderson et .al. [82] described that the solution of aerodynamic problems, can be divided into three approaches. They are namely : (1) analytical, (2) numerical and (3) experimental .

The first approach, an analytical approach , requires simplification of the governing equations in order to make the equation become mathematically tractable.

Consequently the solutions are limited in their application or may deviate significantly from reality. However, the analytical approach still continues to be developed for use in the preliminary stages of design/analysis or as a comparison tool for any new numerical approach.

In the numerical approach, a limited number of assumptions are made and a high speed digital computer is used to solve the resulting governing fluid dynamic equations. Hence, a numerical approach can treat a wider range of flow problems. This type of method is generally not restricted to the linear case , thus allowing complicated physical flow conditions to be solved and the time evolution of the flow, if needed, to be obtained. This approach concentrates on the solution of differential equations which represent the fluid problem in hand. In addition, this approach may not be limited to a specific fluid media, and so a wide range of fluid media can be treated by this approach. The ability of this approach to treat different types of fluid has resulted in this numerical approach being called Computational Fluid Dynamics for its generality. Although the numerical approach offers some advantages, for example the wide range of flow problems it can tackle, it also has some disadvantages. These are associated with truncation errors, boundary conditions and computer costs [82].

The nonlinearity of fluid motion, as well as the complexity of boundary conditions, for some engineering problems may render the flow problem unsolvable. At the same time, information on aerodynamic behaviour for the problem needs to be available. This situation has often resulted in the solution being obtained via an experimental approach. It is true that experimental work often offers more realistic results, but there are often problems encountered , due to : equipment failures, scaling factors, tunnel corrections, measurement processes and the operating costs.

The escalating operating costs and time requirement for experimental methods may represent the main factor to limit such an approach. Conversely, the rapid progress

in the computer industry, which offers rapid growth in computer power and, at the same time, a lower price, has encouraged the numerical approach to become a powerful tool in the aerodynamics field. A survey of the relative cost of computation as function of years since 1953 by Chapman [83], showed that the relative cost of computation has decreased an order of magnitude every eight years and it will continue to drop. It is interesting to note that today in much of the aircraft industry , the testing of preliminary designs for new aircraft, which used to be carried out via numerous wind tunnel tests, is performed almost entirely on the computer and the wind tunnel is only used to fine-tune the final design [84].

The solution of the Navier Stokes equations, combined with the required boundary conditions for complex configurations such as a complete aircraft, is prohibitive in terms of cost and is generally beyond current computer resources. MacCormack [85] and Kutler[86] estimated that a substantial number of grid points would be needed and that solution times would be of the order of up to 2000hours on the most modern computers[87] for this type of problem.

In some circumstances, aerodynamic problems are not always solved using full Navier Stokes equations. There are two things which need to be assessed, namely, the degree of accuracy of numerical simulation needed to be achieved and the available computer resources. In addition, although super computers are already available, not all users have access to them. It seems that the development of efficient algorithms capable of obtaining the same results as current schemes may represent the most demanding achievement in this area.

From the above considerations, the idea of solving aerodynamic problems following Hirsch [88] represents a good approach. He suggested that the solution of aerodynamic problems, using the governing equations of fluid motion, can be simplified via three levels of approximation. They are namely : dynamical, spatial and steadiness levels of approximation. These three approximations can be simultaneously implemented or may be applied in isolation..

The dynamical level approximation is derived from the stand point that all component forces working on a fluid element may not have the same order of magnitude or the same degree of significance. Neglecting low order of magnitude terms will result in a simplified Navier-Stokes model; for instance the Thin Shear Layer, Parabolized Navier - Stokes, and Full potential Equation sets. As given in Ref. 88, this approach produces a hierarchy of the governing equations of fluid motion as shown in Fig. 2.1. The highest level of equation is the time averaged Navier Stokes and the lowest level is the Potential Small perturbation.

The spatial approximation level is introduced from consideration of the variation of flow variables in the spatial direction. This indicates whether the problem should be solved in a fully three dimensional, quasi - three dimensional, two dimensional or just as a one dimensional problem. In addition, from the geometry of the flow system , one can solve problems in terms of cylindrical, spherical or canonical coordinate systems. The last is suitable for the external flow problem around wave rider or delta wing configurations.

The steadiness approximation level corresponds to the presence of various time constants of the flow being considered and the choice of the lowest time constant being taken into consideration in the modelling system. The best example of this procedure is the system of averaged Navier -Stokes equations for mean turbulent flows.

The implementation of these three level approximations to the flow system under consideration may allow the problem to be solved analytically or by numerical solution. Currently, progress in computer technologies and the success of numerical approaches has resulted in a reduction in the number of assumptions required for the earlier example of the solution around complete aircraft configurations. For this case, Paterson et . al [89] gave an estimate of the required computer resource with reference to the ability of a fourth class computer machine for different levels of approximation applied to the Navier Stoke equations as shown in Table 2.1.

Strictly speaking, the solution of flow problems numerically or computational fluid dynamics can be said to be the art of replacing the governing partial differential equations of fluid flow with numbers, and advancing these numbers in space and / or time to obtain a final numerical description of the complete flow field of interest. Hence ingredients of typical computational procedure may consist of successive steps as shown in Fig. 2.2 Considering this diagram , time discretization is always needed whenever the governing equation is time dependent. However, for the steady state flow problem, the time dependent approach is,sometimes, adopted, in order to cast the system of equations in a uniform way. For instance, in the case of transonic flow where the governing equations are a mixed elliptic/ hyperbolic according to the local value of Mach number, the equations can be made purely hyperbolic by considering the steady state problem as a time dependent problem. Time discretization can be divided into three schemes, they are namely : explicit, implicit and hybrid explicit - implicit schemes [90,91].

Continuing with Fig. 2.2, after time discretization, the following step is space discretization. This type of discretization can be done using various different techniques, namely : Finite difference, Finite element, Control volume or spectral method. Details of these techniques can be obtained in Refs. 92-97. Of these schemes, the Finite difference method represents the most widely used in the area of Computational Fluid Dynamics and is the oldest method compared to the other three mentioned above. The philosophy of this method is to replace the partial derivatives appearing in the governing equations of fluid dynamics with algebraic difference quotients, yielding a system of algebraic equations which can be solved for the flow field variables at specific, discrete grid points in the flow. Hence, the solution of a system of algebraic equations represents the next step after space discretization, as described Fig. 2.1.

If the problem in hand is steady state then the solution of the system of algebraic equations represents the final stage in the calculation process . However, for the time dependent problem, it is necessary to continue to check on the stage of convergence

[time asymptotic problem], or whether the time upper limit has been achieved. If such conditions are not satisfied the procedure returns to the stage of time discretization.

Computational fluid dynamics represents one way of solving flow problems. An other approach might be to use the singularities approach . This approach has been commonly applied for the case of incompressible flow at high Reynolds number and low Mach Number. The essence of this approach is to use combinations of simple flow models like sources, sinks, doublets or vortices to build up a complex flow system. Mathematically this approach is correct if the problem in hand can be treated as a potential flow problem. Although this approach needs a numerical solution, the way in which the flow problem is solved is quite different from that usually adopted in Computational Fluid Dynamic methods. Consider, for instance, the case of the flow around a lifting wing at high Reynolds number. Here the solution does not start from the Navier Stokes equations with some progressive simplification to those governing equations, but from consideration of how the vortex system may appear on the wing. For an unswept wing with high aspect ratio, the problem can be solved using a Lifting line approach or Lifting surface approach or a vortex Lattice Method. An excellent review of solutions using the singularity approach can be obtained in Ref. 98, and Ref. 99 . The last reference gives an overview of flow solutions on the basis of vortex singularities .

When considering the flow around rotating bodies like helicopter rotors, propellers, and wind energy devices, almost all methods which have been developed use the singularity type approach. The next following section presents an overview of methods in this area and concentrates on the problem of the flow around vertical axis wind devices.

2.2 Aerodynamic Prediction Methods For the Flow around Rotating Bodies.

There is some practical engineering interest involved with the flow passing through a rotating body, for instance, the flow around a helicopter rotor , propeller, or wind energy device. These represent a few examples of the case of external flow, while for internal flow, this problem can be found in the propulsion system of a jet engine, where the flow passes through a row of rotating blades. Amongst the various external flow problems, the aerodynamics of the helicopter rotor have received more attention than other problems. The commercial driving force and the wide range of helicopter applicability for public and military purposes has made the helicopter's aerodynamics well understood and has allowed them to be used as a source of reference in developing new methods for other flow problems. References 100 & 101 provide good background material on helicopter aerodynamics.

Generally speaking, the equations of fluid motion for any flow situation, whether the flow passes around a rotating body or a body at rest, are governed by the same laws of conservation. Namely mass, momentum and energy are conserved. If such a statement is transformed into a mathematical model, the result is the Navier Stokes equations. These equations , if supplemented by empirical laws for the dependence of viscosity and thermal conductivity on the flow variables and by a consitutive law defining the nature of fluid flow, can describe all flow phenomena which may appear for any kind of flow condition. The form of the governing equations for the flow around a rotating body is more complex than their counterparts for the flow around stationary bodies. Currently, aerodynamic prediction methods can be said to be limited, particularly in the trade off between solving the problem as a simple flow with complex geometry or a complex flow with simple geometry [89 & 102]. The terms, complex geometry and complex flow are relative and have no precise definition. For instance, two dimensional flow around a circular cylinder can be said to be geometrically simple. However under certain conditions the flow problem becomes extremely complex. This is because it contains the unsteadiness generated

by the presence of Von Karman vortex streets [although the incident flow condition is stationary], separation and compressibility effects [Hirsch,(88)]. An attempt to solve this problem using the full Navier-stokes equations in the absence of turbulence modelling has been made by Iishi et al.[88], at various Mach numbers and Reynolds numbers. This calculation required approximately 7-9 hours CPU time, on a super computer Hitachi S810, for every pair of Mach and Reynolds Numbers. In addition, Nixon [103] stated that for even a simple simulation of turbulence at a low Reynolds number around 5000, approximately 100 CPU hours on a Cray-2 would be required.

Flows around rotating bodies, generally, fall into the category of complex flow problems. In addition, for meaningful applications, the system normally has a complex geometry. However, in some respects, when the detailed flow field itself is not required, as in most solutions of the aerodynamics of wind energy devices, a solution may be obtained by a method other than a simplification of the Navier Stokes equations. Typical approaches which are commonly adopted are based on Momentum theory, blade element theory or vortex theory. The description of these methods in the context of vertical axis wind turbines will be discussed later.

The three methods mentioned above might not suit the case of a helicopter rotor or the flow past a row of blades in a propulsion system due to the high Mach number in these situations. An attempt to solve such a problem which included the compressibility effect, using the Full Potential equations for the helicopter rotor, has been carried out by Caradonna. et. al.[104, 105]. An extended version of this method, using the Inviscid Compressible Euler-Equations, has been reported by the same researcher in Ref. 106. This equation set has the ability to capture all non smooth solutions like shock waves as well as surface discontinuities. However, the complex flow field past a helicopter rotor requires a very fine grid resolution and a sophisticated grid system for capturing all non smooth solutions. Thus, obtaining a high quality solution will involve a large number of grid points which, in turn, will demand a large computer memory and computation time.

In the work by Caradonna et. al [104 - 106], to simplify the required grid system, the same numerical procedure as applied for the case of the compressible flow problem around a fixed wing was used. In the case of the fixed wing, the incoming velocity is equal to the velocity at infinity but, in the rotor case, the incoming velocity is replaced by the resultant velocity relative to the rotor blade. This velocity is equal to the summation of three velocity vectors, namely, the free stream velocity vector , the blade rotational velocity and the induced velocity. The induced velocity is calculated by another technique such as a free wake method or obtained from available codes like the Camrad Code [107] or Tanair Code [106].

The work of Caradonna et. al and Wake and Sankar [107] indicates that further development in the aerodynamics of rotary wings, which in the past was mostly based on vortex methods, may be achieved by implementing the success of Computational Fluid Dynamics in handling the flow problem of a fixed wing. An excellent review of such developments, which includes the role of computational fluid dynamics, can be found in Ref.108 and Ref. 109 .

In flow problems in propulsion systems, the common approach adopted in the past has been to consider the flow through an array of rotor blades as a two dimensional flow problem over a cascade where a potential flow solution could imposed[110]. At the present time , the solution of flow problems in propulsion systems has seen significant progress. The most complex flow equations, the Time Averaged Navier - Stokes equations, have been applied to solve this problem, by Birch et. al. [111]. With these equations a detailed description of the flow field can now be provided.

Returning to the around a rotary wing, even the case of low Mach number flow, where the compressibility effect can be ignored, still represents a complex flow system due to the presence of field vorticity. Any attempt to capture a vortex as part of the solution forces one to use at least the Euler equations. Therefore, one has to face the problem of solving nonlinear partial differential equations. The work of

Rizzi at. al.[112] represents an example of capturing a vortex as part of the solution for a less complex flow problem . Here the work is concerned with the case of the flow around a 65^{o} swept delta wing with a round leading edge at angle of attack α = 10^{o}. A three dimensional Euler-Equation was employed as the governing flow equation and the finite difference method as the numerical tool. For this problem, the solution required 125x49x65 grid points to be generated in the domain surrounding the body in order to satisfy the finite difference requirement. It is clear that if this approach is to be adopted for solving the rotary wing's flow problem, it will require a larger number of grid points, which in turn, will become costly and will be complicated by the difficulty in providing a proper mesh system. This type of situation has resulted in the solution of the rotating wing problem normally being via a vortex model.

In a vortex model, the wake flow domain is considered as highly concentrated vorticity embedded in the irrotational flow domain. Further simplification can be introduced by assuming the vorticity domain is represented by sheet vortices with zero thickness, where the Helmhlotz-Kelvin law of field vorticity can be applied. This vortex sheet will contain trailing and shed vortices when variations in blade loading in the spanwise and azimuth directions are present. However, dealing with any continuous sheet of vorticity presents a profound mathematically difficulty, and so further simplification may required. For instance, it is possible to replace it by a discrete representation called a wake vortex lattice. In one such technique this wake vortex lattice is free to develop and thus becomes part of the solution. This approach is known as a Free Wake method and represents the most advanced technique in this area. Such a method has been applied to the solution of many problems in engineering, for instance, in the case of helicopter rotor aerodynamic analysis in Refs.113-116. The case of a delta wing undergoing a rolling motion, with the roll axis on the mid span chord, is presented in Ref.117. Other applications of a Free Wake method have been for wind turbine devices of the horizontal type, as given in Ref.118, and for the vertical axis configuration in Ref. 119.

The complexity of the flow behaviour around a rotary wing, whether it is a helicopter rotor or wind energy device, is clear. For wind energy devices, the aerodynamic problem has not yet been fully investigated. Attempts to solve the aerodynamic problem for this type of device started in the early 1970's when the price of oil, as the world's primary source of energy, increased sharply. Therefore, aerodynamic methods applied to the case of wind energy devices are not yet mature and are limited in their approach .

The aerodynamic problem associated with vertical axis wind turbines may not deviate significantly from the aerodynamic problem found in the rotary wing case [Helicopter]. In other words, the aerodynamic approach for the helicopter might be applicable to such devices. Reference [73] indicates the measure of progress in the development of aerodynamic methods for the vertical axis wind turbine. Strickland [73] indicated that aerodynamic methods for vertical axis wind turbines can be classified into two models, namely :

1. Momentum model
2. Vortex model.

The first type of model may further be classified as :

1.a Single disk single streamtube
1.b Single disk multiple streamtube
1.c Double disk multiple streamtube

While vortex models, can be further classified as :

2a. Fixed Wake Method
2b. Free Wake Method
2c. Prescribed Wake method.

The basic concepts behind the two types of scheme can be described ,respectively,

as follows : The momentum model is developed by using a conservation of momentum principle. Namely the aerodynamic force is equal to the change of stream wise momentum through the turbine [121]. The vortex models are based upon some form of the vorticity equation. The advantage of the vorticity equation is that the pressure is not applied explicitly, therefore allowing one to determine the velocity field without any knowledge of the pressure field. Furthermore, Strickland [73] emphasised the fact that in many flow problems, regions of vorticity can be treated as thin sheets or even points of concentrated vorticity. This greatly facilitates numerical analysis.

2.3 The Momentum Model.

The momentum model represents the most simple approach for solving the aerodynamic problem of a rotary wing. The generality of this approach means it can be applied whether the problem in hand is a helicopter rotor or horizontal or vertical axis wind energy device.

As mentioned previously, this model can be further classified in three ways, these are : Single Disk Single Stream-Tube, Single Disk Multiple Stream-Tube and Double Disk Multiple Stream-Tube methods. The Single Disk Single Stream-Tube method represents the simplest method amongst these three. The other two methods are basically extensions of this technique. Since the Single Disk Single Stream-Tube method represents the basic idea of the momentum model, it will now be presented in detail.

2.3.1. Single Disk Single Stream-Tube Method.

In the Single Disk Single Stream-Tube method , the entire rotor is enclosed in one stream tube and the rotor is modelled as an actuator disk across which there exists a pressure drop equivalent to the stream wise force on the rotor divided by the actuator disk area. Hence, the flow passing the rotor blade is modelled as shown in Fig.2.3. Let the incoming uniform velocity, the wake velocity far down stream and the velocity across the actuator disk be denoted by $U_\sim$, U_w and U_d respectively. The power P required to slow down the air stream can, then , be given by :

$$P = [m/2] [U_\sim^2 - U_w^2] \qquad 2\text{-}1$$

Where m is the mass flow rate through the rotor and the remaining terms on the right hand side represent the change of kinetic energy per unit mass. The power P can be presented in terms of the force F on the actuator disk and the disk velocity U as :

$$P = F U_d \qquad 2\text{-}2$$

It should be noted that the force F above represents the time averaged force in the stream tube for a complete revolution of the rotor. In terms of the upstream velocity at infinity $U_\sim$ and the down stream velocity in the far wake U_w , the force F can be written as :

$$F = m [U_\sim - U_w] \qquad 2\text{-}3$$

The rate of mass flow m along a stream tube is constant, therefore this quantity can be written in terms of swept area A and the disk velocity U. If the air stream density is denoted by ρ, the rate of mass flow m is written as :

$$m = \rho A U_d \qquad 2\text{-}4$$

The swept area A in equation 2-4 above, for the vertical axis wind turbine, is defined as swept area. Equating eq. 2-1 and 2-2 and using the relationships given by eq. 2-3 and 2-4, the disk velocity U_d becomes :

$$U_d = [U_\sim + U_w]/2 \qquad 2\text{-}5$$

Using equation 2-5, the force F can be written in terms of the disk velocity U as :

$$\begin{aligned} F &= m[U_\sim - U_w] \\ &= \rho A U_d [U_\sim - (-U_\sim + 2U_d)] \\ &= 2\rho A U_d [U_\sim - U_d] \end{aligned} \qquad 2\text{-}6$$

Equation 2-6 forms the basis for obtaining the unknown value of U_d. If one can define the force F explicitly as a function of U_d, for instance using blade element theory, then the unknown U_d can be obtained. In some cases, equation 2-6 can be solved explicitly for U_d , but in most cases it must be solved iteratively. Such an explicit formulation is, for example, given by Musgrove [122]. His formulation is applied for the case of an NB straight bladed vertical axis wind turbine, with other pertinent geometric data denoted as follows : blade span L, blade radius R, constant blade chord c_r and angular velocity Ω, then the force F is given by :

$$F = NB\,(\delta C_l/\delta\alpha)\,\rho\,\Omega\,R\,c_r\,L\,U_d/4 \qquad 2\text{-}7$$

Where $\delta C_l/\delta\alpha$ is the rate of change of two dimensional lift coefficient at the blade section with respect to the angle of attack α. The detailed derivation of equation 2-7 is given in Appendix A1. For the case of a straight bladed vertical axis wind turbine, the swept Area A can be defined simply as :

$$A = 2 R L \qquad 2\text{-}8$$

Equating eq. 2-6 with eq. 2-7 and using eq. 2-8 for the swept area A, one can obtain the relationship :

$$NB\,(\delta C_l/\delta\alpha)\,\rho\,\Omega\,R\,c_r\,L\,U_d/4 = 2\,\rho\,2\,R\,L\,U_d(U_\sim - U_w) \qquad 2\text{-}9$$

From the above equation , the actuator disk velocity U_d can be written in non dimensional form $U_d/U_\sim$ as :

$$U_d/U_\sim = 1 - 0.5\,[\,NB\,c_r/(2R)\,][\,\Omega R/U_\sim\,]\,\delta C_l/\delta\alpha \qquad 2\text{-}11$$

The $[\,NB\,c_r/2R\,]$ term is known as the solidity factor while the term $[\Omega R/U_\sim]$ is called the tip speed ratio factor λ. The first term is important in identifying the unsteadiness of the flow behaviour, especially in the absence of dynamic stall. For these conditions the unsteady effects can loosely be categorised as those due to fluid inertial added mass and unsteady wake circulation [73]. The unsteady effect due to added mass, has been formulated by Strickland in Ref.123, while the unsteady effect due to the wake can be included automatically into the Free Wake method [73]. The second term $[\,\Omega R/U_\sim\,]$, denoted by λ, is usually used to describe the overall characteristic performance of the wind energy device by plotting the machine's power coefficient Cp as function of the tip speed ratio λ.

An example of a similar formulation for the force F, in the case of a horizontal wind turbine, can be found in Refs. 124 and 125.

2.3.2 Single Disk Multiple Stream-Tube Method.

This approach attempts to improve the solution of the Single Disk Single Stream-Tube method by representing the swept volume of the rotor as a series of adjacent stream tubes. Introducing multiple stream tubes here allows the disk velocity U_d to vary along the transverse direction. An illustration of the Single Disk Multiple Stream-Tube approach is shown in Fig. 2.3b. The relationships as applied in the Single Disk Single Stream-Tube method are valid for any stream tube. Thus, for any given stream tube, the relation between force F and disk velocity is given by equation 2-6. For this application, however, it is necessary to express the relationship in differential form.

$$dF = dm\, 2(U_{\sim} - U_w(r)) \qquad 2\text{-}11$$

Where dm is the differential rate of mass flow . The formulation of momentum theory in this form can be applied whether the problem is a helicopter rotor , propeller, horizontal axis or vertical axis wind turbine . For the first three, the term dm is given by :

$$dm = 2\pi\rho\, dr\, (r\, U_d(r)) \qquad 2\text{-}12$$

While for the vertical axis type of device and for a general curve where the local blade radius r is a function of the vertical axis z (r=r(z)), dm is written as :

$$dm = dz\, dr\, (\rho\, U_d(r(z))) \qquad 2\text{-}13a$$

For a simple case, like a straight bladed vertical axis wind turbine with blade span L, the dm term can be given by :

$$dm = L\, dr\, (\rho\, U_d(r)) \qquad 2\text{-}13b$$

Following the previous section where the blade radius is denoted by R then, if the swept volume is divided uniformly into N stream tubes, the thickness of each stream tube Δr will be 2R/N. However, in order to simplify the formulation for the force dF , the N divisions are normally made in terms of blade azimuth position in the range [$-\pi/2 < \theta < \pi/2$]. In the multiple stream tube method here , the actuator disk velocity U_d is written in the form :

$$\begin{aligned} U_d &= U_\sim + u_i \\ &= U_\sim\, [\, 1+a\,] \end{aligned} \qquad 2\text{-}14$$

Where u_i is the axial induced velocity, which can be written in non-dimensional form as [$a = u_i / U_\sim$] which is called the axial interference factor [48]. For the case of a straight bladed vertical axis wind turbine with blade span L, equation 2-11 can be written in terms of this interference factor a as :

$$dF = 2\, r\, L\, dr\, U_\sim\, a\, [1+a] \qquad 2\text{-}15$$

For this case, Hunt [48] showed that the value of interference factor a for high tip speed ratio λ, can be expressed analytically as :

$$a = [NB\, c_r/(2R)]\ \lambda\ \sin\theta \qquad 2\text{-}16$$

The detailed formulation for the a parameter, as given by eq. 2-16 above, for this Single Disk Multiple Stream-Tube method, is given in Appendix A2.

In practical vertical axis wind turbine applications, use of the Single Disk approach, whether it is a single stream-tube or multiple stream-tube method, would not give an accurate solution. This approach does, however, seem appropriate for the case of

horizontal axis wind turbines or propellers, where the air stream passes the blade only once. It is different for the case of vertical axis devices, where the air stream passes the rotor blade twice, i.e. once at the up stream blade pass and once at the down stream pass. This has given rise to another approach called the Double Disk Multiple Stream-Tube method. This technique uses two disk actuators instead of a single disk actuator and has attracted many researchers, amongst these are Sharpe [126], Read [127], and Paraschivoiu [128]. A short description of this method will be be given in the next section.

2.3.3 Double Disk Multiple Stream-Tube Method.

This approach introduces double disk actuators to simulate the presence of the difference in disk velocity between the upstream and down stream blade passes. Schematically, this Double Disk Multiple Stream-Tube model is depicted in Fig. 2.3c. An extensive development of this approach has been done by Read et. al. [129] and Paraschiovoiu [130] .

In this approach, two disk actuators are introduced and the flow through the wind turbine is considered to be subdivided into a large number of stream tubes. The flow in each stream tube passes through these two disk actuators. The first disk actuator represents the upstream half of the surface swept by the rotor blades [$\pi/2 < \theta < 3\pi/2$] and the second disk actuator represents the downstream half of the rotor [$-\pi/2 < \theta < \pi/2$]. In the presence of two disk actuators, each stream tube has two axial interference factors. These factors are denoted as a_u and a_d for the upstream and down stream interference factors respectively. As a consequence, along any given stream tube, there exists five velocities as depicted in Figure 2-3. In the presence of the upstream axial interference factor a_u , the disk velocity

upstream U_{du} can be written as :

$$U_{du} = U_{\sim} [1+a_u] \qquad 2\text{-}17a$$

The velocity leaving the upstream blade pass is denoted as U_{uw}. Here it can be assumed that the flow is fully expanded,and so U_{uw} can be written following :

$$U_{uw} = U_{\sim} [2 U_{du} - 1] \qquad 2\text{-}17b$$

This velocity U_{uw} provides an input velocity for the second disk actuator, and so the down stream disk velocity U_{dd} can be defined in the same manner as the upstream disk velocity U_{du} , where $U_{\sim}$ and U_{du} are replaced by U_{uw} and U_{dd} , respectively. Hence U_{dd} can be written as :

$$\begin{aligned} U_{dd} &= U_{uw} [1+u_d] \\ &= U_{\sim} [2 U_{du} - 1][1+u_d] \end{aligned} \qquad 2\text{-}17c$$

The down stream velocity U_{dw} behind the second disk actuator, is defined in the same manner as the exit velocity from the upstream disk actuator U_{uw} , hence it can be formulated as :

$$\begin{aligned} U_{dw} &= U_{uw} [2 U_{dd} - 1] \\ &= U_{\sim} [2 U_{du} - 1][2 U_{dd} - 1] \end{aligned} \qquad 2\text{-}17d$$

The value of these two interference factors can be determined using the same procedure as for the interference factor in the case of the Single Disk Multiple Stream-Tube method described in Appendix A2. An attempt to improve this approach by considering that the width of any stream tube is not constant, but rather expanding, has been made by Read et. al. [129] and Parachioviou [130]. However, the result of this change on power coefficient was not significant at moderate tip speed ratios $4 < \lambda < 7$, as shown by Paraschiviou in Ref. 130.

2.4 Vortex Model.

The momentum based model , described in the previous section, offers a simple approach to solving the aerodynamic performance for rotary wing devices. However, such a method suffers from two major deficiencies. Firstly, since the stream tubes are aerodynamically independent, no consideration is given to the aerodynamic influence of any one blade upon the flow field through which any other one is passing. Secondly, each stream tube calculation simultaneously treats both traverses of each blade through the stream tube. The effects of the blade pass through the upwind half of the stream tube are not to fully dealt with when calculating the effect of the blade pass through the down wind half of the stream tube.Such limitations are not serious at low tip speed ratios, where the blade wakes are swept down stream relatively quickly. However, these limitations become more apparent as both the tip speed ratio and the blade wake spatial density increases. In addition to these limitations, Strickland et. al. [120] added another three sources of inaccuracy associated with the momentum based model. These are based on the fact that the momentum based model (1) assumes quasi steady flow through the rotor, (2) assumes a constant stream wise velocity as a function of stream wise position in the vicinity of the rotor and (3) assumes that the flow velocities normal to the free stream velocity direction are zero.

Recognition of the inability of the momentum models to provide an accurate solution has led to the development of another approach, that is the vortex model. All types of vortex methods are basically derived from some form of the vorticity equations. One of the advantages of the vorticity equations is that the pressure does not appear explicitly in the equation, therefore allowing one to determine the velocity without any knowledge of the pressure field [131]. In addition, Strickland [73] further noticed that in many flows, regions of vorticity can be treated as thin sheets or even points of concentrated vorticity which greatly facilitates numerical analysis.

In formulating the flow problem into a vortex model, it is necessary to recognise the fundamental theorems governing vortex properties. In this respect, there are five theorems which address to the properties of vortex motion, they are namely [132].

1. Kelvin's circulation theorem

   This theorem states that :When the external forces are conservative and derived from a single valued potential, the circulation is independent of the time.

   Strictly speaking this statement means that if the gravity force in a fluid dynamic analysis can be ignored then a flow whose circulation is originally zero will expe - rience no change in circulation. If the bound circulation over the lifting surface is changed then it would be accompanied by shed vorticity to ensure that the total circulation of the whole flow domain remains constant.

2. The First theorem of Helmholtz .

   This theorem states that the fluid particles move like a rigid body with translational and rotational velocity and a deformation velocity caused by the shearing action of the particles is superposed on this motion. Hence, if the fluid particle were suddenly frozen, it would begin to rotate with an angular velocity of one-half the fluid vorticity.

3. The second theorem of Helmholtz.

   This theorem together with Kelvin's theorem may represent the theorem which is most often mentioned when applying a vortex model for solving flow problems. This second theorem states that , the product of the magnitude of vorticity and the cross sectional area remains constant along any vortex filament. In other words, the vorticity is conserved and any vortex filament cannot end in the interior of the fluid and must,therefore, form a closed ring or terminate on the boundary.

4. The third theorem of Helmholtz

   The third theorem of Helmholtz states that the fluid which forms a vortex filament continues to form a vortex filament.

5. The fourth theorem of Helmholtz

The fourth theorem of Helmholtz states that the intensity of a vortex filament remains constant as the filament moves about. The intensity here means the product of vorticity and the cross sectional area.

In addition to the theorems mentioned above, there are two other additional theorems to be considered in the context of flow passing a lifting surface. They are namely the theorem and the condition of Kutta-Joukowski. The former states that the generation of lift is directly related to the presence of circulation around the aerofoil or wing. For the case of a two dimensional aerofoil, if the relative velocity vector , the circulation and the lift are denoted by V_r , Γ and **L**, respectively ,then the relationship between lift **L** and the other quantities can be written mathematically as :

$$\mathbf{L} = \rho \, V_r \times \Gamma \qquad \text{2-18a}$$

Where ρ is fluid density. This theorem, if applied to the case of a finite lifting surface, e.g. a wing, can be written as :

$$L = \rho \int_{-b/2}^{b/2} [\, \partial \Gamma(y) / \partial y \,] \, V(y) \, dy \qquad \text{2-18b}$$

Where **L** is the total lift on the wing, b is the wing span and the variable inside the bracket corresponds to the variation in circulation in the span wise Y-direction.
The Kutta - Joukoswky condition is usually imposed when analysing flow problems using a potential flow solution. If this approach is applied for the case of two dimensional aerofoils, then the Kutta-Joukowski condition means that the flow leaves the trailing edge smoothly.

An excellent review of vortex methods for the purpose of flow simulation at the level of understanding of basic fluid flow behaviour was given by Leonard [99].

Information of practical engineering interest, for instance, the case of two dimensional flow separation and the rolling up of vortex sheets shed from a lifting wing of finite span can be found in Ref. 133. In addition, the progress of vortex methods in a wide range of applications for general fluid dynamic problems has been presented by Sarpkaya in Ref. 98 .

The first recognisable use of the vortex method was by Rosenhead [99] when he used it to investigate the evolution of a sinusoidally perturbed two dimensional vortex sheet in 1931. This vortex sheet generated a flow domain divided into two separate streams of equal density and equal velocity but with opposite direction [98]. His approach introduced a discrete vortex approximation by replacing a continuous vortex sheet by a number of line vortices. Since Rosenhead's work, the development of vortex methods has grown rapidly, both in terms of their application [134-135] and the relevant theory [136-137].

However, attempts to use vortex methods for the case of vertical axis wind turbines are more recent. The Vortex models of Fanucci [138] and Holme [139], both two dimensional , appeared in the mid nineteen seventies. These two works promoted further development of the vortex concept. Further development of vortex methods applied for the case of wind turbine devices can be divided into three classes :(1) Fixed Wake methods ,(2) Free Wake methods and (3) Prescribed Wake methods. The last method, which represents the main subject of this study, will be presented in great detail in the following Chapter. The other two vortex methods will be discussed for completeness.

2.4.1 Fixed Wake Method [77,139,140,141]

This approach, which includes the work of Holmes [139],Sharpe[140] ,Wilson [141]

and Wilson and Walker [77] is basically a two dimensional vortex method. However, the Fixed wake method of Wilson and Walker [77], is quite different from the other three models.

Holme [139] considered the vertical axis wind turbine as a system having a great number of straight, very narrow blades and a high height-diameter ratio. The last condition allowed him to approach the problem as a two dimensional flow case. For this very special case, the circular path of the blade was represented by a continuous circular vortex sheet with its strength a function of blade azimuth position. Due to the rotational motion, each blade experiences a change in its bound vorticity when it moves from one blade position to the next. As the blade moves continuously around the circular path, the change of bound vorticity occurs continuously with respect to the blade position and shed vortices are released in the wake in the form of a trailing vortex sheet. Further simplification of the shape of the trailing sheet vorticity from any blade position, can be made by assuming it to be straight and parallel to the free stream velocity. Holme produced a semi analytic solution for this model.

An attempt to improve Holme's approach by introducing an alternative method for the calculation of the induced velocity due to the wake vortex sheet was made by Sharpe[140]. He used a finite element method for this purpose. However, his approach did not work well for high tip speed ratios where his numerical calculation suffered from a divergent solution.

Another approach to use a 2-D vortex model was that of Wilson et. al. [163]. This approach does not strictly belong to the class of Fixed Wake methods but can be said to be a two dimensional Free Wake method, where the flow is considered as the flow past an infinite span blade, and so tip effects can be ignored. The analysis starts by implementing system coordinates based on the aerofoil geometry, which, using Milne-Thomson's Circle theorem is mapped into the circle plane. The complex velocity potential is , then, derived. The wake is modelled using point

vortices, the number of which increases as more are shed at increasing time steps. Thus, the calculation starts with zero point vortices at t= 0. Since this approach uses a semi-analytic definition of the complex velocity potential at any instant in time, it would be difficult to extend it for more than one blade. Therefore, this approach seems only applicable for a single bladed case.

The Fixed Wake method of Wilson and Walker [77] is quite different from all the vortex methods discussed above. This approach follows the idea of the stream tube approach but uses a vortex analysis to define the axial induced velocity upstream or down stream. In this model, it is considered that, in each stream tube, the aerofoil traverses along the path of the stream tube as shown in Fig.2-4a. Between A and B the aerofoil moves parallel to the free stream and generates no forces. When it comes to the point B, the aerofoil suddenly changes direction and moves across the wind, generating both lift and circulation Γ. The same condition occurs when it arrives at point C, hence vorticity is shed again. In this situation the sign of shed vorticity is opposite to that shed at B. Fig.2.4b shows the wake system which is generated by such aerofoil movement along the path of a stream tube.

In line with the notation used in the case of the Double Disk Multiple Stream-Tube method , axial interference factors upstream and down stream are denoted by a_u and a_d respectively. Here Wilson and Walker [77] obtained a relation between the momentum flux deduced from momentum theory and the force deduced from the wake model as :

$$a(1-a) = [NB/4\pi] - [\Omega/U_{\sim}^{2}][\Gamma_u - \Gamma_d] \qquad 2\text{-}19$$

where

$$a_d = [1 - (1-2a)^{1/2}]/2 \qquad 2\text{-}20a$$

and

$$a_u=[1+2a-(1-2a)^{1/2}]/2 \qquad 2\text{-}20b$$

The circulation Γ is the value of circulation at the blade azimuth where the stream tube under investigation passes through, i.e. at the blade azimuth positions θ and $\pi-\theta$. To solve equation 2-19 above requires an iteration process. An initial value a may be deduced from Single Disk Multiple Stream-Tube theory , as suggested by Strickland [77]. By knowing the value of parameter a ,the up and down stream axial interference factors a_u and a_d can be calculated using equation 2-20. If both interference factors have been defined, then, the axial induced velocity follows from equation 2-14. The Blade element theory can, then, be used to obtain the relative velocity, and the local angle of attack, which in turn, can be used to obtain the lift force. Finally, the circulation Γ can be obtained using the Joukowsky theorem as defined by eq.2-18. If the circulation Γ for both upstream and down stream sections has been obtained, the calculation is then repeated by inserting the calculated Γ values into eq.2-19 to obtain a new value of Γ. The calculation terminates when a prescribed convergence criterion between two successive iterations is satisfied.

2.4.2 The Free Wake method. [72,73,120,163]

The basic principle underlying this approach is that the wake is treated as part of the solution in obtaining the aerodynamic performance of a vertical axis wind machine. The first attempt to use this approach is recognised as Fanucci's model. His work is strictly two dimensional with three to eight bound vortices placed along the aerofoil camber line [120]. The numerical procedure is , then, developed by considering the continuous rotation of the blade as a discrete time stepping process towards a steady state condition. Due to the presence of shed vortices released into the flow field, as required by Kelvin-Helhmholtz theorem, the wake shape is

determined by the movement of the vortices. Unfortunately, complete information on the Fanucci model is not available, and so it is unclear whether at every increment time step the number of shed vortices released into the flow field is equal to the defined number of bound vortices,or the vorticity is accumulated into single shed vortices as has been done by Simhan [73].

Other two dimensional Free wake methods were introduced by Vandenberghe et. al [142] and Wilson et. al [163]. The first approach used a Poisson Equation as the governing equation for the field vorticity and the induced velocity was obtained by solving it. The second approach used a complex potential velocity in the mathematical model and was applied for a single blade problem only.

Attempts to improve the Fanucci model to include three dimensional effects can be noticed in the work of Strickland [120] and Simhan [72]. The differences between those two approaches are first in terms of the number of bound vortices and second in treating the unknown bound vortices. The Strickland model used a single lifting line to replace the blade, while Sihman's model replaced it with a blade vortex lattice. In the latter, the blade was divided into a number of panels, each panel consisted of a bound vortex and a pair of trailing vortices. The bound vortex was located at 0.25 of the local panel chord on the centre line and the corresponding control point at 0.75 of the chord. In this Simhan model [72] , a pair of trailing vortices was shed along the panel edges downstream up to an arbitrarily chosen location just beyond the trailing edge of the blade and then closed into a loop with the vortex about to be shed.

The development of the wake shape in the Strickland model and the Sihman[72] model follows the same algorithm. They consider that the shed vortex is assumed to be force free and is convected down stream with the corresponding local velocity and is always connected by a pair of trailing vortices to the shed vortex originating from the preceding time step. A schematic diagram of the two models is shown in Fig. 2.5.

In terms of numerical procedure, Strickland's model has two different iteration processes at each time step of the calculation. In the the first iteration scheme, the strength of trailing vortices is assumed to be equal to the gradient along the blade span from the previous time step. Therefore, there exists a difference between the strength of the circulation attached to the blade and its trailing vortices.This approach may be acceptable for small time steps, where the circulation difference between two successive blade azimuth positions might be small. Such relaxation of certain requirements in computational fluid dynamics is known as an asymptotic algorithm, which allows one to relax on full mass conservation in its numerical implementation [143]. By relaxing the requirement of circulation conservation, all strengths of vortex filaments on the wake are known, and the induced velocities along a lifting line can be calculated directly . If the bound vortex strength becomes available, the induced velocities are corrected again by specifying that the strength of trailing vortices strictly behind the blade correspond to the variations in bound vorticity on the blade and shed vortices from the previous time step are set equal to the difference between the bound vortex at the current blade position and that at the previous blade position. Whilst in Strickland's method ,there are two calculations of induced velocity on the blade, there is one in the Sihman model. In the Simhan method, however, there is a requirement to compute the solution of a set of algebraic equations. In his model, it is considered that the strengths of trailing vortices immediately behind the blade are unknown as well as the attached bound vortex. To solve such unknown quantities, he used a lifting surface approach and set up a system of algebraic equations for the unknown strengths of the bound vortices, by applying zero normal velocities on the blade. This makes the Sihman model more time consuming than the Strickland model. Experience with the VDART3 code based on Strickland's model indicated that one tip speed ratio calculation required about 12 Hours CPU time on a Microvax. The Sihman Model would take around 15 hours of CPU time.

The mathematical formulation of both these free wake approaches is almost the

same as a Prescribed Wake method. The difference can be said to be their numerical strategy. Hence the mathematical formulation for the Prescribed Wake method, to be presented in Chapter 3, was the same as the Free Wake method.

The numerical strategy applied for the free wake method in the Strickland's model can be described briefly as follows :

The calculation starts from time t=0 with a uniform time step Δt. At this time level, there is no wake, hence the induced velocity on the lifting line due to the wake is zero. The induced velocities are required in order to define the resultant velocity and the angle of attack relative to the blade section and, then, using available aerofoil data to obtain the local aerodynamic characteristics of lift and drag. Once the lift coefficient is known , then, using the Kutta-Joukowski theorem as defined by eq. 2-19, the bound vortex can be defined. When the blade moves to the next blade azimuth position from θ to $\theta = \theta + \Delta\theta$, where $\Delta\theta = \Omega \Delta t$ and Ω is the blade angular velocity, a vortex corresponding to the change in bound vorticity is shed and moves to a new position according to the local velocity for the time Δt. Hence, at the first time increment, the wake consists of a single shed vortex and a couple of trailing vortices emanating from the blade at position θ . If the blade span is divided into Ns segments, the shed vorticity will consist of Ns segment filaments, and there will be (Ns+1) trailing vortices. Since the Strickland model avoids solving a system of equations for an incremental time step, two induced velocity calculations are made.The first calculation, fixes the strengths of the trailing vortices emanating from the blade at a new position equal to the strength of the corresponding trailing vortices at the previous time step. This approach ensures that the strengths of all vortex filaments in the wake are known and allows the induced velocity due to the wake to be determined, thus providing a new estimate of the bound vorticity on the blade. The induced velocities on the blade are, then, recalculated based on the already available information on the bound vortex on the blade. The same procedure follows for the next time step until a prescribed number of time steps is achieved.

2.4.3 The Prescribed Wake Method.

Until now, a prescribed wake method for solving the aerodynamic problem for the vertical axis wind machine was not available. However, such an approach has been already applied for the case of a horizontal wind turbine [145] , a propeller [146] and a helicopter rotor [148,149]. The well known lifting line theory, or the lifting surface method, usually applied for aerodynamic analysis for simple wing planforms or swept wings, in some respects, can be considered as a prescribed wake method. The wake shape in this type of problem is prescribed as flat and emanates from the wing and goes to infinity in the direction of the free stream velocity. Fortunately, although the structure of the wake shape rolls up at some distance down stream, it only gives a small influence on the pressure distribution over the wing surface [148]. This allows the assumption of a flat wake shape, to provide a reasonable degree of accuracy. This is quite different from the flow around a rotary wing such as a propeller, horizontal or vertical axis wind turbine or helicopter rotor blade, where the wake geometry has a significant effect on the performance.

If the wake geometry of any rotary wing device can be defined then the aerodynamic analysis can follow the same numerical procedure as in the lifting line theory. Each type of rotary wing device, however, has its own specific wake geometry. Here examples of prescribed wakes for propellers and for helicopter rotors in forward flight will be presented to provide insight into dealing with the prescribing of wake geometries for other rotary wing devices.

2.4.3.1 A Prescribed Wake Method for Propellers. [145]

In this case, the oncoming velocity is directly parallel to the rotational axis and, therefore, the blade loading at any blade azimuth position is constant and only varies in the radial /spanwise direction. The radial variation of blade loading produces a sheet of trailing vortices springing up along the line of the trailing edge. If the lifting line concept is used for the aerodynamic analysis in this situation, the trailing vortex filaments need to be defined. A schematic model of the trailing vortex filament from a certain blade position is depicted in Fig. 2.6. The rotational motion of the propeller combined with the direction of the oncoming free stream velocity generates a trailing vortex filament with a helical form. If one can define that the pitch of the helix is p, then according to McCormick [145], the equation of the helix filament in terms of the generating angle θ, based on the coordinate system shown in Fig.2.6, can be written as :

$$\begin{aligned} z &= r\cos(\theta) \\ y &= r\sin(\theta) \quad 0 < \theta < \sim \\ x &= p\theta/2\pi \end{aligned} \qquad \text{2-21}$$

Where r is the radius of any blade section with respect to the origin. Unfortunately, McCormick does not indicate how to specify the value of p, which represents the key to incorporating equation 2-21 in the lifting line or lifting surface approach. This p parameter is required in order to calculate the induced velocity due to the vortex filament.

If the pitch of the helix p can be defined, the calculation of induced velocity, for instance along the x axis can be obtained as follows. Let **r** be denoted as a vector which defines any control point A located on an element of a helical vortex filament **ds.** With respect to the origin - system coordinates **r** can be defined as :

$$\mathbf{r} = (p\theta/2\pi)\,\mathbf{i} + r\sin\theta\,\mathbf{j} + r\cos\theta\,\mathbf{k} \qquad 2\text{-}22$$

Where **i**, **j**, and **k** are unit vectors in the x,y and z directions respectively, with their orientation as depicted in Fig. 2.7. The equation of the helix vortex element **ds**, then , can be defined as :

$$\mathbf{ds} = (dr/dq)\,dq$$

$$= [\,(p/2\pi)\,\mathbf{i} + r\cos(\theta)\,\mathbf{j} - r\sin(\theta)\,\mathbf{k}\,]\,d\theta \qquad 2\text{-}23$$

If, in this case, one is interested in the induced velocity at any point x_p along the x axis, the vector $\mathbf{L_p}$ which represents the distance between the points A and x_p, can be defined as :

$$\mathbf{L_p} = \mathbf{r} - x_p\,\mathbf{i}$$
$$= [(p\theta/2\pi) - x_p]\,\mathbf{i} + r\sin\theta\,\mathbf{j} + r\cos\theta\,\mathbf{k} \qquad 2\text{-}24$$

The differential vector induced velocity **dw** due to the differential vortex element **ds** with strength Γ follows the Biot-Savart law , and can be written as

$$\mathbf{dw} = (\Gamma/4\pi)\,[\,\mathbf{L_p} \times \mathbf{ds}\,]\,/\,|\mathbf{L_p}|^3$$

$$\mathbf{dw} = (\Gamma/[4\pi\, r_p^3]) \begin{vmatrix} \mathbf{i} & \mathbf{j} & \mathbf{k} \\ (p\theta/2\pi) - x_p & r\sin\theta & r\cos\theta \\ (p/2\pi) & r\cos\theta & -r\sin\theta \end{vmatrix} d\theta \qquad 2\text{-}25$$

Using equation 2-25, one can define the component differential induced velocities in the directions of the unit vectors **i**, **j**, and **k** denoted by dw_x , dw_y and dw_z respectively. For example, for the **i** component , i.e. in the x-axial direction, the

result from eqs. 2-25 provide dw_x as :

$$dw_x = (\Gamma/4\pi) \frac{r\ d\theta}{[\ (p\theta/2\pi)-xp)^2 + r^2\ ]^{3/2}} i \qquad 2\text{-}26$$

The total induced velocity due to the whole length of helical vortex filament running from $\theta=0$ to θ ---> $+_{\sim}$, can be obtained as [145]

$$w_x = \int_0^{\tilde{}} dw_x$$

$$= \int_0^{\tilde{}} \frac{\Gamma}{4\pi} \frac{r^2\ d\theta}{[(p\theta/2\pi) - x_p)^2 + r^2\ ]^{3/2}} i$$

$$= \frac{\Gamma}{p} [\ 1 + \frac{x_p}{[\ r^2 + x_p^2\ ]^{1/2}}\ ] i \qquad 2\text{-}27$$

Equation 2-27 shows that, at the origin, $x_p = 0$, the induced velocity in the axial direction is simply equal to Γ/p and is not a function of the location of the helical trailing vortex filament emanating from the blade. The formulation of induced velocity at any arbitrary control point due to such a helical vortex filament can be easily obtained. It is clear that by specifying the geometry of the trailing vortex system, it is possible to formulate the induced velocity at any point of interest. How to use such induced velocity information in order to find aerodynamic performance on the blade, will depend on the type of approach adopted, namely lifting line or lifting surface .

2.4.3.2 A Prescribed Wake Method for a Helicopter Rotor Under Forward Flight Conditions.

A prescribed wake method is the name for an aerodynamic analysis method where the development of the wake [vortex sheet] from an individual blade is prescribed in advance. This method implies that if the wake geometry can be prescribed, the corresponding induced velocity at the blade can be calculated. This method does not, actually,provide a formulation for wake geometry which is valid for all rotary wing devices. Therefore, each type of rotary wing device has its own wake geometry which must be determined.

In the case of a helicopter rotor in the forward flight condition, Bramwell's work assumed that the uniform convection velocity is opposite to the flight direction. The incoming velocity denoted as $\mathbf{U}_{\sim}$ makes an angle of attack α_d with respect to the plane of rotation. The inflow velocity V_i is specified as the velocity normal to the rotational plane and dictates the wake shape in the z direction. The definition of system coordinates XYZ, as well as the other notation in the following analysis will be as depicted in Fig. 2.7. By knowing these two velocities, Bramwel[78] formulated the vortex filament coordinates shed at azimuth angle posistion Φ as :

$$\begin{aligned} x &= r_1 \cos(\Phi) + |\mathbf{U}_{\sim}| \cos(\alpha_d)\, t \\ y &= x_1 R \sin(\Phi) \\ z &= |\mathbf{U}_{\sim}| \sin\alpha_d\, t - V_i\, t; \qquad x_1 = r_1/R \end{aligned} \tag{2-28}$$

Where t is the time taken for the blade to rotate from Φ to Ψ . With the angular velocity denoted by Ω, then the time t can be defined as :

$$t = (\Psi - \Phi)/\Omega \tag{2-29}$$

Substituting equation 2-29 into 2-28, it follows :

$$x = r_1 \cos(\Phi) + |\mathbf{U}_\sim| \cos\alpha_d \{(\Psi - \Phi)/\Omega\}$$
$$y = x_1 R \sin(\Phi) \qquad 2\text{-}30$$
$$z = |\mathbf{U}_\sim| \sin\alpha_d - V_i] \{(\Psi - \Phi)/\Omega$$

Using eqs. 2-31 above with Ψ ranging from $\Psi = 0$ to Ψ ---> $+\sim$, one obtains the shape of the trailing vortex filament which emanates from the blade at azimuth position Ψ at distance r from the origin. Now if P is an arbitrary control point on the blade at the blade azimuth position Ψ, then the distance $\mathbf{L_p}$ from this to the differential element of the helical vortex filament originated when the blade was at the blade azimuth position Φ, can be written as :

$$\mathbf{L_p} = L_1 \mathbf{i} + L_2 \mathbf{j} + L_3 \mathbf{k} \qquad 2\text{-}31$$

where

$$L_1 = r \cos(\Psi) - r_1 \cos(\Phi) - |\mathbf{U}_\sim| \cos\alpha_d \{(\Psi - \Phi)/\Omega\}$$
$$L_2 = -R [x \sin(\Psi) - x_1 \sin(\Phi)] \qquad 2\text{-}32$$
$$L_3 = [|\mathbf{U}_\sim| \sin\alpha_d - V_i] \{(\Psi - \Phi)/\Omega\}$$

The differential element of the helical vortex filament $\mathbf{ds}$ which originated when the blade was at Φ and in the direction away from the blade can be written as :

$$\mathbf{ds} = ds_1 \mathbf{i} + ds_2 \mathbf{j} + ds_3 \mathbf{k} \qquad 2\text{-}33a$$

where

$$ds_1 = -[r_1 \sin(\Phi) + |\mathbf{U}_\sim| \cos(\alpha_d)/\Omega] d\Phi$$
$$ds_2 = -r_1 \cos(\Phi)\, d\Phi \qquad 2\text{-}33b$$

$$ds_3 = -[\,|\mathbf{U}_\sim| \sin\alpha_d + V_i\,]d\Phi/\Omega$$

The control point P on the blade in question experiences an induced velocity from its own trailing vortices and is also affected by trailing vortices from the preceding blades. Equation 2-31, which represents the distance between the control point P and a differential element, still applies provided we allow for an appropriate phase shift in the translational term of L_1, L_2 and L_3. Hence the equation 2-31 applied to measure the distance from the trailing vortices to another blade can be written as :

$$\begin{aligned} L_{n1} &= r\cos(\Psi) - r_1\cos(\Phi) - |\mathbf{U}_\sim|\cos\alpha_d\,(\Psi - \Phi + (2\pi/NB)n)/\Omega \\ L_{n2} &= r\sin(\Psi) - r_1\sin(\Phi) \\ L_{n3} &= [\,|\mathbf{U}_\sim|\sin\alpha_d - V_i\,]\,(\Psi - \Phi + (2\pi/NB)/n)/\Omega \\ n &= 0,1,2,\ldots, Nb\text{-}1 \end{aligned} \qquad 2\text{-}34$$

Where NB is the number of blades, and n=0, refers to the distance between the control point P and trailing vortices from its own blade. If this aerodynamic problem is treated using a lifting line approach, each blade is replaced by a single bound vortex, and this bound bound vortex influences the induced velocity on the other blades. To calculate the induced velocity from the bound vortices of each blade, we consider two blades separated by angle $\Delta\Psi$ as shown in Fig. 2.9a The coordinates

of bound vortex Γ_b are

$$\begin{aligned} x_{b1} &= -r_{b1}\cos(\Psi + \Delta\Psi) \\ y_{b1} &= r_{b1}\sin(\Psi + \Delta\Psi) \\ z_b &= 0 \end{aligned} \qquad 2\text{-}35$$

With the bound vortex on the blade, a differential bound vortex element $\mathbf{ds_b}$ can be defined as :

$$\mathbf{ds_b} = -\cos(\Psi + \Delta\Psi)\, d r_{b1}\, \mathbf{i} + \sin(\Psi + \Delta\Psi)\, d r_{b1}\, \mathbf{j} + 0\,\mathbf{k} \qquad 2\text{-}36$$

The distance between the control point p on the blade at blade azimuth Ψ and the differential element of bound vortex vorticity, denoted by $\mathbf{L_{bp}}$ [Fig. 2.9b] can be written as :

$$\mathbf{L_{bp}} = [\, r_{b1} \cos(\Psi + \Delta\Psi) - r\cos(\Psi)\,]\,\mathbf{i} + [r_b \sin(\Psi) - r_{b1} \sin(\Psi + \Delta\Psi)\,]\,\mathbf{j} + 0\,\mathbf{k} \qquad 2\text{-}37$$

It has been recognized that as well as the blade loading varying along the blade span [radial direction], it also changes with the blade azimuth position. This produces shed vortices, which Bramwell [78] assumed were convected in the same way as trailing vortices. Hence the equation for the distance between a control point and a differential element of shed vorticity is the same , and the formulation of an element of shed vorticity **ds** is equivalent to the formulation of a differential element of bound vorticity .

At this stage, the formulation still contains unknown values, namely the strength of the vortex filaments , which correspond to the unknown blade loadings. Thus, although, the wake shape is known in advance, the calculation procedure needs an iteration process to determine the unknown strength of the vortex filaments. Further more Bramwell [96] states that such an iteration process may require considerable care to obtain a convergent solution. A similiar formulation for the hover condition can be obtained in Ref. 146.

2.4.3.3 A Prescribed Wake Method for Vertical Axis Wind Turbines.

From geometry considerations, the trailing vortex configuration which emanates from

the tip part of a helicopter blade, actually resembles the trailing vortex which emanates from the blade of a vertical axis wind turbine.The difference between them is there is no inflow velocity which makes the wake trail beneath the rotational plane of the turbine as occurs in the case of the helicopter rotor. The presence of the inflow velocity V_i, as described by Bramwell (78) , precludes the presence of large induced velocities. This can be easily seen by introducing the limiting case that the velocity in the z direction [parallel to the axis of rotation] is zero. This causes a large part of the trailing vortex system to interact with the rotor blade. Application of the Biot -Savart law in this case, would promote unacceptable values of induced velocity and, in turn would give a meaningless solution.

An attempt to use a similar approach to Bramwell, was made during this research, by simply prescribing that the trailing vorticity was convected by the uniform oncoming velocity. The result in terms of power coefficient was an over-prediction compared to other methods. The comparison in the case of the vertical axis wind turbine will be presented in detail in Chapter 4 of this thesis. A complete description of the Prescribed Wake method for the vertical axis wind turbine will be given in Chapter 3.

CHAPTER - THREE : A PRESCRIBED WAKE METHOD.

3.1 Physical flow Phenomena around Vertical Axis Wind Turbines.

There are various physical configurations of wind turbines belonging to the class of vertical axis wind turbines. They are namely, Savonius, Darrieus, V-Type and the straight bladed vertical axis wind turbine. With the exception of the Savonius rotor, these wind turbines have similar aerodynamic characteristics. In particular, the rotor blade experiences a variation in angle of attack with azimuthal blade position and the wake trailed from the blade in clycoid form experiences blade vortex interaction. There are additional influences due to the proximity of the earth surface, and the presence of tower shadow and the rotor blade arms all complicate the flow pattern.

The complexity of such physical flow phenomena can be described schematically, as shown in Fig. 3.1 [149]. It is clear that to obtain an aerodynamic solution in the presence of such flow phenomena is quite complicated. The Free Wake method is commonly accepted as the most appropriate method for solving the aerodynamic problem under such complex flow conditions. Unfortunately, this method is very time consuming and is, therefore inappropriate as a design tool which usually requires a fast solution without losing accuracy.

It has been realised that the main computational effort in the Free wake method is due to the wake calculation. If the wake shape could be defined in advance, the required computer time would drop significantly, since nearly ninety percent of the computer time is spent on building up the wake. The prescribed wake method proposed here is similar to the Free wake method of Strickland [73] but with the wake shape prescribed in advance. The wake shape is a crucial factor which determines the accuracy of the solution, and physical data on the wake shape are not available. Hence, an investigation based on results from the Free Wake method was carried out in this study for the purpose of developing a wake shape for the

Prescribed Wake Method. Therefore, the results from the Free Wake method will be reviewed first before going on to a complete description of the Prescribed Wake Method.

3.2 Free Wake Solution as a Background Study.

The theoretical background of Strickland's Free Wake method has been fully described in Ref. 120. The computer code (VDART3), based on this theory, for specific aerofoil data and the Darrieus configuration was made available for this study. A modified version (MVDART3) was developed to allow the use of any aerofoil data, any rotor blade configuration and the output was configured to facilitate the development of the Prescribed Wake method. Although VDART3 was modified, the modified version could still be used for the Darrieus rotor. It is interesting to note that for each type of vertical axis wind turbine, with the exception of the Savonius rotor which requires a completely different theoretical approach, implementation of the Free wake method requires different programme structures. The code designed for the Darrieus rotor, cannot be used for a V-type or a straight- bladed model and vice versa. However, if the code is configured for a straight bladed machine , it can be applied for other types, if some simplifications are introduced.

3.2.1 Wind Turbine Geometry Under Investigation.

For the purpose of this study, the wind turbine geometry data from Musgrove [122] is used. He used this model in his work on the Multiple Stream Tube method.

The wind turbine data used by Musgrove is as follows :

Type of wind Turbine	: Straight bladed
Radius of cross arm	: 12.5 m
whole blade length	: 18.0 m
Chord length	: 1.25 m
aerofoil type	: NACA 0015
Rotational Speed	: 27.0 rev/min.
Number of blades	: 2

It is recognised that, in actual operation, a vertical axis wind turbine blade undergoes a variation in angle of attack which may extend beyond the range of static stall. The changing angle of attack from one blade position to another implies that the dynamic effect cannot be ignored. Hence, the use of dynamic aerofoil data rather than static data seems , for this case, to be more appropriate. However, implementation of the dynamic response via a semi-empirical model such as the Beddoe's[150] , Gangwani[151] or ONERA dynamic stall models [152] into VDART3 or MVDART3 increases the time required for a solution. Hence, for simplicity, static aerofoil data were used in this study. The particular data used were for the NACA 0015, these data are presented in Table 3.1

3.2.2 Numerical Parameters for the Free Wake Code.

The Free Wake method requires discretization along the blade span, blade azimuth and also an input for the number of rotational calculations. The blade azimuth discretization corresponds to time steps within each rotational calculation. This parameter is denoted by NTI. The number of rotational calculations (NR) relates to the number of wake cycles, and also indicates the extent to which the calculation is close to the steady state solution. It is true that a large NR is favourable but,

consequently, it will result in a high computation time. In this study, the parameters mentioned above were chosen as follows :

No. of uniform blade elements NBE	= 8
Uniform time steps NTI	= 16
Rotational Calculation NR	= 8

In the original Code [VDART3], these parameters had been set at :

No. of blade elements NBE	= 5
Uniform time step NTI	= 16
Rotational calculation NR	= 4

The number of blade span elements, NBE, equal to five, in the original code had been applied to a Darriues rotor, where the blade is a curve. This case might, actually, require more elements to reasonably approximate the blade shape. An even number for NBE was chosen in this study , in order to provide wake vortex filaments at the mid blade span. With NBE as described above, and the blade span divided uniformly, aerodynamic characteristics will be obtained at a distance equal to 1/16 of the blade span from the centre span position.

3.2.3 Wake shape for various Numbers of blades.

In the Prescribed Wake method, the wake geometry is an input to the numerical solution and this shape is a crucial factor for gaining an accurate solution. The flow problem facing a vertical axis wind turbine is quite different from the flow problem past a fixed wing configuration, where the wake structure does not have a significant influence on the wing loading [148].

It is possible for vertical axis wind machines to be built with their rotor consisting of a number of blades This option is usually applied for small scale power output, where more than two blades is common. The effect of increasing blade numbers can be observed by applying the MVDART3-Code to wind turbines with one, two, three and four blades. The comparison of the wake shape for four different numbers of blades at tip speed ratio $\lambda = 4$ is shown in Fig. 3.2. This figure shows the wake geometries at NTIxNR time steps and ,for clarity, the wake from only one blade has been drawn. It is clear that with increasing numbers of blades the wake shape becomes more complicated.

3.2.4 Wake Shape for Various Tip Speed Ratios For a Two Bladed Configuration.

Whilst a wind turbine designed for small scale rated power output may use a large number of blades, for medium to large scale wind turbines, due to fatigue and structural considerations, the number of blades is normally restricted to two . Hence, the work on the Free and Prescribed Wake method is mostly directed to the two bladed configuration. A comparison of wake shapes at the mid blade span, for various tip speed ratios in the range $2 \leq \lambda \leq 7$ is shown in Fig. 3.3. Again, for clarity, the wake shape shown in Fig. 3.3 is that generated by one of the blades. It is clear that by increasing the value of tip speed ratio, the cloud of the wake around the blade becomes dense. Since the wake represents a source of induced velocity on the blade, any deviation in prescribing the wake shape, especially for high tip speed ratios, will significantly alter the result obtained.

3.2.5 Variation in Wake Shape with Azimuth and Blade Span Position For a Two Bladed Configuration.

In this section special attention is focused on the particular value of tip speed ratio λ = 4 . This value can be considered to represent a moderate tip speed ratio and is, thus, appropriate for most wind turbines which are designed to operate at moderate tip speed ratios. Hence, it will provide the ideal case to illustrate the behaviour of the vortex model . Using the numerical parameters described above, i.e. NR = 8 and NTI = 16 time steps, Fig. 3.4 shows the wake development from time step to

time step at the mid blade span for λ = 4 . However, for space considerations, this figure only presents the development of the wake from the 113 th to 128th time step.

Fig. 3.5 shows the wake shape variations along the blade span at the end of the 128th time step for three different values of tip speed ratio [λ = 4, 5 and 6]. From the above figures, it is clear that there is a variation in the wake shape trailed from the tip and from the mid blade span. During the time stepping process, however, when the development of the wake had reached a large number of time steps, the wake shape did not vary very much with azimuth.

3.2.6 The rate of convergence of the Free wake method

Of the three numerical parameters mentioned above, NR represents the most pertinent parameter in the context of required computation time. This parameter can provide an estimate for the possibility that the solution will be close to the steady state solution. Consider a calculation at the N th time step. At this time, every

trailing vortex filament will contain N-1 shed vortices. If the blade is divided uniformly into NBE elements, there will be (N-1)xNBE shed vortices and (N-1)x(NBE+1) trailing vortex filaments behind each blade. Since the Free Wake approach requires the calculation of induced velocity to obtain the local velocity for the movement of a vortex filament at the next time step, the total number of calculations of induced velocity for the case of an NB bladed system at the Nth time step is approximately NBxNx(N-1)(NBE+1) [2x NBE +1]. Thus, a complete calculation using a Free Wake method will involve a total number of calculations of induced velocity given by :

$$= \sum_{J=1}^{NRxNTI} NBxJx(J-1)(NBE+1)(2\ NBE\ +\ 1) \qquad 3\text{-}1$$

From the above equation, it is clear that reducing NR reduces the number of induced velocity calculations. For the Free Wake model, the rate of convergence can be easily examined by plotting the behaviour of power coefficient with respect to the number of rotational calculations. Fig. 3.6 shows the rate of convergence in terms of Cp versus rotational calculation for various values of tip speed ratio. The rate of convergence becomes faster for low tip speed ratios $\lambda < 4$. In this range of tip speed ratio, when the method has reached the 5 th rotational calculation, the power coefficient Cp starts to approach the steady state solution. This can be understood since, at low tip speed ratios, the axial induced velocity in the opposite direction to the free stream is much lower than the free stream velocity itself. Hence, the wake is swept further down stream. Consequently, the induced effect of the change of wake shape is not felt as much by the rotor blade. From Fig.3.6, it can be concluded that NR equal to 8 is appropriate for any value of tip speed ratio as being within the limit of a steady state solution.

3.2.7 Some Examples of the Detailed Aerodynamic Performance Resulting From the Free Wake Method.

An interesting result of the Free Wake method is its ability to provide detailed aerodynamic characteristics along the blade span at any azimuth position. Such a result is important for the purpose of fatigue or structural analyses which require detailed information about aerodynamic forces along the blade span. Such detail, at some degree of accuracy, could not be achieved by any other approach. For instance, the stream-tube methods can provide overall performance in good agreement with experiment but their local aerodynamic loads are known to be in error, as reported by Wilson et. al [75].

Typical results from the Free Wake method in terms of two component induced velocities in the free stream and transverse direction [X and Y direction], the relative angle of attack α, and normal and tangential force coefficients [C_{Fn} and C_{Ft}] near the mid blade span, as a function of blade azimuth position for three different value of tip speed ratio ($\lambda = 2, 5$ and 7) are shown in Fig. 3.7.

It is clear that at low tip speed ratios, given the static stall angle for this type of aerofoil [NACA 0015] is around $\alpha_s = 15.0^o$, the blade experiences an angle of attack above static stall for most of the range of blade azimuth.

Figs. 3.8 a,b and c for $\lambda = 2, 4$ and 7, respectively, show the variation of the parameters along the blade span, The variation along the blade span is, generally, not significant except at the blade tips.

Fig. 3.9 shows the detailed aerodynamic characteristics [the induced velocity, angle of attack etc.] as a function of blade azimuth near the steady state solution.

From this figure, it is clear that increasing the number of rotational calculations, after NR = 7, did not make a significant difference to the result, and confirms that eight rotational calculations seems appropriate for convergence.

3.3 Field Velocity According to the Free Wake Method.

Before presenting the flow behaviour calculated by the Free Wake method, the wake convection velocity calculated from momentum theory considerations will be introduced. Momentum theory indicates that the wake convection velocity of a vertical axis wind turbine is related to the velocity at a corresponding blade position by :

$$U_w = 2\,U_b - U_f \qquad 3\text{-}2$$

Where the incoming velocity U_f may depend on whether the upstream or downstream blade pass is being considered. Application of equation 3-2, via double disk momentum theory, gives the wake convection velocity behind the upstream blade U_{wu}, in a given stream tube as :

$$U_{wu} = 2\,U_{bu} - U_{\sim} \qquad 3\text{-}3$$

The upstream disk velocity U_{bu} can be written in terms of the upstream blade induced velocity W_{xbu} and free stream velocity $U_{\sim}$ as :

$$W_{xbu} = U_{bu} - U_{\sim} \qquad 3\text{-}4$$

Then equation 3-2, becomes

$$U_{wu} = U_{\sim} + 2\,W_{xbu} \qquad 3\text{-}5$$

Following equation 3-2, and assuming that the incoming velocity to the downstream blade pass is equal to the wake convection velocity from the upstream pass, the downstream wake convection velocity U_{wd} can be written as :

$$U_{wd} = 2\,U_{bd} - U_{wu} \qquad 3\text{-}6$$

If the downstream disk velocity U_{bd} is also referenced to the free stream velocity, it follows :

$$W_{xbd} = U_{bd} - U_{\sim} \qquad 3\text{-}7$$

Where W_{xbd} is the induced velocity on the blade downstream pass. Combining equations 3-2, 3-5, 3-6 and 3-7, one can obtain :

$$U_{wd} = U_{\sim} + 2\,W_{xbd} - 2\,W_{xbu} \qquad 3\text{-}8$$

Hence, equations 3-5 and 3-8 provide the relationship between the induced velocities at the blades and the wake convection velocities for a given stream tube.

Alternatively, the velocity behaviour in the flow field can be examined using the free wake solution. A complete wake development from time step to time step is depicted in Fig. 3.4. for tip speed ratio $\lambda = 4$. This figure does not represent the development of the wake from the beginning but after the main body of the wake has been established since, here, the steady state configuration is of interest. The induced velocity at each shed vortex can be deduced from the change of wake shape from one step to the next, and then, using an averaging process, the average value for one complete rotational calculation can be determined. However, another approach is possible by considering the wake development at the (NR-1)xNTI th and NRxNTI th time steps.

Fig. 3.10a shows the wake shape development at these two time steps for tip speed ratio $\lambda = 4$, while Fig. 3.10b shows the breakdown of the wake shape into its component cycles. Similar diagrams for tip speed ratios $\lambda = 2$ and 7 are shown in Figs. 3.11 and 3.12, respectively. From these three figures, the change in wake shape from one rotation to the next can be observed. Curve cycle AB [Fig. 3.10b] becomes A'B', CD becomes C'D' and so on.

Here, to gain information from the wake shape development about the field velocity behaviour it is convenient to consider the vector wake convection velocity $\mathbf{U_w}$ as being composed of the free stream velocity and the induced velocity due the vortex system. This can be written as :

$$\mathbf{U_w} = U_{\sim}\mathbf{i} + W_{xw}\,\mathbf{i} + W_{yw}\,\mathbf{j} \qquad 3\text{-}9$$

Where W_{xw} and W_{yw} represent the induced velocities in the flow field in the X and Y - directions respectively. By considering how the wake shape changes, the average induced velocity in both directions in the flow field can be deduced. The resulting induced velocity components in the X direction, due to the change of wake shape from the (NR-1)th to the NRth rotational calculation, are compared to the induced velocities on the blade in Fig. 3.13a for tip speed ratio $\lambda = 4$. The same comparison for the Y direction is shown in Fig. 3.13b. The other two values of tip speed ratio, $\lambda = 2$ and 7, are presented in Figs. 3.14 and 3.15, respectively.

The conclusion which can be drawn from these three figures is that the X - component induced velocity W_{xw}, from the up and downstream blade passes, has a tendency to equalise at some distance downstream from the blade. The Y-induced component W_{yw} does not show any regularity and does not seem to be influenced by the value of tip speed ratio.

The flow field induced velocities calculated above, were then compared to the relationships derived from momentum theory ,as given in equations 3-5 and 3-8. It

was found that substantial agreement existed between the velocities calculated for the first cycle of the vortex model and those obtained from momentum theory. In particular , the upstream wake convection velocity was almost identical for the range of tip speed ratio considered. At tip speed ratios greater than four, however, equation 3-8 produced slightly lower convection speeds than those measured from the vortex method.

It had been recognised that the basic momentum analysis used to derive equation 3-8 assumes full expansion of the wake from the upstream pass prior to calculation of the downstream losses. This assumption, therefore, does not include any upstream influence of the downstream blade and its associated vortex system. It is apparent, from the Free Wake method, that the wake structure is very concentrated near the turbine at high tip speed ratios and, thus, does exert strong influence' on upstream conditions. The momentum theory above was, therefore, modified to include this effect. A satisfactory expression for the incoming velocity to the downstream blade was found to be :

$$U_{wu} = U_{bd} - W_{xbu} \qquad 3\text{-}10$$

In this way, the incoming velocity to the downstream pass is influenced by the velocity at the downstream blade [U_{bd}] and the velocity induced on the blade upstream pass [W_{xbu}]. The downstream wake convection velocity, as previously expressed by equation 3-8, then becomes :

$$U_{wd} = U_{\sim} + W_{xbd} + W_{xbu} \qquad 3\text{-}11$$

Substitution of the induced blade velocities, predicted by the Free Wake method, into equation 3-5 and 3-11 result in an accurate reproduction of the first vortex wake cycle.

The process whereby the wake convection velocities from the upstream and downstream blade passes equalise in the far wake was also examined. In the Free

Wake method, a uniform convection velocity, equivalent to the average of the upstream and downstream components of the first wake cycle, is established by the third wake cycle. This equalisation process appears virtually independent of tip speed ratio. The convection speed of the wake from the third cycle onward can, thus, be related to the velocities in the near wake by :

$$U_{wf} = [\, U_{wu} + U_{wd} \,]/2 \qquad 3\text{-}12$$

The second wake cycle can then be approximated by assuming a linear variation in velocity between the first and the third cycles. The velocity of the section corresponding to the upstream blade pass is given by :

$$U_{wu2} = [\, U_{wu} + U_{wf} \,]/2 \qquad 3\text{-}13a$$

and that of the downstream section by

$$U_{wd2} = [\, U_{wd} + U_{wf} \,]/2 \qquad 3\text{-}13b$$

As mentioned before, the Y-component of induced velocity showed no such regularity and, hence, an appropriate relationship could not be formulated in the same way as for the X - component. However, it was found that the rate of expansion of the first wake cycle was equivalent to the average cross-stream velocity induced at the turbine blades. It was, therefore, possible to include the effects of wake expansion in the first cycle of the Prescribed Wake model by consideration of the induced velocity field at the turbine blades . The other cycles in the prescribed wake are fixed and do not expand or contract.

As an example , wake shapes based on equations 3-5, 3-11, 3-12 and 3-13, but without Y-convection, were generated using the blade induced velocities from the Free Wake method. Figs. 3.16 - 3.19 show comparisons of these wakes with those of the Free Wake method in terms of induced velocities in the flow field and the

shape of wake cycles at four different values of tip speed ratio; λ = 2, 4, 5 and 7 respectively. From these figures, it is apparent that the above equations permit accurate reconstruction of the wake shape once the induced velocities on the turbine blades are known. Based from this study , a Prescribed Wake method was developed. Further study, was, however, required to determine a suitable initial wake shape which would provide the required blade induced velocities . The next section presents the mathematical representation of aerodynamic performance used in the Prescribed Wake method, while the next chapter presents the stages in the development of the Prescribed Wake method.

3.4 Basic Concept of the Prescribed Wake Method.

The basic concept behind this method is simply that the wake shape can be considered as an input rather than as part of the solution. If the wake shape at any blade azimuth position is known, the aerodynamic performance analysis can proceed as in the Free Wake method described by Strickland et. al. in Ref. 120 . Strictly speaking, the aerodynamic characteristics and rotor blade performance in the Prescribed Wake method are formulated using blade element theory. On the other hand, the induced velocity, which represents the unknown element in the blade element theory , is obtained using a vortex method.

In this case, application of blade element theory means that the aerodynamic force on the blade is calculated by imagining that the blade is composed of aerodynamically independent, chord-wise oriented, narrow strips or elements. The vortex method follows lifting line or lifting surface theory. Here the replacement of the rotor blade by a single lifting line or lifting surface is used to deduce the behaviour of blade loading. There are two possible blade loading behaviour patterns. The blade loading may only vary along the blade span or in both the spanwise and azimuthal

directions. If the blade loading is a function of both span and azimuthal blade position it seems appropriate to use a single lifting line rather than a lifting surface approach, since the complexity of the calculation and the time required for a solution will be reduced.

In the Prescribed Wake method, the blade is replaced by a single lifting line, the aerodynamic performance formulations are derived on the basis of blade element theory and a preliminary wake shape is initiated at first in order to allow the induced velocity on the blade to be made available. In the second stage, a new wake shape is created using information from the first stage and following the relationships had been presented in section 3.3. If the first stage wake can provide induced velocities close to those predicted by the Free Wake solution, it could be expected that the creation of the wake shape at the next stage would correspond well with the Free Wake solution. If such conditions could be obtained , recalculation of aerodynamic performance based on the updated wake shape would produce a result which was close to the Free Wake method.

3.5 Mathematical Formulation of the Prescribed Wake Method

The replacement of the rotor blade by a single lifting line was chosen in this approach. However, to accommodate the variation in blade loading along the blade span, the blade was divided into a number of blade elements. Since the blade undergoes rotational motion, this motion promotes a variation in blade loading with azimuth position. Consequently, each time the blade moves to a new blade azimuth position, the movement must be accompanied by shed vortices in order to satisfy Helmholtz-Kelvin's theorem [132]. In the Prescribed Wake method, the simple representation of the vortex system associated with a blade element in the Free Wake method of Strickland et. al. [120] is still applicable. Hence, the simple vortex

system , shown in Fig. 3.20, has been used to develop the mathematical formulation for the Prescribed Wake approach.

3.5.1 System Coordinates of the Vertical Axis Wind machine.

Here two coordinate systems, namely Cartesian and polar coordinates , will be used in order to describe the physical coordinates of the configuration. The Cartesian coordinates XYZ include their unit vectors **i**, **j** and **k** . The positive X-axis is taken in the direction of the free stream velocity with the Y-axis as its counterpart. The Z-axis is attached to the rotational- axis of the wind machine and the origin of the system coordinates is as shown in Fig. 3.21a. The definition of polar coordinates $[r,\theta]$, to describe the blade azimuth position, is shown in Fig 3.21b, with the zero degree blade azimuth position coinciding with the positive X-axis . Blade rotation is in the anticlockwise direction.

3.5.2 The Aerodynamic Characteristics and Power Coefficient Derivation.

The concept of blade element theory has been known for fifty years and was first introduced by Drzewiwcki. The aerodynamic forces, say, on a differential blade element of chord c_r with width ΔL located at blade azimuth position θ, are calculated by imagining that the blade is composed of aerodynamically independent, chord wise-oriented, narrow strips or elements.

Now, consider a differential blade element at a radius r from the z-axis as shown in Fig. 3.22a. In terms of velocity relative to the blade, the differential blade element

is shown acting under the influence of the rotational blade motion V_r , the oncoming free stream velocity $U_\sim$ and the induced velocity W as presented in Fig. 3.22b. Here, for the purpose of aerodynamic analysis, the first two velocities [$U_\sim$ and V_r] are, usually, known and the induced velocity is unknown and is estimated, in this case by a vortex technique.

If the induced velocity is known, the resultant velocity U_R , as well as the angle of attack α, on the differential blade element can be defined. By using a look up table of airfoil data , the local aerodynamic characteristics in terms of the lift and drag coefficients [C_l and C_d] can then be obtained. However, representation of these two coefficients in terms of normal and tangential coefficients [C_n and C_t] is more useful for the purpose of the calculation of power and structural bending moment. For a given angle of attack α, the normal and tangential coefficients can be defined from C_l and C_d as follows [Strickland et. al. 120] :

$$C_n = C_l \sin\alpha - C_d \cos\alpha \qquad 3\text{-}14a$$

$$C_t = - C_l \sin\alpha + C_d \cos\alpha \qquad 3\text{-}14b$$

Hence, for a given resultant velocity U_R, local chord c_r and blade element width ΔL, one can define the differential normal and tangential forces ΔF_n and ΔF_t at the element, as :

$$\Delta F_n = 1/2\, \rho U_R^2\, C_n(\alpha)\, c_r\, \Delta L \qquad 3\text{-}7a$$

$$\Delta F_t = 1/2\, \rho U_R^2\, C_t(\alpha)\, c_r\, \Delta L \qquad 3\text{-}7b$$

Where ρ is the fluid density. If the local blade radius r with respect to the rotational axis [z-axis] is known, a differential torque ΔT_e produced by the blade element can be computed by :

$$\Delta T_e = r \Delta F_t$$

$$= 1/2\, \rho U_R^2\, C_t(\alpha)\, c_r \Delta L\, r \qquad 3\text{-}15$$

In addition, if the tangential blade velocity at the rotor equator, which represents the maximum velocity, is denoted by U_T, the instantaneous rotor power ΔP_e produced by the differential blade element can be formulated as :

$$\Delta P_e = \Delta T_e\, U_T$$

$$= 1/2\, \rho U_R^2\, C_t(\alpha)\, c_r \Delta L\, r\, U_T \qquad 3\text{-}16$$

or, in nondimensional form, when divided by a factor $1/2\, \rho\, R\, A_f\, U_\infty^3$, as :

$$\Delta Cp_e = \frac{\Delta T_e\, U_T}{0.5\, \rho\, R\, A_f\, U_\infty^3}$$

$$= \frac{0.5\, \rho\, U_R^2\, C_t\, c_r\, r\, \Delta L\, U_T}{0.5\, \rho\, R\, A_f\, U_\infty^3}$$

$$= C_t \frac{c_r}{R} \frac{r \Delta L}{A_f} \lambda \frac{U_R^2}{U_\infty^2}$$

3-17

Where A_f is the total projected frontal area of the rotor and λ is the tip speed ratio. If NB is the nimber of blades, NBE is the number of blade elemental divisions and NTI represents the number of blade azimuth positions, the averaged power coefficient $Cp_{ave.}$ can be obtained by a summation of the differential power coefficients ΔCp_e divided by the number of blade azimuth positions (NTI) under investigation, i.e. :

$$Cp_{ave.} = \frac{1}{NTI} \sum_{1}^{NTI} \sum_{1}^{NB} \sum_{1}^{NBE} \Delta Cp_e \qquad 3\text{-}18$$

3.5.3 The Induced Velocity.

Although, in this case, a simplified wake shape has been introduced, dealing with a continuous vortex sheet presents a profound mathematical difficulty. Hence, replacing the continuous sheet by an array of vortex filaments has been commonly adopted for solving flows around three dimensional lifting bodies.

Consider a given finite segment vortex filament with strength Γ, as shown in Fig. 3.23, with end points A [Xa,Ya,Za] and B [Xb,Yb,Zb]. The direction of the vortex filament vector points out from A to B. The coordinates of some control point C in the flow field are denoted as [Xc,Yc,Zc]. Hence the three component induced velocities W_x ,W_y and W_z in the direction of the unit vectors **i**, **j** and **k** at any control point C, due to the vortex filament AB, can be written as [153] :

$$W_x = [\Gamma/4\pi] [(Yc-Ya)(Zc-Zb)-(Yc-Yb)(Zc-Za)] K_1 /K_2 \qquad 3\text{-}19a$$

$$W_y = - [\Gamma/4\pi] [(Xc-Xa)(Zc-Zb)-(Xc-Xb)(Zc-Za)] K_1 /K_2 \qquad 3\text{-}19b$$

$$W_z = [\Gamma/4\pi] [(Xc-Xa)(Yc-Ya)-(Xc-Xb)(Yc-Ya)] K_1 /K_2 \qquad 3\text{-}19c$$

where :

$$K_1 = \{[(Yc-Ya)(Zc-Zb)-(Yc-Yb)(Zc-Za)] + \{[(Xc-Xa)(Zc-Zb)-(Xc-Xb)(Zc-Za)]\} + \{[(Xc-Xa)(Yc-Yb)-(Xc-Xb)(Yc-Yb)]\} \qquad 3\text{-}20a$$

$$K_2 = [(Xb-Xa)(Xb-Xa)+(Yb-Ya)(Yc-Ya)+(Zb-Za)(Zc-Za)]/E1$$

$$- [(Xa-Xa)(Xc-Xb)+(Yb-Ya)(Yc-Yb)+(Zb-Za)(Zc-Zb)]/E2 \qquad 3\text{-}20b$$

$$E_1 = [\,(Xc - Xa)^2 + (Yc - Ya)^2 + (Zc - Za)^2\,]^{1/2} \qquad 3\text{-}21a$$

$$E_2 = [\,(Xc - Xb)^2 + (Yc - Yb)^2 + (Zc - Zb)^2\,]^{1/2} \qquad 3\text{-}21b$$

3.5.4 Strength of Shed and Trailing Vortex Filaments.

The small variation of blade loading along the span, as well as around the blade azimuth, means that the wake contains trailing and shed vortices. Hence, discretization of the wake should accommodate these two vortex types. A simplified model of the discretized wake from a differential blade element is shown in Fig. 3.20. The strength of the vortex filament representing the blade is denoted by Γ_b , and the trailing and shed vortices are denoted by Γ_t and Γ_s , respectively. The strength of the trailing vortex Γ_t is defined as the difference between the strengths of the bound vorticity on two adjacent differential blade elements. If the strengths of two successive differential blade elements i and i+1, are denoted by Γ_{bi} and Γ_{bi+1} respectively, the strength of the trailing vortex Γ_{ti} springing up between them, can be defined as :

$$\Gamma_{ti} = \Gamma_{bi+1} - \Gamma_{bi} \qquad 3\text{-}22a$$

If the blade is divided into NBE elements, there will be (NBE) finite segments of bound vorticity, Γ_{bi} , i = 1,2, ..., NBE, and (NBE+1) trailing vortex filaments. The

strength of each trailing vortex Γ_{ti} for $1 < i < (NBE+1)$ is defined by equation 3-10a, while for $i = 1$ and $i = NBE+1$, the strength of the trailing vortex will be :

$$\Gamma_{ti=1} = \Gamma_{b1} \qquad 3\text{-}22b$$

$$\Gamma_{ti=NBE+1} = \Gamma_{bNBE+1} \qquad 3\text{-}22c$$

If the bound vorticity on a blade element at a given azimuth position is $\Gamma_b(\theta_n)$. and the corresponding shed vortex is denoted as Γ_{sn}, where n = N, N-1, N-2, ..., 1, an expression for the shed vortices can be developed as follows :

$$\Gamma_{sn} = -\Gamma_b(\theta_n) + \Gamma_b(\theta_n - \Delta\theta) \; ; \; \Gamma_{sn-1} = -\Gamma_b(\theta_n - \Delta\theta) + \Gamma_b(\theta_n - 2\Delta\theta)$$

$$\Gamma_{sn-j} = -\Gamma_b(\theta_n - (j-1)\Delta\theta) + \Gamma_b(\theta_n - (j-2)\Delta\theta) \qquad 3\text{-}23$$

3.5.5 The Angle of Attack Formulation.

In a previous section, the manner in which the aerodynamic characteristics of the blades are determined, if the resultant velocity and angle of attack relative to the differential blade element are available, were discussed. The way that the angle of attack can be defined is now described.

To obtain the angle of attack , let us first consider Fig. 3.22[a,b] which represents an arbitrary blade element Ds viewed from above [Fig. 3.22a] and from the side [Fig. 3.22b]. In the diagrams, the control points are located at both edges of the element, and are denoted as C_j and C_{j+1}. This blade element is located at blade azimuth position θ , and the coordinates of the two control points are denoted as [X_j , Y_j, Z_j] and [X_{j+1}, Y_{j+1}, Z_{j+1}], respectively.

In this approach, the induced velocity due to the wake is calculated at these two points rather than at a control point located at the mid element. The two values are, however, used to obtain aerodynamic characteristics at the mid element. This procedure follows that adopted in the VDART3-code. Namely, the induced velocity at the mid element represents the average value of the induced velocities from these two control points. Such a procedure was adopted in VDART3 in order to reduce the number of control points considered in the calculation of induced velocity.

In order to calculate the effective angle of attack α, at the mid element, we introduce three new unit vectors **c**, **s** and **n** . The unit vector **c** represents a unit vector in the chord wise direction [Fig. 3.22]. The unit vector **s** is defined as a unit vector in the direction from point C_j to C_{j+1}, while the **n** vector is the normal vector of the plane [**c** x **s**] with positive sign in the outward direction. For the problem in hand these three unit vectors can be formulated as follows :

$$\mathbf{c} = \sin\theta\ \mathbf{i} - \cos\theta\ \mathbf{j} + 0\mathbf{k} \qquad 3\text{-}24$$

$$\mathbf{s} = [\,\Delta x_j \mathbf{i} + \Delta y_j \mathbf{j} + \Delta z_j \mathbf{k}\,]/\Delta L \qquad 3\text{-}25a$$

$$\Delta L = [\,\Delta x_j^2 + \Delta y_j^2 + \Delta z_j^2\,]^{1/2} \qquad 3\text{-}25b$$

where

$$\Delta x_j = X_{j+1} - X_j$$

$$\Delta y_j = Y_{j+1} - Y_j \qquad 2\text{-}26$$

$$\Delta z_j = Z_{j+1} - Z_j$$

$$\mathbf{n} = -\mathbf{s} \times \mathbf{c}$$

$$\mathbf{n} = \frac{1}{\Delta L}\begin{bmatrix} \mathbf{i} & \mathbf{j} & \mathbf{k} \\ \Delta x_j & \Delta y_j & \Delta z_j \\ \sin\theta & -\cos\theta & 0 \end{bmatrix}$$

$$= [\, -\Delta z_j \cos\theta\, \mathbf{i} - \Delta z_j \sin\theta\, \mathbf{j} + (\Delta x_j \cos\theta + \Delta y_j \sin\theta)\, \mathbf{k} \,] / \Delta L$$

3-27

The induced velocity described by equation 3-4 is already written in Cartesian coordinates. The vector free stream velocity $\mathbf{U}_\sim$ and the vector tangential velocity $\mathbf{U}_t$ can , also, be written in Cartesian coordinates, respectively as follows :

$$\mathbf{U}_\sim = |U_\sim|\,\mathbf{i} \qquad 3\text{-}28$$

$$\mathbf{U}_t = \left|U_\sim \lambda \frac{r}{R}\right| [\, \sin\theta\, \mathbf{i} - \cos\theta\, \mathbf{j} \,] \qquad 3\text{-}29$$

λ : tip speed ratio

r : local blade radius

R : maximum blade radius

Hence the vector resultant velocity $\mathbf{U}_R$ relative to the blade can be obtained as :

$$\mathbf{U}_R = [\, U_\sim + (U_\sim \lambda \frac{r}{R}) \sin\theta + W_x \,]\,\mathbf{i} +$$

$$+ [\, -U_\sim \lambda \frac{r}{R} \cos\theta + W_y \,]\,\mathbf{j} + W_z\,\mathbf{k} \qquad 3\text{-}30$$

And the effective angle of attack can be obtained by noting that :

$$\tan \alpha = - \frac{\mathbf{U_R} \bullet \mathbf{n}}{\mathbf{U_R} \bullet \mathbf{c}} \qquad 3\text{-}31$$

A complete form of the angle of attack equation can be written as follows:

$$\begin{aligned} \mathbf{U_R} \bullet \mathbf{n} = \{ [U_\infty + (U_\infty \lambda \frac{r}{R}) \sin\theta + W_x][- \Delta z \cos\theta] \\ + [- (U_\infty \lambda \frac{r}{R}) \cos\theta + W_y][- \Delta z \sin\theta] \\ + [\Delta x \cos\theta + \Delta y \sin\theta] W_z \} / \Delta L \end{aligned} \qquad 3\text{-}32a$$

and

$$\begin{aligned} \mathbf{U_R} \bullet \mathbf{c} = [U_\infty + (U_\infty \lambda \frac{r}{R}) \sin\theta + W_x] \sin\theta \\ + [- (U_\infty \lambda \frac{r}{R}) \cos\theta + W_y][- \cos\theta] \end{aligned} \qquad 3\text{-}32b$$

then

$$\begin{aligned} \tan\alpha = \{ [- (U_\infty + W_x) \Delta z \cos\theta + (- W_y \Delta z \sin\theta) + \\ + (- \Delta x \cos\theta + \Delta y \sin\theta) W_z] / \Delta L \} / \\ \{ (U_\infty + W_x) \sin\theta - W_y \cos\theta + U_\infty \lambda \frac{r}{R} \} \end{aligned} \qquad 3\text{-}32c$$

With knowledge of the angle of attack α, then, using a look up table of airfoil data, the aerodynamic characteristics C_l and C_d at the blade element can be determined. The non dimensional blade bound vortex Γ_b can be obtained as :

$$\frac{\Gamma_b}{R\,U_\infty} = \frac{1}{2} C_l \left(\frac{c_r}{R} \right) \left| \frac{U_R}{U_\infty} \right| \qquad 3\text{-}33$$

c_r : local airfoil chord

3.6 The Numerical Strategy for the Prescribed Wake Method.

Implementation of the Prescribed Wake method can be divided into two steps. The first step involves creating the wake shape and the second step is the calculation of rotor blade performance.

The study of the field induced velocity from the Free Wake method, as presented in section 3.3, was intended to gain insight into the wake shape development. Since the induced velocity on the blade is easier to define than the flow field itself, this was used as the starting point for the wake shape development.

If an appropriate wake shape could be implemented into the prescribed wake method, then a result close to the free wake method could be found. Unfortunately, it is difficult to obtain an induced velocity on the blade close to that given by the free wake method. A number of different schemes designed to provide this information were studied. These are discussed in the following chapter. The numerical scheme adopted for the prescribed wake model is presented in a simplified form in Fig. 3.23, while a detailed form is presented in Appendix B.

3.7 A Programming Strategy for the Implementation of a Prescribed Wake Approach

The physical configuration of the wake shape trailing behind the turbine blade of a vertical axis wind machine is complex. However, we can deduce that the wake shape is cycloid and consists of an array of wake circles. In addition, if the quasi steady flow condition has been achieved, all rotor blades passing the same blade azimuth position will have the same wake shape trailing from them. The Prescribed Wake method only considers the induced velocity on the blade and not in the flow field, and hence the part of the wake which is very far from the blade can be ignored. This allows the wake shape to be approximated by a finite configuration, i.e. the wake can be considered as consisting of NR wake circles. In addition, the vortex system is discretized by replacing the blade by a single lifting line, and dividing the blade span into a number of elements. The continuous rotation of the blade is also considered as a discrete time stepping motion. Thus, the azimuth range of the blades , $\theta = 0^o$ to $\theta = 360^o$, is divided into NTI blade azimuth positions at which aerodynamic calculations are under taken. Hence there are NTI wake shapes to be defined for a wind machine with only one blade. However, if there are NB blades, NBxNTI wake configurations are required, since each blade at any blade azimuth position has its own wake shape. This represents a computational overhead which can be alleviated if all the blades visit the same NTI blade azimuth positions during a calculation. In this case, only NTI wake configurations are required.

The numbering system used for the blade azimuth positions, which is shown in Fig.3.24a, starts from 1 at blade azimuth position $\theta_1 = 90^o$ and 2 at $\theta_2 = 90^o + 360^o$ /NTI, etc .. until the NTIth position $\theta_{NTI} = 90^o - 360^o$ /NTI. As an example of how the wake shapes were created in this study, we take NTI = 16, with the number of wake cycles NR = 3, and assume that the shed vortices are convected by a uniform free stream. For this case, the wake at blade position number 1[$\theta_1 = 90^o$] will contain NRxNTI shed vortices. The number of shed

vortices in the wake will increase with each azimuth step. Hence, at the NTI th blade position it will contain (NR+1)xNTI-1 shed vortices.

The wake shapes generated for blade positions 1, 9 and 16 , for this simple case, are shown in Fig. 3.24b. The points in the figure indicate the position of shed vortices within the wake . These vortices are numbered in a consecutive manner beginning from 1 at the wake end and increasing towards the turbine. The number assigned to each vortex gives an indication of the blade position from which it was shed. For example shed vortex 1 resulted from the change in blade circulation between blade position 1 and 2. Similarly, all shed vortices whose number are given by jxNTI+1; j=1,2, ... were shed from the same blade position and have the same strength.

The manner in which shed and trailing vortices are defined in the Prescribed Wake method is slightly different from the VDART3-Code. VDART3 used a fixed strength-backward approach. Fixed strength means that the strength of each vortex in the flow field remains equal to the strength at the time when it was released to the flow field. Hence, some of the vortices have strengths calculated at the time when the vortex system only consisted of a few shed vortices in the early stages of wake development. The backward approach assumes that the movement of the blade from one position to the next does not incur a change in blade attitude. Thus, the strength of a trailing vortex strictly behind the blade is equal to the gradient of bound vorticity attached to the blade at the previous time step. In the forward approach , the strength of the trailing vortex released from the blade depends on its bound vorticity at that time. By increasing the number of blade azimuth positions, the two different approaches are likely to give a similar result, since the difference in flow conditions between two successive blade positions will be small. Both techniques were examined for the Prescribed Wake method and the results are presented in the next chapter.

CHAPTER -FOUR : STAGES IN THE DEVELOPMENT OF THE PRESCRIBED WAKE METHOD

4.1 The First Version of the Prescribed Wake Method : Wake Shape Based on Uniform Free Stream Velocity [PRESWK - Org. Version].

This approach represents the simplest approach amongst the various schemes discussed in this chapter. Here, it is assumed that shed vortices are convected by the free stream velocity only.

As described in the previous chapter, if the wake shape can be defined, then the calculation of aerodynamic performance can proceed. Fig. 4.1 shows the numerical algorithm for this approach in the form of a flow diagram. The first step is to define the wake shape for all chosen blade azimuth positions. The wake sheet is then split into a wake vortex lattice containing trailing and shed vortices of unknown strength. The relationship between the strength of vortex filaments in the wake and the bound vorticity on the blade follows the Helmholtz-Kelvin Theorem as presented in Chapter 3. However, the bound vortex strengths on the blades are also unknown, hence an iteration procedure is required. The iteration procedure begins by setting all vortex filament strengths in the wake vortex lattice equal to zero. These values are updated, as the calculation proceeds from one blade position to the next. A number of full iterations is needed to obtain a convergent solution, numerical experiment shows that four iterations are adequate.

Since, the development of the Prescribed Wake method was referenced to the Free Wake method, all calculation results presented in this chapter were obtained using the same numerical parameters applied in MVDART3, as presented in Chapter 3. The parameters were : 7 wake circles, 8 spanwise elements and 16 blade azimuth positions. Six values of tip speed ratio λ, in the range $2 \leq \lambda \leq 7$, were used to

assess the accuracy of the solution with respect to the Free Wake solution.

There are nine versions of the Prescribed Wake method discussed in this chapter. Results for each version will be compared to the Free Wake method in terms of power coefficient and instantaneous incidence and loadings. Based on the results , it was clear that further improvement in prescribing the wake was required. Such an improvement will be presented in section 4.10. The following chapter presents an investigation of numerical parameter effects such as the span wise spacing, blade azimuth divisions, the cut off for Biot -Savart's law and the influence of aerofoil data.

In the first approach , the wake shape is defined by using the free stream velocity for the convection of shed vortices. The method is denoted as PRESWK-Org. The comparison of the wake shape trailed from the mid blade span , between the Free Wake method and PRESWK-Org, for various values of tip speed ratio [$2 \leq \lambda \leq 7$] , is shown in Fig. 4.2. It is clear that using the free stream velocity for the convection of shed vortices creates a wake shape which travels down stream faster than its counterpart, especially for increasing tip speed ratio. The wake shape in this model, therefore, has less influence on the induced velocity on the blade and, consequently, the effective angles of attack on the blade are greater than those obtained by the Free Wake method. As a result, the overall performance, in terms of power coefficient , is over predicted as shown in Table 4.1 .

The detailed aerodynamic characteristics, presented in terms of induced velocities in the X and Y-directions, the effective angle of attack α , and the normal and tangential force coefficients [C_{Fn} and C_{Ft}] near the mid blade span, are plotted as function of blade azimuth position for tip speed ratios λ = 2 and 7 , in Figs. 4.3a and 4.3b. These results are also compared to the results of the Single Disk Multiple Stream-Tube [SDMST] and Double Disk Multiple Stream-Tube [DDMST] methods for completeness. The Single Disk and Double Disk Multiple Stream-Tube methods are

basically two dimensional models, and so give no variations along the blade span. As can be observed, these methods do not give accurate representations of the instantaneous loading patterns on the blades either.

4.2 The Second Version of the Prescribed Wake Method : Wake Shape Based on Uniform Free Stream Velocity and Single Disk Multiple Stream -Tube induced Velocity [PRESWK - SDMST Version].

Using the free stream velocity for the convection of shed vortices generated a wake shape which travelled down stream faster than the wake shape from the Free Wake method and consequently produced an over prediction of the power coefficient. Here, an attempt to improve the Prescribed Wake solution was made by prescribing the wake shape based on the resultant of the free stream velocity and an induced velocity. The simple way to obtain an induced velocity is on the blade where information can be derived from other methods which involve far less computation time than the Free Wake method; for instance by using Single Disk or Double Disk Multiple Stream-Tube methods. Both methods will be used in this study, with the results obtained using the Single Disk's induced velocity presented first and the case of the Double Disk discussed in the next section.

Both momentum models provide the induced velocity in X - direction only. The presence of the induced velocity, which is in the opposite direction to the free stream, will result in the wake shape being swept down stream at a slower speed than in the previous case.

Strictly speaking this scheme uses the same numerical procedure as described in the previous section, the only difference is in terms of the velocity used for the convection of shed vortices. Fig. 4.4 shows the flow diagram for this scheme and the

box containing information written in bold characters shows the difference between this scheme and the last. In order to distinguish with the previous one , this scheme is denoted by PRESWK - SDMST. All calculations were again done using the same values for the required numerical parameters.

As in the previous section, various values of tip speed ratio in the range $2 \leq \lambda \leq 7$ were used to asses the accuracy of the solution with respect to the Free Wake method. However, only three values of tip speed ratio are presented to illustrate the results. The comparison of the new wake shape is compared to the Free Wake method in Fig. 4.5. For low to moderate tip speed ratios $2 \leq \lambda \leq 4$, this approach could provide a good approximation to the Free Wake solution, but agreement deteriorated with increasing tip speed ratio.

Table 4.2 shows the comparison of power coefficient between the Free Wake method, PRESWK - SDMST and also the Single Disk Multiple Stream-Tube method itself. This table shows that, in general, the Single Disk Multiple Stream-Tube method could provide a good result in terms of power coefficient; for instance at tip speed ratio $\lambda = 4$, this method produced Cp = 0.4841, while PRESWK - SDMST gave Cp = 0.5028, which is much higher than the Free Wake method where Cp is equal to 0.4769. However, if we look at the detailed aerodynamic performance near the mid blade span, as a function of blade azimuth position, for three different values of tip speed ratio $\lambda = 2,4$ and 7 as depicted in Figs. 4.6 a,b and c, respectively, it is clear that the Single Disk Multiple Stream-Tube method gives an error over the whole blade azimuth position range when compared to the Free Wake method.

Although PRESWK - SDMST provides an over approximation , in terms of detailed performance this method gives better agreement with the Free Wake solution than the Single Disk Multiple Stream -Tube momentum model.

4.3 The Third Version of the Prescribed Wake Method : Wake Shape Based on Uniform Free Stream Velocity and Double Disk Multiple Stream -Tube's induced Velocity [PRESWK - DDMST Version].

The advantage of the Double Disk method is that it can provide a solution which distinguishes between the up and down stream blade passes. Thus, two different induced velocities are calculated in each stream tube and can be used to generate a prescribed wake . This technique follows the same procedure as that based on the Single Disk Multiple Stream -Tube method in the previous section. Namely, the wake is generated using a convection velocity for the shed vortices resulting from the summation of the induced velocity on the blade and the free stream velocity. The difference between this and the Prescribed Wake generated using the Single Disk Multiple Stream-Tube approach is that the convection velocity depends on whether the shed vortices originated from the up stream or down stream blade pass. With the wake shape defined, the same numerical procedure as in the two previous schemes [PRESWK - Org. and PRESWK - SDMST] was applied.

Calculations were conducted for this version over the same range of tip speed ratios and using the same numerical parameters as mentioned previously.

A comparison of wake shapes with the Free Wake method, at various tip speed ratios, is shown in Fig. 4.7. This figure shows the wake shape trailed from the mid blade span, and from one blade for clarity .

The conclusion that can be drawn from the comparison between the previous method and PRESWK - DDMST is that, for increasing tip speed ratio, the wake produced by PRESWK - DDMST travels downstream at a slower speed than PRESWK - SDMST. The impact of wake shape is quite significant both in terms of overall power coefficient as well as detailed aerodynamic characteristics. The wake shape generated using DDMST's induced velocity still, however, travels faster than

that from the Free Wake method. As a result , the power coefficient from PRESWK - DDMST is greater than the Free Wake method as shown in Table 4.3. This table also presents the prediction of power coefficient according to DDMST itself. In the range $2 \leq \lambda \leq 3$, both methods [DDMST and PRESWK -DDMST] showed good agreement with the Free Wake method, but produced an over prediction at higher tip speed ratios.

Experience with the first three versions showed that, at low tip speed ratios , i.e. around $\lambda = 2$, the three methods provided good agreement with the Free Wake results, in terms of both power coefficient and detailed aerodynamics. Clearly, at this tip speed ratio, the wake moves quickly down stream and, therefore, has a reduced influence and creates a low induced velocity with respect to the total resultant velocity relative to the blade.

The result presented in Fig. 4.8a , for tip speed ratio $\lambda = 2$, shows a comparison between the Free Wake method, Double Disk Multiple Stream-Tube method and PRESWK - DDMST. Although DDMST apparently produced large deviations in terms of induced velocity in the X- direction, the average order of magnitude of these deviations is less than 0.1 of the free stream velocity . Hence, when transformed in terms of angle of attack, and all other pertinent aerodynamic characteristics, the deviations are relatively insignificant and close agreement with the other schemes is obtained.

The result presented in Fig. 4.8b, shows a comparison of detailed aerodynamic characteristics near the mid blade span, as a function of blade azimuth position, between the Free Wake method, PRESWK - Org. and PRESWK - DDMST for tip speed ratio $\lambda = 4$. The last two methods, PRESWK - Org. and PRESWK DDMST produced power coefficients equal to 0.5723 and 0.5338, respectively, which are higher than the result from the Free Wake method at Cp = 0.474. This was due to the prescription of the vortex system associated with the down stream blade since

both approaches provided good agreement with the Free Wake method in the upstream domain. This can be understood, since the down stream blade is closer to the domain of flow where the density of vortex filaments is high. Although in terms of numbers of shed vortices and trailing vortex filaments , the three methods are equal, the difference in the location of these vortices changes the aerodynamic characteristics produced by the calculation.

An interesting result is depicted in Fig. 4.8c, which shows the comparison of detailed aerodynamic characteristics between the Free Wake method, PRESWK - SDMST and PRESWK - DDMST for tip speed ratio λ = 7. The power coefficients produced are equal to 0.222, 0.245, and 0.328 , respectively. It is clear that the power coefficient from PRESWK - DDMST is much higher than that from PRESWK - SDMST. When, however, the detailed aerodynamic characteristics are examined , especially in terms of tangential force coefficient C_{Ft} , it can be seen that PRESWK - DDMST provides a better approximation to the shape of the Free Wake curve than PRESWK - SDMST. The close agreement with the Free Wake method in terms of power coefficient for PRESWK - SDMST is due to a lower average error of C_{Ft}'s around the whole blade azimuth.

4.4 The Fourth Version of the Prescribed Wake Method : Wake Shape Based on Uniform Free Stream Velocity and SDMST's Induced Velocity Modified According to Equations 3.5 & 3.11-3.13 [PRESWK - SDMST - D Version].

In section 3.4, relationships between the velocities in the first three wake cycles and the velocity induced on the blade in the Free Wake method were developed. It was considered that, if the induced velocity on the blade could be approximated in some way, it would be possible to use these relationships to prescribe a wake shape. The fourth version of the Prescribed Wake model used the blade induced velocity,

calculated from SDMST, to construct such a wake . Unfortunately, the initial estimate of blade induced velocity as given by SDMST was so much in error, particularly at high tip speed ratios, that unrealistic wake shapes were produced. A higher level approximation to the blade induced velocity was, therefore, required.

4.5 The Fifth Version of the Prescribed Wake Method : Wake Shape Based from Uniform Free Stream Velocity and Double Disk Multiple Stream-Tube's Induced Velocity Modified According to Equations 3.5 & 3.11-3.11 [PRESWK - DDMST - D Version].

Detailed aerodynamic characteristics of the X-component induced velocity on the blade, for the Double Disk Multiple Stream -Tube method [DDMST], were presented in section 4.1., at tip speed ratios 2 and 7. For those two values of tip speed ratio, the DDMST's result, in terms of X - component induced velocity showed substantial agreement with the Free Wake method. It could, therefore, be expected that implementation of the relationships developed in section 3-3, could produce a wake shape close to that of the Free Wake method, if the blade induced velocity from DDMST was used . The resulting version of the Prescribed Wake method, which uses this approach, is called PRESWK - DDMST - D. Figure 4.9 shows its flow diagram.

The wake shape produced by transforming DDMST's induced velocity is compared to the wake shape provided by the Free Wake method, for a wide range of tip speed ratios $2 \leq \lambda \leq 7$, in Fig. 4.10. For tip speed ratio $\lambda = 2$, this version gave the first three wake cycles in close agreement with the Free Wake method. Similar results were also found at tip speed ratios 3 and 4. However, if the tip speed ratio was increased further, the locations of the first three wake cycles moved further upstream than the Free Wake results.

From momentum considerations, it can be deduced that a wake which is convected faster than that of the Free Wake method will correspond to a higher power coefficient, since there is a lower momentum loss. If the opposite occurs, either an under prediction will be obtained or unexpected blade vortex interactions will take place due to the wake density and may destabilise the solution.

Table 4.4 shows the comparison of power coefficients between the Free Wake method, PRESWK - DDMST and PRESWK - DDMST - D. Here the result of PRESWK - DDMST is included in this table to examine the progress made by introducing a transformed induced velocity to this version. For the first three tip speed ratios λ = 2, 3 and 4 , this version produced power coefficients in good agreement with the Free Wake method. The difference was no more than 3% with respect to the Free Wake solution.

An interesting result appeared at tip speed ratio λ = 4. The PRESWK - DDMST code produced a power coefficient equal to 0.5338, whereas the Free Wake solution was 0.4789. By using the transformed induced velocity in PRESWK - DDMST - D, a power coefficient equal to 0.4781 was obtained. In this case, direct use of DDMST's induced velocity created a wake shape which convected faster than the Free Wake method , while application of the transformation produced a wake shape in close agreement with Free Wake method .

In addition, this version also made a significant change to the value of power coefficient at tip speed ratio λ = 6. For this case, PRESWK - DDMST produced a Cp equal to 0.4394, which is around 20% higher than that produced by the Free Wake method (0.3572). Using the present approach gave a lower Cp (0.3168). It can, thus, be concluded that a change of wake shape, especially a change in convection speed , can alter the overall result significantly. Figure 4.11a shows the comparison of the detailed aerodynamics for these three methods at λ = 6 .
Another interesting result appeared at tip speed ratio λ = 7. In this case,

PRESWK-DDMST-D gave a significant over prediction [see Table 4.4]. It is clear that this was due to unexpected blade vortex interactions which the Free Wake method did not exhibit. The comparison of detailed aerodynamic characteristics is shown in Fig. 4.11b. From this figure, it can be seen that the implementation of the induced velocity transformation in this version , unfortunately , produced blade vortex interactions at four blade azimuth positions. Namely at $\theta = 0^{o}$, 22.5^{o}, 45^{o} and 297.5^{o}. This occurred as a result of the increased proximity of the wake to the turbine blades.

4..6 The Sixth Version of the Prescribed Wake Method : Wake Shape Based on Inconsistent Approach and the First Y-Modification [PRESWK - INCON - Y1 Version].

If one considers the wake shapes produced by PRESWK-DDMST and PRESWK - DDMST - D , it appears that the first version [PRESWK - DDMST], is superior in producing a wake shape which nearly matches the Free Wake method when the tip speed ratio is greater than 5. The second version provides a better approximation up to tip speed ratio 5.

A hybrid scheme which, if the tip speed ratio was greater than 5, followed PRESWK - DDMST and, at lower tip speed ratios, followed PRESWK - DDMST - D was possible. In addition, this hybrid version could be configured to include wake convection in the Y-direction. The study of the results of the Free Wake method presented in section 3-3, showed that there were no regular features of the Y-component of induced velocity in the flow field. This prevented a relation ship being developed between the Y-component of induced velocity on the blade and in the flow field which was similar in form to that for the X-component. Hence, as a

first approximation, wake convection in the Y- direction was only applied to the first wake cycle using the Y-component velocity at the blade. The rest of the wake cycles were defined to have the same Y-ordinates as the first wake cycle. Such a modification could not be made at the same time as the X-coordinates of the wake were defined, since Y-induced velocities were not available from the Double Disk Multiple Stream-Tube method. A simple approach was, therefore, adopted by adding one additional iteration to that used in the previous version. For this new version the number of iterations was equal to 5. At the end of the fourth iteration, a new wake based on the Y-modification was introduced and the aerodynamic characteristics recalculated. This new version was called PRESWK - INCON - Y1 . The flow diagram for this version is shown in Fig. 4.12

Figure 4.13 shows the comparison of wake shapes between the Free Wake and PRESWK - INCON - Y1. It shows good placement of the wake cycles for almost all tip speed ratios, with the exception at tip speed ratio $\lambda = 5$. Table 4.5 shows the comparison of power coefficients . The first three tip speed ratios from $\lambda = 2$ to 4 showed good agreement with the Free Wake solution. At tip speed ratio $\lambda = 5$, the new version gave an under prediction.

An important aspect of the wake modelling procedure was observed with this version. It was found that introducing a Y-modification produced a lower power coefficient than without Y-modification . Considering again Table 4.5, it may be observed that the inclusion of the Y-modification brought the results closer to the Free Wake solutions. In general, introducing a Y-convection , produced a significant reduction in Cp, over the predictions of PRESWK - DDMST. The most significant reduction appeared at tip speed ratio $\lambda = 5$, from Cp equal to 0.4982 to 0.4002. Although the last result does not match the Free Wake solution [Cp = 0.4445] , the introduction of Y- convection eliminated the presence of vortex interactions.

4.7 The Seventh Version of the Prescribed Wake Method : Wake Shape Based on Inconsistent Approach and the Second Y-Modification [PRESWK - INCON - Y2 Version].

In the previous section a method which attempted to include wake convection in the Y-direction was examined. The method only modified the first wake cycle and fixed the remaining wake cycles to have the same y - ordinate as the first. In the Free Wake method, it is clear , that, wake convection in the Y-direction occurs for the whole wake and not just the first cycle. However, investigation of the behaviour of the Y-component induced velocity in the Free Wake method, as presented in section 3-3, did not show any regular behaviour. Consequently, a suitable mathematical relationship, to relate the behaviour of the Y-component induced velocity on the blade to the gross flow field, could not be defined. By specifying that only the first wake cycle experienced wake convection in the Y- direction, the wake shapes presented in Fig. 4.13 were produced. The resulting wakes did not exhibit as much initial expansion as the Free Wake method. It was, therefore, decided to attempt to allow the wake convection to continue to the second wake cycle and then fix the rest of the wake cycles to have the same Y-ordinates as the second wake cycle. Although, in the Free Wake method the far wake contracts, it was considered that, due to the distance of the far wake from the blade, this could be ignored. This version had , essentially, the same numerical algorithm as PRESWK - INCON - Y1 and was denoted by PRESWK - INCON - Y2.

The comparison of results in terms of wake shape between the Free Wake method and PRESWK - INCON - Y2 is shown in Fig. 4.14. The power coefficient comparison, including the result of PRESWK - INCON - Y1, is shown in Table 4.6.

The main feature found here was that introducing further convection in the Y - direction reduced the value of power coefficient at all values of tip speed ratio. At

certain values of tip speed ratio, namely λ = 2,3 and 7, this version produced results which were closer to the Free Wake method, with an average difference of no more than 5%. At other tip speed ratios, the method produced slightly higher values than the Free Wake method. In general, this version was more accurate than the first six versions.

4.8 The Eighth Version of the Prescribed Wake Method : Wake Shape Based on Inconsistent Approach with a Second Y&X-Modification [PRESWK - INCON- (Y? + X) and PRESWK - INCON - (Y?)+(X) Version]

Seven methods of defining the wake to match the Free Wake solution have been proposed. Amongst these, most can provide good agreement with the Free Wake solution especially at low tip speed ratios. The last two versions represented further development [sixth and seventh version] of the third and fifth versions where the basic concept of wake development was to use information on induced velocity from the Double Disk Multiple Stream-Tube method. Unfortunately, this information, whether used directly or via transformation , did not give a correct wake which was valid for a wide range of tip speed ratio. In general, however, this approach did produce detailed aerodynamic characteristics with similar behaviour to those of the Free Wake solution .

The deficiencies of the first seven versions warranted a further attempt to introduce a second modification to the wake shape.There were two possible schemes which could be applied to make a second stage X-Modification. They were (a) the second stage X-modification at the same time as the Y modification, (b) the second stage X-modification after the Y - modification had been implemented. Implementation of the first scheme would not change the number of iterations in PRESWK - INCON - Y1/Y2, whereas the second scheme would require one additional iteration. The

first scheme would, therefore, absorb less CPU time than the second one. It was, however, difficult to assess in advance whether the first scheme would be superior to the second or vice versa.

It should be noted that the first scheme mentioned above entails a simultaneous second stage modification of the wake shape in terms of XY - coordinates. In this case, the necessary induced velocity information would be obtained from the results produced by PRESWK - DDMST or PRESWK -DDMST - D . The second scheme would utilise the induced velocity from PRESWK - INCON - Y?.

Since there were two schemes deployed in this new proposed version, they were called PRESWK - INCON - (Y?+X) and PRESWK - INCON - (Y?) + (X), respectively. The question mark (?) following Y means that Y? could be Y1 or Y2. Thus, for this version, there were four variants. The predictions, in terms of power coefficients, are presented in Table 4.7. This table shows that the second stage modification where X & Y alterations take place simultaneously, offers better results than a step by step approach. In this section ,the detailed aerodynamics will not be presented, but it is sufficient to say that the typical results did not deviate significantly in form from the other versions presented in the last two sections but were closer to the Free Wake solution. As an example, the wake shapes created by PRESWK-INCON-(Y1) + X, for the range of tip speed ratio $2 \leq \lambda \leq 7$, are given in Fig. 4.15. This example shows that the wake shapes are close to those produced by the Free Wake method. Indeed, this is true for all schemes in the range of tip speed ratio $2 \leq \lambda \leq 4$. Above this range, wake convection velocities are over predicted , especially by INCON-(Y?) + X. This produces an under prediction of the result. [see table 4.7]

4.9 The Ninth Version of the Prescribed Wake Method : The Extension of PRESWK -DDMST to Include a Second Modification in the X and Y - Directions in a Simultaneous Manner [PRESWK - DDMST - (Y?+X) Version].

This version was introduced in order to reduce the complexity of the method produced in version eight. This simplified approach used the direct induced velocity from the Double Disk Multiple Stream -Tube method to initiate the wake shape. A process of four iterations was, then, carried out to achieve a converged solution for that wake shape. The result from this stage of the calculation was , then, used to modify the wake shape in the X and Y directions simultaneously. The numerical algorithm of this method was, therefore, the same as PRESWK - INCON - (Y?+X) . Again, the X modification in this version used the same transformation to define the flow field as had been used in the previous versions. The two different Y modification schemes were, again, used, to assess which was most appropriate. Since both Y - modifications were attempted, two versions were created named PRESWK - DDMST - (Y1+X) and PRESWK - DDMST - (Y2 + X). These two versions only differed in terms of how the Y-wake coordinates were modified.

As with previous versions, the numerical input parameters and values of tip speed ratio were standard. For the range of tip ratio considered, Figure 4.16 shows the wake shape comparisons between the Free Wake method and PRESWK - DDMST - (Y1+X) , while Fig. 4.17 shows the comparisons with PRESWK - DDMST - (Y2+X). The first thing to note is that each component wake cycle shows good agreement in the X-directions with the Free Wake method. Experience with previous versions established that the first three wake cycles, which are close to the blade, had great influence on the solution. In other words, the proposed version would give a result close to the Free Wake solution if the first few wake cycles matched the wake shape from the Free Wake method. Such a condition was satisfied by this version and, so close agreement with the Free Wake solution was obtained.

Table 4.8 shows the comparison of power coefficient between the Free Wake method

and these two versions .This table also includes the result from PRESWK - DDMST in order to indicate the improvement achieved by these two versions. The result was encouraging for the entire range of tip speed ratio with the exception being at tip speed ratio $\lambda = 4$, which showed a slightly higher Cp than that produced by the Free Wake method, but still provided a better solution than PRESWK - DDMST itself.

From the results for power coefficient shown in Table 4.8, it seems an appropriate scheme could be applied by switching the type of Y-modification according to the tip speed ratio. Namely , for tip speed ratios less than 6, the scheme could use a Y2 - type modification, while for higher tip speed ratios it could use a Y1- type modification.

Typical calculation results, in terms of detailed aerodynamic characteristics near the mid blade span as a function of blade azimuth position, are compared to the Free Wake solution for tip speed ratio $\lambda = 7$ in Fig. 4.18. This case was selected , since the difference in power coefficient between PRESWK - DDMST - (Y2+X) and the Free Wake method was significant at $\lambda = 7$, while, PRESWK - DDMST - (Y1+X) gave close agreement with the Free Wake method. It can be said that, generally , the detailed aerodynamic characteristics for other values of tip speed ratio, show good agreement with the Free Wake method for most of the range of blade azimuth position.

4.10 Further Improvement of the Wake Shape.

The manner in which the wake shape is developed, for various versions of the Prescribed Wake method, has been presented in the first nine sections of this chapter. The results from those schemes showed a lack of agreement with the Free Wake

solution for tip speed ratios greater than 5. This is simply due to the fact that the field induced velocity derived from momentum considerations does not accurately model the time dependent physical phenomena in the flow around a vertical axis wind turbine. Conversely, the Free Wake method does provide a good simulation of the velocity field. Thus, any wake development schemes based on the momentum equation would always be limited in accuracy. It is clear , from the previous section that, as a result, all the developed schemes suffered from low convection velocities in the flow field at high tip speed ratios and hence gave under predictions of power coefficients. However, it was possible that the formulation for field induced velocity could , still, be used if the time dependent nature of the flow field could be taken into account. To do this, the field induced velocity behaviour with time, according to the Free Wake solution, was examined by considering the behaviour of two particular shed vortices from the upstream and downstream blade passes from one time step to the next.

Figure 4.19 shows how the field induced velocity changes from time to time for these two point shed vortices as they travel downstream. This figure has four parts : Fig. 4.19 a, shows the induced velocities at the point shed vortices when they are part of the first wake cycle, Fig. 4.19.b when they are in the second wake cycle and so on. This figure is for the case of tip speed ratio $\lambda = 4$, while the corresponding behaviour for $\lambda = 3$ and 5 is shown in Figs. 4.20 and 4.21, respectively. The two straight lines drawn on each of these figures represent the induced velocities calculated from the formulae given in Chapter 3. It may be observed that, at tip speed ratio $\lambda = 4$, the formulation for induced velocity on the first and second wake cycles matches the Free Wake method. At lower tip speed ratios the formulae give an under estimate whilst, at higher tip speed ratios, they give an over estimate. In addition, one can notice that, for $\lambda = 3$, the far wake condition is achieved at the third wake cycle. More wake cycles are required with increasing tip speed ratio. For instance, the induced velocities at the front and rear point vortices only converge at the fourth wake cycle for $\lambda = 4$ etc. Furthermore, Fig. 4.22 shows the field induced velocities as a

function of the vortex position, in terms of number of wake cycles, for the range of tip speed ratio $2 \leq \lambda \leq 7$. From this figure one can estimate the actual value of far wake induced velocity predicted by the Free Wake method.

For analysis purposes, the induced velocity deduced from momentum considerations is called an approximate induced velocity $W_{appr.}$ and that from the Free Wake solution is called the actual induced velocity $W_{act.}$. In the far wake, the flow is considered to be equivalent in the up and downstream wake sections. This is not the case in the flow domain near the rotor blade, i.e. for the domain of flow in the first, second ... etc wake cycles. The induced velocity in the near wake could be determined from the Free Wake solution, but the far wake velocity given by the Free Wake method was known to be in error due to the inappropriate starting conditions of the scheme. However, using Fig. 4.22, the far wake induced velocity could be deduced from the convergence characteristics of the two curves. Fig. 4.23a shows a comparison between the actual up stream induced velocities [based on the Free Wake solution] and the approximate values [based on momentum considerations] for the first wake cycle, as a function of tip speed ratio. The downstream wake component of the first wake cycle is given in Fig. 4.23b , while the far wake is depicted in Fig. 4.23c. A difference between the approximate induced velocity $W_{appr.}$ and actual induced velocity $W_{act.}$ is apparent in all the figures. This difference caused the various schemes described in the previous sections fail to accurately reproduce the Free Wake solution at high tip speed ratios. The difference can be eliminated by application of a correction based on the comparison of approximate and actual field induced velocities. An appropriate expression can be developed as follows :

$$W_{corr.} = [\, 1. - f(\lambda) \,] W_{appr.} \qquad 4\text{-}1$$

Where $f(\lambda)$ represents the correction factor as a function of tip speed ratio λ . If W_{corr} is replaced with W_{act} in equation 4-1, the correction factor $f(\lambda)$ can be written as :

$$f(\lambda) = [\, W_{appr.} - W_{act.} \,]/W_{appr.} \qquad 4\text{-}2$$

The non-dimensional difference on the right hand side of equation 4.2 was plotted against tip speed ratio λ for the upstream and downstream segments of the first wake cycle and the far wake condition in Fig. 4.23. This figure shows the functional forms of the generated correction factor curves. The correction factor for the upstream part of the first wake cycle $f_{up}(\lambda)$ is, then, given by :

$$f_{up}(\lambda) = - 0.82284 + 0.28238\,\lambda + 0.016621\,\lambda^2 \qquad 4\text{-}3a$$

While, for downstream part, the correction factor $f_{dw}(\lambda)$ is given by :

$$f_{dw}(\lambda) = - 0.62869 + 0.22355\,\lambda + 0.014947\,\lambda^2 \qquad 4\text{-}3b$$

For the far wake condition , the correction factor $f_{fw}(\lambda)$ has the form :

$$f_{fw}(\lambda) = - 0.31395 + 0.051593\,\lambda + 0.032978\,\lambda^2 - 0.002484\,\lambda^3 \qquad 4\text{-}3c$$

Once the induced velocity for the first wake cycle and far wake position had been corrected, the next problem was to determine the variation of induced velocity between these two domains. Fig. 4.24a shows how the actual induced velocities for the up stream part of a wake cycle changed from the first wake cycle to the far wake condition, for various values of tip speed ratio, plotted with respect to the real time t. The equivalent diagram for the downstream part is given in Fig. 4.24b. Considering Fig. 4.24a, one can notice that the upstream - induced velocity varies linearly to the far wake condition. For this special case, it seems that a constant time T equal to 7 units represents the approximate time when the far wake condition is achieved whatever value of tip speed ratio. This constant time T is important, since it allows the number of wake cycles before the far wake condition is satisfied to be defined. For

example at tip speed ratio $\lambda = 3$, which corresponds to a unit time for one rotation of 2.094. units, the far wake condition would be achieved at the third wake cycle. Examination of Fig. 4.20 indicates that this is true. For the downstream part [Fig. 4.24b], it is difficult to define a single time constant which is independent of tip speed ratio. Careful examination of the figure , however, shows that the far wake condition is nearly always achieved at the second wake cycle. Thus , considering that the second wake cycle represents the far wake condition for the downstream part seems acceptable.

Strictly speaking the improvement of the wake shape can be described as follows :

1. The induced velocities for the first and far wake cycles are defined using the formulation described in section 3.3, then corrected using the relationships given by equations 4.1-4.3.

2.A time constant equal to 7, is used to define the number of wake cycles NFW when the far wake condition is reached by the upstream wake segment. A linear variation of induced velocity is applied between the first and the NFW th wake cycle.

3. For the downstream part , the far wake condition is reached at the second wake cycle, Subsequent wake cycles has an induced velocity equal to the far wake condition in their downstream segment.

The improvements described above produced a wake shape in good agreement with the Free Wake method for the range of tip speed ratio $2 \leq \lambda \leq 7$, when the blade induced velocities predicted by the Free Wake method were used as the input to the wake generation procedure. However, as an example, reconstruction of the wake shape based on the new scheme is only presented for three values of tip speed ratio λ = 5,6, and 7 as shown in Fig. 4.25. This figure also presents the wake shapes

according to the old wake scheme. From this figure, it can clearly be seen that the new wake scheme provides a wake shape closer to the Free Wake method. Thus, implementation of this new wake scheme should give a similar result to the Free Wake method. This will be presented in the following section.

4.11 The Prescribed Wake Method Using the New Wake Scheme [PRESWK-DDMST-(Y2+XN?)] .

The scheme presented here is similar to PRESWK-DDMST-(Y2+X), but now, in reconstructing the second stage of the wake shape, the wake scheme described in section 4.10 is used . In addition, PRESWK-DDMST-(Y2+X) had only one iteration process at the second stage, i.e. the recalculation of aerodynamic performance after wake reconstruction was only done once. An attempt to iterate towards a final solution had been made, but this approach failed when the solution became divergent for λ above 5. This was due to an excessive axial induced velocity provided by the old wake scheme which, in turn, created a wake configuration which was much more closely packed than that of the Free Wake method. Since there is a mutual relationship between the strength of bound vortices and the strength of shed vortices in a flow field, a significant error in the calculation at a particular blade azimuth spreads up to other blade positions and a divergent solution can occur.

The algorithm for this new version is exactly the same as PRESWK-DDMST-(Y2+X). However, due to the more appropriate nature of the wake shape prescription at the second stage of the calculation , a number of iterations can be made. In order to distinguish between versions, this version is called PRESWK-DDMST-(Y2+XN?). The question mark (?) following XN means that there are some variants belonging to this scheme. Here, four variants denoted as PRESWK-DDMST -(Y2+XN1), (Y2+XN2), (Y2+XN3) and (Y2+XN4) , respectively , are proposed.

Their algorithms are the same, in that the number of iterations in the second stage is equal to the number in the first stage , i.e. four iterations in each stage. The differences appear in the way in which the wake shape is updated during the iteration process in the second stage.

In the first variant [PRESWK-DDMST-(Y2+XN1] , the wake shape is created once at the second stage and is kept fixed during the subsequent iteration process. The second version [PRESWK-DDMST-(Y2+XN2)], splits the second stage modification into a two level process in which each level consists of two iterations. Here, the wake shape created at the second stage is fixed for two iterations, then updated again and kept fixed for the last two iterations. Hence, with the wake initiation in the first stage included, there are three stages of wake construction in this scheme. In the third scheme (PRESWK-DDMST-(Y2+XN3)), the wake shape is reconstructed at each of the first three iterations in the second stage. The wake shape is then fixed for the final iteration to achieve a convergent solution. The fourth scheme [PRESWK-DDMST-(Y2+XN4)], involves the wake always being updated during the second stage iteration process. This procedure was also found to produce a convergent solution.

Considering that the differences in the above schemes were not very significant, the flow diagram for PRESWK-DDMST-(Y2+XN4) will only be presented here as shown in Fig. 4.26.

The wake shapes produced by these new wake schemes are compared to the Free Wake method for high tip speed ratios, λ = 5, 6 and 7, in Fig. 4.27. The comparison in terms of power coefficient is presented in Table 4.9 and in graphical form, including a comparison with PRESWK-DDMST-(Y2+X), in Fig. 4.28. In general, these four versions provide good agreement with the Free Wake method, with the most promising result given by PRESWK-DDMST-(Y2+XN4). The detailed aerodynamic characteristics are as shown in Fig. 4.29 for tip speed ratio λ = 7.

The conclusion which can be drawn from this work is that the wake shape is crucial , if accurate predictions are to be obtained. A wake shape which has a similar form to that of the Free Wake method can be generated in an iteration process and can produce a converged solution.

4.12 The Strength of Shed Vortices : Forward and Backward Approach.

The theoretical background of Strickland's Free Wake method has been fully described in Ref. 120. This was translated into a computer - code called VDART3 which was only applicable to the Darrieus type of wind turbine. Here, MVDART3 was developed during this work, as a modified version of VDART3 which allowed straight bladed configurations to be considered. The modification required to the original version was considerable, but the main features of the code were retained. For instance, the manner in which the movement of the wake from one time step to the next was defined, and the definition of the strength of vortex filaments was the same in both methods. The way in which the vortex strength is defined in the Free Wake method differs with theory and appears to be configured for simplicity in programming. This can be explained as follows :

In the Free Wake scheme, the wake is developed as part of the solution in a step by step manner as the calculation proceeds.At each time step, shed vortices are released from the blade and, together with other shed vortices which are already in the flow field, are convected by local field velocities. If the calculation is at the Nth time step, corresponding to blade azimuth position θ_N and bound vortex Γ_{bN}, the wake trailed behind the blade contains [N-1] shed vortices. At the previous time step, the blade located at azimuth position θ_{N-1} has bound vortex Γ_{bN-1}. In VDART3, for a particular element, when the calculation proceeds to the next time step N+1, i.e at the

bladea zimuth θ_{N+1}, the new shed vortex released into the flow field and has strength $\Gamma_{sN} = \Gamma_{bN} - \Gamma_{bN-1}$. The line drawn to connect the point representing the convected position of the blade control point and the control point on the blade, represents the trailing vortex shed from the blade. Here, the strength of this trailing vortex is determined from Γ_{bN} . The strength of the bound vortex on the blade is unknown and in order that it can be calculated, VDART3 uses $\Gamma_{bN+1} = \Gamma_{bN}$ as an initial value. This approach is correct since, without knowing this value, one cannot calculate the induced velocity. After the induced velocity on the blade has been obtained, it is used to calculate the bound vortex strength Γ_{bN+1} and the process is repeated for a second time. However, during the second recalculation, the strengths of the rest of the vortex filaments in the wake do not change, i.e. the change applies only to the strength of the bound vortex Γ_{bN+1}. This approach represents an attempt to simulate the time stepping process during the blade movement from one step to the next by considering that the attitude of the blade does not change as it moves , and that a sudden change occurs when the blade reaches its destination. Therefore, the strength of the trailing vortex behind the blade corresponds to the bound vortex at the old blade position. For simplicity, this technique is called the backward approach.

Another approach considers that the blade at the current time step is always in equilibrium with the wake. This means that the strength of the trailing vortex strictly behind the blade corresponds to the variations of the bound vortex on the blade at that time step. This approach was not applied in MVDART3, but it will be mentioned in the context of possible future work in the next chapter. This approach has, however, been adopted in the Prescribed Wake method.

In contrast with the backward approach mentioned above, this alternative may be called a forward approach. Based on the comparison of results between MVDART3 and various proposed versions of the Prescribed Wake, as described in the previous section, it was decided to use PRESWK-DDMST-(Y2+XN4) to investigate the

forward approach. To distinguish with the original ,the version using the forward approach for the strength of shed vortices, was called PRESWK-DDMST-(Y2+XN4)-F.

In general, the manner in which the strength of vortex filaments was defined , i.e back ward and forward approach , did not produce a significant difference in terms of power coefficient , as shown in Fig. 4.30. An exception occurred at tip speed ratio λ = 7. At this value, PRESWK-DDMST-(Y2+XN4)-F failed to obtain a converged solution. For other values of tip speed ratio, for instance λ = 4 and 6, this version provided Cp = 0.483 and 0.378 respectively, while MVDART3 gave Cp = 0.477 and 0.357 and PRESWK-DDMST-(Y2+XN4) produced Cp = 0.481 and 0.371. The forward approach did, however, change the detailed aerodynamic characteristics as shown in Fig. 4.31 at these two tip speed ratios, particularly over the downwind blade pass.

The failure of the forward approach for tip speed ratio λ = 7 was due to the failure in creating an appropriate wake shape at the second stage, since the induced velocity calculated from the wake shape in the first stage was too excessive. Fig. 4.32 shows the induced velocity from the last two iterations in the first stage of the calculation. This figure also includes the recalculated induced velocities obtained from the first iteration of the second stage. It should be noted that, this second stage result is derived from the wake shape developed using the induced velocities from the first stage. The over prediction of induced velocities for the down stream blade pass in the first stage produced a wake shape which was quite different from the Free Wake solution [see Fig. 4.32]. An attempt to remedy this problem is proposed here. Namely, the backward approach is applied in the first stage of the iteration process followed by the forward approach for the second stage. This produced a convergent solution and, at tip speed ratio 7, gave a Cp equal 0.2412, while the Cp result from the Free Wake method was equal to 0.2215.

The conclusion which can be drawn is that the back ward and forward approaches provide very nearly the same solution in terms of overall Power coefficient. They do, however, differ in terms of detailed aerodynamic characteristics.

CHAPTER - FIVE : THE ASSESSMENT AND APPLICATION OF THE PRESCRIBED WAKE METHOD

5.1 Introduction

An attempt to develop a Prescribed Wake method, suitable for vertical axis wind machines has been presented in Chapter 4. It was found that there are various schemes which can be created, ranging from a simple approach for wake generation to a complex step by step reconstruction of the wake shape. More than 20 versions of the Prescribed Wake method were introduced and investigated. The conclusion reached was that a version called PRESWK-DDMST-(Y2+XN4) offered the solution in closest agreement with the Free Wake method. An alternative method for defining the strength of shed vortices was also incorporated into PRESWK-DDMST-(Y2+XN4), and the result presented in section 4.12 showed that close agreement in terms of overall power coefficient was obtained with MVDART3, but significant differences were evident in detailed aerodynamic characteristics especially, at high tip speed ratios. Since in the present work, the aim was to develop a Prescribed Wake method which could reproduce the result of MVDART3, further study presented in the next section is based on the basic PRESWK-DDMST-(Y2+XN4) version. It was recognised that replacing a continuous wake sheet as a wake vortex lattice raised questions as to how to implement this in an appropriate manner. For example, the optimum number of time steps [NTI] and the most appropriate blade element spacing in the spanwise direction had to be determined. There were also some questions concerning a suitable cut off radius for the vortex influence when close to control points. Such problems will be discussed first before presentations on the effects of aerofoil data and application of the model to specific cases, i.e. Darrieus wind machines. However, first an assessment of the most appropriate location for control points on the blade will be made.

5.2 Effects of the Placement of Control Points.

The fact that the wake is part of the solution in the Free Wake method, makes this method too time consuming for design purposes due to the large number of induced velocity calculations on the blade and in the flow field. In the calculation process , there is no difference between the method of calculation for induced velocities on the blade or in the flow field.

In the case of NB blades, NTI steps in each full rotation and NBE spanwise elements , in MVDART3 the vortex system at the Nth time step will contain (NBE+1)xNBxN vortex filaments. If the calculation proceeds until the steady state solution is achieved after NR rotations, then, the value of N will have ranged from 1 to NTIxNR. This is generally a large number; for example if N= 100, NBE=8, NTI=16, NR=8 and NB=2, at the 100th step there are 1800 control points where an induced velocity calculation should be made. Each control point is influenced by 16 finite segment bound vortices, 1584 shed vortices, and 1782 finite segments of trailing vorticity. Such quantities had , actually, been minimised in MVDART3, by taking the induced velocities at the mid element control point to be the average of the induced velocities from the control points at the element edges. The induced velocities on both edges of element are required in MVDART3 in order to develop the wake as part of the solution.

The Biot -Savart law is a non linear formulation, as is the relationship between the strength of bound vorticity and the induced velocity since these two quantities are related via angle of attack and rely on non linear aerofoil data. This made it difficult to analyse mathematically the difference between averaging induced velocities from the element edges at the mid element or doing a direct calculation. The most simple calculation scheme involves calculation of the induced velocity directly at the mid element . Here, in order to avoid the averaging approach, the total number of control points along the blade span with NBE elements is (2xNBE+1). The first (NBE+1)

control points represent the control points located at the element edges and the other NBE points represent the control points at the mid elements. The calculation of induced velocity was carried out in PRESWK-DDMST-(Y2+XN4) at these control points. This approach was not attempted in the Free Wake method, since it would be too time consuming, i.e. around 20 hours on a DEC-MICROVAX computer system.

A different result could be expected due to this different approach to the calculation of induced velocity on the mid element control point. The calculation of induced velocity at a control point located at the edge of a blade element automatically eliminates the segment of the trailing vorticity from this point. The averaging process for the induced velocity on the mid element, therefore, means losing the influence from two segments of trailing vorticity. These two segments of trailing vorticity represent the part of the vortex system closest to the blade element under investigation. For this reason, their presence actually cannot be ignored. However, since the Biot-Savart law does not allow calculation of the induced velocity at a point located on the vortex filament, MVDART3 was unable to take account of this important trailing vorticity.

The length of this segment of trailing vorticity is inversely proportional to the number of time steps per rotational calculation NTI. If the blade induced velocity in the free stream direction, at any blade azimuth position, is denoted as W_x, then, for a given tip speed ratio λ, the segment of trailing vorticity has length ΔL_t given by :

$$\Delta L_t = 2\pi R/NTI + [U_\sim + W_x] [2\pi R]/[NTI x \lambda x U_\sim] \qquad 5\text{-}1$$

Where R is the blade radius and $U_\sim$ is the free stream velocity. From equation 5-1, it is clear that increasing the number of time steps (NTI) decreases the length of the segment of trailing vorticity. Consequently, the influence on the induced velocity is reduced.

In the present work, the NTI which was used was equal to 16 and the blade radius R, as well as the free stream velocity, were set equal to one unit of length and one unit of

speed, respectively. Hence, the first term of the right hand side of the above equation contributed 0.398 units to the length of the vortex segment. The second term of equation 5-1 will automatically add to this value, since its contribution is always positive . By increasing the tip speed ratio, the contribution from the second term decreases. Thus, whatever the value of tip speed ratio, the minimum length of this particular segment of trailing vorticity is equal to 0.398. This value is nearly four times the length of the aerofoil chord of the wind machine under current study. Hence, neglecting this trailing vorticity is likely to have significant influence on the result.

To distinguish between the original version of PRESWK-DDMST-(Y2+XN4) and the variant, the new scheme is called PRESWK-DDMST-(Y2+XN4)-M. In the range of tip speed ratio [$2 \leq \lambda \leq 7$], Table 5.1 shows the comparison of results in terms of power coefficients between MVDART3, PRESWK-DDMST-(Y2+XN4) and PRESWK-DDMST-(Y2+XN4)-M. The same comparison is made in graphical form in Fig. 5.1

Considering the results given in Table 5.1, the power coefficient given by the variant dropped by around 0.03, in the range of tip speed ratio $3 \leq \lambda \leq 7$, with respect to MVDART3 or PRESWK-DDMST-(Y2+XN4). It seems that the calculation of induced velocity applied directly to the control point at the mid element is more appropriate, since all vortex filaments can be taken into account. This approach was , therefore, adopted in the following section.

For completeness, Fig.5.2 shows the comparison of results in terms of wake shape, for tip seed ratios λ=5,6 and 7. Figs. 5.3a and Fig.5.3b show the comparison of detailed aerodynamic characteristics at $\lambda = 7$ between the above three schemes at the mid blade span and near the blade tip , respectively. At the mid blade span, the results show good agreement, but are slightly different near the blade tip section. This difference causes the disagreement in terms of power coefficient Cp. It is likely that

the scheme which includes the influence of all vortex filaments will give a more accurate representation of the true spanwise loading on the blade.

5.3 The Effects of the Type of Spacing in the spanwise Direction

A cosine spacing in the spanwise direction represents a common approach adopted in the aerodynamic analysis of fixed wings using Lifting line theory. This approach is, especially, required for the case of a swept wing configuration, due to the presence of a strong gradient of wing loading in the spanwise direction near the tip region. Meanwhile, for other cases, say a simple wing planform with high aspect ratio A_r, the implementation of a uniform spacing into a lifting line approach could provide a good solution. For such a wing planform , where the wing span and the aerofoil chord are denoted as b and c respectively , the aspect ratio A_r can be defined as the ratio between b and c [$A_r = b/c$]. In the aerodynamics of an aeroplane, the wing configuration termed " high aspect ratio " corresponds to A_r greater than 6. In line with the geometry of the wind turbine in the present work, where the blade span b and aerofoil chord c are equal to 1.44 R and 0.1 R respectively [R : blade radius], the aspect ratio A_r of this machine is equal to 14.4., and so can be considered as high aspect ratio. The use of uniform spacing, as had been used in the previous sections, therefore, seems justifiable.

It has been recognised that the wake shapes corresponding to these two physical configurations, fixed and rotary wing, are quite different. The rotational motion of the rotor blade creates the wake shape in a cycloid form, while a simple wing planform, has a wake which is trailed in the direction of the free stream. The purpose of introducing a cosine spacing in the spanwise direction here is to investigate whether such spacing has a significant effect on the PRESWK-DDMST-(Y2+XN4) solution. This work is, also, applied to the PRESWK-DDMST-(Y2+XN4)-M version, since

this alternative approach is likely to produce a better solution. The calculation will use the same numerical parameters as described in chapter 4, i.e. NB=2, NBE=8 and NTI = 16. The tip speed ratio range under investigation will be $2 \leq \lambda \leq 7$. This work is also carried out using MVDART3 but, due to computer limitations, the calculations are applied only to certain values of tip speed ratio, i.e. $\lambda = 4, 6$ and 7.

Table 5.2 shows the comparison of power coefficients between the uniform and cosine spanwise spacing. These data are also presented in graphical form in Fig. 5.4. Here, one can notice that the different type of spanwise spacing, has produced a difference result in the Free Wake method itself. For the three values of tip speed ratio considered, the result shows that the cosine distribution produces a higher Cp at the moderate tip speed ratio , but a lower value at the highest tip speed ratio $\lambda = 7$. The same tendency at moderate tip speed ratios is observed in both Prescribed Wake methods but, in these two cases, the value of Cp at $\lambda = 7$ is increased with the cosine distribution. Such a difference in the Free Wake method can be explained as follows : The cosine spacing ensures that more vortex filaments are present in the domain near the tip. At the same time , a high tip speed ratio generates a wake which is dense and close to the rotor blade. All of this increases the mutual influence between the stage of wake development and the feed back to rotor blade aerodynamic performance. Hence, at high tip speed ratios, unlike the Prescribed Wake model, the wake shape developed by the Free Wake method will be strongly dependent on this mutual influence.

The results above are for the case where the number of blade elements NBE is equal to 8. Due to computer constraints it was not possible to use a Free Wake method to examine the effects of discretization and the number of blade elements over a range of tip speed ratios. As a result, calculations to investigate these parameters were only done at tip speed ratios $\lambda = 4$ and 7. With more emphasis being given to $\lambda = 7$, where the wake configuration is closer to the rotor blade. It is likely , that the solution would be more sensitive to these parameters at this tip speed ratio. The

previous results presented for the Free Wake method, using a uniform and cosine spacing in the spanwise direction , were produced with the number of blade elements NBE set equal to 8. The number of blade elements was changed to NBE=12 and NBE=16 in this investigation . Both uniform and cosine spacing of spanwise elements were applied , but all other parameters were as in the previous work. The result at tip speed ratio $\lambda = 7$, showed that each set of numerical parameters had its own solution. A uniform blade spacing with NBE = 8, 12 and 16 provided Cp equal to 0.2215, 0.2190 and 0.2089 respectively. On the other hand, a cosine spacing produced Cp equal to 0.2193, 0.2103 and 0.2341. All these values represented a convergent solution as is clearly shown in Table 5.3a or, in graphical form, in Fig. 5.5a. The table shows how the power coefficient changed from one iteration to the next for the six variants of the Free Wake method. For the uniform element spacing, an increasing number tended to reduce the power coefficient. The cosine spacing exhibited an oscillation in result with changing blade element number. This oscillation also occurred at tip speed ratio $\lambda = 4$, as presented in Table 5.3b and Fig.5.5b. Although the difference between the cases was not significant, it may be concluded that there is no exact solution for the Free Wake method. In other words the solution depends on the numerical parameters used.

The uniform and cosine blade spacings cause the trailing vortices to be released at different locations along the blade. In the case were the blade is divided into 12 elements, however, there are five trailing vortices which have the same initial coordinates whether the blade is divided uniformly or using a cosine spacing . They are namely , the trailing vortices which are released from (1) the blade tips, (2) blade section 0.36R and (3) at exactly the mid blade span. Since the blade loading is symmetrical, only the wake from half of the blade span will be presented here. Fig. 5.6 shows a comparison of the wake shapes along half of the blade span for the Free Wake method using both uniform and cosine spacings with NBE = 12. From this figure, it is clear the different types of spacing created slightly different wake shapes.

The conclusion which can be drawn from this parametric study is that, using NBE greater than 8, both uniform and cosine spacings gave a solution which did not exceed 7% above or below the solution obtained using a uniform spacing with NBE = 8. Hence, the complete set of solutions from the Free Wake with NBE=8, in the range $2 \leq \lambda \leq 7$, are adequate as reference results for the Prescribed Wake model.

Considering, again, the results presented in Table 5.2., the discrepancy between the Free Wake method and Prescribed Wake method using a cosine spanwise spacing, is probably due to the inadequate way in which the wake expansion in the Y-direction is prescribed. PRESWK-DDMST-(Y2+XN4)-M gave higher values of power coefficient with a cosine spacing than with a uniform spacing.

For completeness, Fig. 5.7 shows a comparison of the wake shapes along the half blade span released from blade azimuth position 67.5^{o} for tip speed ratio $\lambda = 7$ with NBE=8. This figure consists of two parts; the first part presents the comparison of wake shapes generated using a uniform spacing, while the second part is the equivalent diagram for a cosine spacing. From these figures, it is clear that the way in which the wake shape is derived in the Prescribed Wake method produces good agreement with the Free Wake method, especially in terms of the x-coordinates . The differences between the Prescribed and Free Wake solution appear to be mostly due to inadequate prescription of the wake shape in the Y-direction

To end this section, Fig. 5.8a shows the comparison of detailed aerodynamic characteristics as function of blade azimuth near the mid blade span for various numerical parameters at $\lambda = 7$. The results shown in this figure, show clearly that there is no significant difference between using a uniform or cosine spacing near the mid blade span. However, as may be expected, the differences become apparent near the blade tip, as shown in Fig. 5.8b. In this case, the result corresponding to a uniform spacing relates to blade section 0.09 R, while the result from the cosine spacing relates to blade section 0.03 R.

5.4 Numerical Effects of the Number of Blade Elements and Time Steps.

This section presents an assessment of the effects on the solution of the number of span wise elements [NBE] as well as the number of time steps [NTI]. To limit the number of calculations , the NTI and NBE numbers investigated are :

NBE = 8, 12 and 16
NTI = 16, 24 and 32

Experience from the work on the Free Wake method presented in the previous section, showed that uniform and cosine distributions of blade elements gave similar results, when NBE = 12 and NTI = 16. Thus, a complete series of calculations for the full range of tip speed ratio was carried out using the two Prescribed Wake schemes with NBE=12 and NTI = 16. Other combinations of numerical parameters were only applied at certain tip speed ratios. Namely for λ = 4 and/ or 7.

A more restrictive calculation series was applied for the Free Wake method, with only four calculations being carried out. The calculations used both types of spacing with the numerical parameters NBE and NTI set equal to 8 and 24 respectively. This was applied to the case of tip speed ratios λ = 4 and 7 only. No attempt was made to calculate the problem in hand using NTI = 32 since, within the present ability of the MicroVax computer system working in batch processing mode, it would have required more than 4 days for such a calculation. In addition, NBE = 8 was used in the Free Wake method, since it was shown that an increase in the number of blade elements in the span wise direction did not significantly change the result obtained.

Firstly, results for Cp at tip speed ratio λ = 7, for various sets of numerical parameters, are presented for the three schemes [MVDART3-Code, PRESWK-DDMST-(Y2+XN4) and PRESWK-DDMST-(Y2+XN4)-M] in Table 5.4. Table 5.5,

shows the results at tip speed ratio $\lambda = 4$.

From these two tables, one can notice that the results from the Free Wake method vary from 0.2048 to 0.2341 for the case of $\lambda = 7$ and in the range 0.4706 to 0.4853 for the case of $\lambda = 4$. An increasing number of elements in the span wise direction and the cosine distribution both tend to increase the power coefficient above the result obtained using a uniform blade spacing with NBE = 8 and NTI = 16 or NTI = 24. It is interesting to note that, whether the solution reached Cp = 0.2048 or to 0.2341, a converged solution was obtained. This is due to the fact that, in the Free Wake method, different numerical parameters create different initial values of power coefficient at the first rotational calculation. Although these differences are small at first, they tend to be amplified as the calculation progresses. It is clear, therefore, that the choice of numerical parameters influences the solution obtained. However, further observation of the results, as presented in these two tables, suggests that the Free Wake method with uniform NBE = 8 and NTI = 16 , which was used as the basis for the development of the Prescribed Wake method, represents an appropriate solution with respect to numerical parameter effects. This may be argued, since the solutions from the Free Wake method, using different values of numerical parameters, do not deviate significantly from the solutions obtained with numerical parameters as mentioned above.

The results obtained in this study, for the Free Wake method, can be described as follows : At tip speed ratio $\lambda = 7$, from 9 calculations, the power coefficient obtained was in the range $0.2048 \leq Cp \leq 0.2341$. While at tip speed ratio $\lambda = 4$, from 7 calculations, the solution was in the range $0.4706 \leq Cp \leq 0.4853$. The great variation at $\lambda = 7$ can be under stood since, at high tip speed ratio, the wake is closer to the rotor blade than at lower tip speed ratios and ,hence, the solution is more susceptible to the vortex distribution in the wake.

The numerical effects observed for the Prescribed Wake method can be described as follows : The PRESWK-DDMST-(Y2+XN4) version provided 5 out of 9 solutions in the same range of solution as the Free Wake method for $\lambda = 7$. The other results were, on average, no more than 7% above the highest value of Cp from the Free Wake method. At $\lambda = 4$, this Prescribed Wake version provided 4 out of 6 results in the domain between $0.4813 \leq Cp \leq 0.4858$, as opposed to the Free Wake method which gave the range $0.4706 \leq Cp \leq 0.4858$. The other two results were around 4% below the lowest Cp value from the Free Wake method.

The other version, PRESWK-DDMST-(Y2+XN4) - M, produced solutions, at tip speed ratio $\lambda = 7$, in the range $0.1930 \leq Cp \leq 0.2508$, with 5 out of 8 calculations falling in the range of $0.2281 \leq Cp < 0.2433$.

Table 5.6 shows a comparison of power coefficients produced by the three schemes with NBE=12 and NTI = 16, in the range of tip speed ratio $2 \leq \lambda \leq 7$. Fig. 5.9 shows the comparison in graphical form. Close agreement is apparent between PRESWK-DDMST-(Y2+XN4) and the Free Wake method [MVDART3-Code], while PRESWK-DDMST-(Y2+XN4)-M does not correspond as well with the other two. This can be understood, since PRESWK-DDMST-(Y2+XN4) uses exactly the same procedure in calculating the induced velocity at a control point as MVDART3, whereas the other scheme uses an alternative approach. The differences in the results shown in Table 5.6 are quite small, and so the detailed aerodynamic characteristics will be very similar to the results presented in the previous section .

5.5 The Numerical Effects of the Radius Cut off in the Biot-Savart Law.

Replacement of a continuous wake sheet with a discrete wake vortex lattice represents

a common approach for solving flow problems using a vortex method. This is done in order to avoid the mathematical difficulty in defining the velocity induced by the presence of such a wake sheet. In this type of calculation, the Biot-Savart Law is used for the induced velocity calculation at any control point in the flow field. For simple flow problems, such as the flow past a fixed wing configuration, where the wake can be considered straight in the direction of the free stream velocity, the implementation of the Biot-Savart law does not pose a serious problem. This is true since the wake geometry of the flow problem, when represented by a discrete wake vortex lattice, does not have control points on the wing which fall in the domain of a vortex singularity. However, when it comes to problems such as the flow past a rotary wing, the wake may come close to or interact with the blade. The singularity associated with a vortex filament may, therefore, become significant in the computational process, and may prevent a solution from being obtained.

In the present work, the induced velocity produced by a vortex was taken as being equal to zero within a finite radius of the vortex core as described in Fig. 5.10a. Many other alternative representations of the core effect were possible including the linear induced velocity variation depicted in Fig. 5.10b. During the development of the Prescribed Wake model a number of these vortex core representations were studied, but it was found that the model was relatively insensitive to core type. A more influential parameter was the vortex core radius. For this reason, this section concentrates on the effect of cut off radius R_c. In the Prescribed Wake model, if the distance between a vortex filament and a given control point was less than R_c, the induced velocity at that control point, due to the vortex filament, was set to zero. Since R_c is arbitrary, an appropriate value of R_c had to be determined.

In the previous section, all calculations presented, for both the Prescribed Wake method and the Free Wake method, used R_c equal to 0.001 R. This value represents 1% of the blade section aerofoil chord. The best way to investigate the effect of varying R_c, is by using the Free Wake method since this method requires calculation of induced velocities in the flow field. In addition, there is no difference in the way

that the induced velocity at a control point on the blade or in the flow field is calculated. Since vortex filaments are more concentrated around a control point in the flow field , rather than around the blade, the Free Wake method will be more sensitive to the choice of R_c. Therefore, the limit of R_c for the Free Wake method can be considered as the limit of applicability in the Prescribed Wake method.

Initially, an investigation of the effect of reducing R_c on the Free Wake method was conducted. It was not possible to investigate over the full range of tip speed ratios due to computer limitations. Therefore, only two values of tip speed ratio, $\lambda = 4$ and 7, were considered. The table below shows the effect of R_c, in terms of power coefficient, on the Free Wake method at those two tip speed ratios.

Cp result - Free Wake method

Tip speed ratio	Rc = 0.001 R	0.0001 R	0.00001 R
4	0.4769	0.4780	0.4781
7	0.2215	0.2392	0.2640

From this result , one can notice that the power coefficient tends to increase with reducing R_c. The effect of R_c becomes more significant with increasing tip speed ratio. This can be understood, since at high tip speed ratio, the wake structure is closer to the blade and the vortex filaments are more densely packed. It was also found that, at tip speed ratio $\lambda = 7$ and with Rc = 0.00001 R, the Free Wake method did not reach a steady state solution. This was not the case for calculations using R_c = 0.001 R or 0.0001 R. The table below shows the change in Cp with respect to rotational calculation number for the three different values of R_c at $\lambda = 7$.

Cp result with respect to the rotational calculation number - Free Wake method [$\lambda = 7$]

Rot. numb.	Rc = 0.001 R	0.0001 R	0.00001 R
1	1.0392	1.0432	1.0358
2	0.6922	0.6446	0.6625
3	0.4554	0.4738	0.4701
4	0.3371	0.3629	0.3523
5	0.2827	0.2668	0.2872
6	0.2624	0.2466	0.2838
7	0.2361	0.2437	0.3002
8	0.2215	0.2392	0.2640

The result given above suggests that a choice of R_c less than or equal to 0.00001R will not produce a converged solution. The choice between R_c = 0.001 R or R_c = 0.0001 R can , of course, be decided only via comparison with experimental results, since both produce a converged solution. However, if the results from these two R_c values at tip speed ratio $\lambda = 4$ and 7, are examined, no significant differences between the two are apparent.

It is interesting to examine how the wake shape changes due to the choice of R_c. Fig. 5.11 shows a comparison of wake shapes along the half blade span from the Free Wake method for the three different values of R_c mentioned above at tip speed ratio $\lambda = 7$. For R_c = 0.001 R and 0.0001 R, the wake shapes are very similar. A significant change, especially near the blade tip, appears at R_c = 0.00001 R. This change in wake shape manifests itself in the detailed aerodynamic characteristics shown in Fig. 5.12. This figure clearly shows the Biot-Savart singularity at certain blade azimuth positions, where a discontinuity in the parameter curves is observed. This behaviour, which is also observed at other spanwise locations , prevents a

converged solution being obtained.

On the basis of the above study, a complete set of calculations in the range $2 \leq \lambda \leq 7$ was only carried out using the Prescribed Wake method with R_c = 0.0001 R. Table 5.7 shows a comparison of the Cp values obtained using R_c = 0.001 R and 0.0001 R. From this table it is clear that the Cp values from the Prescribed Wake method do not change much with R_c. A comparison of these power coefficients in graphical form is shown in Fig. 5.13.

5.6 The Influence of Aerofoil Data.

The rotational motion of a vertical axis wind machine causes the blades to experience changes in angle of attack. The angle of attack, at the local blade element, may vary from -40^o to $+ 40^o$ depending on the ambient wind speed, tip speed ratio and blade shapes. At the same time, performance prediction methods require blade element section data to perform a calculation. Hence, certain difficulties have arisen in obtaining these data, since the aerofoil operating range in terms of both angle of attack and Reynolds number, is not normal for typical aeronautical applications. In this section , it will be shown that the aerofoil data have a significant influence on the solution obtained from the Free Wake method and the Prescribed Wake method. It will also be shown that the Prescribed Wake method, although based on the solution of the Free Wake method using Naca 0015 aerofoil data, is applicable for other aerofoils.

In addition to the Naca 0015 data, results from the Prescribed Wake method for the same geometry of wind machine but with three other types of aerofoil data are presented . The other aerofoil data are :

1. Aerofoil data from Musgrove [122]
2. Naca 0012
3. Eppler-data [155]

Using the above aerofoil data, calculations were also carried out using the Free Wake method. However, again due to computer limitations, calculations were only done for certain values of tip speed ratio. It is important to note that the results presented below were obtained using the same numerical parameters as in the previous chapter; namely NBE = 8, NTI = 16 and NR = 8. The cut off radius, R_c, for the Biot - Savart law was 0.001 R.

The aerofoil data of Musgrove [122] were used to derive an analytical expression for the overall performance of a straight bladed vertical axis wind machine. The lift and drag coefficients [C_l , C_d] as a function of angle of attack α , were given by :

$$C_l(\alpha) = (\delta C_l/\delta\alpha)\,\alpha \qquad 5\text{-}2a$$

$$C_d(\alpha) = C_{do} + k\,C_l^2 \qquad 5\text{-}2b$$

Using these aerofoil data, in a momentum model, Musgrove [122] found the overall performance of a straight bladed vertical axis wind machine could be written in terms of tip speed ratio λ as :

$$Cp = 0.5\,\sigma\,l\,[\,(a_l - k\,a_l^{\,2})(\,1 - \sigma\,a_l\,\lambda/8\,)^2 - 2\,C_{do}\,\lambda^2] \qquad 5\text{-}3$$

Where $a_l = (\delta C_l/\delta\alpha)$ is the lift slope and σ is the solidity factor defined as :

$$s = NB\,c_r/(2R) \qquad 5\text{-}4$$

NB : number of blades

c_r : aerofoil chord

R : blade radius.

In his analysis, the performance of a Naca 0015 aerofoil at Reynolds number Re ~ 2 10^6, was modelled by setting the unknown coefficients of C_l and C_d in equations 5-2 to be :

$$\begin{aligned} a &= 6.25 \\ C_{do} &= 0.007 \\ k &= 0.005 \end{aligned} \qquad 5\text{-}5$$

The above Cp formulation, combined with the aerofoil data defined using these coefficients, when applied to the case of a wind machine with solidity factor $\sigma = 0.1$, gave Cp as :

$$Cp = 0.303\,\lambda - 0.0473\,\lambda^2 + 0.0015\,\lambda^3 \qquad 5\text{-}6$$

Three example Cp calculations using these aerofoil data, for tip speed ratios λ =4,5 and 7 , are shown in the table below :

Aerofoil data from Musgrove [122] - Cp results.

Tip speed rat.	MVDART3	PRESWK-DDMST-(Y2+XN4)	Musgrove[122]
4	0.5306	0.5194	0.5288
5	0.5211	0.5153	0.4762
7	0.3752	0.3760	0.1978

From the example calculations shown above, it is clear that the Prescribed Wake method provided good agreement with the Free Wake solution. On the other hand, Musgrove's results were far below the Free Wake's solution at high tip speed ratios. Here one can notice that the aerofoil data given by eqs. 5.2 produced higher Cps than using the previous aerofoil data . The Naca 0015 data , at tip speed ratio $\lambda = 7$, produced Cp equal to 0.2215. Whilst the simplified aerofoil data gave a Cp equal to 0.3752. It is known that at high tip speed ratios the rotor blade operates at low angles of attack, where the simplified representation of the lift coefficient versus angle of attack, given above [equation 5.2], seems appropriate. The big difference in power coefficient present in this case is probably due to an inaccurate specification of C_d , since this is the major contributor to the tangential force at low incidence. From this example, it is clear that the aerofoil data used has a significant effect on the solution or, in other words, the aerofoil data will determine the overall performance of the wind machine. This statement will be further confirmed when results for other aerofoils are examined.

The NACA 0012 data were already incorporated in the VDART3-Code and covered a range of Reynolds numbers. Hence, the variation of Reynolds number around the blade azimuth could be taken into account in the analysis. Four example calculations at tip speed ratios λ = 2,4,5 and 7 were carried out. The comparison of power coefficients obtained is as shown in the table below, which clearly shows good agreement between the Free Wake method and the Prescribed Wake scheme. At the lowest tip speed ratio, $\lambda = 2$, both methods provide a negative power coefficient. Here, one can again notice the effect of the different type of aerofoil data on the calculated Cp at a given tip speed ratio. This case also produced a different λ_{max}. These aerofoil data gave the peak power coefficient Cp_{max} at around $\lambda = 5$ while , for the previous data [Naca 0015], it occurred at around $\lambda = 4$.

NACA 0012- data - Cp results.

Tip speed rat.	MVDART3-Cd	PRESWK-DDMST-(Y2+XN4)
2	-0.0011	-0.0009
4	0.3170	0.3180
5	0.4100	0.4132
7	0.2059	0.2207

The Eppler data was for the Naca 0015 aerofoil at Reynolds number Re = 10^6. The difference with the previous Naca 0015 data was in terms of the Reynolds number and the range of angle of attack covered by the data. The original data set was for Re = 3×10^6 with an angle of attack range $-70^o \leq \alpha \leq +70^o$, while the present data covered the range $-180^o \leq \alpha \leq 180^o$. The difference between the range of the two data sets is relatively unimportant, since a normal vertical axis wind turbine would normally not exceed an operating incidence of around 45^o. Calculated Cp values for MVDART3 and PRESWK-DDMST-(Y2+XN4) using the Eppler data are as shown in the table below :

Eppler-Data - Cp results.

Tip speed rat.	MVDART3-Cd	PRESWK-DDMST-(Y2+XN4)
2	0.0707	0.0709
4	0.5193	0.4813
7	0.3583	0.3586

From the results presented above it is clear that, although the analysis was carried out using different aerofoil data, PRESWK-DDMST-(Y2+XN4) still provided a solution which gave good agreement with the Free Wake method.

From the above analysis, it may be concluded that the aerofoil data has a significant influence on the overall predicted performance of the wind machine. It, therefore, follows that in any aerodynamic performance analysis of a vertical axis wind turbine , appropriate aerofoil data are required.

Considering the variation in power coefficient produced by the aerofoil data, it may be expected that different wake shape configurations would be generated. This was, in fact, observed although the gross characteristics of the wakes were similar.

5.7 Application of the Prescribed Wake Method to the Darrieus Wind Machine : First Model - The Circle Arc Darrieus Wind Turbine.

The original Free Wake code from which MVDART3 originated, i.e. VDART3 was designed for a Darrieus configuration in which the blade shape took the form of a circular arc. If z represents the vertical axis of the wind machine, then , the local blade radius r(z) in this code is defined as :

$$r(z) = 1.- 4 [(z/H_r - 0.5)]^2 \qquad 5\text{-}7$$

Where H_r is the overall height and the other terms in the above equation have been non dimensionalised by the maximum blade radius R_m. In VDART3, the blade radius R_m, as well as the free stream velocity , is set to unity. All quantities which have dimensions of length and velocity are non dimensionalised with respect to these

two quantities.

The frontal Area A_f for a straight bladed vertical axis wind turbine with blade span H_r and blade radius unity, is simply defined as 2 x H_r . However, for a curved blade with local blade radius z(r), the frontal area A_f can be obtained from :

$$A_f = 2\ R_m^2 \int_0^{H_r} (r/R_m)\, \partial(z/R_m) \qquad 5\text{-}8$$

For the circular arc form defined by equation 5-7, equation 5-8 provides a frontal area A_f equal to 1.33 H_r .

The blades of a Darrieus wind machine have two meeting points at the bottom and the top of the central tower. At these points, the local blade radius is equal to zero. A finite radius is, however, required in the Prescribed Wake method when the Double Disk Multiple Stream Tube method is used to generate the wake shape at the first stage of the calculation. Therefore, to avoid a zero local blade radius, the model assumes that the blades are terminated just before the top and bottom. If the height of the turbine is H_r , then, the bottom cut off point is set at 0.025 H_r, while the top cut off point is at 0.975 H_r . Applying this cut off scheme allowed MVDART3 to be applied to this problem. It was also checked that this small cut off did not significantly affect the solution. The original code [VDART3] for this type of configuration, at tip speed ratios λ = 3 and 6 , gave Cp equal to 0.3350 and 0.3083. MVDART3 with the cut off scheme produced Cp equal to 0.3335 and 0.3127 respectively.

For this configuration, the models used the same parameters as in the case of the straight bladed configuration, i.e. blade number NB = 2, blade span H_r = 1.44 R and the ratio of chord- blade radius c_r = 0. 1 R. Two sets of aerofoil data were applied within the model. The first data set , i.e. for the Naca 0012, was already available

in VDART3 and the second data [Naca 0015] was that used in the previous work on the straight bladed configuration. The range of tip speed ratio examined for this configuration was the same as for the straight bladed machine, i.e. $2 \leq \lambda \leq 7$. The number of calculations carried out using the Free Wake method were, however, limited by available computational resources.

Table 5.8a shows a comparison of power coefficients produced by the methods using the aerofoil data for the Naca 0015. The following Table [Table 5.8b] gives the result using the Naca 0012 data. The result shows that good agreement is achieved below tip speed ratio λ=4. Above this tip speed ratio , the Prescribed Wake scheme [PRESWK-DDMST-(Y2+XN4)] provided higher Cp values than the Free Wake solution. The different result stems from the wake shape in the Prescribed Wake scheme not correctly reproducing that of the Free Wake method. The conclusion which can be drawn from the present analysis is that the curved blade of the Darrieus turbine produces a wake with behaves differently along the blade span compared with the straight bladed case. Strictly speaking, the formulation for the wake shape used in the Prescribed Wake method [see section 4.9] requires to be corrected for application to the case of a curved bladed machine. This was beyond the scope of the present work but it is suggested for future work [See chapter 6]. As guidance, results for this case obtained using the version of the Prescribed method described in Section 3.4, which is described in Table 5.8a as the old wake scheme, are also presented. This version of the Prescribed Wake model in the straight bladed case generated wakes with lower convection speeds than the Free Wake method and so always gave a lower power coefficient than the Free Wake method [See Table 4.7]. Considering the result in Table 5.8a, it is clear that this version of the Prescribed Wake method is more appropriate to the Darrieus turbine. Since , in this case , it provided results closer to the Free Wake method.

Fig. 5.14 shows the comparison of power coefficient versus tip speed ratio between PRESWK-DDMST-(Y2+XN4) and MVDART3, in graphical form, for this wind machine. For this range of tip speed ratio, results along the full blade span were

obtained. Fig.4.15 shows the comparison of results at tip speed ratio $\lambda = 7$ for the Naca 0015 data. Good agreement with the Free Wake method is achieved near the mid blade span. But , from the mid span to the blade tip, the deviation in the two results increases. In terms of induced velocities in stream wise direction , it is clear that the Free Wake method produces a more negative result. This corresponds to a slower moving wake in the Free Wake method.

5.8 Application of the Prescribed Wake Method for the Darrieus Wind Machine : Second Model - Sandia - 17 m wind machine.

Experimental results of power coefficient with respect to tip speed ratio λ for this machine are widely available, for instance in Refs. 156, 77, 157 and 164. Amongst these references , only the last provides a complete description of the wind turbine geometry. The blade geometry adopted from Ref. 164 for the Sandia - 17m wind machine is shown below :

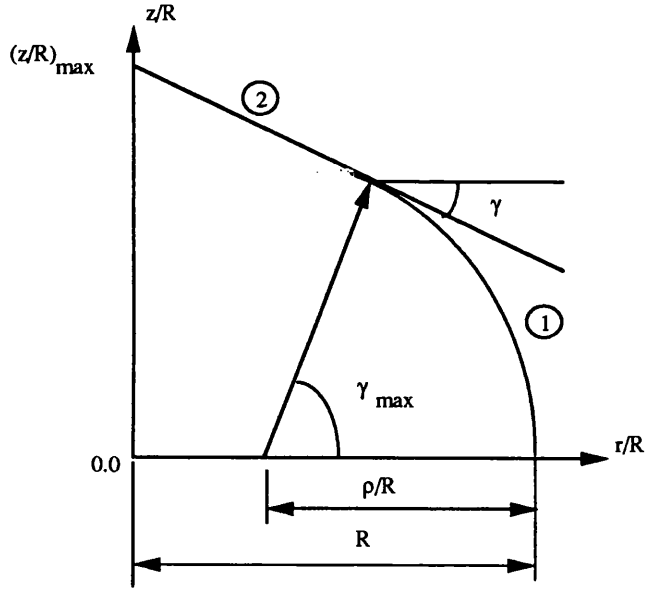

Rotor blade geometry - Sandia - 17 m Wind machine

region 1 : $r/R_m = (1. - r_1/R_m) + [(r1/R_m)^2 - (z/Rm)^2]^{1/2}$ 5-9a

$\cos\gamma = [1 - (z/r_1)]^{1/2}$ 5-9b

region 2 : $r/R_m = C_1 - C_2 (z/r_1)$ 5-9c

The constants C_1, C_2, r_1 and other pertinent data related to this machine can be described as follows :

Sandia - 17 m Wind Machine.

==========

Blade number	: 2	r1/Rm	: 0.66286
Aerofoil section:	Naca 0015	C1	: 1.552253
Chord	: 24"	C2	: 1.48256
R_m	: 325.86"	γ_{max}	: 56.^{o}
c/R_m	: 0.07365	z_{max}/R_m	: 0.54953
x_o/c	: 0.38		

With the data given above, the frontal area A_f for this configuration can be obtained easily, i.e $A_f = 2.6741$. For calculation purposes, the aerofoil data for the Naca 0015 from Eppler and the previously used Naca 0015 data were most appropriate. The calculations covered the tip speed ratio range $2 \leq \lambda \leq 9$, where Cp values obtained from field tests were available. The field tests showed that the power coefficient depended on the wind machine's rotational speed. The main difference in overall performance, due to the wind machine's rotational speed became apparent in the range of tip speed ratio $4 < \lambda < 10$. Fig. 5.16 shows the overall performance of the machine for four different rotational speeds from field data [164].

The RPM of the machine corresponds to the mean value of Reynolds number around the azimuth which, in turn, corresponds to the aerofoil's aerodynamic characteristics. The difference in performance due to the wind machine's rotational speed can,

therefore, be said to be due to the Reynolds number effects. For example , if the density ρ and viscosity μ are assumed to be approximately 1.2251 kg/m^3 and 1.7894×10^{-5} kg/ms respectively and the maximum blade radius of the Sandia machine is R_m = 325.86 inc. = 8.2768 m, the corresponding mean blade Reynolds numbers for the four values of RPM for this machine are as shown in the table below:

RPM's wind machine	Reynolds number Re
38.7	2.3×10^6
42.2	2.5×10^6
46.7	2.8×10^6
50.6	3.0×10^6

The Naca 0015 data from Eppler was obtained from experimental work at Reynolds number Re ~ 10^6 . It would , therefore, be appropriate to compare a result obtained using these data with the 38.7 RPM case. The other data correspond with the test results at a Reynolds number of approximately 3.0×10^6 and are thus applicable to the Sandia wind machine operating somewhere between 46.7 and 50.6 RPM.

Table 5.9 shows a comparison of power coefficients between the Sandia field data and the Prescribed Wake scheme. The comparison is given graphically in Fig. 5.17. Considering Fig. 5.17, the Prescribed Wake scheme using the Eppler data provided good agreement with the field data at 38.7 RPM. However, using the data for Reynolds number Re ~ 3. 10^6, correspondence was only obtained with the 50.6

RPM data below tip speed ratio $\lambda = 5$. Above it, the scheme under predicted the Cp values. When, however, comparison is made with the field results at 42.7 RPM, substantial agreement is apparent. The discrepancy with the experimental result at 50.6 RPM is also suffered by the Free Wake method. Two possible causes for this discrepancy exist. Firstly, the second data set was only available for the range of angle of attack $-70 \leq \alpha \leq 70$. This, however, would only affect the top and bottom regions of the turbine and would, therefore , be unlikely to contribute significantly to the discrepancy. Secondly, the local blade radius of the turbine varies from one unit at the mid blade span to zero at the top or the bottom. Consequently , when the wind machine is operated at 50.6 RPM, only the local blade element at the mid span has a mean Reynolds number around 3×10^6. Other blade elements experience a lower Reynolds number. In addition to these two problems, the sensitivity of the solution to accurate drag data complicates the problem.

5.9 Dynamic Stall Effects : An Overview Description

The physical configuration of a vertical axis wind turbine, whether in the form of a Darrieus type or a straight bladed wind machine, is such that the rotor blades experience changes in angle of attack, as they traverse their circular trajectory. As a result, the rate of change in angle of attack becomes a significant parameter in the vertical axis wind machine. Noll and Ham [158] suggested that dynamic stall may be encountered by aerofoils or lifting surfaces which are oscillating or subjected to cyclic inputs. In addition to the presence of the changing rate of angle of attack due to the rotational motion of the blade, there are other factors which make the wind machine susceptible to dynamic stall. These factors include the use of variable pitch and the blades being subjected to periodic forces such as gust and tower shadow effects.

Dynamic stall was described by Carr [159] as the complex series of events that result in the dynamic delay of stall on an aerofoil or wing experiencing unsteady motion to angles significantly beyond the static stall angle. Furthermore, Noll and Ham [158] noted that the presence of dynamic stall may produce lift coefficients and nose down pitching moments with peak values much greater than the corresponding static stall loads. The maximum aerodynamic load due to dynamic stall may be as much as three times the magnitude predicted without dynamic stall effects . Additionally, the nose down moment may be five times the static value. As a result, load variations of these magnitudes may exceed structural static margins and may reduce the fatigue life of the machine. In this respect, the performance of the machine may deviate from predicted values which, in turn, may create problems for the matched performance of the rotor/gear box/ alternator design.

The consequences of dynamic stall are, undoubtedly, that the wind machine suffers severe conditions which can shorten its fatigue life. As shown by Veers [159], an error of 30% in the prediction of dynamic air loads on VAWTs, can result in a reduction by a factor of 70 in the expected life span of a wind turbine. Unfortunately , dynamic stall is a complex flow phenomenon , which is dependent on a large number of parameters. McCrosky [160] identified these parameters and their effects are as shown in Table 5.10. Furthermore, McCrosky indicated that dynamic stall can be further classified into two categories, i.e. light stall and deep stall. In the first category, the dynamic characteristics share some of the general features of classical static stall, such as loss of lift and a significant increase in drag and nose down pitching moment. The second category, deep stall, is identified by the presence of the vortex shedding phenomenon. The passage of the dynamic stall vortex over the upper surface of the aerofoil produces aerodynamic forces and moment coefficients far in excess of their static counterparts. In addition, a large amount of hysteresis is experienced during the cycle. The complexity of dynamic stall is immense and its effects are generally detrimental . At the same time there are a variety of current applications in aeronautics, hydrodynamics and wind engineering where dynamic stall effects are present. Such conditions have resulted in impressive progress being made

in the analysis and prediction of dynamic stall effects [160]. Amongst the applications mentioned above , helicopter rotor aerodynamics represent the field to which most efforts in analysis and the development of prediction methods have been directed. At the same time, dynamic stall prediction methods developed for helicopter applications can also be applied to the case of a wind turbine.

In general, prediction methods for dynamic stall can be classified into two approaches, i.e. theoretical methods and semi-empirical techniques. The theoretical methods encompass Navier-Stokes techniques, the discrete vortex method and the zonal method [161]. Semi-empirical methods, however, have received more interest than their theoretical counterparts [162]. Generally, this type of approach attempts to simulate the gross features of stall via static data with a dynamic correction. This is advantageous, since static data can be easily generated and automatically includes the effects of Reynolds number, Mach number and aerofoil shape. A scheme of this type is, therefore, computationally more efficient and can be incorporated into an aerodynamic code for a rotor blade of a helicopter or wind device. There are several semi-empirical methods currently available. Amongst these are the Boeing-Vertol gamma function method[144], the Beddoe's model [150], Gangwani's model[151] and ONERA's model [152]. All of these were developed for use in the aerodynamic analysis of helicopter rotor blades. The Boeing-Vertol gamma function method may represent the simplest model of the four. Attempts to use this method for the aerodynamic analysis of a vertical axis wind machine have been made by Sharpe [126] and Vandenberghe et. al. [163]. Sharpe [126] found that the incorporation of the dynamic model in a Multiple Stream-Tube method produced poorer results than without dynamic stall effects. Conversely, Vandenberghe et. al. [142] found that including dynamic stall effects in a vortex method provided better agreement, in terms of power coefficient, with experimental results.

Attempts to use a more complicated method than the Boeing Vertol gamma function method are not common. However, the Beddoe's model [150] has been successfully incorporated into a Fixed Wake method. Implementation of the Beddoe's model into

the prescribed wake method is currently under way. Due to the early stage of development, results from this hybrid model are not yet available.

VI. CHAPTER - SIX : CONCLUSIONS AND FUTURE WORK

6.1 Concluding Remarks :

The complexity of the wake geometry of vertical axis wind machines is considerable and precise wake data from experimental work are not currently available. For this reason, the wake geometry provided by the Free Wake vortex method was used as the source of information in developing a Prescribed Wake scheme. It is generally accepted that the Free Wake method is the most accurate prediction method currently available for the aerodynamic performance of vertical axis wind turbines. This method is, however, simply too time consuming for design purposes. The determination of the wake shape during the solution is the cause of the large amount of computation required. In the Prescribed Wake scheme, the intent was to prescribe the wake geometry in advance, and so reduce the computation time significantly. In fact, prescribing a wake shape, equivalent to that from the Free Wake method,was not an easy task. An investigation of the flow field induced velocities in the stream wise and transverse directions, given by the Free Wake solution, was carried out for a wide range of tip speed ratio $2 \leq \lambda \leq 7$. It was found that some regularity was apparent for the stream wise induced velocities in the flow field but not for the induced velocity in the transverse direction. Alternatively, an approximate induced velocity in the stream wise direction at the blade could easily be provided by other means , such as a momentum based model. For this reason, an initial induced velocity at the blade, calculated using momentum theory, was used used to develop the induced velocity in the flow field and, hence, to generate the wake shape. Momentum considerations were applied in order to define a relationship between the stream wise induced velocity at the blade and those in the flow field. Since no regularity was found for the transverse induced velocity, the wake shape in that direction was assumed to convect at the induced velocity on the blade until the second wake cycle, after which no further expansion took place.

Various possible Prescribed Wake schemes,were introduced and compared to the Free Wake solution . At low tip speed ratios $\lambda \leq 4$, close agreement with the Free Wake method was provided by most of the schemes. Significant deviations from the Free Wake solution became apparent at increasing values of tip speed ratio. This was due to the fact that, in these schemes , near-wake cycles close to the rotor blade were not modelled correctly. As a result, a further investigation of the time dependent behaviour of the induced velocity in the stream wise direction was carried out. It was concluded that the original relationship between the induced on the blade and that in the flow field required correction for the time dependent nature of the wake development. By applying a deficiency function to the original relationship, a new wake scheme called PRESWK-DDMST-(Y2+XN4) was developed. This version provided good agreement with the solution of the Free Wake method at all tip speed ratios.

A study of numerical parameter effects, such as the type of blade span wise spacing, the number of elements in the span wise direction and the number of time steps was carried out. An increase in the number of span wise elements had a significant influence, especially if a cosine type spacing was applied. This was also true for the Free Wake method. This can be understood, since the cosine spacing concentrates the trailing wake in the domain of the blade tip and, as a result, captures the large variation of circulation at the tip. This approach is, however, more prone to strong interactions. In this work, the blade span divided into 12 elements was found to represent the best choice since, for this number of blade elements , the type of span wise spacing did not have a significant effect on the solution. At the same time, the result obtained using 8 elements was close to the result with 12 elements and a solution was obtained in 2/3 of the time. Consequently, most calculations were carried out using 8 elements.

The cut off radius R_c , which identified the extent of the vortex core, was also investigated using the Free Wake method. Values of R_c equivalent to 1% and 0.1% of the aerofoil chord gave solutions in close agreement with each other. However,

when $R_c = 0.01$ % of the aerofoil chord length was used, it was found that the Free Wake method had a non-convergent solution due to blade vortex interaction.

It was also found that aerofoil data had a significant influence on the result. The same aerofoil data for different Reynolds numbers could provide different power coefficients. Regardless of the aerofoil data used, the Prescribed Wake scheme gave a solution in good agreement with the Free Wake method.

Two Darrieus wind turbine configurations were also examined. The first configuration was already available in VDART3 and was investigated using two sets of aerofoil data. The Prescribed Wake model did not give the same results as the Free Wake method at high tip speed ratios [$\lambda > 5$]. Conversely, close agreement, in terms of detailed characteristics near the mid blade span, was achieved. This was not true at the top and bottom of the blades. Strictly speaking, the Prescribed Wake scheme produced an over prediction in Cp at high tip speed ratios. This is due to the fact that, whilst the Prescribed Wake method produces a wake at each blade element which is developed by calculating the influence of the whole wake structure on the blade element, the full three dimensionality of the problem is not fully addressed. This is because the local influence of adjacent wake elements on each other is only weakly represented by this approach. In the case of the Darrieus turbine, this local influence is likely to be very significant due to the relative strength of the wake shed from the centre of the turbine when compared to that produced near the extremities. The likely result of such a cross wake influence would be the retardation of the wake near the extremities. The fact that the Free Wake method, which includes these local effects, produced a wake which, at the turbine extremities, convected at a slower speed than those of the Prescribed Wake model, appears to confirm this.

The second type of Darrieus wind machine studied was the Sandia - 17 m wind turbine. Field results showed that the overall performance of this machine varied with the speed of rotation and hence was influenced of the value of Reynolds number experienced by the rotor blade. Two sets of data for the Naca 0015 aerofoil, at

Reynolds number Re ~ 10^6 and Re ~ 3.0 x 10^6 were, therefore, used to study this effect. These Reynolds numbers corresponded to experiments carried out on the Sandia-17 m wind machine at 38.7 and 50.6 RPM. In both cases, the Prescribed Wake scheme was found to provide results in good agreement with experiment for almost the whole range of tip speed ratio $2 \leq \lambda \leq 9$. It was clear from this analysis, that it is necessary to use aerofoil data which corresponds to a Reynolds number appropriate to that experienced by the turbine blade, if accurate predictions of performance are to be obtained.

6.2. Suggestions for Future work

- In the case of the straight bladed wind machine, the proposed Prescribed Wake method provided good agreement with the Free Wake method. A number of numerical parameters were investigated, but the work only covered one basic geometric configuration. Further assessment of the scheme for other configurations with , for example, different values of solidity may be valuable.

- The Prescribed Wake scheme, throughout this study, used a wake which consisted of 7 wake cycles. This number was chosen, since the Free Wake method, for a wide range of tip speed ratios, achieved a converged solution with 7 wake cycles. The first three wake cycles close to the rotor are important, since virtually the total induced velocity due to the vortex system comes from this part. If the rest of the wake cycles, which are quite far from the rotor blade, could be modelled in such a way that the calculation of induced velocity, on the blade, due to these cycles was simplified, it would reduce computation significantly. This approach , which is quite common in helicopter rotor modelling will be, especially , beneficial when dynamic stall effects are included in the scheme. This is true, since the inclusion of dynamic effects, via a

semi-empirical model requires high resolution of the forcing functions and hence small time steps.

- For the Darrieus wind turbine configuration, further comparison with experimental work is required for further assessment of the accuracy of the solution. Complete aerofoil data in the range $-180^{o} \leq \alpha \leq 180^{o}$, which include the effect of Reynolds number , should be provided, since the solution is sensitive to aerofoil data. Further improvement of the wake shape might be required in the case of the curved blade to include local wake effects resulting from the highly three - dimensional nature of the Darrieus wake.

- It would be valuable to do a similar numerical parameter study on the VDART3-Code as was done on the Prescribed Wake method. In particular, the manner in which the induced velocity at the mid element control point is calculated should be examined. The forward approach to the definition of shed and trailing vortices should also be applied to the method and the wake vortex strengths should be continually updated. In this way, a more precise solution may be obtained from the Free Wake method.

REFERENCES.

1. Hall R . *"Update World Population Trends"* , Cambridge University Press, Cambridge UK, 1989

2. Tapp, B.A. and Watkins, J.R. *"Energy and Mineral Resources System "*. Cambridge University Press, Cambridge UK, 1990

3. Oliver, D., Miall, H., Nectoux, F. and Opperman, M. ,*" Energy - Efficient Futures : Opening the solar Options. "* , Earth Resources Research Ltd. London, UK, 1983

4. Dept. Of Energy , Energy Paper 39. : *" Energy Technologies For The United Kingdom . "* HMSO, London 1979

5. *"World Economic Outlook "* , A Survey by The Staff of The International Monetary Fund, April 1989

6. Guilmot, J.F., MacGlue, D., Valette P., and Waterloos, C. *" Energy 2000. "* Cambridge University Press, Cambridge UK, 1986

7. Nielsen, J.H. *" Denmark's Energy Future. "*, Energy Policy, Vol.18, No. 1, January/February, 1990 pp 80-85

8. Hedly, D. *" World Energy : The Facts and The Figures. "*, 2nd Ed. Euromonitor Publication Ltd., London, 1986

9. Radetzki M. *"Plausible shocks in World Energy in the 1990s."*, Energy Policy, Vol. 17, No.4, August. 1989, pp 331-336

10. Labys, W.C. and Lesourd, J.B., *"The New Energy Markets in Modern Applied Energy Conservation."*, edited by : Jacques J.K. et al., Ellis Horwood Ltd., UK, 1988

11. Petroleum Economist, January 1990.

12. EIA/OECD : *" Energy Technology Policy "*, Paris, France, 1985

13. Ellis, L.A. " *Hydraulic Resources* ", World Energy Conference, IPC Science and Technology Press, UK, 1978

14. Crabe, D. and Macbride, R. *"The World Energy Book."*, Kogan Page Ltd., London. Uk, 1978

15. Baum, W. *"World Electricity : Watt Next in Power.* ", Petroleum Economist, January 1991

16. Crocker, V.S. [Editor] : " *OECD Electricity Generation Break Down."* Nuclear Energy. Vol. 30 No.2, April, 1991 pp. 72

17. *"Energy Balance of OECD Countries 1970/1980"*, OECD/IEA , Paris, France, 1987

18. Baum, V. " *Survey Electricity : Nuclear Power after Chernobyl."* , Petroleum Economist. November, 1987, pp 395-397

19. Simnad, M.T. *"Analysis of The Factors Contributing to One Trillion Dollars Wasted on Nuclear Power."*, J. of Energy, Vol. 14. No.9, pp. 503-511, 1989

20. Basu, A. et. al. *"Solar Derived Power* " , Handbook Of Engineering System : Production and Utilisation, ed. by : Wilbur L.C., John Wiley & Sons Inc., Canada, 1985

21. Wood, D.W. and Acharya H.K. *"Demographic* " , Handbook of Energy Systems Engineering, ed. by Wilbur L.C., John Wiley & Son, Inc. USA, 1985

22. Hubbert, M. *"The Energy Resources of The Earth* " in Scientific American Book : Energy and Power. Scientific American Inc.,USA, 1971

23. Twidell, J. and Weir, T. *"Renewable energy resources."*, E & F.N. Spon, London, 1986

24. Grubb, M.J. *"The Cinderella Options : A Study of Modernised Renewable Energy Technologies Part 1-A : Technical Assessment .* ", Energy Policy, Vol. 18, No.6, July/August 1990, pp. 525-542

25. Auer, P.L., Bos, B.P., Robert ,V.W. and Gough, W.C., " *Unconventional Energy Resources* ", World Energy Resources 1985-2020., The World Energy conference 1978, IPC Science and Technology Press, Guildford, UK, 1978

26. Edward, L.M. et. al. " *Handbook of Geothermal Geothermal Energy.*" Gulf Publ. Company, Houston, USA, 1982

27. Acharya, H.K. " *Geothermal Energy* ." , in : Handbook of Energy Systems Engineering ed. by Wilbur L.C. John Wiley & Son, Inc. USA, 1985

28. Okandon, E. *"Importance of Geothermal Engineering."*, In The assessment of Geothermal Sources in Geothermal Reservoir Engineering ed. by : Okandan, E., Kluwer Academic Publisher, Dordrecht, The Netherlands, 1988

29. Department of Energy (UK) . *"Renewable Energy In The UK : The Way Forward ."* Energy Paper No. 55, HMSO Publ., 1988

30. Government Publ. Dept. Of Energy UK. " *Renewable Energy In Britain* . " Brightman & Stratton Ltd., UK, 1989

31. Dorf, R.C. " *Energy , Resources and Policy.*" , Addison - Wesley Publ. Company, Philippines, 1978

32. Wilson, D. *"Qualifying and Comparing Fuel Cycle Green House - Gas Emission : Coal, Oil and Natural Gas Consumption."*, Energy Policy , July/August 1990

33. Wilbur, L.C. [ed.] *"Handbook of Energy Systems Engineering : Production and Utilisation"* John Wiley & Sons, Inc. Canada, 1985

34. Laughton, M.A. [editor]. *"Renewable Energy Sources."*, Watt Committee Report, Rep. Num. 22, Elsevier Science Publ. Ltd., Essex, England.

35. Weingart, J.M. *"Solar Energy as Global Energy Option For mankind."* , Solar Thermal Power Generation Conference The Royal Institution " July, 1978 , UK-ISES, London, UK, 1978

36. Duret, M.F., Phillips, G.J., Veeder, J.I. and Wolfe, W.A., *"The Contribution of Nuclear Power to World Energy Supply 1975 to 2020 "*, World Energy Resources 1985-2020. The World Energy conference 1978, IPC Science and Technology Press. Guildford, UK, 1978

37. Surrey, J. *"Beyond 1992-The single Market and EEC Energy Issue."* Energy Policy, Vol.18, No. 1, January/February, 1990, pp 42-54.

38. Eldridge, F.R. *"Wind Machines."*, 2nd ed. Van Nostrand Reinhold Company, New York, USA, 1980.

39. Jaras, T.F. *"Wind Energy 1987 : Wind Turbine Shipments and Applications "* , Stadia Inc, USA, 1987.

40. Robinson, M.L. *"The Darrieus Wind Turbine for Electrical Generation."* Aeronautical Journal, June, 1981.

41. Lipman N.H., Musgrove, J.P., and Pontin, G W-W (ed.) *"Wind the energy of the Eighties ."* , Peter Pregirinus Ltd., UK, 1982

42. Lynnete, R . *"Status of The US Wind Power Industry."*, 10th BWEA Wind Energy Conference, Mechanical Engineering Publ. Ltd., London, 1988.

43. Scheffler, R.L. and Wehrey M.C. *" Wind Power ."* , Handbook of Energy Systems Engineering : Production and Utilisation ed. by : Wilbur L.C John - Wiley & Sons, New York, 1985.

44. McVeigh J.C *" Sun Power : An Introduction The Applications Of Solar Energy. "* Pergamon Press, Oxford, England, 1977.

45. Selzer, H. *"Wind Energy : Potential of Wind Energy in The European Community An Assessment Study ."*, Series G. Vol. 2., D. Reidel Publ. Company, Dorderch, Holland, 1986.

46. Palz, W. and Schnell, W. (ed.), *"Wind Energy. "*, Series G. Vol. 1 D Reidel Publ. Company, Dorderch, Holland, 1983.

47. De Renzo *"Wind Power - Recent Developments."* , Energy Technology Review 46, USA, N.J. Noyes Data Corp., 1979

48. Hunt, V.D. *"Wind Power : A Handbook on Wind Energy Conversion Systems. "* Van Nostrand Reinhold Company, New York, USA, 1981.

49. Bedford, L.A.W. *"Wind Energy For The United Kingdom - A Status Report."*, Wind Energy Conversion , 1984, ed. by Musgrove, P.J. Cambridge University Press, UK, 1984.

50. Musgrove, P.J. *"Wind Energy Evaluation for The European Communities."* EUR 8996 EN Report. Commission of The European Communities, Luxembourg, 1984.

51. Divone, L.V. *"The Current Perspective on Wind Power Based on Recent U.S Result s."*, 3nd International Symposium Wind Energy System, Copenhagen, Denmark, 1980. BHRA Fluid Engineering, Cranfield, England, 1980.

52. Schmid, J. and Palz, W. *"European Wind Energy Technology : State of The Art of Wind Energy Converters In the European Community ."*, Series G. Vol. 3, D. Reidel Publ. Company, Dorderch, Holland, 1986.

53. Abrahamvich, H. *"Vertical Axis Wind Turbine : A Survey and Bibliography."* J. of Wind Engineering and Industrial Aerodynamic, Vol. 11,No. 6, 1987.

54. Sutton-Vane, V. *" A New Form of Straight Bladed VAWT : A Preliminary Report."* Wind Engineering Journal. Vol. 12, No. 1, 1988, pp 27-46.

55. Cheremisinoff, N.P. *" Dynamics of Wind Machines."*, in Encyclopedia of Fluid Mechanics, Vol.8 : Aerodynamics and Compressible Flows, Ed. by : Cheremisinoff, N.P., Gulf Publ. Company, Houston, 1989.

56. Fujisawa, N. and Shirai, H. *"Experimental Investigation on the Unsteady Flow Field Around a Savonius Rotor at the Maximum Power Performance."*, J. of Wind Engineering and Industrial Aerodynamic, Vol. 11, No. 4, 1987.

57. Ushiyama, I. and Nagai H. " *Optimum Design Configuration and Performance of Savonius Rotors* "., J. of Wind Engineering and Industrial Aerodynamics, Vol. 11,No. 1, 1988

58. Aldoss, T.K.and Obeidat, K.M. *"Performance Analysis of Two Savonius Rotors Running Side by Side Using The Discrete Vortex Method."* J. of Wind Engineering and Industrial Aerodynamic, Vol. 11,No. 1, 1987.

59. Ogawa, T. *"Theoretical Study on The Flow about a Savonius Rotor."* J. of Fluids Engineering Vol. 11, 1984, pp 85-91.

60. Aldoss, T.K. and Kotb, M.A. *"Theoretical Calculation of the Flow Field Around a Savonius Rotor."*, J. of Wind Engineering and Industrial Aerodynamics, Vol. 11 No. 1, 1988, pp 194-203

61. Backwell, B.F. et.al. *"Engineering Development Status of The Darrieus Wind Turbine."*, J. Energy, January. 1977, pp 50-64.

62. Mays J. D.,*"Developing the Variable geometry Vertical Axis Wind Turbine for Production."*, Proceedings of the third International Conference on Future Energy Concepts, IEE Conference Pub., 1981

63. Grylls, W., Dale, B. and Sarre, E.P. *"A Theoretical and Experimental Investigation into The Variable Pitch Vertical Axis Wind Turbine."* 2nd International Symposium on Wind Energy Systems, Amsterdam, Netherlands, 1978. BHRA Fluid Engineering, Cranfield, England, 1978.

64. Musgrove, P.J. *"The Variable Geometry Vertical Axis Windmill."* International Symposium on Wind Energy Systems, Cambridge, England , 1976. BHRA Fluid Engineering, Cranfield, England, 1976.

65. Musgrove, P.J and Mays, I.D. *"Development of the Variable Geometry Vertical Axis Windmill."*, International Symposium on Wind Energy Systems, Cambridge, England, 1978.

66. Clare, R. and Mays, I.D *"Development of the Musgrove Variable Geometry Vertical Axis Win Turbine."* , 4th International Symposium on Wind Energy Systems, Stockholm, Sweden, 1982.

67. Mays, I.D., Musgrove, J.P. and Morgan, C.A., *"The Evolution of the Straight Bladed Vertical Axis Wind turbine."*, 10th BWEA Wind Energy Conference ed. by. Milborrow D.J., 1988 Mechanical Engineering Publ. Ltd. 1988.

68. Mays, I.D.and Rhodes, H., *"Progress with The U.K Vertical Axis Wind Turbine Programme "*, European Wind Energy Conference 1984, ed. by Palz W., H.S. Stephen and Associates Publ, Bedford, England, 1985.

69. Powles, S.J.R., Anderson M.B., Harris, A. and Groechel, K., *"Results from the UK 25 m Vertical Axis Wind Turbine Programme."*, 10th BWEA Wind Energy Conference ed. by. Milborrow D.J., 1988, Mechanical Engineering Publ. Ltd. 1988.

70 Sharpe, D.J. and Taylor, D.A. " *The Aerodynamic Performance of the Vee -Type Vertical Axis Wind Turbine* " , Proc. 7th BWEA Wind Energy Workshop, March, 1985

71. Amos, G.W. and Bragg, G.M.,*"A Comparison of Analytic Prediction Methods For Vertical Axis Wind Turbines. "* EWEC, Hamburg, F.R. Germany,1984. ed. by. Palz, W., H.S. Stephens and Associates Publ. Bedford, England, 1985.

72. Simhan, K. *"A Review of Calculation Methods For The Determination of Performance Characteristics of Vertical Axis Wind Energy Converters With Special Reference to The Influence of Solidity and Starting Characteristic. "* EWEC, Hamburg, F.R. Germany,1984. ed. by. Palz W., H.S. Stephens and Associates Publ. Bedford, England, 1985.

73. Strickland, J.H. *"A Review of Aerodynamic Analysis methods for Vertical Axis Wind urbine."*, 5th. ASME Wind Energy Symposium ed. by : Swift, A.H.P., 1986.

74. Paraschivoiu, I. *"Double Multiple Stream tube Model for Studying Vertical Axis Wind Turbines."*, J. Propulsion, Vol. 4, No.4, August, 1988.

75. Wilson, R.E. and Mckie, W.R., *" A Comparison of Aerodynamic Analyses for The Darrieus Rotor."*, 2nd International Symposium on Wind Energy Systems, 1978.

76. Hirsch, Ch. and Mandal, A.C., *"Flow Curvature Effect on a Vertical Axis Darrieus Wind Turbine having High Chord-Radius Ratio."*, EWEC, Hamburg, F.R. Germany,1984. ed. by. Palz W., H.S. Stephens and Associates Publ. Bedford, England, 1985.

77. Wilson, R.E and Walker, R.N., *"Fixed Wake Theory for Vertical Axis Wind Turbines."*, ASME 83-WA/FE-14

78. Bramwell, A.R.S. *"Helicopter Dynamics."*, Edward Arnold Publ. Ltd. London, UK, 1976

79 . Graham, J.M.R. *" A Free Wake Vortex Model of the Wake of a Vertical Axis Wind Turbine"*, Wind Energy Conversion 1990, Mechanical Engineering Publications Ltd.,London, 1990

80. Anderson, J.D.Jr., *"Fundamental Aerodynamics ."* , Academic Press, New York, 1986.

81. Schlicting, H. *" Boundary Layer Theory ."* , 7th. Ed. MacGraw Hill Book Company, New York, 1979.

82. Anderson, D.A., Tannehill, J.C. and Pletcher, R.H., *" Computational Fluid Mechanics and Heat Transfer ."*, Hemisphere, New York, 1984.

83. Chapman, D.R. *"Computational Aerodynamics , Development and Outlook."* AIAA Journal, Vol. 17, 1293-1313, 1979

84. Anderson, J.D. Jr *"Short Course In Computational Fluid Dynamics ".* Lecture Series Von Karman Institute, Belgium, 1986.

85 MacCormack ,R.W., *"The Numerical Solution of The Compressible Viscous Flow Field About a Complete Aircraft .",* In Computational Methods In Viscous Flow ed. By : G.W. Habashi, Pineradge Ltd., Swansea, UK, 1984.

86. Kuttler, P. *"A Perspective of Theoretical and Applied Computational Fluid Dynamics "* AIAA J., Vol. 23, No. 3, March, 1985, pp 328-34.

87. Hayes, J.L. *"Programming of Super Computers. "*, Handbook of Numerical Heat Transfer" ed. Minkowiycs W.J. et . al. John Wiley & Son Inc., New York, 1988.

88. Hirsch, C. *" Numerical Computation of Internal and External Flow ."*, Vol. I :" Fundamental of Numerical Discretization " , John Wiley and Son, UK, 1988.

89. Peterson, V.L., Ballhaus, W.F.Jr. and Bailey, F.R., *"Numerical Aerodynamic Simulation [NAS]. "* , Ed. by Pater S.V in. Large Scale Scientific Computation , Academic Press, Inc., New York, 1984.

90 Strikwerda, J.C. *" Finite Difference Schemes and Partial Differential Equations "*, Wadsworth & Books/Cole Ltd., New York, 1990

91 Strang, G. *" On the Construction and Comparison of Difference Schemes "*. SIAM Journal of Numerical Analysis, Vol. 5, 1968

92. Pyret R. and Taylor T.D. *" Computational Methods For Fluid Flow ."* Springer Verlag, New York, 1984.

93. Sod G.A. *"Numerical Methods in Fluid Dynamics ."* Cambridge University Press, London, 1985.

94. Abbot. M.B and D.R. Bassco, *"Computational Fluid Dynamics : An Introduction For Engineers. "*, Longman Scientific and Technical, Longman Singapore Publ. Ltd., 1989.

95. Boss T.K *"Computational Fluid Dynamic. "*, John Wiley & Son, Wiley Eastern Ltd., New Delhi, 1988.

96. Baker A.J. *"Finite Element Computational Fluid Mechanics."* MacGraw-Hill Book Company Ltd., Singapore, 1985.

97. Thompson J.F., Z.U.A. Warsi and C.W Mastin ,*" Numerical Grid Generation : Foundation and Applications "*., Elsevier Science Publ. Co. Inc, 52 Vanderbilt Avenue, New York , 1985.

98. Sarpkaya, T. " *Computational Methods With Vortices-The Freeman Scholar Lecture .*" Journal of Fluids Engineering, Vol. 111, March 1988.

99 Leonard, A. " *Review : Vortex Methods for Flow Simulation.* " Journal of Computational Physic, Vol. 37, 1980.

100 Stepniewski W.Z. and Keys C.N. " *Rotary Wing Aerodynamics .* " Dover Publ. Inc., USA, 1984.

101 Johnson W. " *Helicopter Theory .*" , Princeton University Press. New Jersey, USA, 1980.

102 Fletcher C.A.J. *"Computational Techniques for Fluid Dynamics ."* Springer-Verlag, New York, 1988

103 Nixon, D. " *Basic Equation for Unsteady Transonic Flow .",* in Unsteady Transonic Aerodynamics . Progress In Astronautics and Aeronautics Vol. 20, ed. by : Nixon D, American Institute of Aeronautics and Astronautics, Washington D.C, 1989.

104 Caradonna F.X. and Strawn R., *"An Experimental and Computational study of Rotor -Vortex interactions.",* Vertica Vol. 12, No. 4 pp 315-327, 1988.

105 Jones H.E. and Caradonna F.X. *"Full Potential Modelling of Blade Vortex Interaction."* Vertica Vol. 12, No.1/2 pp 129-145, 1988

106 Caradonna F.X. *"Application of Transonic Flow Analysis to Helicopter Rotor Problems for Unsteady Transonic Flow .* " , in Unsteady Transonic Aerodynamics., Progress In Astronautics and Aeronautics Vol.20, ed. by : Nixon D, American Institute of Aeronautics and Astronautics, Washington D.C, 1989.

107 Wake B.E. and Sankar L.N., *"Solution of The Navier Stokes Equations for The flow about a Rotor Blade."* Journal of American Helicopter Soc., April, pp 12-23, 1989.

108 Davis S.S and Chang I-C., *"The Critical Role of Computational Fluid Dynamics In Rotary Wing Aerodynamics."* Vertica Vol. 11. no1/2, pp 43-63,1987.

109 Johnson W. *"Recent Development in Rotary Wing Aerodynamic Theory."* AIAA Journal, Vol. 24, No. 8, August, 1986, pp 1219-1245.

110 Gostelaw, J.P. *" Cascade Aerodynamics "*, Oxford Pergamon Press, UK, 1984.

111 Birch N.T, Northall J.D and Stow P. *"Navier Stokes Method For Turbo-machinary Blade Design."*, Computational Methods In Aeronautical Fluid Dynamics, ed. by. P. Stow, Oxford Science Publ. Claredon Press, Oxford, 1990.

112 Rizzi, A. and Muller, B. *"Vortex flow modelling With Euler and Navier Stokes Equations. "* , Computational Method In Aeronautical Fluid Dynamics, ed. by. P. Stow, Oxford Science Publ., Claredon Press, Oxford, 1990.

113 Morino L. et al. *" Free wake Analysis of Helicopter Rotors. "*, Vertica Vol. 9, No. 2, 1985.

114 Grabel A. and Rosen A. *"A Parametric Investigation of Free Wake Analysis of Hovering Rotors."* Vertica, Vol. 12, No. 1/2, 1988.

115 Quakenbush T.R. and Bliss D.B *"Free Wake Flow Field Calculation for Rotor craft Interactional Aerodynamics. "*, A.H.S. Forum, 1984

116 Miller , R.H. *" A Simplified Approach to the Free Wake Analysis of a Hovering Rotor ."* Vertica, Vol. 6, 1982

117 Konstandipoulos P. et al. *"Vortex lattice method for general Unsteady Aerodynamics."* J. of Aircraft, January, 1985, pp 43-49.

118 Afjeh, A.A. and Keith, T.G. Jr. *" A Simplified Free wake Method for Horizontal Axis Wind Turbine Performance Prediction. "*, Journal of Fluids Engineering, Vol. 108, Dec. 1986.

119 Rosen, A., Lavie, I. and Seginer, A.“ *A General Free Wake Efficient Analysis of Horizontal Axis Wind Turbines.* “ Wind Engineering, Vol. 14, No. 6, 1990.

120 Strickland, J.H., Webster, B.T. and Nguyen, T. *“A Vortex Model of The Darrieus Turbine : An Analytical and Experimental Study . “* J . of Fluids Engineering, Vol. 101, Dec. 1979.

121 Strickland, J.H. *“A Performance Prediction Model for the Darrieus Turbine “* International Symposium on Wind Energy System, Sept. 1976.

122 Musgrove P.J. *“Aerodynamics of Vertical Axis Wind Turbines.”*, Lecture Note, University of Reading.

123 Strickland, J.H., Smith, T. and Sun, K. *“A Vortex Model of The Darrieus Turbine : An Analytical and Experimental Study . “* Sandia Report SAND81-7017, June 1981.

124 Yamane T. Tsutsui Y. and Orita T., *“The Aerodynamic Performance of a Horizontal Axis Wind Turbine in Large Induced Velocity state.”* 4th International Symposium on Wind Energy System , Stockholm , Sweden, 1982.

125 Anderson M.B , Milborrow D.J and Ross J.N., *“Performance and Wake Measurements on A-3M Diameter Horizontal Axis Wind Turbine : Comparison of Theory, Wind Tunnel and Field Test. “*, 4th International Symposium on Wind Energy System , Stockholm , Sweden, 1982.

126 Sharpe, D.J. *“Refinements and Development of the Multiple Stream Tube Theory for the Aerodynamic Performance of the Vertical Axis Wind Turbine.”* Proc. 6nd BWEA Wind Energy Conference , University of Reading, U.K, 1984.

127 Read, S. and Sharpe, D.J., *“An extended multiple stream tube theory for vertical axis wind turbines.”*, Proc. 2nd BWEA Wind Energy Workshop , Cranfiled U.K, 1980.

128 Paraschivoiu, I. “ *Aerodynamic Loads and Performance of the Darrieus Rotor* “ AIAA J. Energy , Vol. 6, No. 4, Nov.-Dec. 1982.

129 Read, S. and Sharpe D.J., *" A Critical Analysis of the Extended Multiple Stream Tube Theory for Vertical Axis Wind Turbine."*, Proc. Wind and Solar Energy Conference , Kansas City , Miss, 1982

130 Paraschiviou, I. and Delclaux *" Double Multiple Streamtube Model with Recent Improvements"*, J. of Energy, Vol. 7, No. 3, 1982.

131 Speziale, C.G. *" On the Advantage of the Vorticity-Velocity Formulation of the Equations of Fluid Dynamics "* J. of Computational Physics, Vol. 73, 1987

132 Hall , J.F. *" An Introduction to The Vortex Break Down and Vortex Core. "* Aeronautics Note NAE-AN-28, NCR No. 24336, March 1985, Ottawa.

133 Clements, R.R. *" Flow Representation, Including a Separated Region Using Discrete Vortices."* AGARD LS-86, 1977.

134 Leonard, A. *" Computing Three Dimensional Incompressible Flow s With Vortex Elements."* Ann. Rev. Fluid Mechanic, Vol. 17, 1985.

135 Inomura, T., Saito, T. and Adachi, T. , *" A Numerical Analysis of Unsteady Separated Flow by the Discrete Vortex Method Combined With a Singularity Method. "*, Computer and Structures, Vol. 19, No. 1-2, 1984.

136 Beale J.T. and Mayda, A. *" Vortex Method II : Higher Order Accuracy in Two and Three Dimensions ."* Mathematics Computation, Vol. 39, 1982.

137 Anderson, C. and Greengard, C. *" On Vortex Methods "*, SIAM J. of Numerical Analysis, Vol. 22, No. 3, June, 1985.

138 Klimas, P.C. *"Vertical Axis Wind turbine Aerodynamic Performance Prediction Methods ."* Proceedings of the Vertical Axis Wind Turbine Design Technology Seminar for Industry, New Orleans, August 1980.

139 Holme, O. *" A Contribution to The Aerodynamic Theory of the Vertical Axis Wind Turbine."*, Proceeding. of the International Symposium on Wind Energy System, St. John's College, England, 1976.

140 Sharpe, D.J. *" A Vortex Flow Model for the Vertical Axis Wind Turbine."* 1st BWEA Workshop, 1979.

141 Wilson R.E. *" Vortex Sheet Analysis of The Giro Mill ."* Journal Of Fluids Engineering, Vol. 100, September, 1978.

142 Vadenberghe, D. and Dick, E. *" A Theoretical and Experimental Investigation into The straight Bladed Vertical Axis Wind Turbine With a Second Harmonic Pitch Control. "* Wind Engineering Vol. 10. No. 3, 1986.

143 Oran, E.S. and Boris, J. P. *" Numerical Simulation of Reactive Flow. "* Elsevier, New York, 1987

144 Anderson, M.B. *" A Vortex Wake Analysis of a Horizontal Axis Wind Turbine and a Comparison With a Modified Blade Element Theory. "* Third International Symposium on Wind Energy Systems, Denmark, August 1980.

145 McCormick, B.W. Jr. *" Aerodynamics of V/STOL Flight ."*, Academic Press, New York, 1967.

146 Kocurek, J.D. and Tangler , J.L *" A Prescribed Wake Lifting Surface Hover Performance Analysis."* 32nd Ann. National Forum of the Helicopter Society, Washington D.C., May 1976.

147 Landgrebe, A.J. *" The Wake Geometry of a Hovering Helicopter Rotor and Its Influence on Rotor Performance ."* , J. of the American Helicopter Society, Vol. 17, No. 4, 1972.

148 Hoeijmakers H.W.M. *" Methods for Numerical Simulation of Leading Edge Vortex Flow ."*, in Studies of Vortex Dominated Flows ed. by : Hussaini, M.Y., and Salas, M.D., Springer-Verlag, 1985.

149 Basuno, B., Coton, F.N. and Galbraith, R.A.McD. *"On the Aerodynamic Modelling of Vertical Axis Wind Turbines ."*, Aerodynamic Aspects of Wind Energy Convertors, London, 1990 (IMECHE).

150 Beddoes, T.S. *" A Synthesis of Unsteady Aerodynamic Effects Including Stall Hysteresis ."* , Vertical, Vol. 1, 1976.

151 Gangwani S.T. " *Prediction of Dynamic Stall and Unsteady Airloads for Rotor Blades.* ", Proc. 37th Ann. Forum American Helicopter Soc., New Orleans, 1981.

152 Tran, C.T. and Petot, D. " *Semi Empirical Model for the Dynamic Stall of Airfoils in View of the Application to the Calculation of the Responses of a Helicopter Blade in Forward Flight.* ", Vertica, Vol. 5, 1981.

153 Bertin, J.J. and Smith, M.L. " *Aerodynamic for Engineers .*" Prentice-Hall, Inc., Englewood Cliffs, New York, 1979

154 Wilson, R.E., Lissaman P.B.S., James, M. and Mckie, W.R., " *Aerodynamic Loads on a Darrieus Rotor Blade .*", J. of Fluids Engineering, Vol. 105, March 1983

155 Sheldahl, R.E. and Klimas, P.C. " *Aerodynamic Charecteristics of Seven Symmetrical Airfoil SectionsThrough 180-Degree Angle of Attack for Use in Aerodynamic Analysis of Vertical Axis Wind Turbines.* " Sandia National Labs., SAND80-2114, March 1981

156 Klimas, P.C. " *Darrieus Rotor Aerodynamics .*", J. of Solar Energy Engineering, Vol. 104, May 1982.

157 Worstell, M.H. " *Aerodynamic Performance of the DOE/Sandia 17-M-Diameter Vertical Axis Wind Turbine* ", AIAA J. Energy, Vol. 5, No. 1, Jan.-Feb. 1981.

158 Noll, R.B and Ham, N.D. " *Effects of Dynamic stall on SWECs .*" J. of Solar Energy Engineering, Vol. 104, May 1982.

159 Carr, L.W. " *Progrees in Analysis and Prediction of Dynamic Stall .* " J. Aircraft, Vol. 25, January 1988.

160 McCroskey, W.J. " *The Phenomenon of Dynamic Stall* " Nasa TM-81264, March 1981

161 Galbraith R.A.McD . " *Comments on the Prediction of Dynamic Stall* " G.U. Aero Report 8501, Univ. of Glasgow, March 1985

162 Reddy T.S.R. and Kaza K.R.V., *" A Comparative Study of Some Dynamic Stall Models "* , NASA-TM-88917, 1988

163 Vandenberghe, D. and Dick, E. *" Performance Optimazation of Vertical Axis Wind Turbines by Pitch Control "* in Encyclopedia Fluid Mechanics, Vol.8 : Aerodynamics and Compressible Flows, Ed. by : Cheremisinoff, N.P., Gulf Publ. Company, Houston, 1989

164 Wilson, R.E. and Walker, S.N. , *"Fixed Wake Analysis of the Darrieus Rotor "*, Sandia National Labs., SAND81-7026, 1981

Table 1.1 : EEC energy consumption 1980 and 1987 in MTOE

	1980	1987
A. Final energy by sector:		
- Industry	245	215
- Transport	170	199
- Homes, shops and offices	278	289
Total	693	703
B. Final energy by fuel :		
- Solid fuel	63	58
- Oil products	397	365
- Gas	127	155
- Electricity	102	120
- Heat	4	5
total	693	703
C. Primary fuel :		
- Coal	238	230
- Oil	551	477
- Natural Gas	171	196
- Nuclear	46	136
- Hydro	17	17
total	1023	1061

source : Surrey, J., [37]
MTOE : Million Tonnes of Oil Equivalent.

Table 1.2 : Total world energy consumption for 1972-1983 and estimated demand for 1990 and 2000.

Year	MTOE	% change from previous year
1972	5630.7	4.3
1973	5923.2	5.2
1974	5964.5	0.7
1975	5968.0	0.1
1976	6291.4	5.4
1977	6490.6	3.2
1978	6707.7	3.3
1979	6944.3	3.5
1980	6812.3	-0.6
1981	6771.2	-0.6
1982	6744.3	-0.4
1983	6832.0	1.3
1990*)	8346.0	-
2000*)	10761.0	-

Source : Ref. 1

*) : estimated value

Table 1.3 : Distribution of world energy consumption

Year	MTOE					
	Oil	Coal	Nat. Gas	Nuclear	Hydro	Total
1972	2592.4	1629.4	1045.0	38.4	325.5	5630.7
%	46.0	28.9	18.6	0.7	5.8	100 %
1976	2894.4	1786.4	1141.0	106.4	362.5	6291.4
%	46.0	28.4	18.1	1.7	5.7	100 %
1980	3001.5	2006.5	1306.1	169.4	420.2	6903.7
%	43.5	29.1	18.9	2.4	6.1	100 %
1982	2818.8	2041.2	1312.1	216.6	446.0	6836.7
%	41.2	29.9	19.2	3.2	6.5	100 %
1983	2794.0	2097.1	1328.9	236.3	469.2	6925.5
%	40.3	30.3	19.2	3.4	6.8	100 %
1990*)	3008.0	2586.6	1652.0	504.4	595.0	8346.0
%	36.3	30.4	20.0	6.1	7.2	100 %
2000*)	3333.0	3560.0	2286.0	857.0	725.0	10761.0
%	30.9	33.1	21.3	8.0	6.7	100 %

Source : Hedly, D.[8].

* : estimated value.

Table 1.5 : Historical development times of some selected technologies

Technology	Time from Scientific Demonstration to First Commercial Unit (years)	Additional Time Required to Capture Significant Percentage of the Market (years)
Nuclear	16	20
Diesel Engines	60	30 - 50
Pulverised Coal Combustion	25	15 - 18
Solar Heating	60	30 (variable)
Low Head Hydropower	50	20 - 30
Heat Pumps	30	20

Source : EIA/OECD, [12].

Table 1.6 : Average cost of electricity production for various power plant ($1984)

Type of plant	Hydro	Nuclear [PWR 2x1100 MW]	Coal [2x600MW]	Oil [2x600MW]
Investment	1000	1300	1000	750
Discount rate	5%	5%	5%	5%
Construction	5 years	10 years	4 years	3 years
Operating costs (per Kw)	$2/year	$5/year	$5/year	$4.2/year
Fuel cost (per Kw)	-	$9/year	$20/year	$43/year
Average cost ($/Kw-h)	0.023	0.031	0.036	0.036

Source : Lasby, W.C. and Lesourd, J.B.[10]

Table 1.7 : World production and reserves of primary energy

Type Resources	Rate of production	Reserves
Oil	3150 MTOE [1990][1]	96 000 MTOE [1987][5]
Natural gas	1927 10^9 m^3 [1986][4]	110 683 10^9 m^3 [1988][3]
Coal :		
Anthracite+bituminous	3.23 10^9 Tons[1988][4]	559 10^9 Tons [1988][4]
Sub-bituminous+lignite	1.46 10^9 Tons(1988][4]	443 10^9 tons [1988][4]
Nuclear [uranium]	37 000 Tons [1988][4]	2.196 10^9 Tons [1978][6]
Hydro power	2.12 10^{12} KWh[1989][2]	19.19 10^{12} KWh[1980][7]

Source :

1. Petroleum Economist, January, 1990 [11]
2 Lasby, W.C and Lesourd, J.B.[10]
3. Petroleum Economist, August, 1991 [15]
4 Wilson, D. [32]
5. Petroleum Economist, November, 1987 [18]
6 Duret, M.F. et. al. [36]
7 Wood, D.W. et al. [21] [Technical usable potential at 50% load factor]

Note :

The relation between coal and natural gas with respect to crude oil can be deduced as follows [32] :

1 MTOE = 1.5 10^6 Tonnes Anthracite + Bituminous coal
= 3.0 10^6 Tonnes Sub-bituminous + lignite
= 111.1 10^9 m^3 Natural Gas .

Table 1.8 : A comparison of capital cost, overall efficiency and the cost of power output amongst renewable resources.

Renewable Resources	Capital Cost $/Kw	Overall Load Factor (%)	Generation cost pence/Kw-h
wind energy	600.0	53.51	1.35
OTEC	4400.0	82.86	9.25
Geothermal-HDR	2563.0	81.0	4.22
Tidal	845.0	20.27	3.23
Geothermal-Doublet	1718.0	81.00	3.01
Offshore wave calm	840.0	21.25	5.0
Inshore wave	830.0	29.40	3.17
Solar active	500.0	10.38	7.15
solar process heat	500.0	10.49	6.57
solar-passive	200.0	11.39	1.66
solar-photovoltaic	6000.0	11.04	1.82

source : Laugthon, M.A. (Editor) [34]

Table 1.9 Quality of wind resource.

Annual mean wind speed V_a at 10 m height	Indicated level of wind source
$V_a < 4.5$ m/s	poor
4.5 m/s $< V_a <$ 5.4 m/s	marginal
5.4 m/s $< V_a <$ 6.7 m/s	good to very good
$V_a > 6.7$ m/s	exceptional

Source : Cheremisinoff, N.P.[55]

Table 3.1 Aerofoil Data NACA 0015 at Reynolds Number Re = 3.0 x 10^6

α (deg)	C_l	C_d	α(deg)	C_l	C_d
-70.1	- 0.673	1.802	70.1	0.673	1.802
-60.2	- 0.914	1.634	60.2	0.914	1.634
-50.2	- 1.101	1.392	50.2	1.101	1.392
-40.2	- 1.185	1.064	40.2	1.185	1.064
-35.2	- 1.161	0.892	35.2	1.161	0.892
-30.1	- 1.065	0.682	30.1	1.065	0.682
-28.1	- 1.000	0.598	28.1	1.000	0.598
-26.1	- 0.923	0.515	26.1	0.923	0.515
-24.1	- 1.270	0.260	24.1	1.270	0.260
-22.1	- 1.309	0.208	22.1	1.309	0.208
-20.0	- 1.090	0.0859	20.0	1.090	0.0859
-19.0	- 1.14	0.0775	19.0	1.14	0.0775
-18.0	- 1.19	0.0691	18.0	1.19	0.0691
-17.0	- 1.24	0.0607	17.0	1.24	0.0607
-16.0	- 1.37	0.0525	16.0	1.37	0.0525
-15.0.	- 1.38	0.0349	15.0.	1.38	0.0349
-14.0	- 1.34	0.0355	14.0	1.34	0.0355
-13.0	- 1.27	0.0286	13.0	1.27	0.0286
-12.0	- 1.19	0.0236	12.0	1.19	0.0236
-11.0	- 1.09	0.0210	11.0	1.09	0.0210
-10.0	- 1.00	0.0193	10.0	1.00	0.0193
- 9.0	- 0.90	0.0180	9.0	0.90	0.0180
- 8.0	- 0.80	0.0168	8.0	0.80	0.0168
- 7.0	- 0.71	0.0157	7.0	0.71	0.0157
- 6.0	- 0.61	0.0147	6.0	0.61	0.0147
- 5.0	- 0.51	0.0139	5.0	0.51	0.0139
- 4.0	- 0.42	0.0131	4.0	0.42	0.0131
- 3.0	- 0.32	0.0124	3.0	0.32	0.0124
- 2.0	- 0.22	0.0118	2.0	0.22	0.0118
- 1.0	- 0.09	0.0105	1.0	0.12	0.0111
0.0	0.02	0.0106			

source : Dept. of Aerospace Eng. Univ. of Glasgow.

Tip Speed rat.	MVDART3 - Code	PRESWK - Org.
2	0.1387	0.1402
3	0.4336	0.4684
4	0.4769	0.5723
5	0.4445	0.6020
6	0.3572	0.5589
7	0.2215	0.4933

Table 4.1 A comparison of power coefficients between the Free Wake method [MVDART3] and PRESWK - Org.

Tip speed rat.	MVDART3 - Code	SDMST.	PRESWK - SDMST
2	0.1387	0.1363	0.1402
3	0.4336	0.4540	0.4533
4	0.4769	0.4841	0.5028
5	0.4445	0.4412	0.4745
6	0.3572	0.3316	0.3745
7	0.2215	0.1643	0.2448

Table 4.2 A comparison of power coefficients between the Free Wake method [MVDART3] , SDMST and PRESWK -SDMST.

Tip speed rat.	MVDART3 - Code	DDMST.	PRESWK - DDMST
2	0.1387	0.1354	0.1389
3	0.4336	0.4557	0.4526
4	0.4769	0.5288	0.5338
5	0.4445	0.5088	0.4982
6	0.3572	0.4201	0.4391
7	0.2215	0.2874	0.3280

Table 4.3 A comparison of power coefficients between the Free Wake method [MVDART3] , DDMST and PRESWK -DDMST .

Tip speed rat.	MVDART3-Cd	PRESWK-DDMST.	PRESWK-DDMST-D
2	0.1387	0.1389	0.1391
3	0.4336	0.4526	0.4462
4	0.4769	0.5338	0.4781
5	0.4445	0.4982	0.4292
6	0.3572	0.4394	0.3168
7	0.2215	0.3280	0.5142

Table 4.4 A comparison of power coefficients between the Free Wake method [MVDART3], PRESWK - DDMST and PRESWK - DDMST - D.

Tip speed rat.	MVDART3 - Code	P - DDMST.	P - INCON - Y1
2	0.1387	0.1389	0.1386
3	0.4336	0.4526	0.4399
4	0.4769	0.5338	0.4698
5	0.4445	0.4982	0.4002
6	0.3572	0.4394	0.4154
7	0.2215	0.3280	0.2766

Table 4.5 A comparison of power coefficients between the Free Wake method [MVDART3], PRESWK -DDMST and PRESWK-INCON-Y1.

Tip speed rat.	MVDART3 - Code	P -INCON-Y1	P-INCON -Y2
2	0.1387	0.1389	0.1386
3	0.4336	0.4399	0.4354
4	0.4769	0.4698	0.4448
5	0.4445	0.4002	0.3690
6	0.3572	0.4154	0.3919
7	0.2215	0.2766	0.2401

Table 4.6 A comparison of power coefficients between the Free Wake method [MVDART3], PRESWK-INCON-Y1 and PRESWK-INCON-Y2.

T.s.r .	MVDART3	P-I-(Y1+X)	P-I-(Y2+X)	P-I-(Y1)+X	P-I-(Y2)+X
2	0.1387	0.1386	0.1386	0.1387	0.1836
3	0.4336	0.4418	0.4398	0.4386	0.4344
4	0.4769	0.4807	0.4710	0.4807	0.4598
5	0.4445	0.4266	0.4045	0.3930	0.3503
6	0.3572	0.3628	0.3398	0.3412	0.2897
7	0.2215	0.2138	0.1568	0.1867	0.1074

Table 4.7 A comparison of power coefficients between the Free Wake method [MVDART3], PRESWK- INCON - (Y1+X), PRESWK-INCON-(Y2+X), PRESWK-INCON-(Y1)+X and PRESWK-INCON-(Y2)+X.

T.s.r .	MVDART3	P-DDMST	P-DDMST-(Y1+X)	P-DDMST-(Y2+X)
2	0.1387	0.1389	0.1386	0.1385
3	0.4336	0.4526	0.4456	0.4437
4	0.4769	0.5338	0.4991	0.4902
5	0.4445	0.4982	0.4628	0.4437
6	0.3572	0.4394	0.3628	0.3398
7	0.2215	0.3280	0.2138	0.1567

Table 4.8 A comparison of power coefficients between the Free Wake Method [MVDART3], PRESWK -DDMST , PRESWK - DDMST - (Y1+X) and PRESWK - DDMST - (Y2+X).

T.s.r .	MVDART3	P-D-(Y2+XN1)	P-DDMST-(Y1+X2)	P-DDMST-(Y2+X3)	P-DDMST (Y2+X4)
2	0.1387	0.1388	0.1386	0.1386	0.1386
3	0.4336	0.4340	0.4329	0.4329	0.4325
4	0.4769	0.5912	0.4850	0.4851	0.4813
5	0.4445	0.4676	0.4578	0.4581	0.4524
6	0.3572	0.4985	0.3804	0.3807	0.3713
7	0.2215	0.2746	0.2369	0.2373	0.2245

Table 4.9 A comparison of power coefficients between the Free Wake Method [MVDART3] and PRESWK - DDMST +(Y2+XNi) , i=1,2, ..., 4 versions.

Tip Speed rat.	MVDART3 - Cd	P.-D.-(Y2+XN4)	P.-D.-(Y2+XN4)-M
2	0.1387	0.1386	0.1399
3	0.4336	0.4338	0.4186
4	0.4769	0.4813	0.4469
5	0.4445	0.4524	0.4180
6	0.3572	0.3713	0.3336
7	0.2215	0.2245	0.1930

Table 5.1 A comparison of power coefficients between the Free Wake method [MVDART3], PRESWK-DDMST-(Y2+XN4) and PRESWK-DDMST -(Y2+XN4)-M.

Tip Speed ratio	MVDART3 - Cd		P.-D.-(Y2+XN4)		P.-D.-(Y2+XN4)-M	
	u.s	c.s	u.s	c.s	u.s	c.s
2	0.1387	-	0.1386	0.1369	0.1399	0.1396
3	0.4336	-	0.4338	0.4370	0.4186	0.4282
4	0.4769	0.4850	0.4813	0.4858	0.4469	0.4665
5	0.4445	-	0.4524	0.4626	0.4180	0.4418
6	0.3572	0.3766	0.3713	0.3958	0.3336	0.3742
7	0.2215	0.2193	0.2245	0.2631	0.1930	0.2490

u.s : uniform spacing; c.s : cosine spacing

Table 5.2 A comparison of power coefficients between the Free Wake method [MVDART3] , PRESWK-DDMST-(Y2+XN4) and PRESWK -DDMST -(Y2 +XN4) -M in respect with type of spacing

Case at Tip speed ratio $\lambda = 7$

Rotational Calculation Numbers	Uniform spacing			Cosine Spacing		
	NBE=8	12	16	8	12	16
1	1.0397	1.0134	1.0136	1.0638	1.0073	1.0449
2	0.6412	0.6326	0.6432	0.6629	0.6277	0.6616
3	0.4554	0.4397	0.4413	0.4744	0.4376	0.4669
4	0.3371	0.3249	0.3146	0.3347	0.3178	0.3408
5	0.2827	0.2733	0.2716	0.2831	0.2753	0.2935
6	0.2624	0.2558	0.2531	0.2660	0.2545	0.2735
7	0.2361	0.2315	0.2286	0.2332	0.2289	0.2465
8	0.2215	0.2190	0.2089	0.2193	0.2103	0.2341

Table 5.3a The rate of convergence of power coefficient in the MVDART3 Code [Free Wake method] in relation to blade spacing at tip speed ratio $\lambda = 7$

Case at Tip speed ratio $\lambda = 4$

Rotational Calculation Numbers	Uniform spacing			Cosine Spacing		
	NBE=8	12	16	8	12	16
1	0.7554	0.7461		0.7701	0.7438	0.7618
2	0.5865	0.5772		0.5991	0.5753	0.5916
3	0.5259	0.5189		0.5294	0.5125	0.5267
4	0.5030	0.4976		0.5083	0.4929	0.5061
5	0.4884	0.4858		0.4977	0.4835	0.4969
6	0.4812	0.4814		0.4894	0.4780	0.4917
7	0.4791	0.4781		0.4866	0.4745	0.4880
8	0.4769	0.4752		0.4850	0.4723	0.4853

Table 5.3b The rate of convergence power coefficient in the MVDART3 Code [Free Wake method] in relation to blade spacing a tip speed ratio $\lambda = 4$.

Case at tip speed ratio $\lambda = 7$

Code name	Type span wise spacing	NBE	NTI	Cp's result
MVDART3-CODE :				
	uniform	8	16	0.2215
	uniform	12	16	0.2190
	uniform	16	16	0.2089
	cosine	8	16	0.2193
	cosine	12	16	0.2103
	cosine	16	16	0.2341
	uniform	8	24	0.2048
	cosine	8	24	0.2098
PRESWK-DDMST -(Y2+XN4) :				
	uniform	8	16	0.2245
	uniform	12	16	0.2212
	uniform	16	16	0.2447
	cosine	8	16	0.2631
	cosine	12	16	0.2162
	uniform	8	24	0.2374
	cosine	8	24	0.2449
	uniform	8	32	0.2201
	uniform	12	24	0.2221
PRESWK-DDMST -(Y2+XN4) - M :				
	uniform	8	16	0.1930
	uniform	12	16	0.2281
	cosine	8	16	0.2490
	cosine	16	16	0.2433
	uniform	8	24	0.2387
	uniform	8	32	0.2329
	uniform	12	24	0.2338
	cosine	12	24	0.2508

Table 5.4 A comparison of power coefficient Cp between the Free Wake method [MVDART3], PRESWK-DDMST-(Y2+XN4) and PRESWK -DDMST - (Y2 +XN4) -M versions in respect of numerical parameter effects at tip speed ratio $\lambda = 7$.

Case at tip speed ratio $\lambda = 4$

Code name	Type span wise spacing	NBE	NTI	Cp's result
MVDART3-CODE :				
	uniform	8	16	0.4769
	uniform	12	16	0.4752
	cosine	8	16	0.4850
	cosine	12	16	0.4723
	cosine	16	16	0.4853
	uniform	8	24	0.4706
	cosine	8	24	0.4822
PRESWK-DDMST -(Y2+XN4) :				
	uniform	8	16	0.4813
	uniform	12	16	0.4676
	cosine	8	16	0.4858
	cosine	16	16	0.4840
	uniform	8	24	0.4685
	cosine	8	24	0.4821
PRESWK-DDMST -(Y2+XN4) - M :				
	uniform	8	16	0.4469
	uniform	12	16	0.4845
	cosine	8	16	0.4669
	uniform	8	24	0.4803
	uniform	8	32	0.4763

Table 5.5 A comparison of power coefficient Cp between the Free Wake method [MVDART3], PRESWK-DDMST-(Y2+XN4) and PRESWK -DDMST -(Y2 +XN4) -M versions in respect of numerical parameter effects at tip speed ratio $\lambda = 4$.

Tip Speed ratio	MVDART3 - Cd (*)	P.-D.-(Y2+XN4)	P.-D.-(Y2+XN4)-M
2	0.1387	0.1345	0.1299
3	0.4336	0.4268	0.4324
4	0.4769	0.4676	0.4845
5	0.4445	0.4378	0.4527
6	0.3572	0.3568	0.3672
7	0.2215	0.2212	0.2281

(*) : MVDART3-Code with uniform NBE = 8 and NTI = 16

Table 5.6 A comparison of power coefficient Cp between the Free Wake method [MVDART3] , PRESWK-DDMST-(Y2+XN4) and PRESWK - DDMST - (Y2+XN4) -M versions with uniform NBE = 12 and NTI =16.

Tip Speed ratio	MVDART3 - Cd Rc = 0.001R	P.-D.-(Y2+XN4) Rc = 0.001 R	P.-D.-(Y2+XN4) Rc=0.0001 R
2	0.1387	0.1386	0.1385
3	0.4336	0.4338	0.4252
4	0.4769	0.4813	0.4702
	0.4780*)		
5	0.4445	0.4524	0.4588
6	0.3572	0.3713	0.3686
7	0.2215	0.2245	0.2432
	0.2392*)		

*) : MVDART3-Code with Rc = 0.0001 R

Table 5.7 A comparison of power coefficient Cp between the Free Wake method [MVDART3] and PRESWK-DDMST-(Y2+XN4) with variation of R_c.

Tip Speed ratio	MVDART3 - Cd	P.-D.-(Y2+XN4)	P.-D.- Old wake
2	0.1255	0.1276	-
3	0.3335	0.3386	-
4	0.3931	0.4054	-
5	0.3803	0.4160	0.3997
6	0.3127	0.3401	-
6.5	0.2554	0.3055	0.2768
7	0.2095	0.2402	0.2089

Table 5.8a A comparison of power coefficient between the Free Wake method [MVDART3] and PRESWK-DDMST-(Y2+XN4) for a Circle Arc Darrieus wind turbine with Naca 0015 airfoil section

Tip Speed ratio	MVDART3 - Cd	P.-D.-(Y2+XN4)
2	-	0.0036
3	-	0.0692
4	0.2465	0.2492
5	-	0.3352
6	0.2472	0.2886
7	0.1547	0.2344

Table 5.8b A comparison of power coefficients between the Free Wake method [MVDART3] and PRESWK-DDMST-(Y2+XN4) for a Circle Arc Darrieus wind turbine with Naca 0012 airfoil section.

Tip Speed ratio	Field data of the Sandia-17 m Rpm : 38.7	50.6	P.-D.-(Y2+XN4) Eppler dt	Glasgow U. dt
2	0.0660*)	-	0.0501	-
3	0.2047	0.2086	0.2282	0.2102
4	0.3543	0.3584	0.3805	0.3687
5	0.4173	0.3976	0.3970	0.3870
5.5	0.4409	0.4015	0.4352	0.3804
6	0.4606	0.4094	0.4422	0.3744
6.5	0.4527	0.3976	0.4462	0.3641
7	0.4370	0.3700	0.4200	0.3295
7.5	0.4724	0.3464	0.4060	0.3103
8	0.4094	0.3228	0.3800	0.2517
9	0.2952	0.2519	0.3102	0.1296

*) : extrapolate

Table 5.9 A comparison of power coefficient Cp between PRESWK - DDMST -(Y2 + XN4) and the field data for the Sandia-17m Darrieus Wind turbine.

Stall Parameter	Effect
Airfoil shape	Large in some cases
Mach number	Small below M ~ 0.2
	Large above M ~ 0.2
Reynolds number	Small at low Mach number
	Unknown at high Mach number
Reduced frequency	Large
Mean angle, amplitude	Large
Type of motion	Virtually unknown
Three dimensional effects	Virtually unknown
Tunnel effects	Virtually unknown

Source : McCrosky W.J. Ref. 160

Table 5.10 Importance of Dynamic Stall Parameters

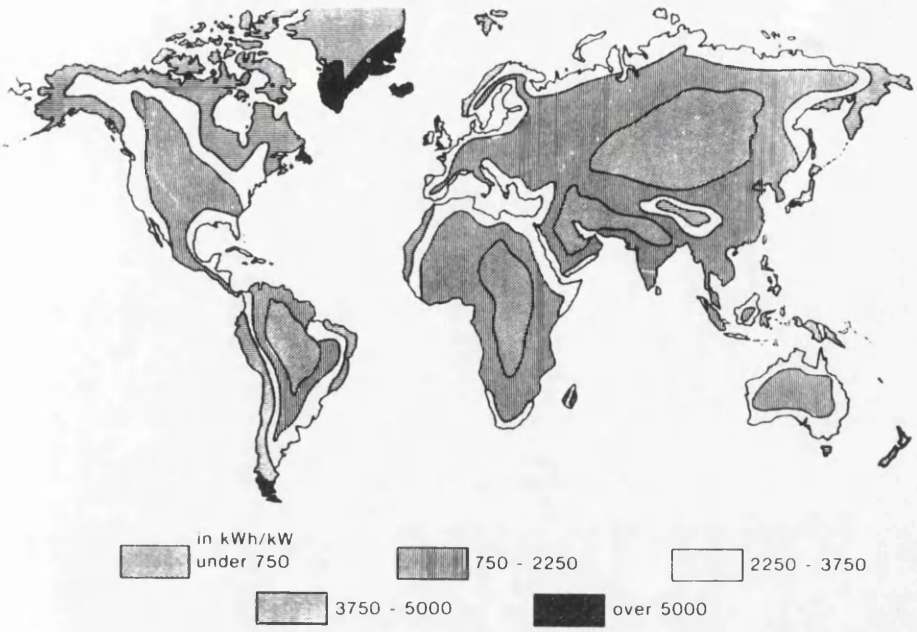

Fig. 1.1 Annual availability of wind energy in different part of the world [Ref. 40].

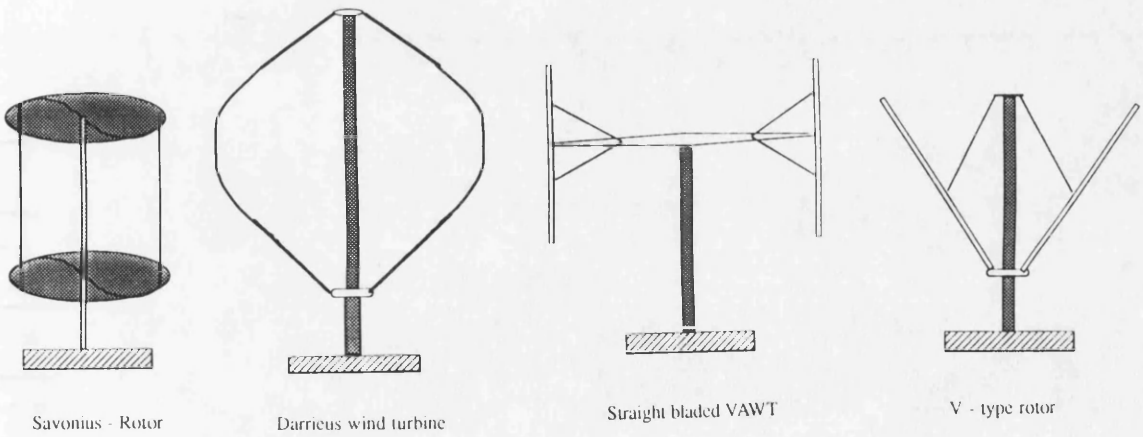

Fig. 1.2 Schematic configuration of typical vertical axis wind machines.

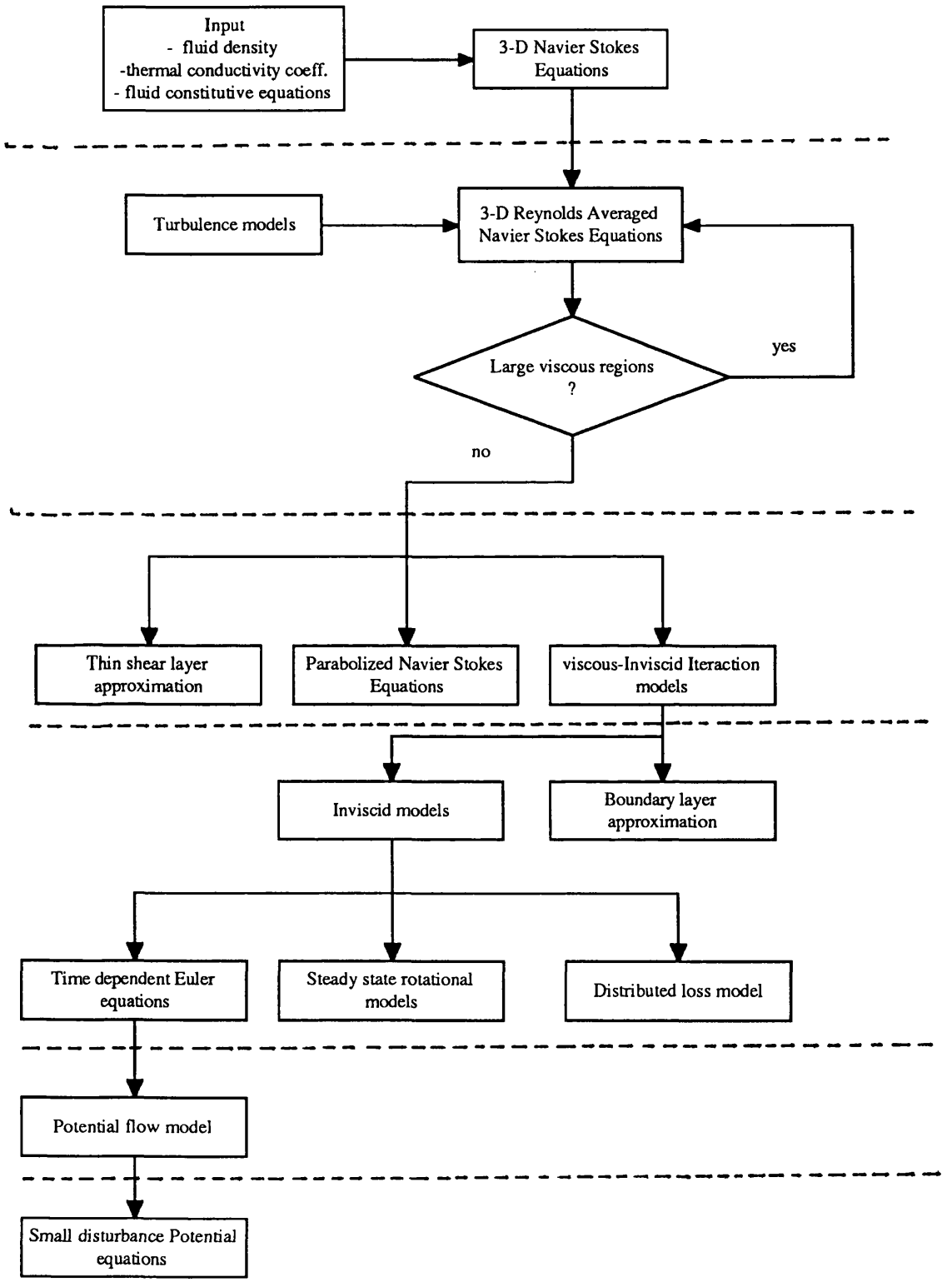

Fig. 2.1 Levels of governing equations in fluid dynamic flow problems [Ref. 88].

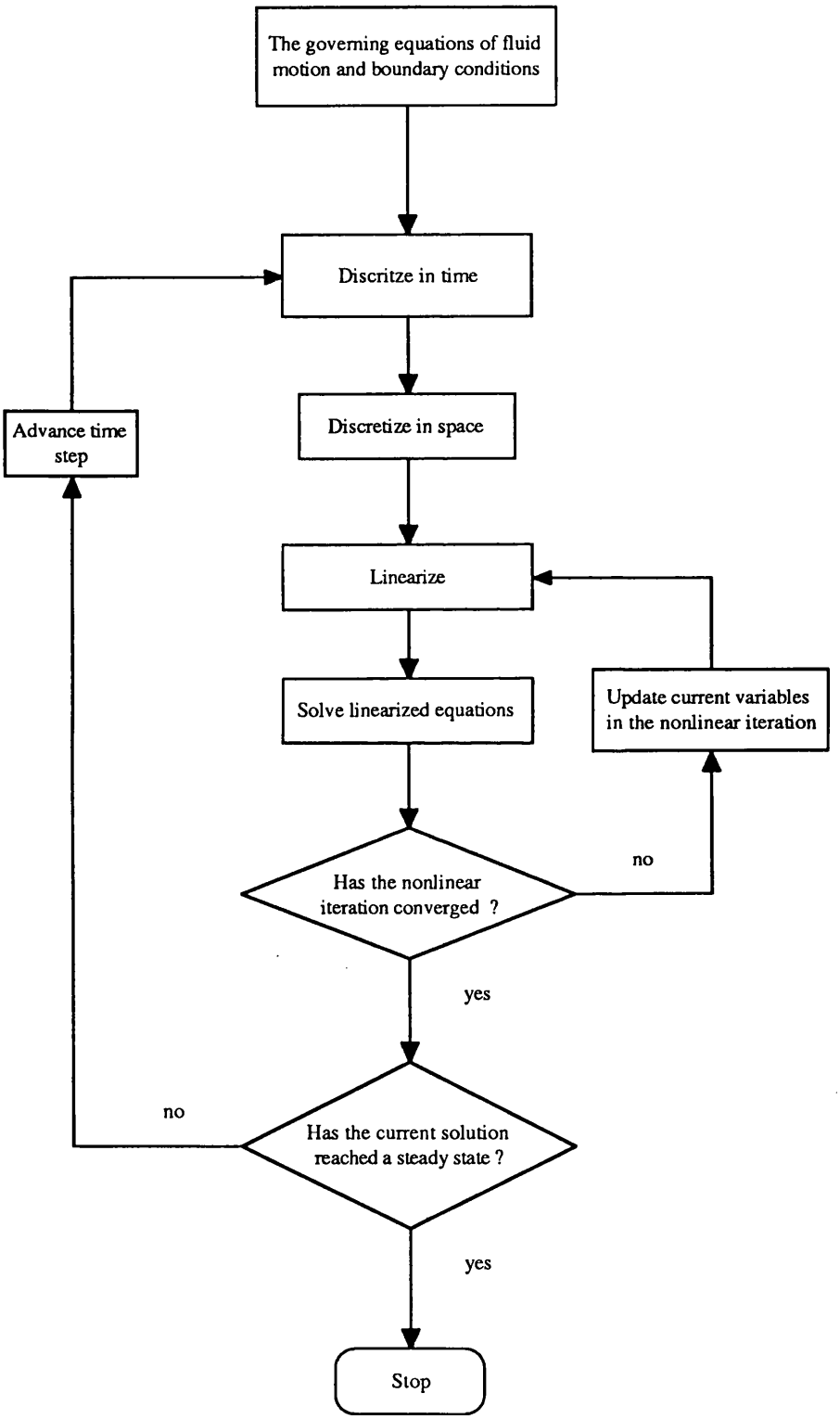

Fig. 2.2 Flow diagram of the solutions of governing equations in Computational Fluid Dynamics.

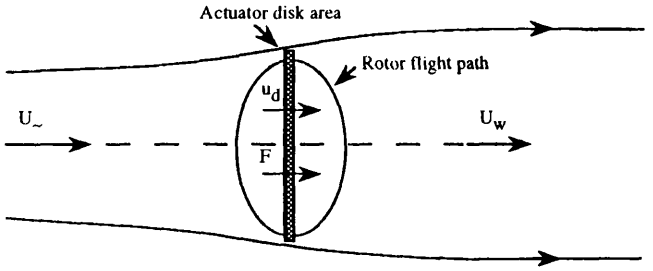

(a) Single disk single stream tube model

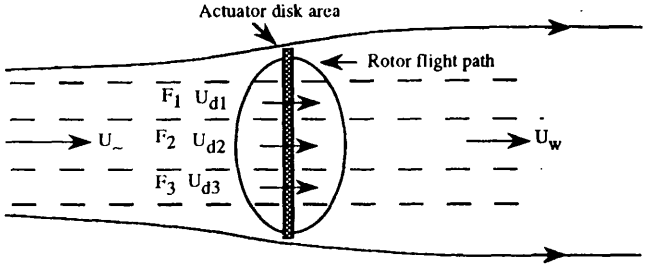

(b) Single disk multiple stream tubes model

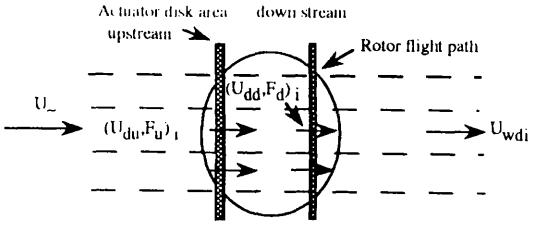

(c) Double disk multiple stream tubes model

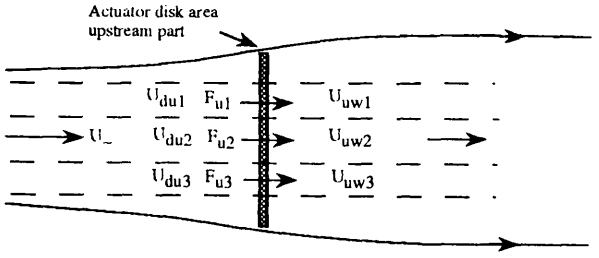

(c1) Schematic upstream part

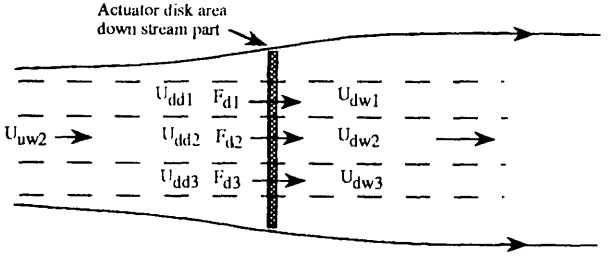

(c2) Schematic down stream part

Fig. 2.3 The Stream tube models.

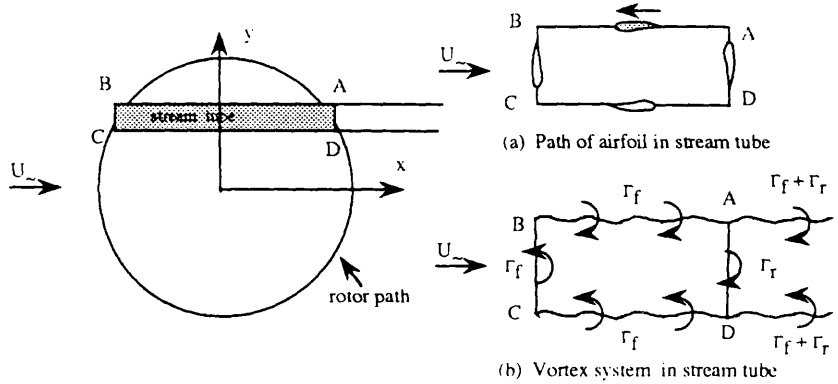

Fig. 2.4 Fixed Wake model due to Wilson and Walker [Ref. 77].

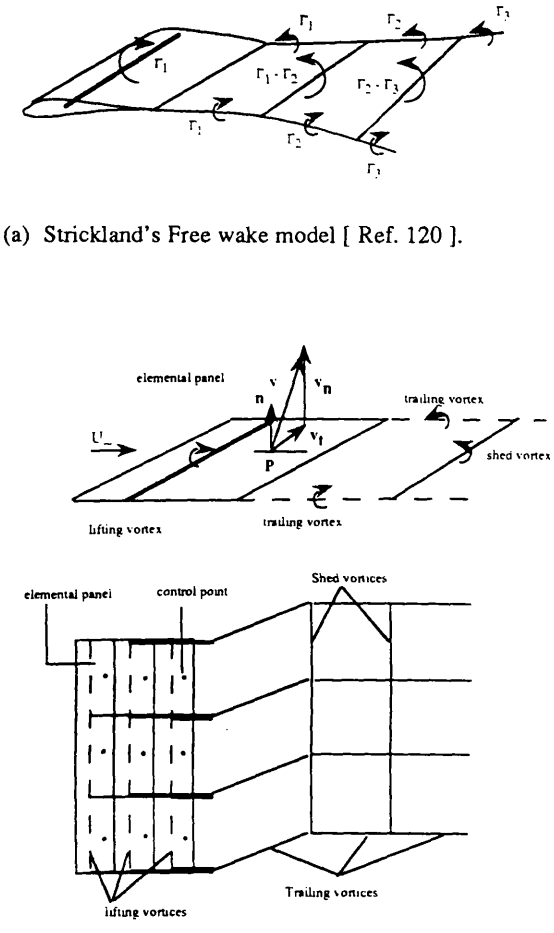

Fig. 2.5 Two types of Free Wake model for VAWT.

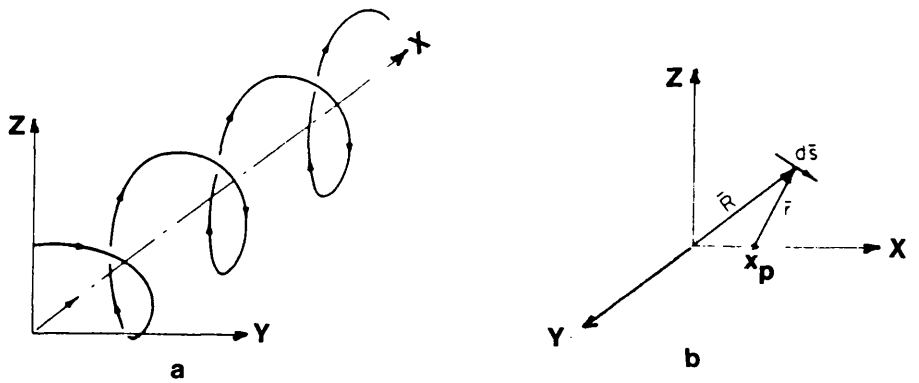

Fig. 2.6 The geometry of a helical vortex of the propeller.

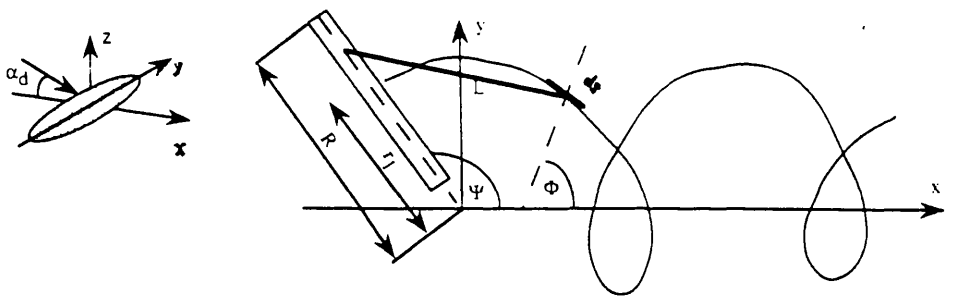

Fig. 2.7 Plan view of vortex filament of the helicopter rotor in forward flight.

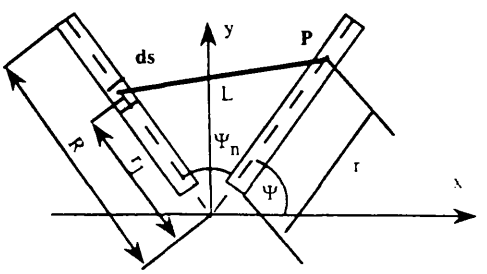

Fig. 2.8 Effect of bound vortex on succeeding blade.

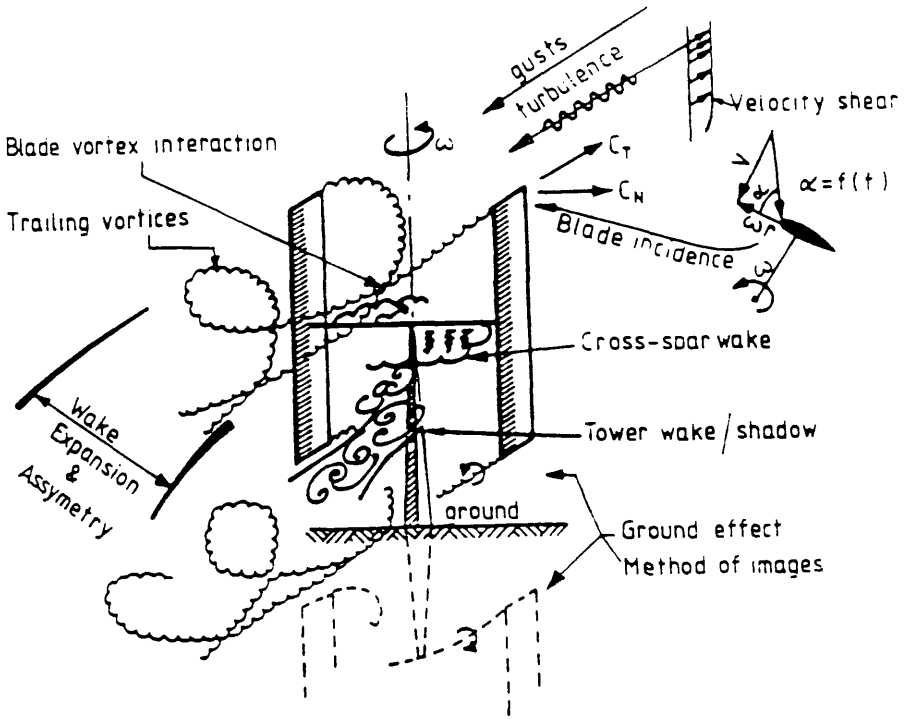

Fig. 3.1 Physical flow phenomena around vertical axis wind turbines.

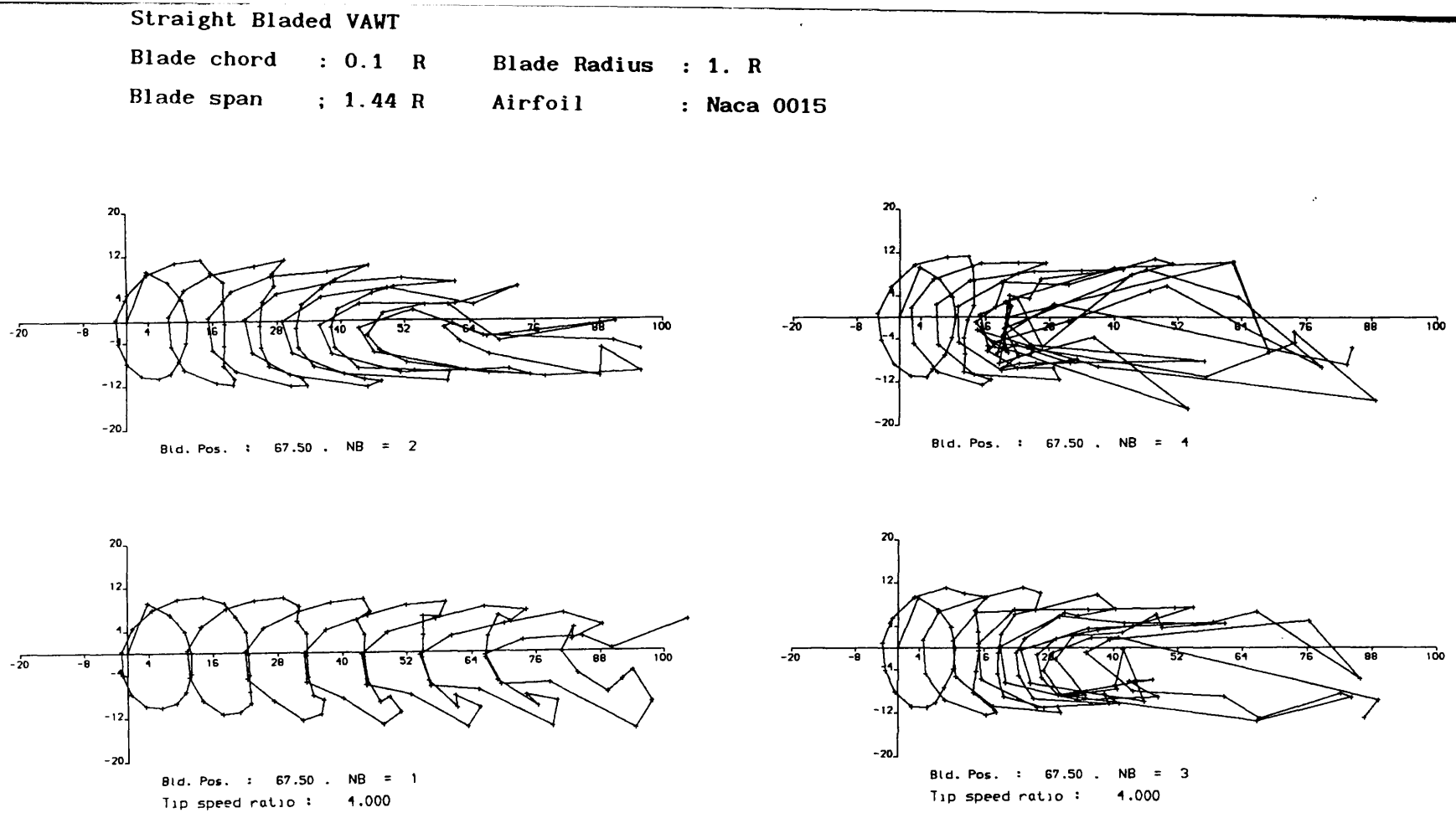

Fig. 3.2 Typical wake shape produced by the Free wake method [MVDART3-Code] for straight bladed VAWT with different numbers of blade at λ=4.

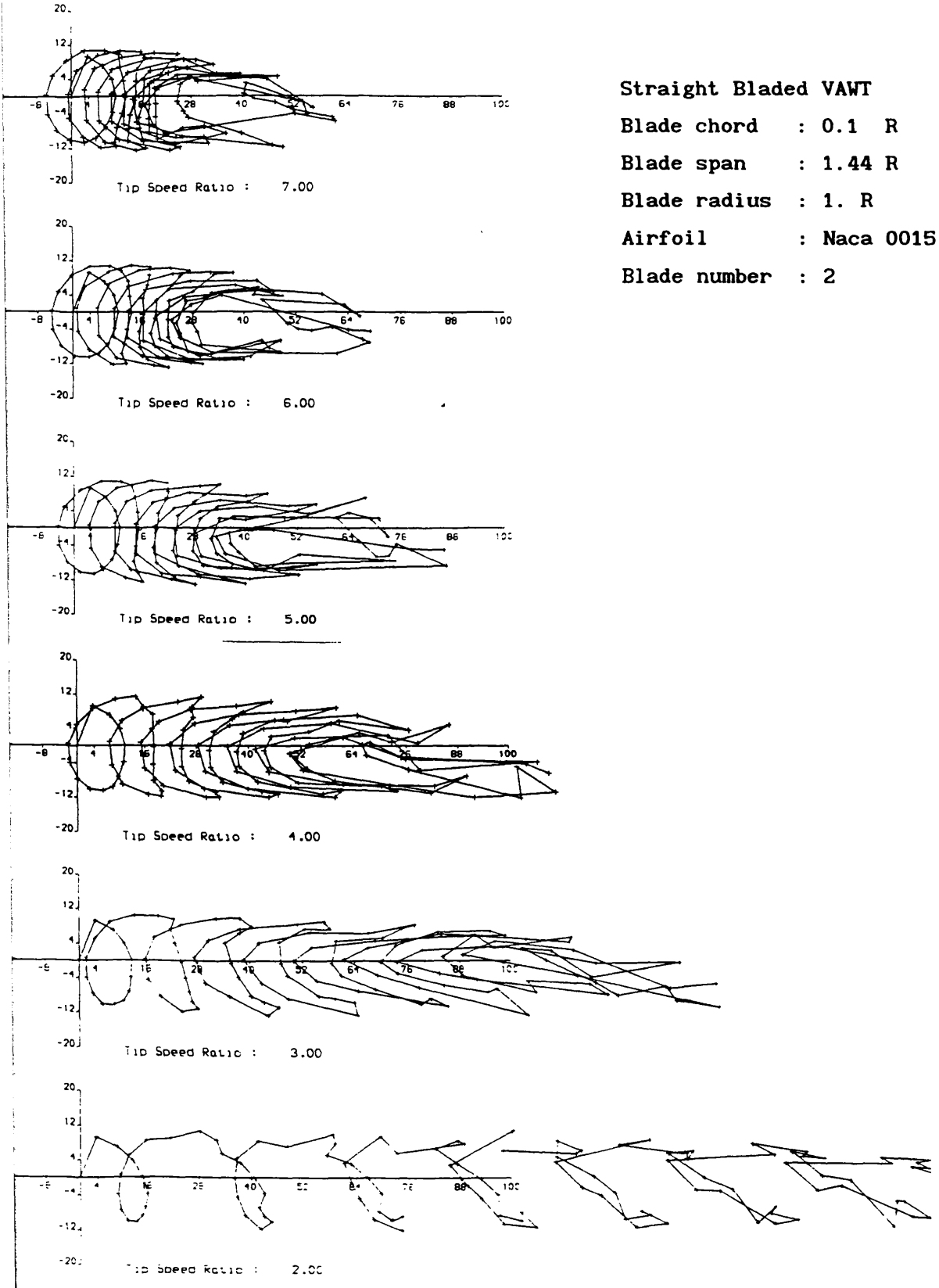

Fig. 3.3 Wake shape for two blade VAWT at different values of tip speed ratio.

Blade chord	: 0.1 R	Blade radius	: 1. R
Blade span	: 1.44 R	Airfoil	: Naca 0015
Blade number	: 2	Tip speed rat.	: 4

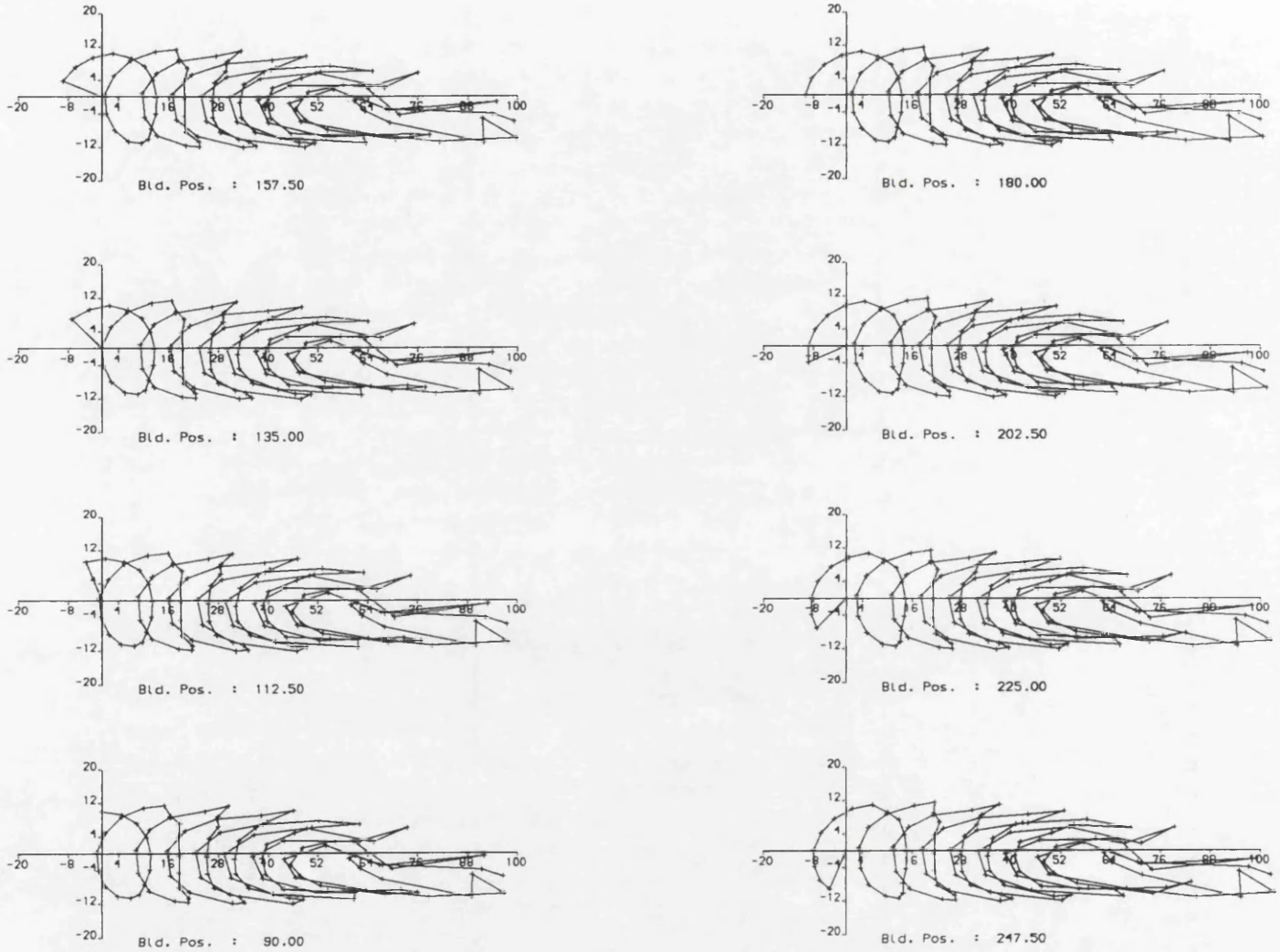

Fig. 3.4a Wake shape development with changing azimuth position at $\lambda = 4$.

Blade chord	: 0.1 R	Blade radius	: 1. R
Blade span	: 1.44 R	Airfoil	: Naca 0015
Blade number	: 2	Tip speed rat.	: 4

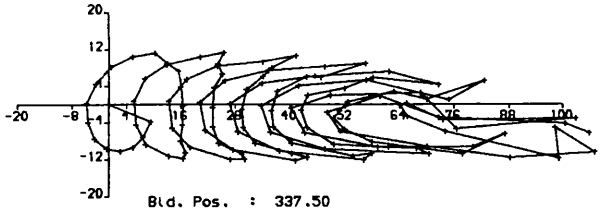

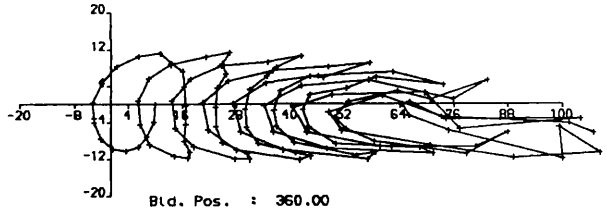

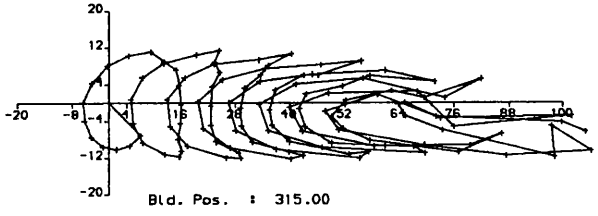

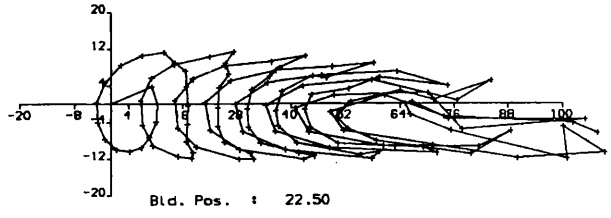

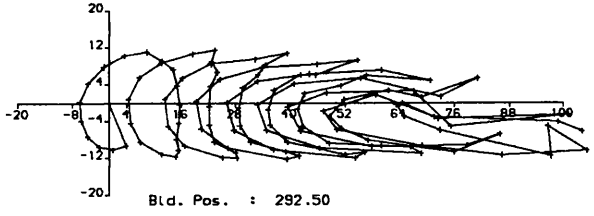

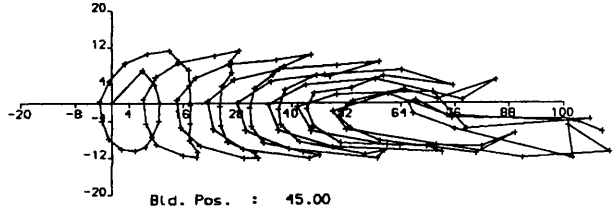

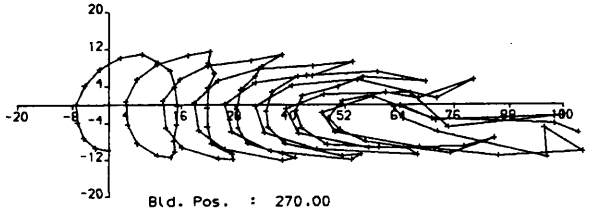

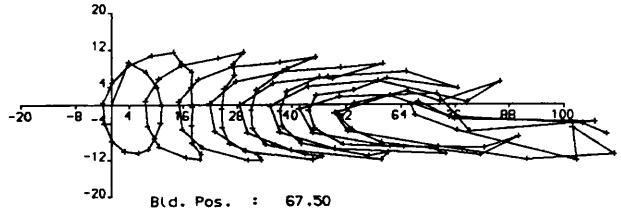

Cont'n from Fig. 3.4a.

27-JAN-92

Straight Bladed VAWT — Blade radius : 1. R
Blade chord : 0.1 R — Airfoil : Naca 0015
Blade span : 1.44 R — Blade number : 2

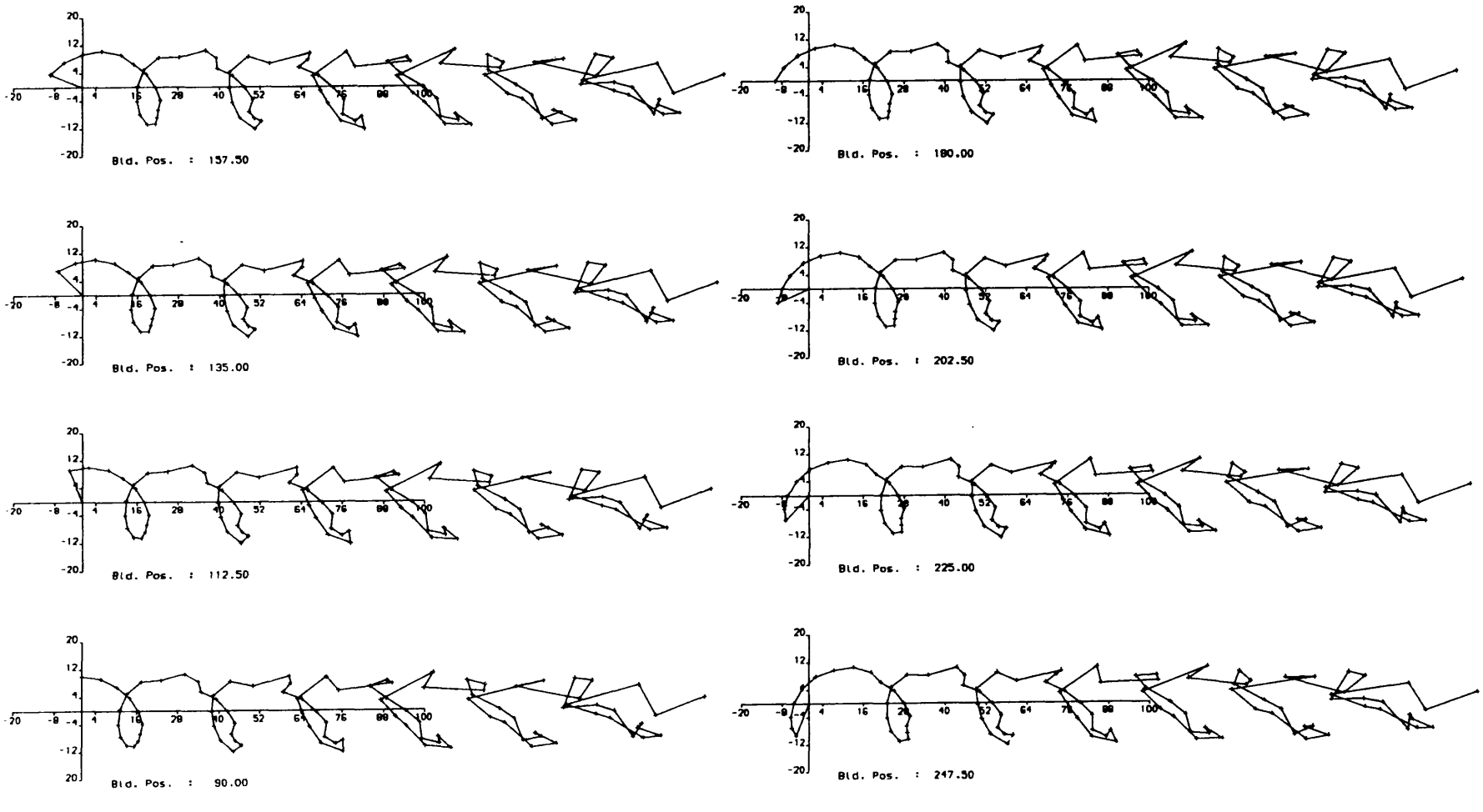

Fig. 3.4b Wake shape development with changing azimuth position at $\lambda = 2$.

Straight Bladed VAWT | Blade radius : 1. R
Blade chord : 0.1 R | Airfoil : Naca 0015
Blade span : 1.44 R | Blade number : 2

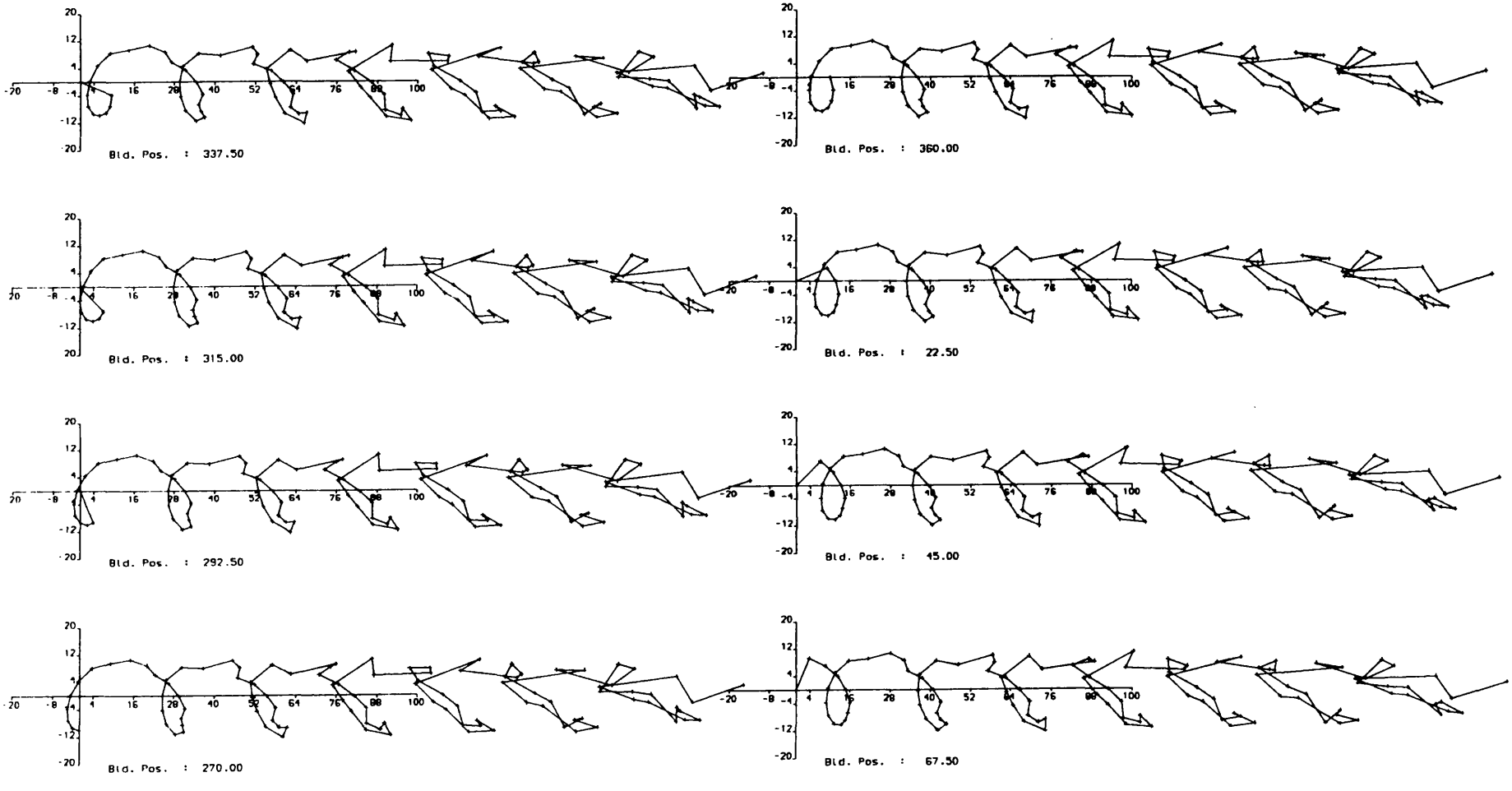

Cont'n from Fig. 3.4b

Straight Bladed VAWT | Blade radius : 1. R
Blade chord : 0.1 R | Airfoil : Naca 0015
Blade span : 1.44 R | Blade number : 2

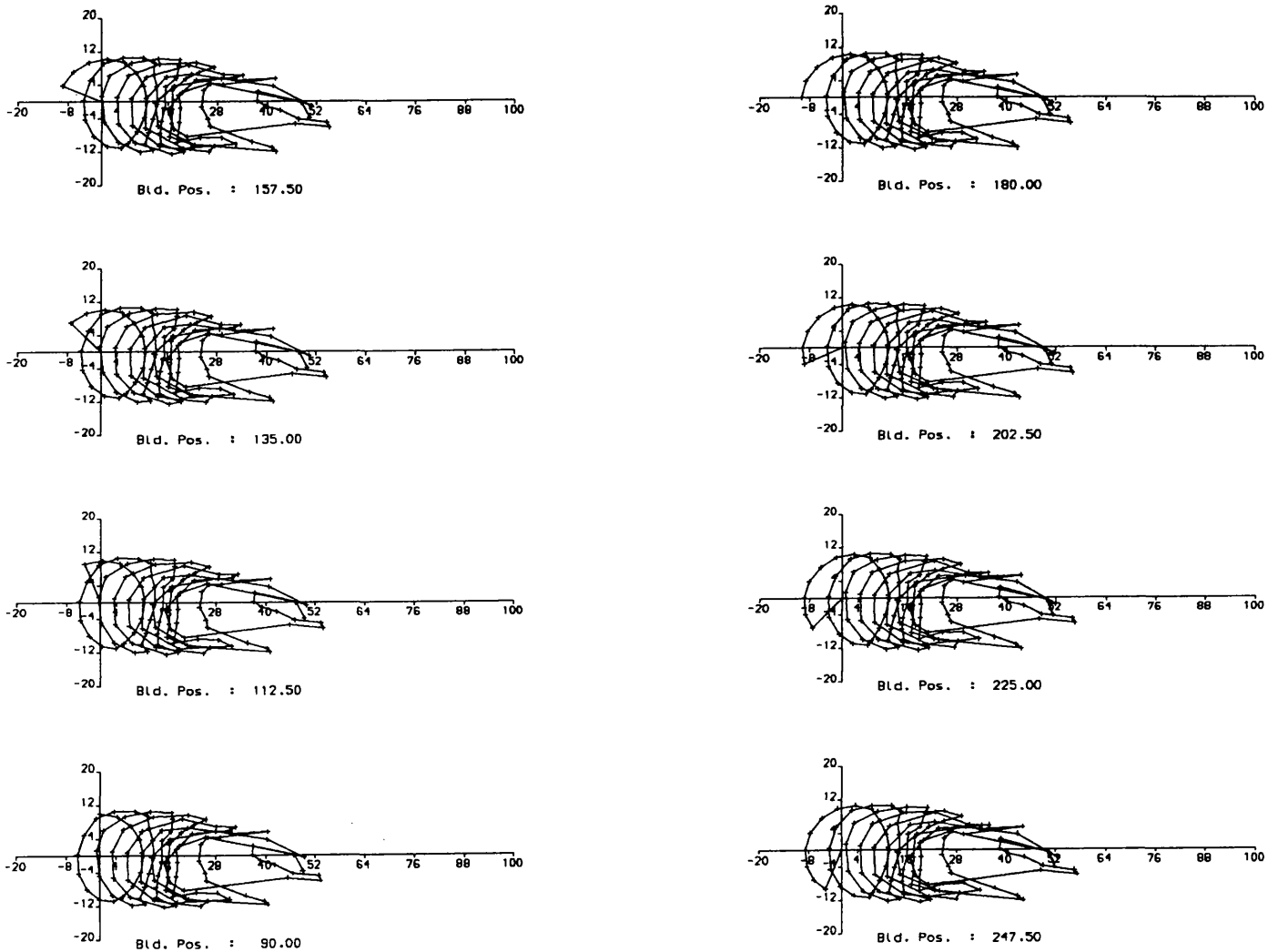

Fig. 3.4c Wake shape development with changing azimuth position at $\lambda = 7$.

Straight Bladed VAWT | Blade radius : 1. R
Blade chord : 0.1 R | Airfoil : Naca 0015
Blade span : 1.44 R | Blade number : 2

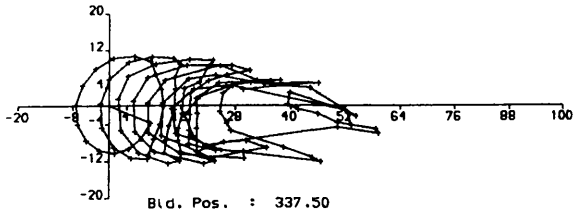

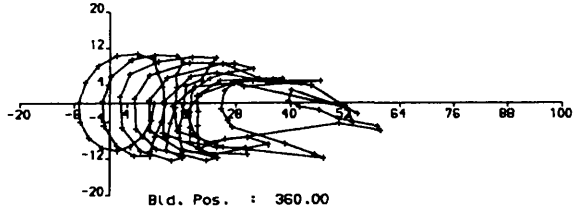

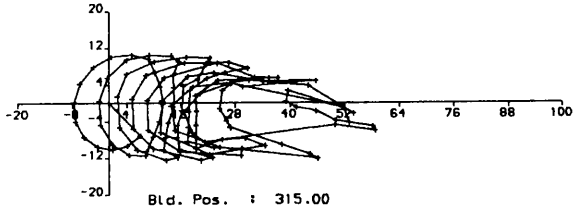

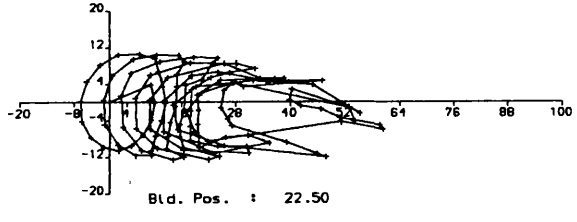

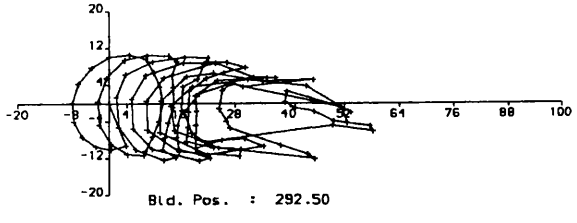

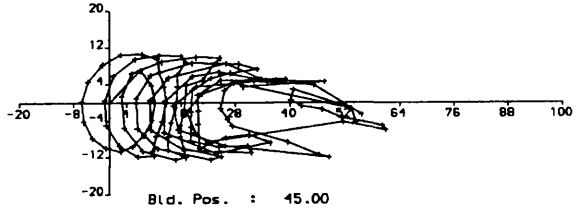

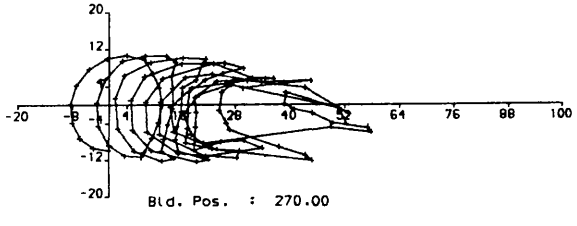

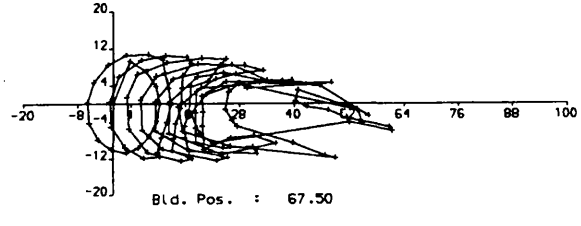

19-SEP-91

Cont'n from Fig. 3.4c

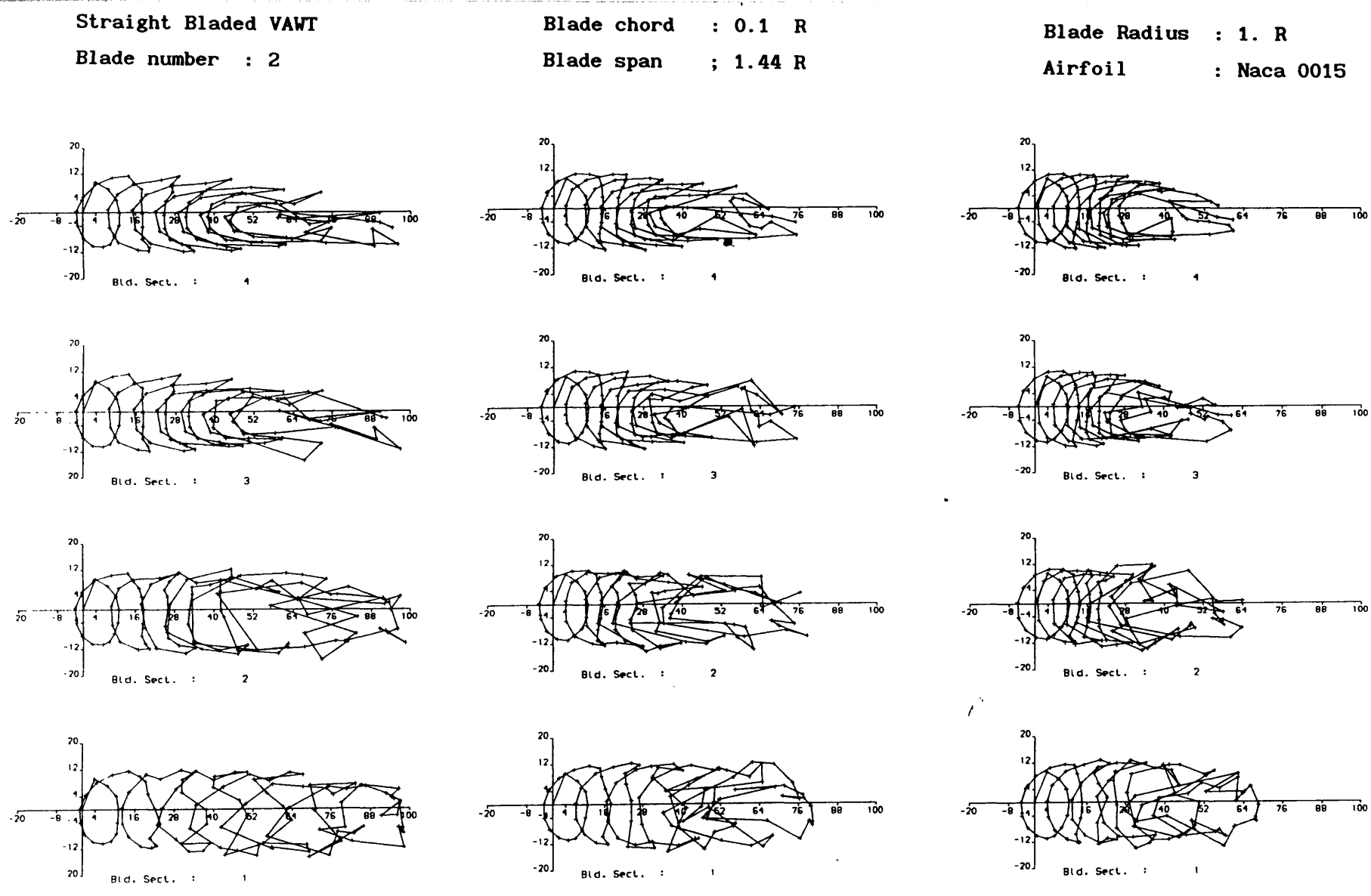

Fig. 3.5 Variation in wake shape along half blade at three different tip speed ratios.

Straight Bladed VAWT		Blade radius	: 1. R
Blade chord	: 0.1 R	Airfoil	: Naca 0015
Blade span	: 1.44 R	Blade number	: 2

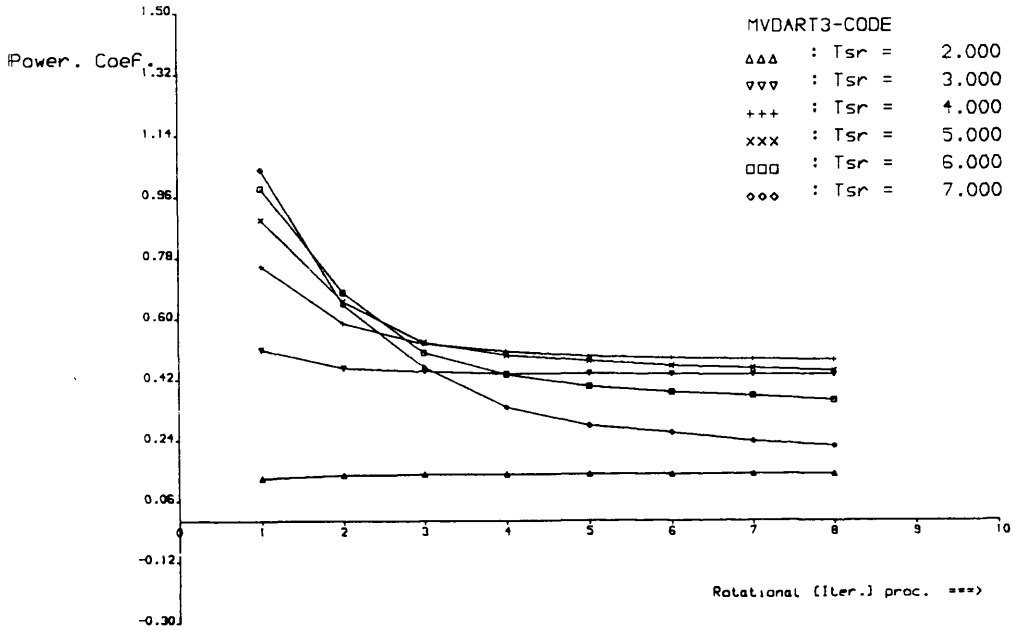

Fig. 3.6 Typical rate of convergence of the Free wake method [MVDART3-Code] for different tip speed ratios.

17-SEP-91

Straight Bladed VAWT — Blade radius : 1. R
Blade chord : 0.1 R — Airfoil : Naca 0015
Blade span : 1.44 R — Blade number : 2

+ + + : VDART3-CODE TSR = 2
[Cp = 0.139]
× × × : MVDART3-CODE TSR = 4
[Cp = 0.477]
□ □ □ : MVDART3-CODE TSR = 7
[Cp = 0.222]

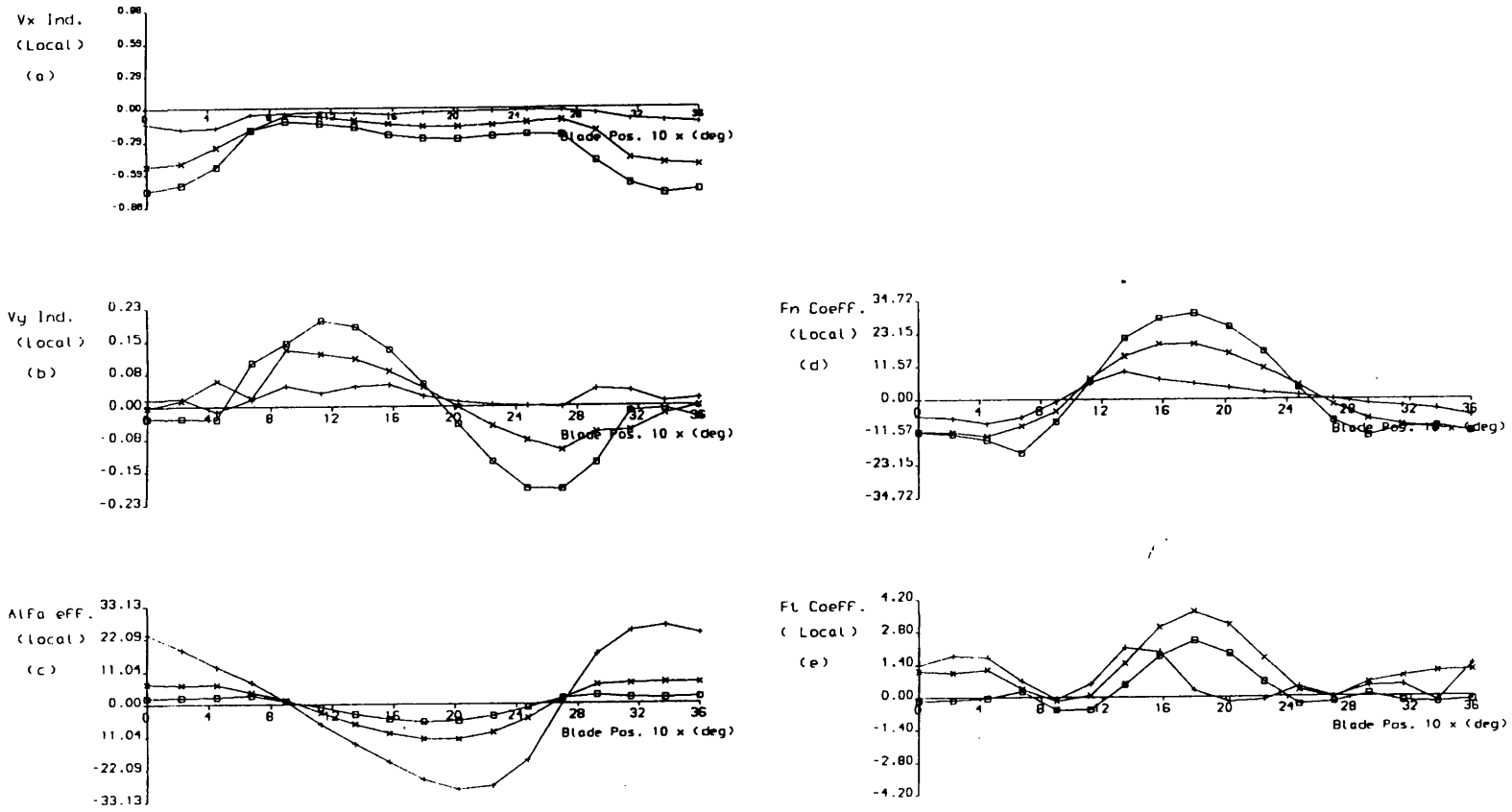

Fig. 3.7 Typical result of detailed aerodynamic characteristics near the mid blade span versus blade azimuth position from MVDART3-Code at different tip speed ratios.

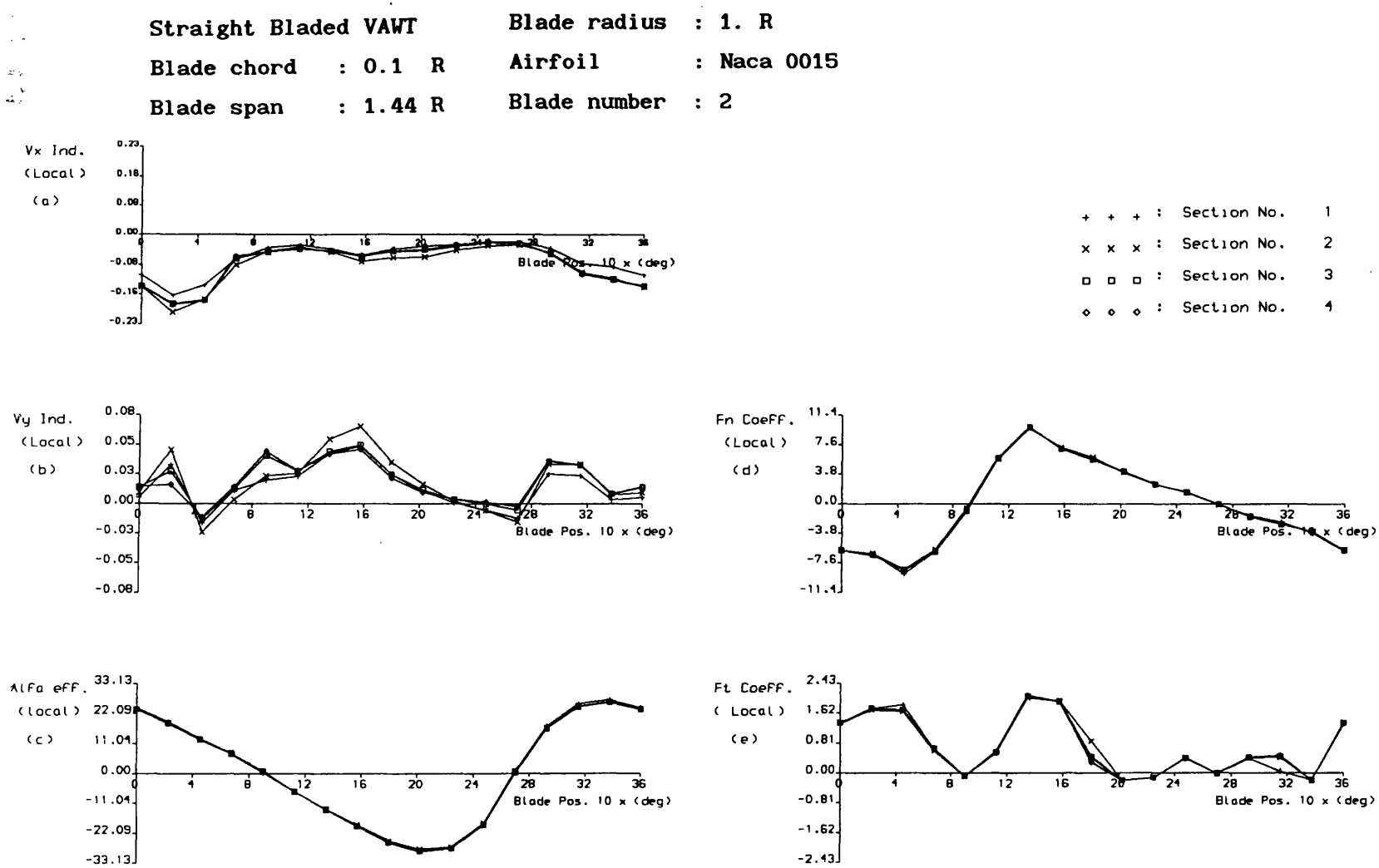

Fig. 3.8a Typical result of detailed aerodynamic characteristics along half blade span versus blade azimuth position from MVDART3-Code at $\lambda = 2$.

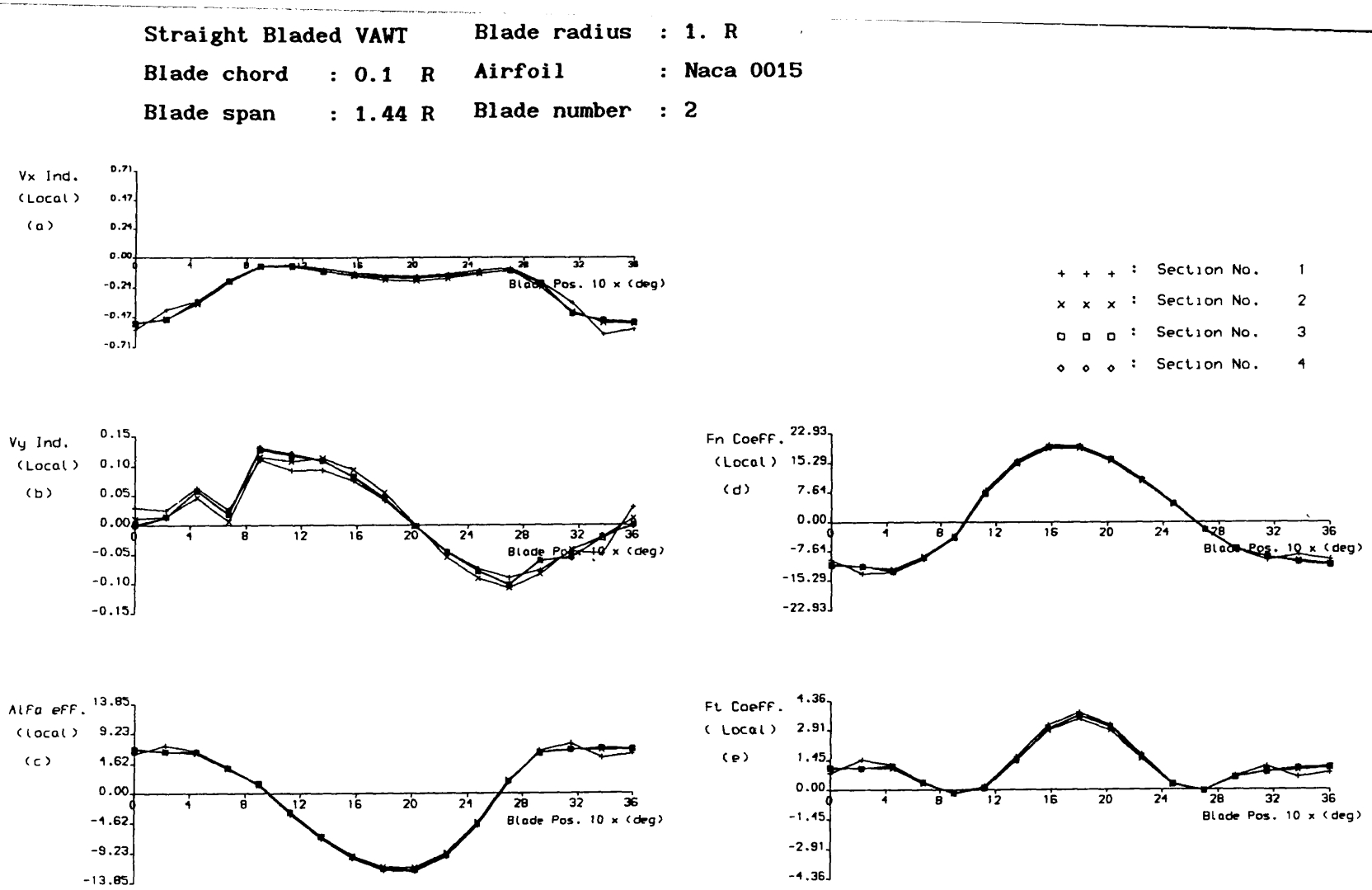

Fig. 3.8b Typical result of detailed aerodynamic characteristics along half blade span versus blade azimuth position from MVDART3-Code at $\lambda = 4$.

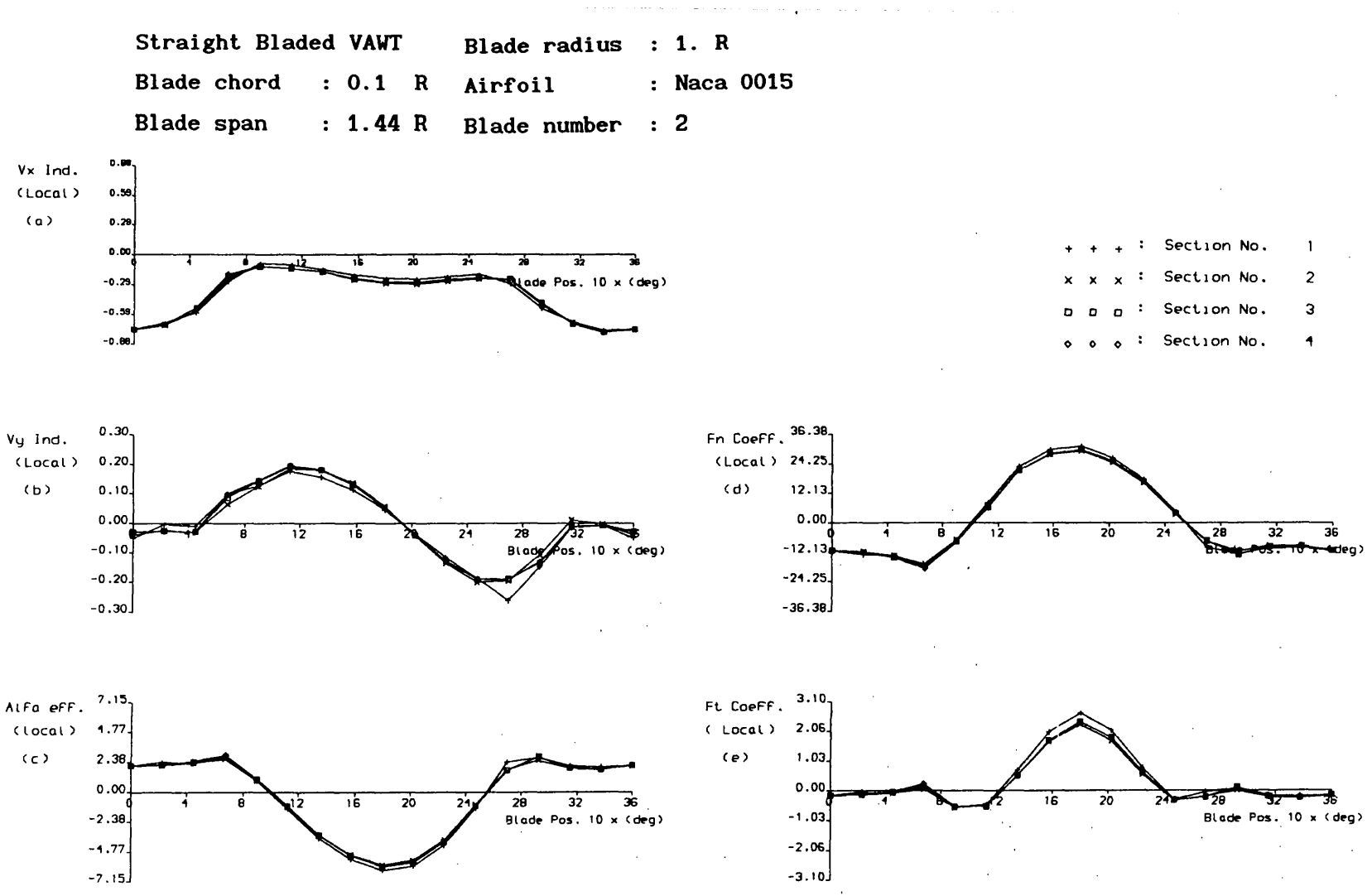

Fig. 3.8c Typical result of detailed aerodynamic characteristics along half blade span versus blade azimuth position from MVDART3-Code at $\lambda = 7$.

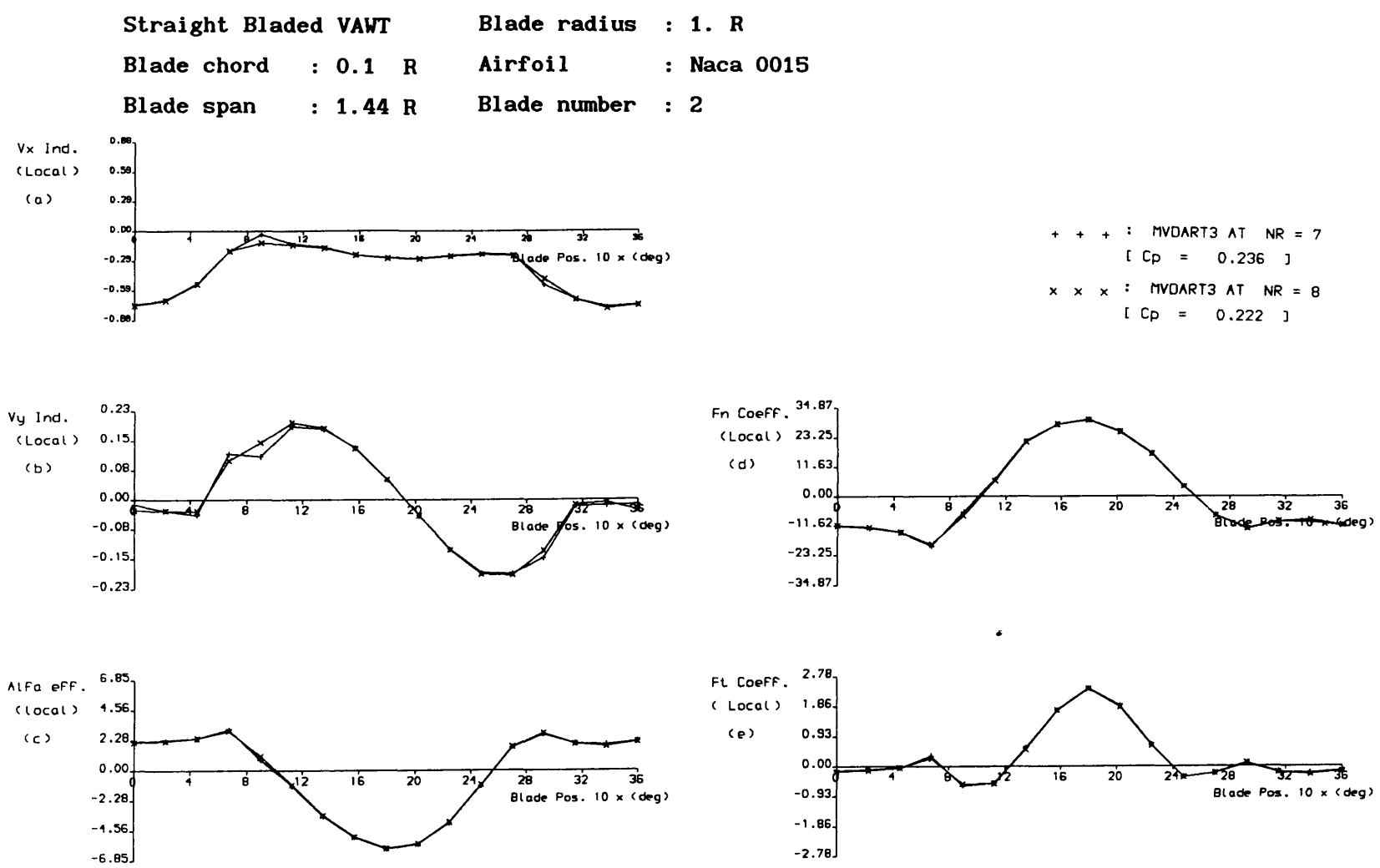

Fig. 3.9 A comparison of detailed aerodynamic characteristics at two successive rotational calculation NR = 7 & 8.

Straight Bladed VAWT

Blade chord	: 0.1 R	Blade Radius	: 1. R
Blade span	: 1.44 R	Airfoil	: Naca 0015
Blade number	: 2	Tip speed r.	: 4

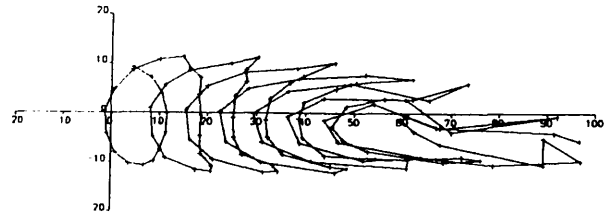

The wake shape at (NR-1)TI time step

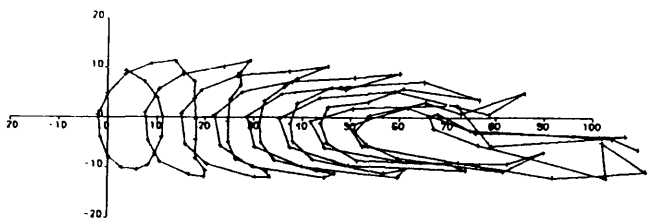

The wake shape at NRTI time step

Fig. 3.10a A comparison of wake shapes at two successive rotational calculations NR = 7 & 8 for $\lambda = 4$.

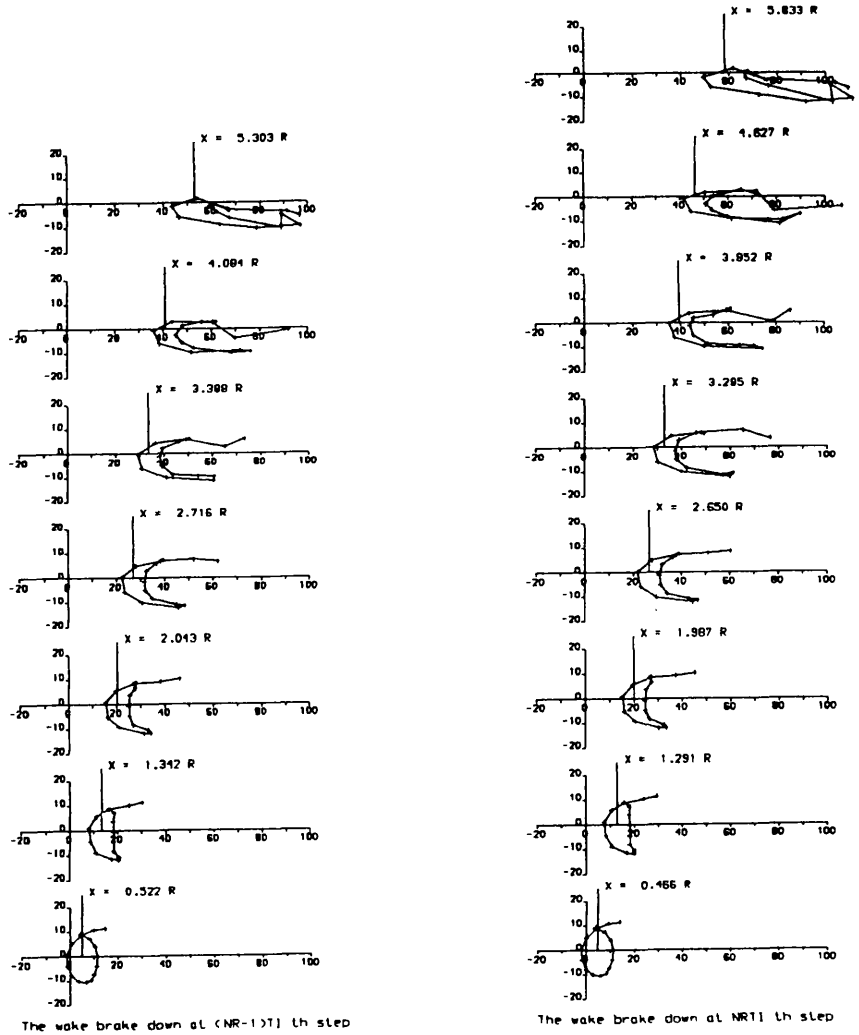

Fig. 3.10b The break down of wake shape into wake cycle components for λ=4.

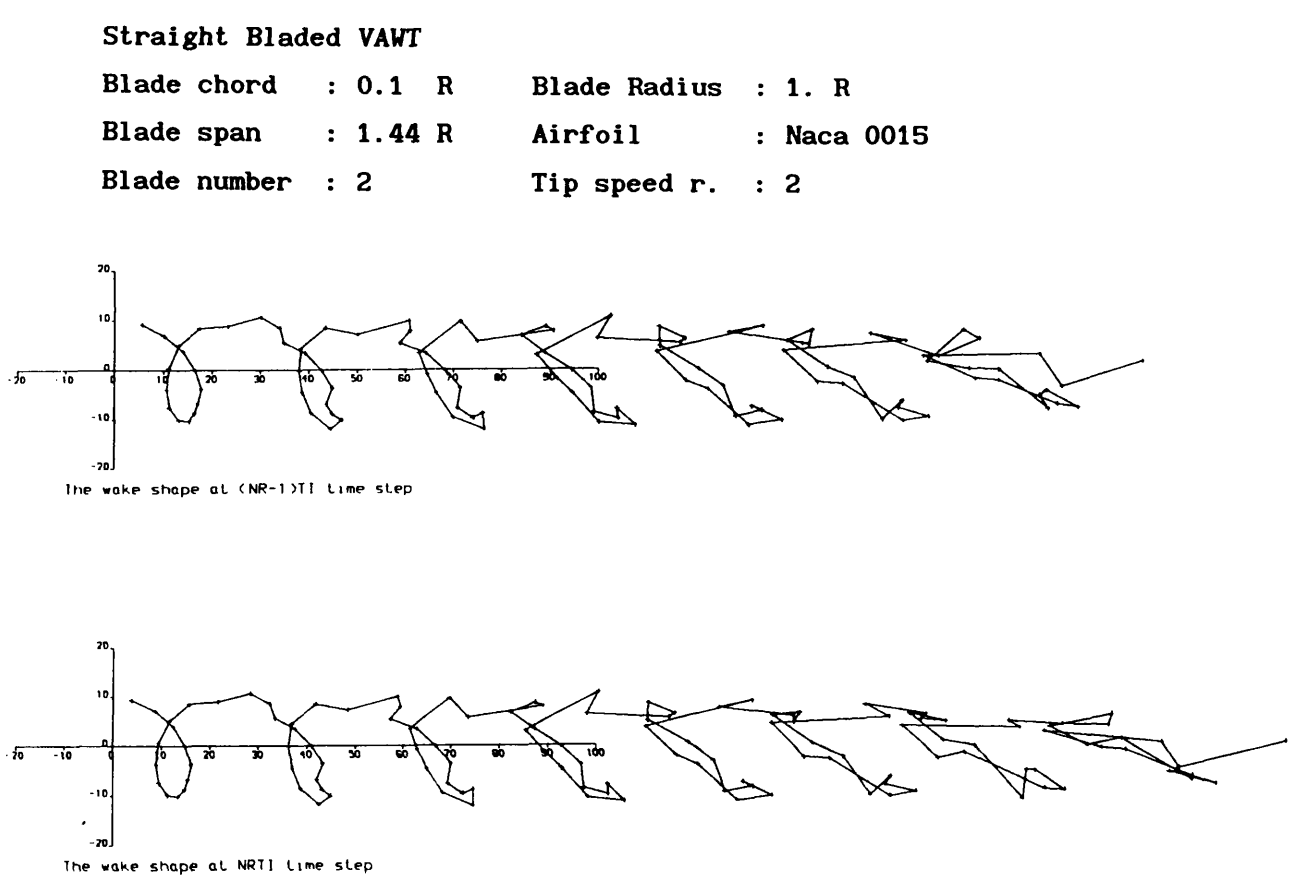

Fig. 3.11a A comparison of wake shapes at two successive rotational calculations NR = 7 & 8 for $\lambda = 2$.

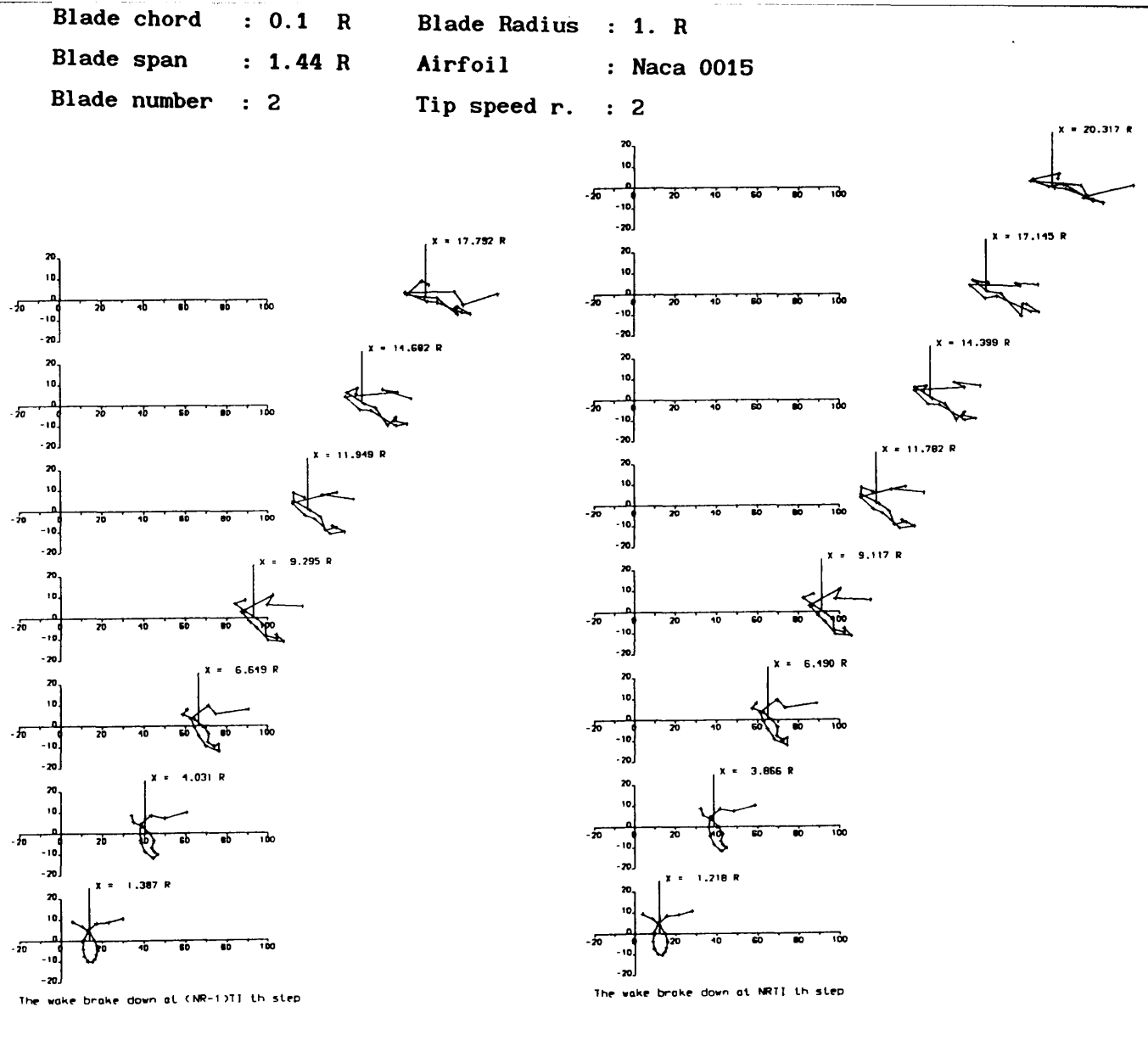

Fig. 3.11b The break down of wake shape into wake cycle components for λ=2.

Straight Bladed VAWT

Blade chord	: 0.1 R	Blade Radius	: 1. R
Blade span	: 1.44 R	Airfoil	: Naca 0015
Blade number	: 2	Tip speed r.	: 7

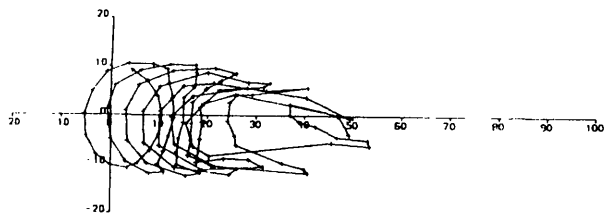

The wake shape at (NR-1)T] time step

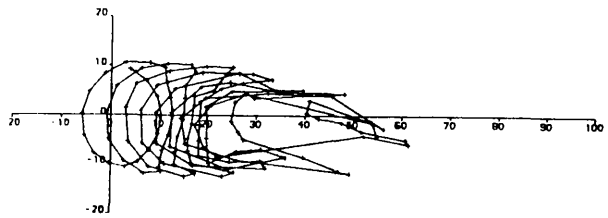

The wake shape at NRT] time step

Fig. 3.12a A comparison of wake shapes at two successive rotational calculations NR = 7 & 8 for λ =7 .

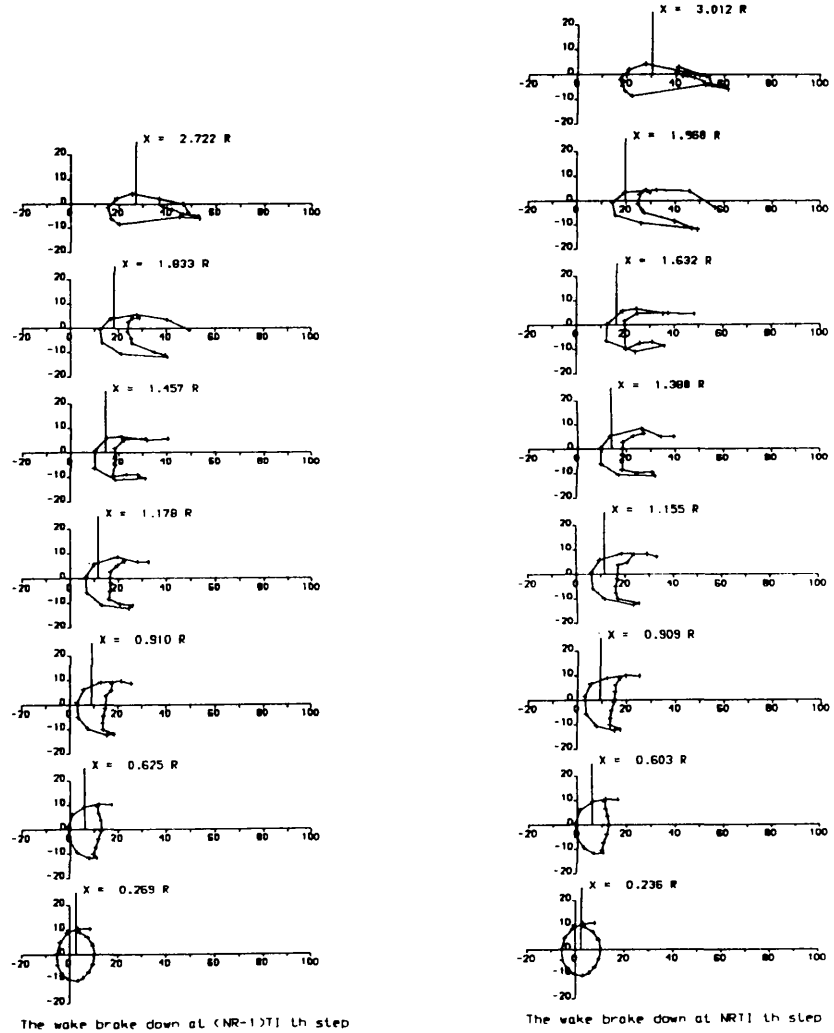

The wake brake down at (NR-1)T] th step

The wake brake down at NRT] th step

Fig. 3.12b The break down of wake shape into wake cycle components for λ=7.

Straight Bladed VAWT

Blade chord	: 0.1 R	Blade radius	: 1. R
Blade span	: 1.44 R	Airfoil	: Naca 0015
Blade number	: 2	Tip speed ratio	: 2

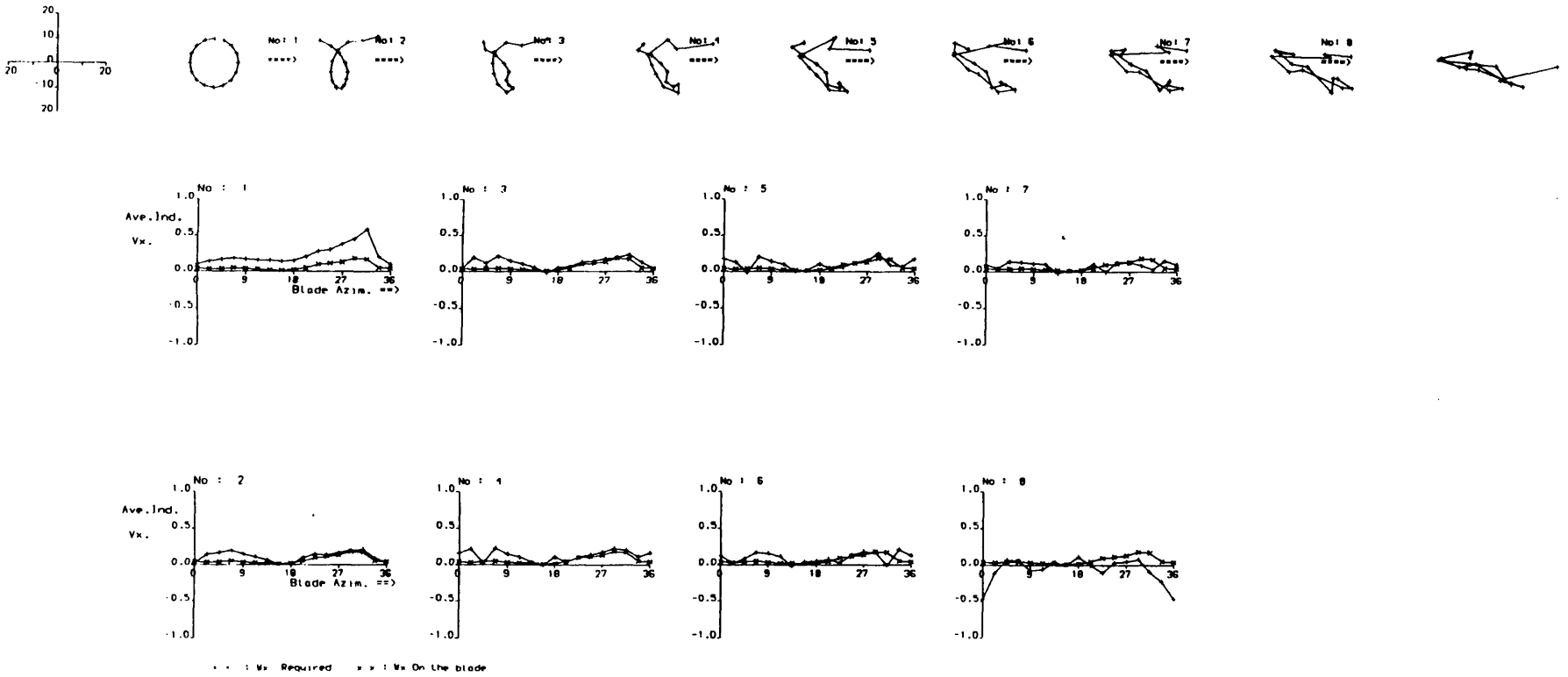

Fig. 3.13a A comparison of required X-component induced velocity in the flow field and on the blade at $\lambda = 2$.

Straight Bladed VAWT

Blade chord	: 0.1 R	Blade radius	: 1. R
Blade span	: 1.44 R	Airfoil	: Naca 0015
Blade number	: 2	Tip speed ratio	: 2

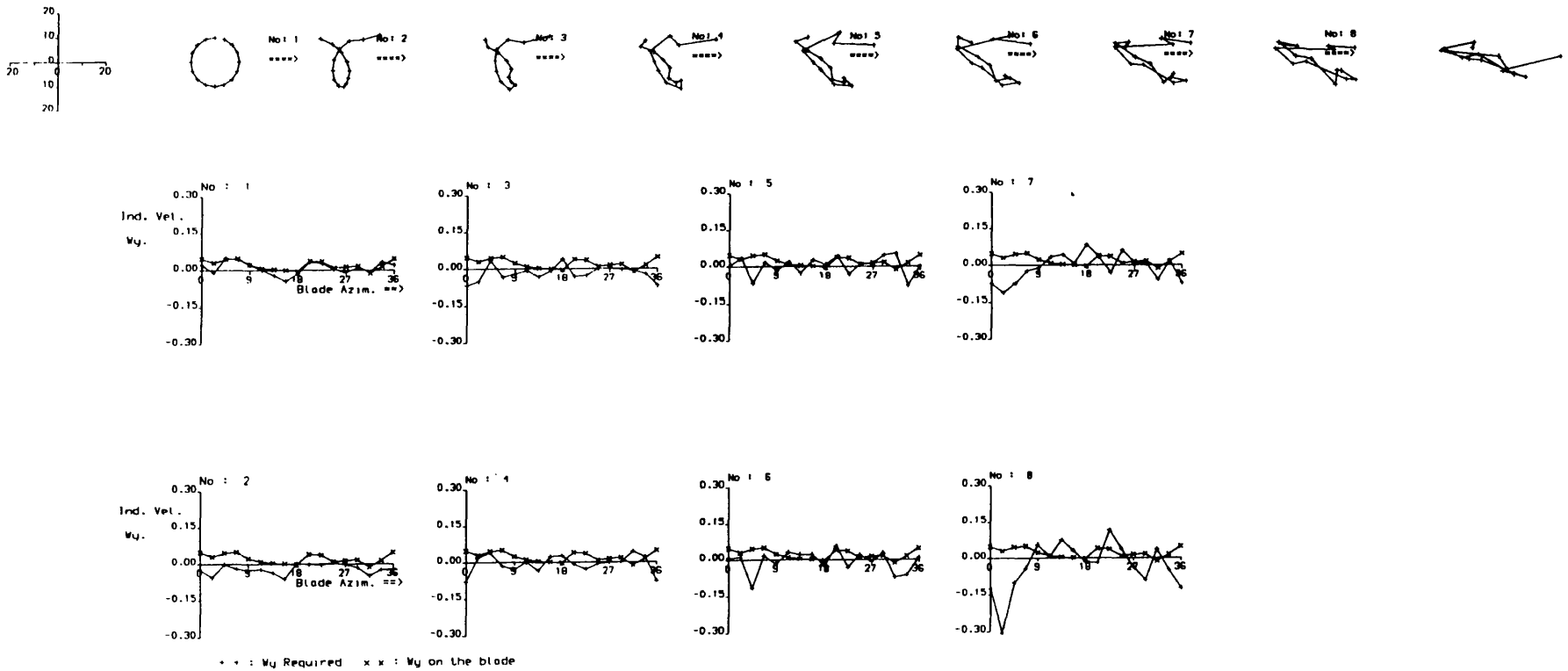

Fig. 3.13b A comparison of required Y-component induced velocity in the flow field and on the blade at $\lambda = 2$.

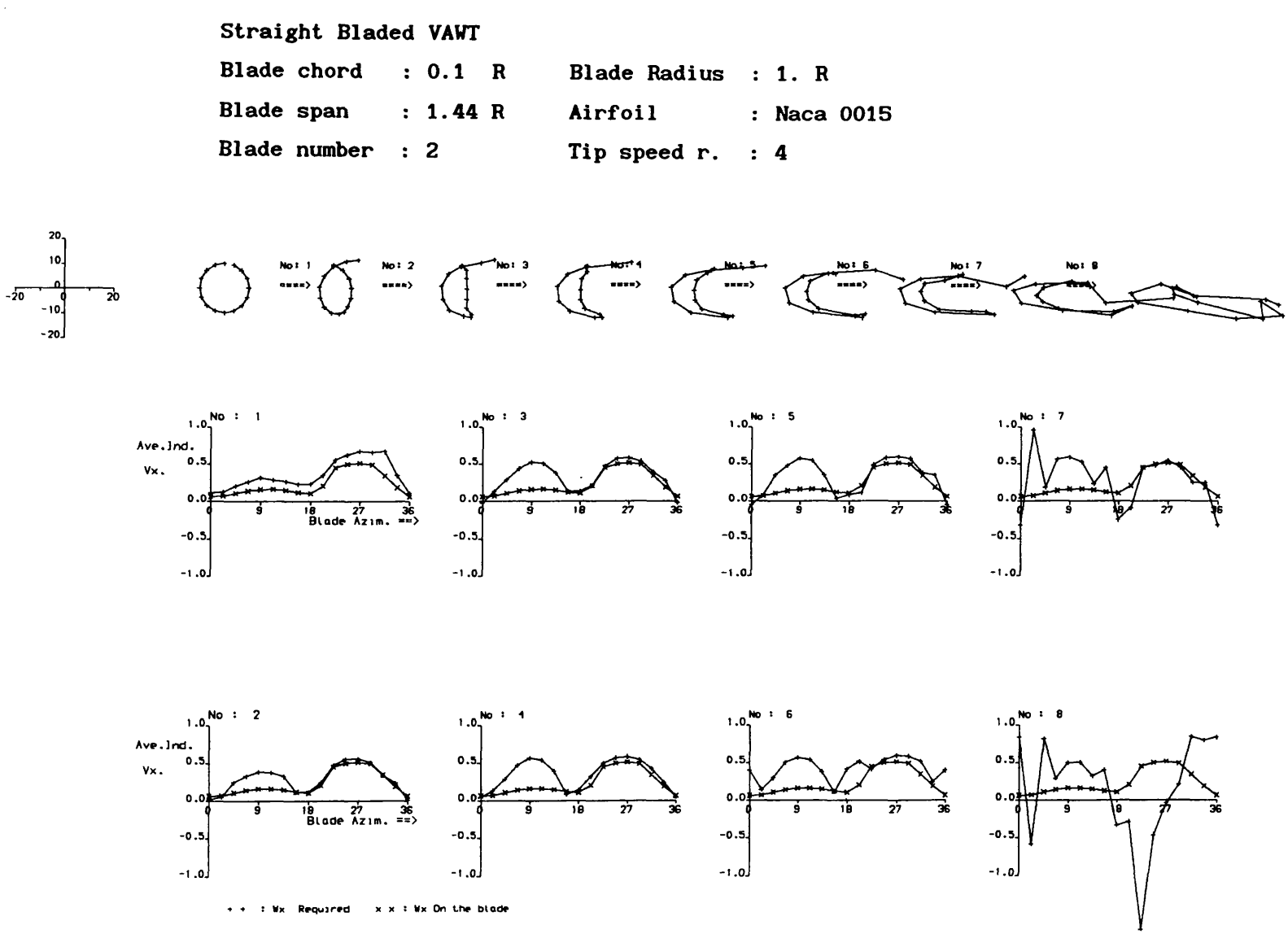

Fig. 3.14a A comparison of required X-component induced velocity in the flow field and on the blade at $\lambda = 4$.

Straight Bladed VAWT

Blade chord	: 0.1 R	Blade radius	: 1. R
Blade span	: 1 44 R	Airfoil	: Naca 0015
Blade number	: 2	Tip speed ratio	: 4

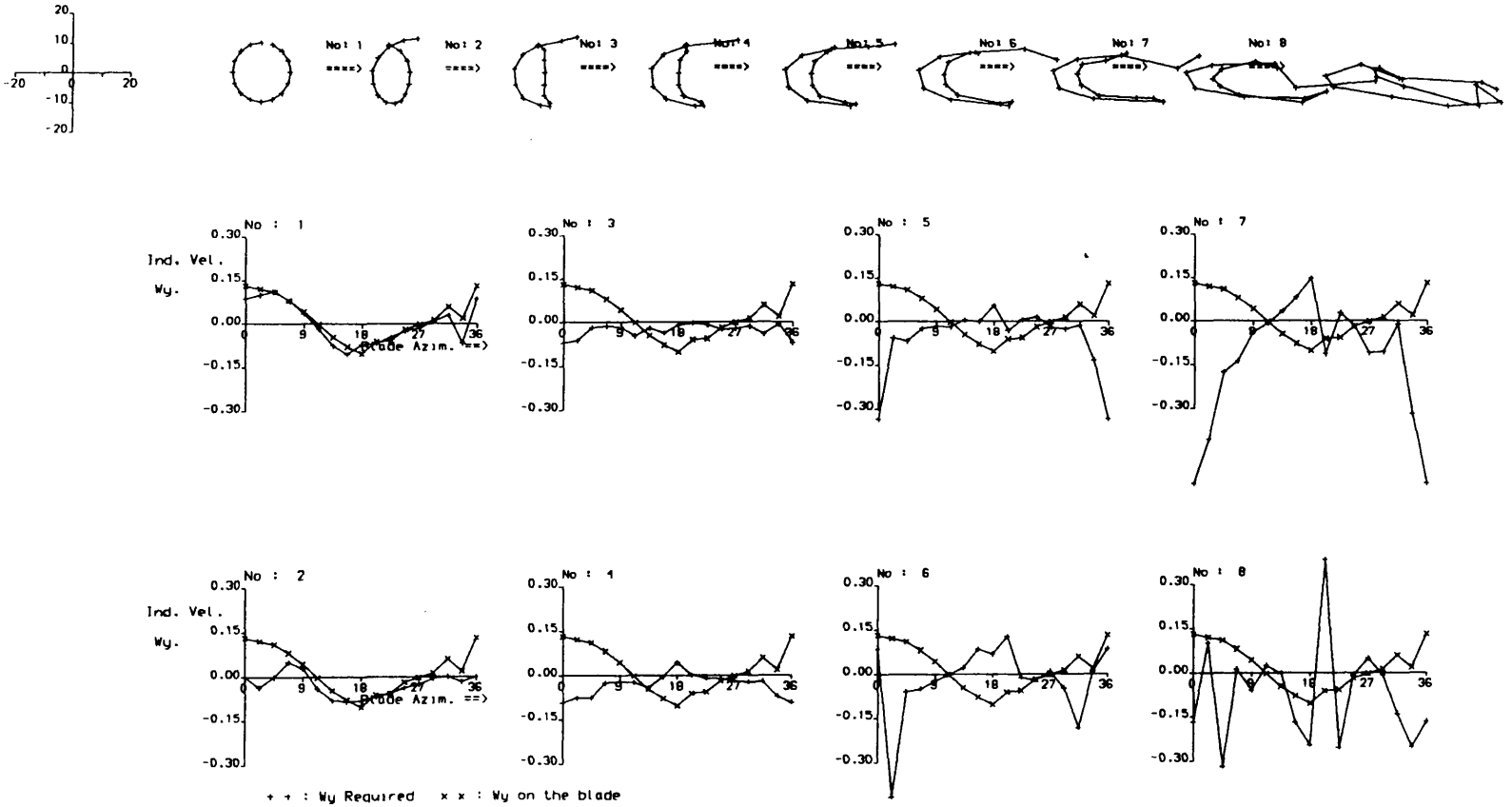

3.14b A comparison of required Y-component induced velocity in the flow field and on the blade at $\lambda = 4$.

Straight Bladed VAWT

Blade chord	: 0.1 R	Blade radius	: 1. R
Blade span	: 1.44 R	Airfoil	: Naca 0015
Blade number	: 2	Tip speed ratio	: 7

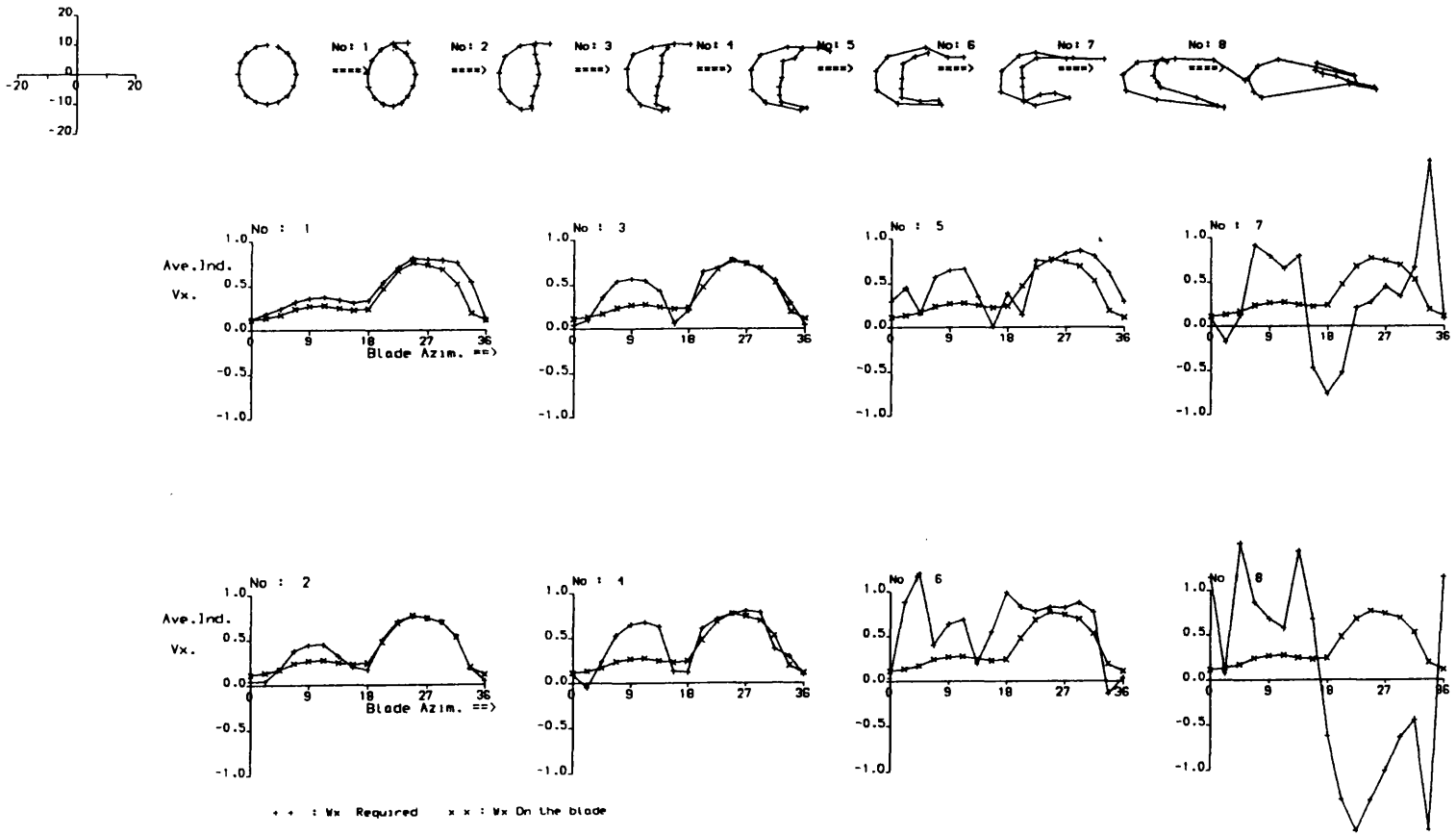

Fig. 3.15a A comparison of required X-component induced velocity in the flow field and on the blade at $\lambda = 7$.

Straight Bladed VAWT

Blade chord	: 0.1 R	Blade radius	: 1. R
Blade span	: 1.44 R	Airfoil	: Naca 0015
Blade number	: 2	Tip speed ratio	: 7

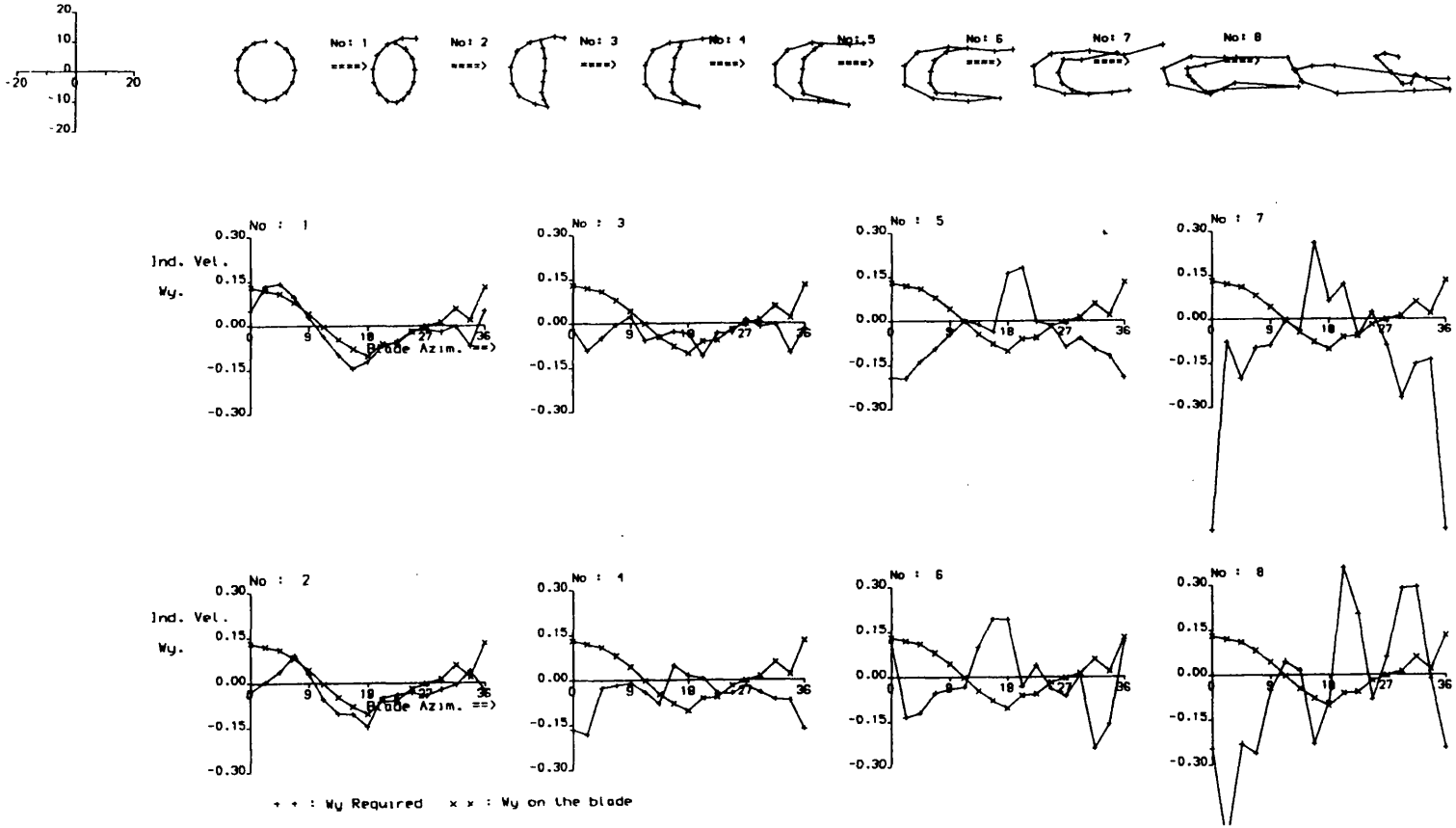

Fig. 3.15b A comparison of required Y-component induced velocity in the flow field and on the blade at $\lambda = 7$.

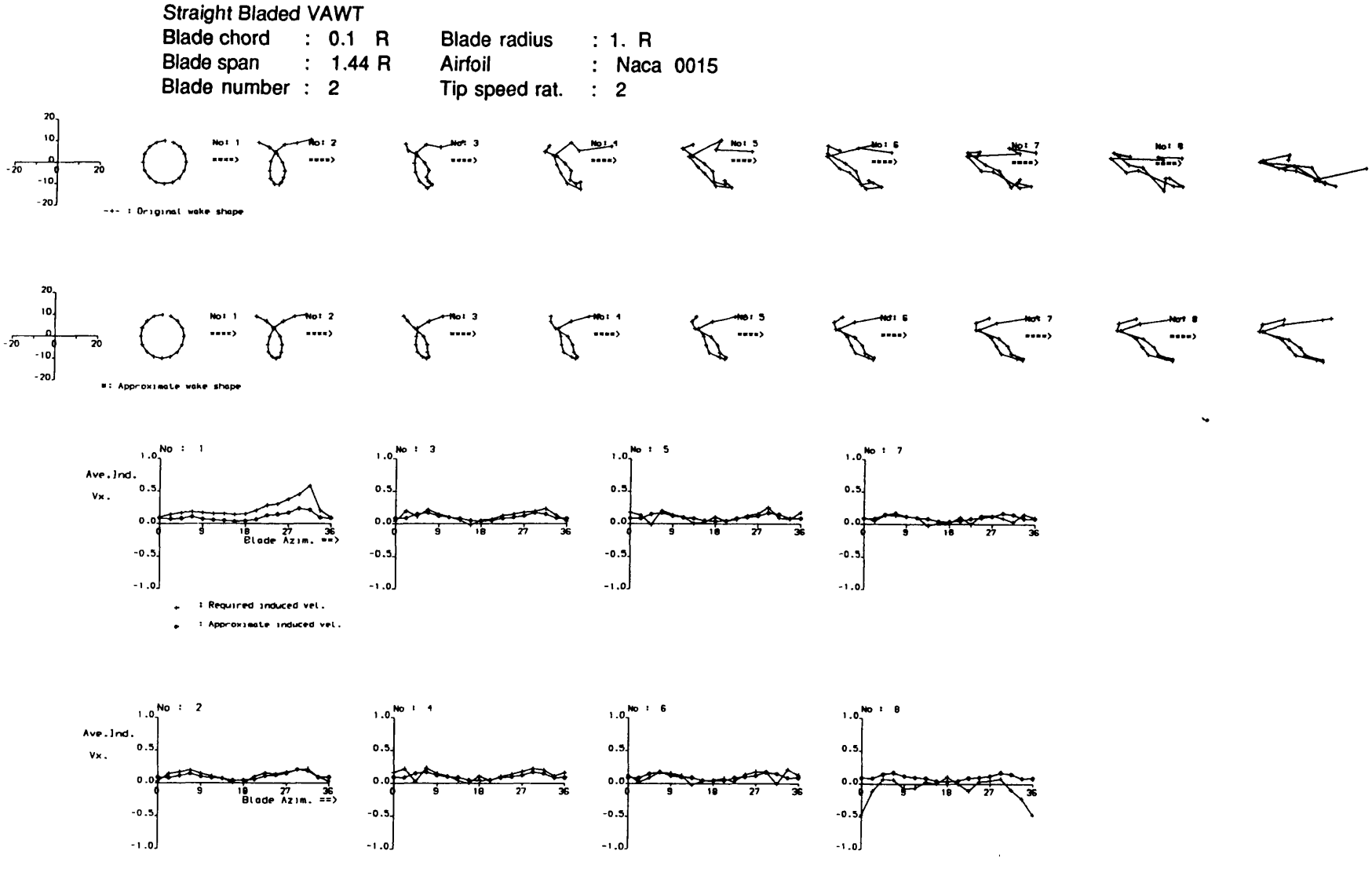

Fig. 3.16 A comparison of actual and approximate wake shape derived using X-component induced velocity at $\lambda = 2$.

Blade chord	: 0.1 R	Blade radius	: 1. R
Blade span	: 1.44 R	Airfoil	: Naca 0015
Blade number	: 2	Tip speed rat.	: 4

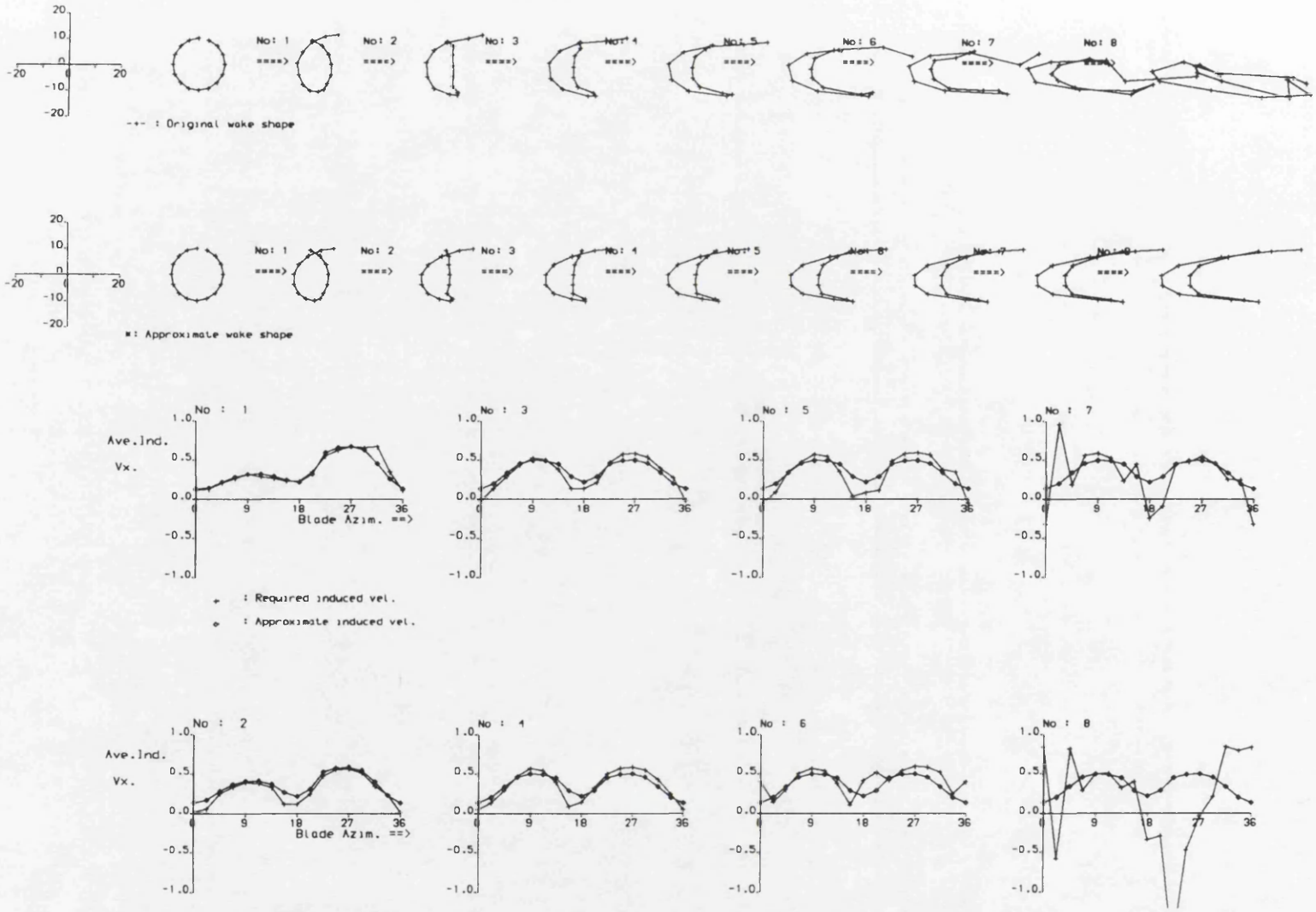

Fig. 3.17 A comparison of actual and approximate wake shape derived using X- component induced velocity at $\lambda = 4$.

Blade chord	: 0.1 R	Blade radius	: 1. R
Blade span	: 1.44 R	Airfoil	: Naca 0015
Blade number	: 2	Tip speed ratio	: 5

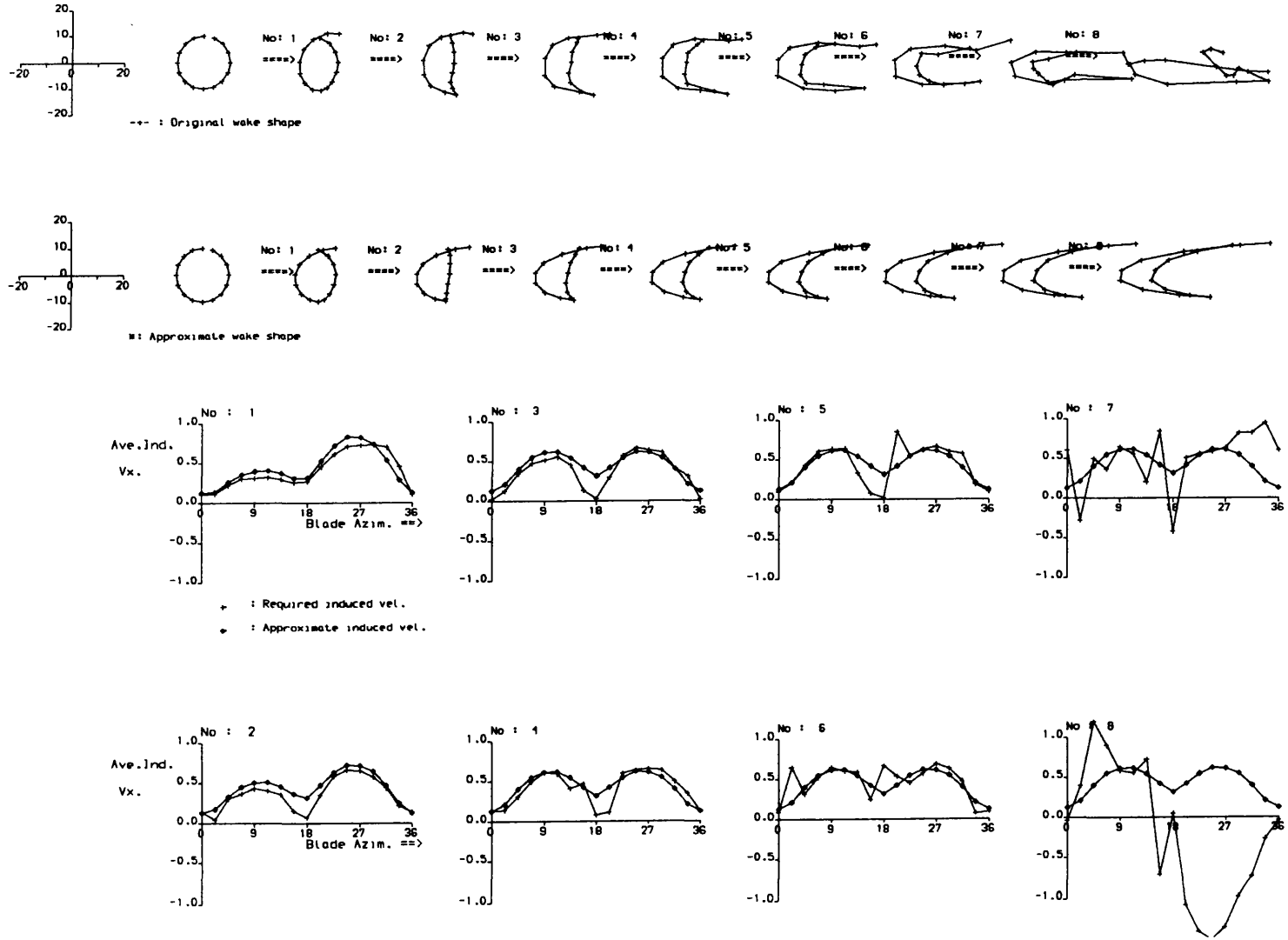

Fig. 3.18 A comparison of actual and approximate wake shape derived using X- component induced velocity at $\lambda = 5$.

Blade chord	: 0.1 R	Blade radius	: 1. R
Blade span	: 1.44 R	Airfoil	: Naca 0015
Blade number	: 2	Tip speed ratio	: 7

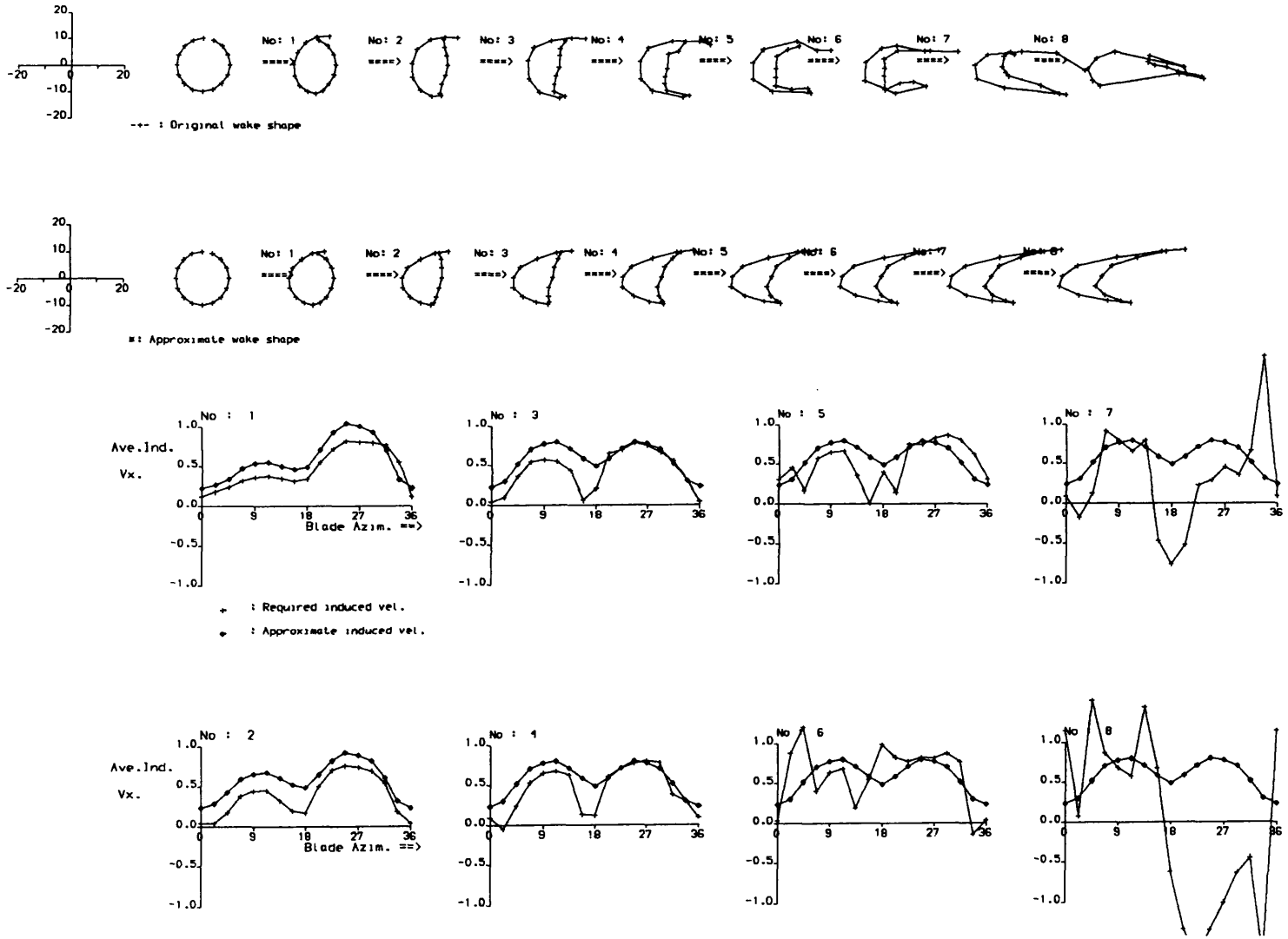

Fig. 3.19 A comparison of actual and approximate wake shape derived using X- component induced velocity at $\lambda = 7$.

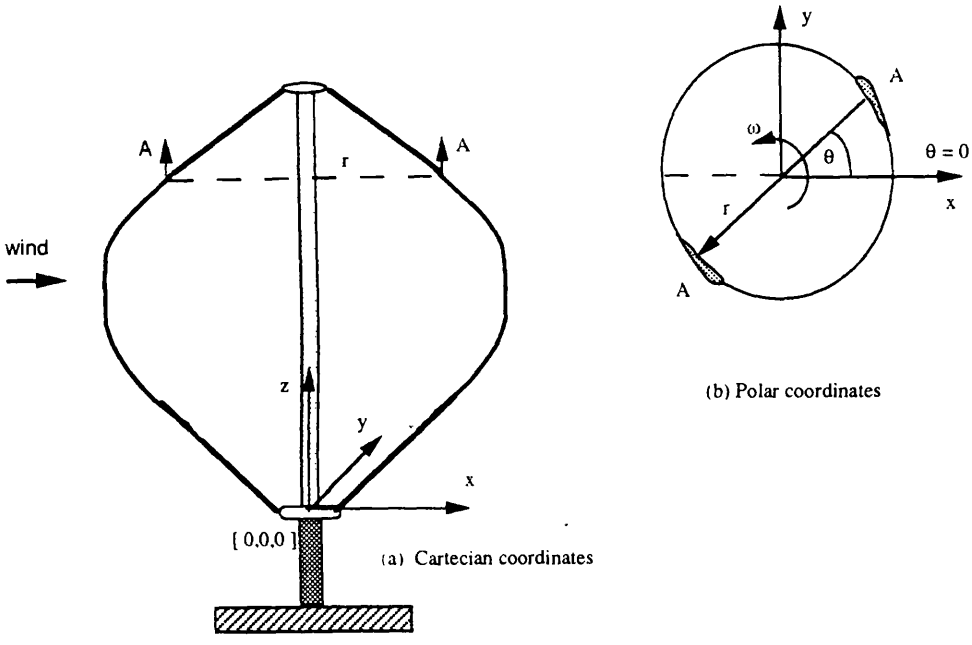

Fig. 3.20 VAWT's system coordinates.

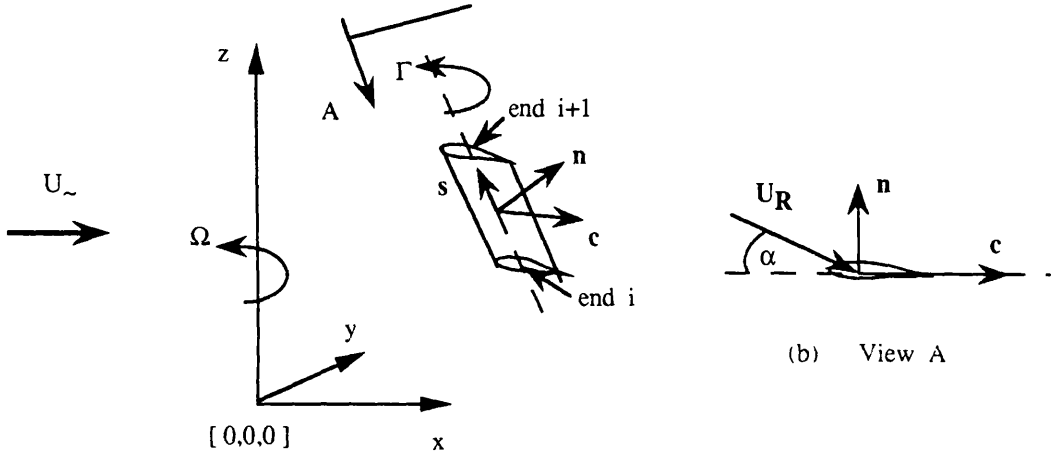

Fig. 3.21 The definition of unit vector in the blade element and the velocity resultance's diagram.

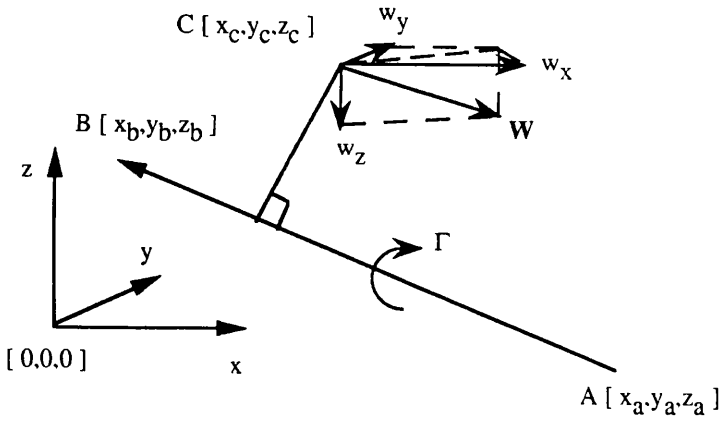

Fig. 3.22 The Vortex filament and the induced velocity.

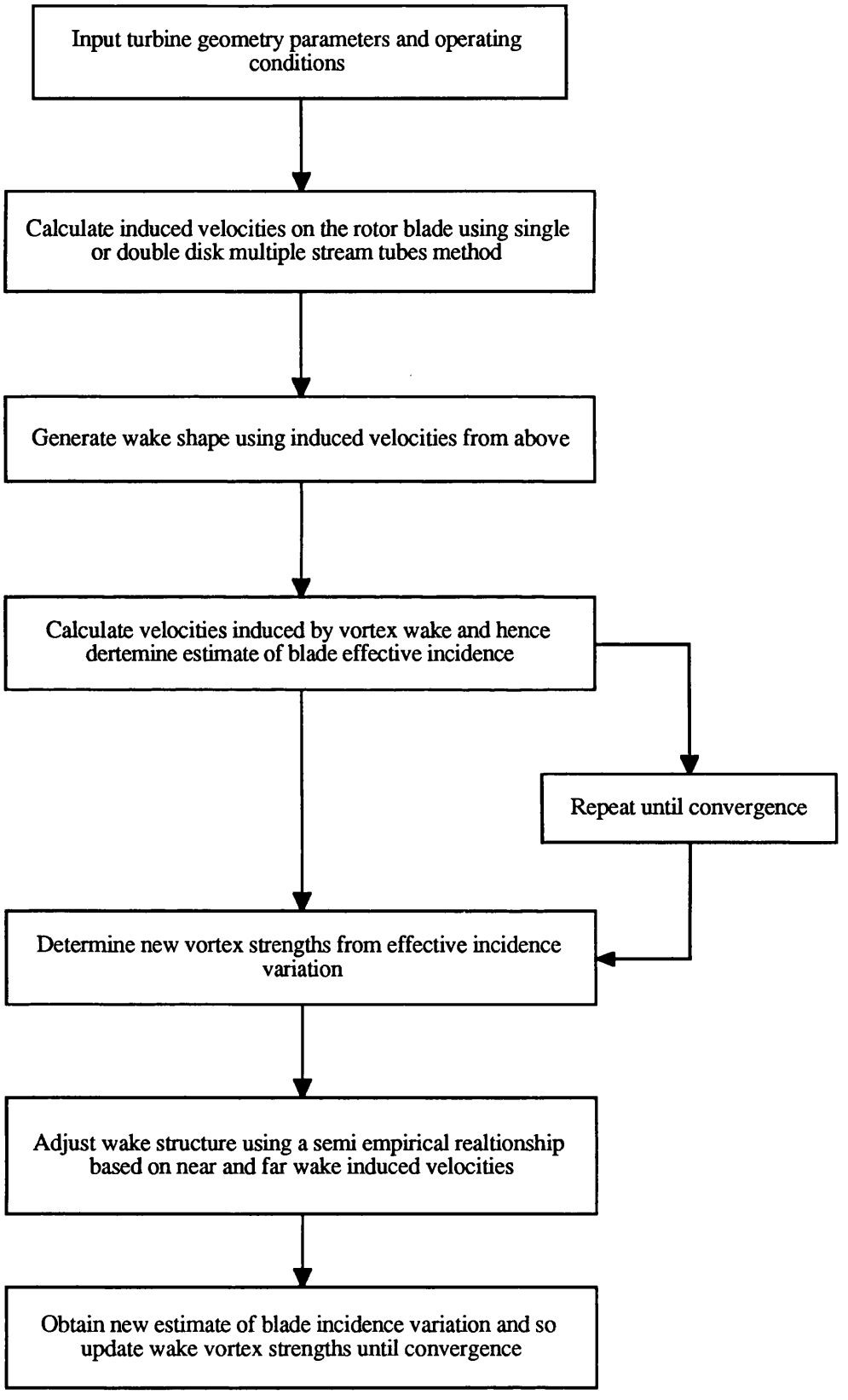

Fig. 3.23 The proposed prescribed wake calculation scheme

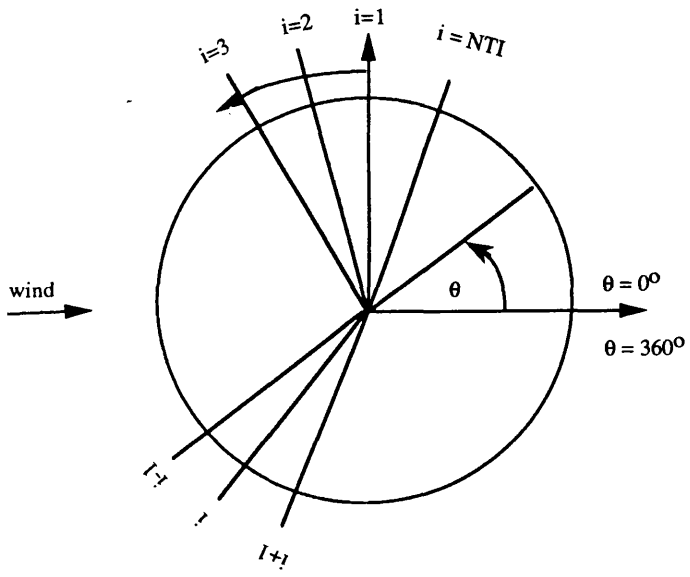

Fig. 3.24 The numbering system of blade azimuth position and shed vortices.

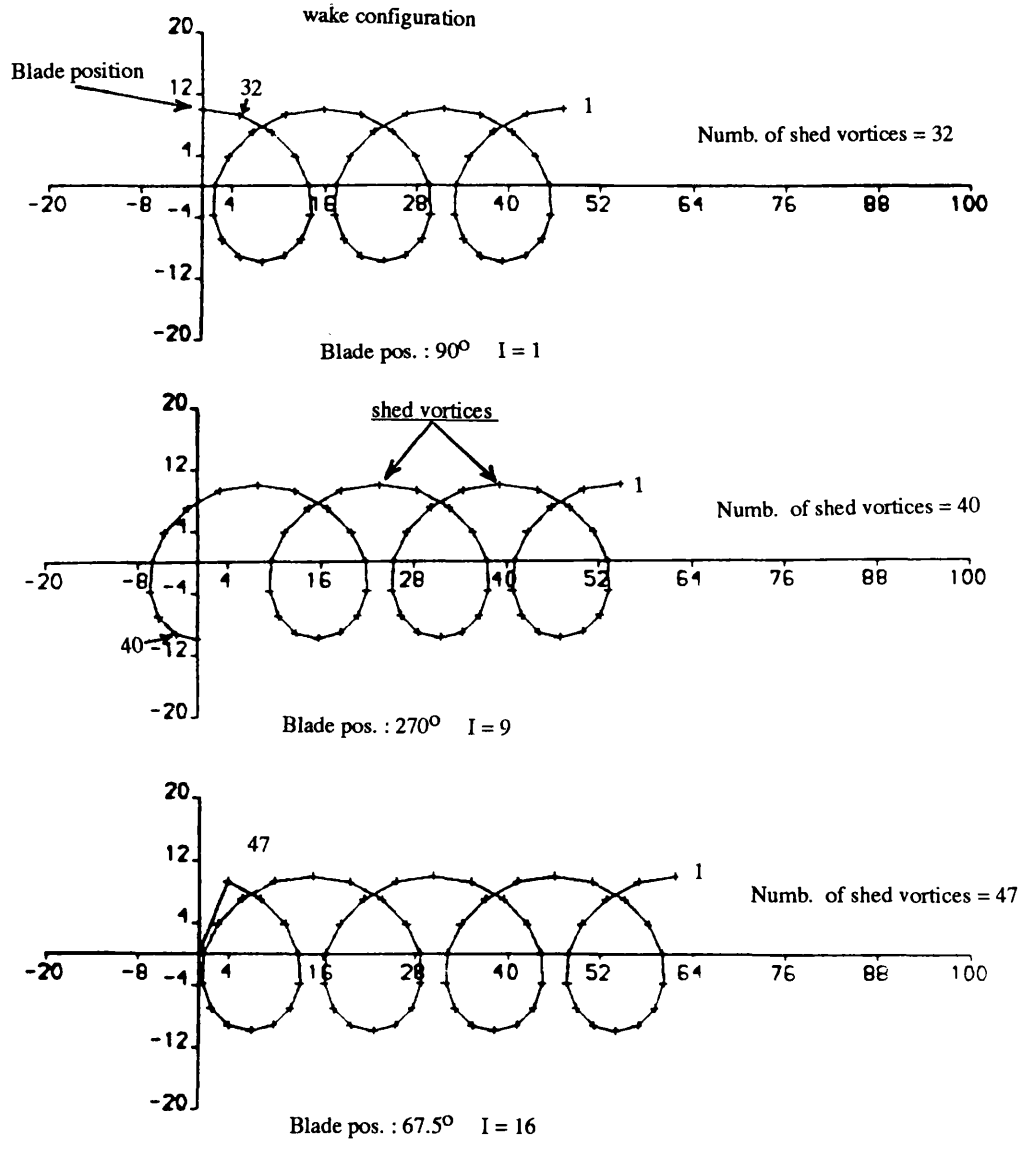

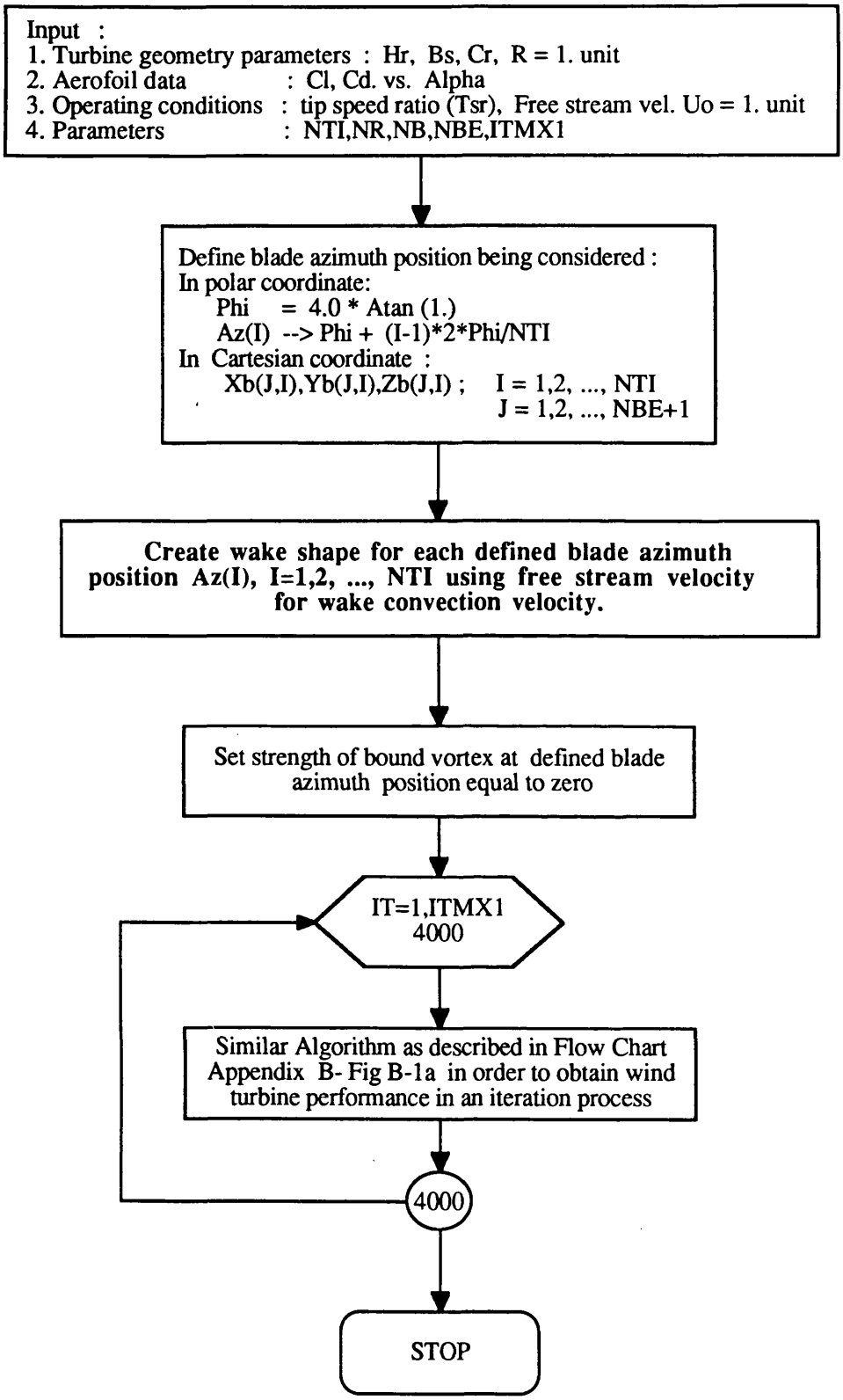

Fig. 4.1 Flow diagram PRESWK-Org. version

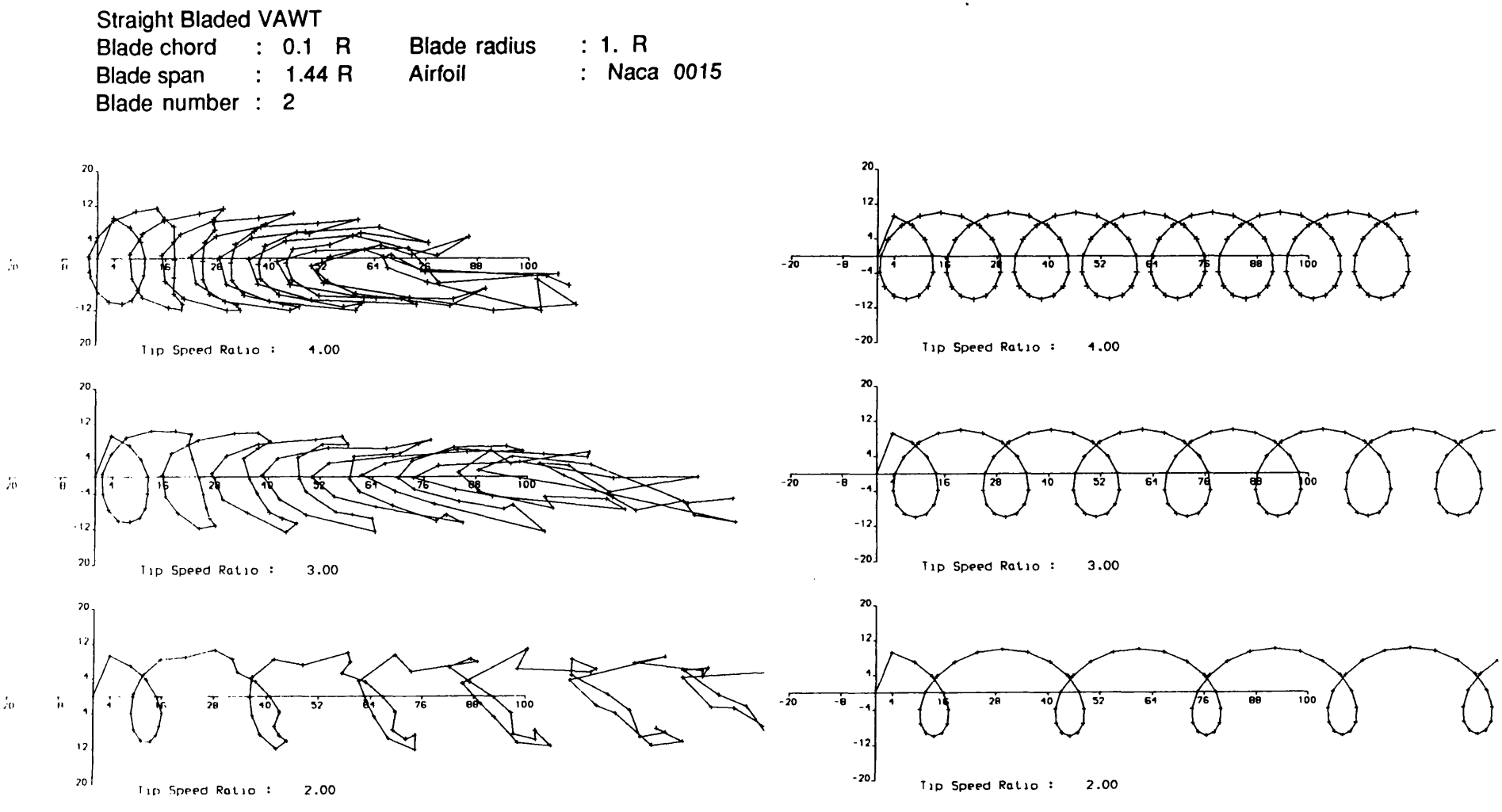

Fig.4.2 A comparison of the wake shapes at the mid blade span between the Free wake method [MVDART3] and PRESWK-Org. version for different values of tip speed ratio.

Straight Bladed VAWT

Blade chord	: 0.1 R	Blade radius	: 1. R
Blade span	: 1.44 R	Airfoil	: Naca 0015
Blade number	: 2		

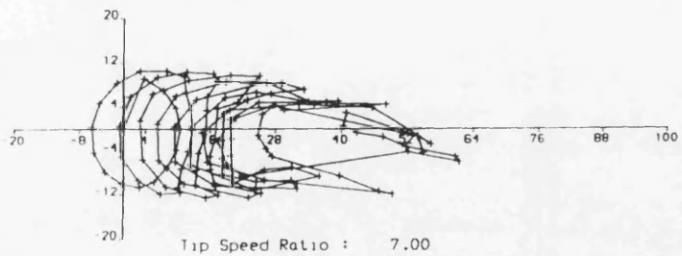

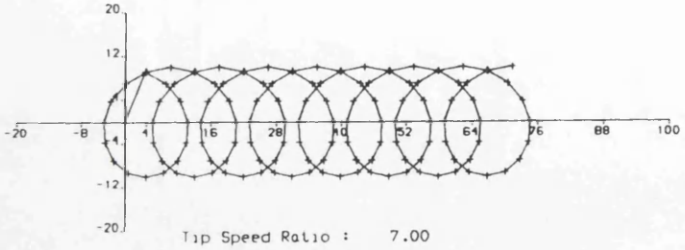

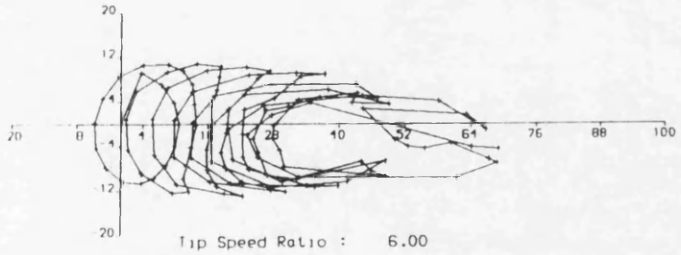

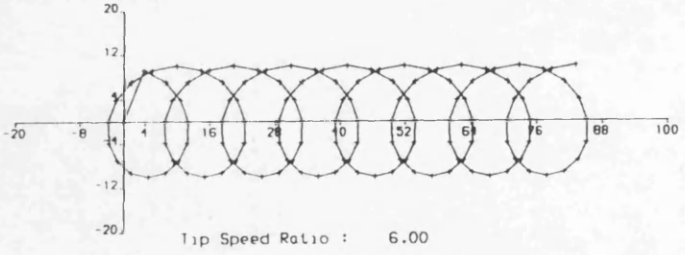

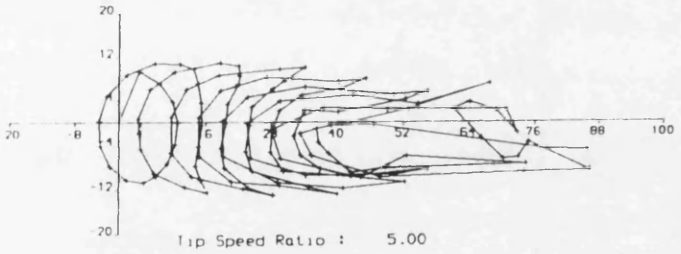

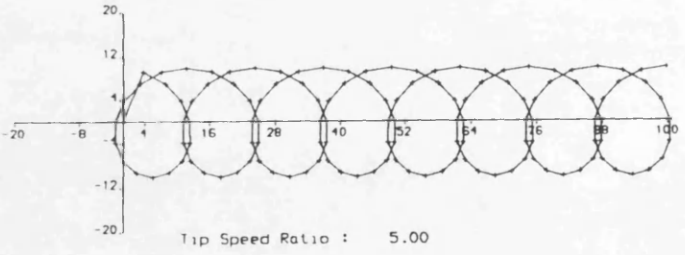

Cont'n from Fig. 4.2

Straight Bladed VAWT

Blade chord	: 0.1 R	Blade radius	: 1. R
Blade span	: 1.44 R	Airfoil	: Naca 0015
Blade number	: 2	Tip speed rat.	: 2

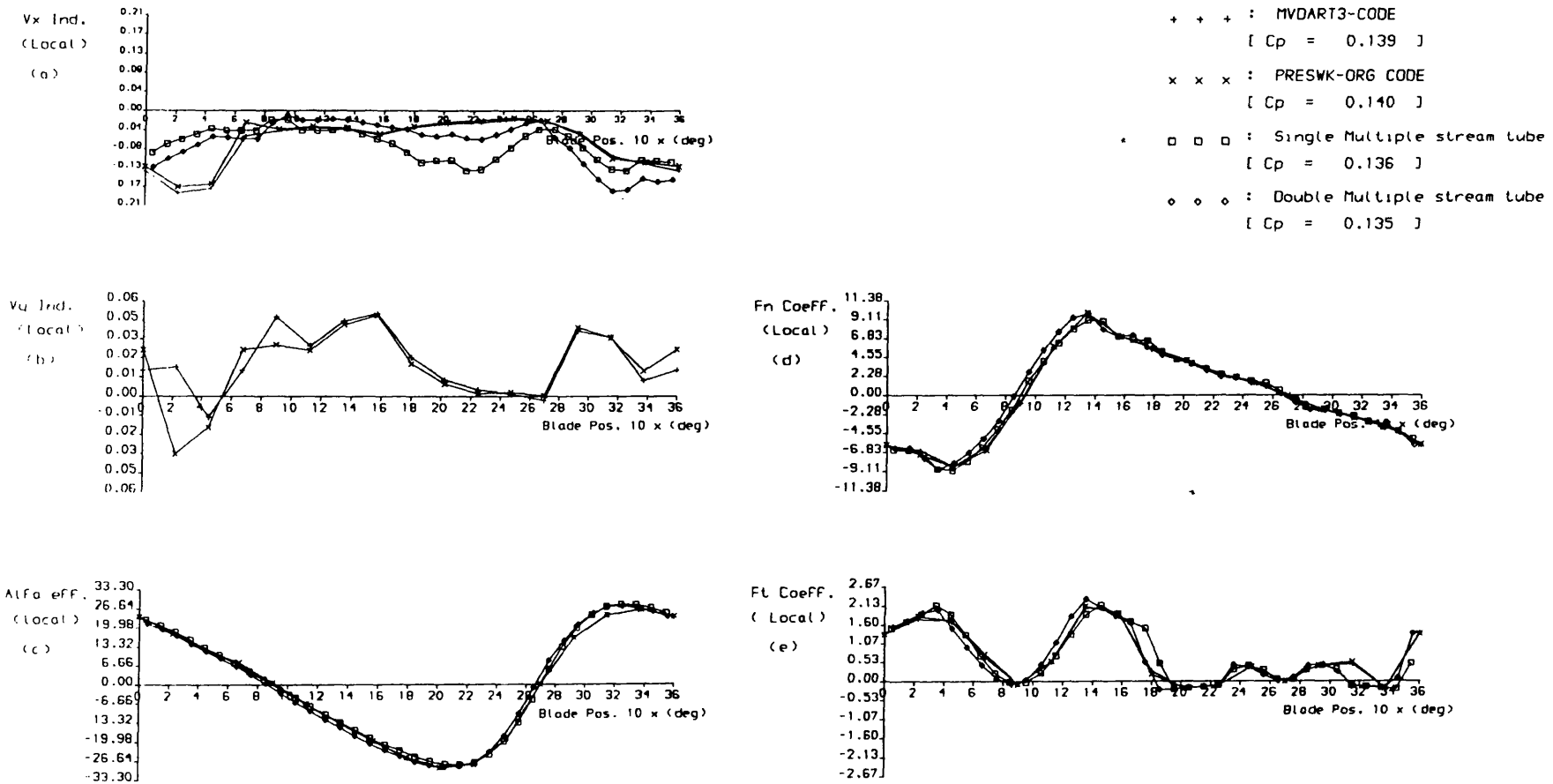

Fig.4.3a A comparison of detailed aerodynamic characteristics near the mid blade against blade azimuth position, between the Free wake method [MVDART3] and PRESWK - Org. for $\lambda = 2$.

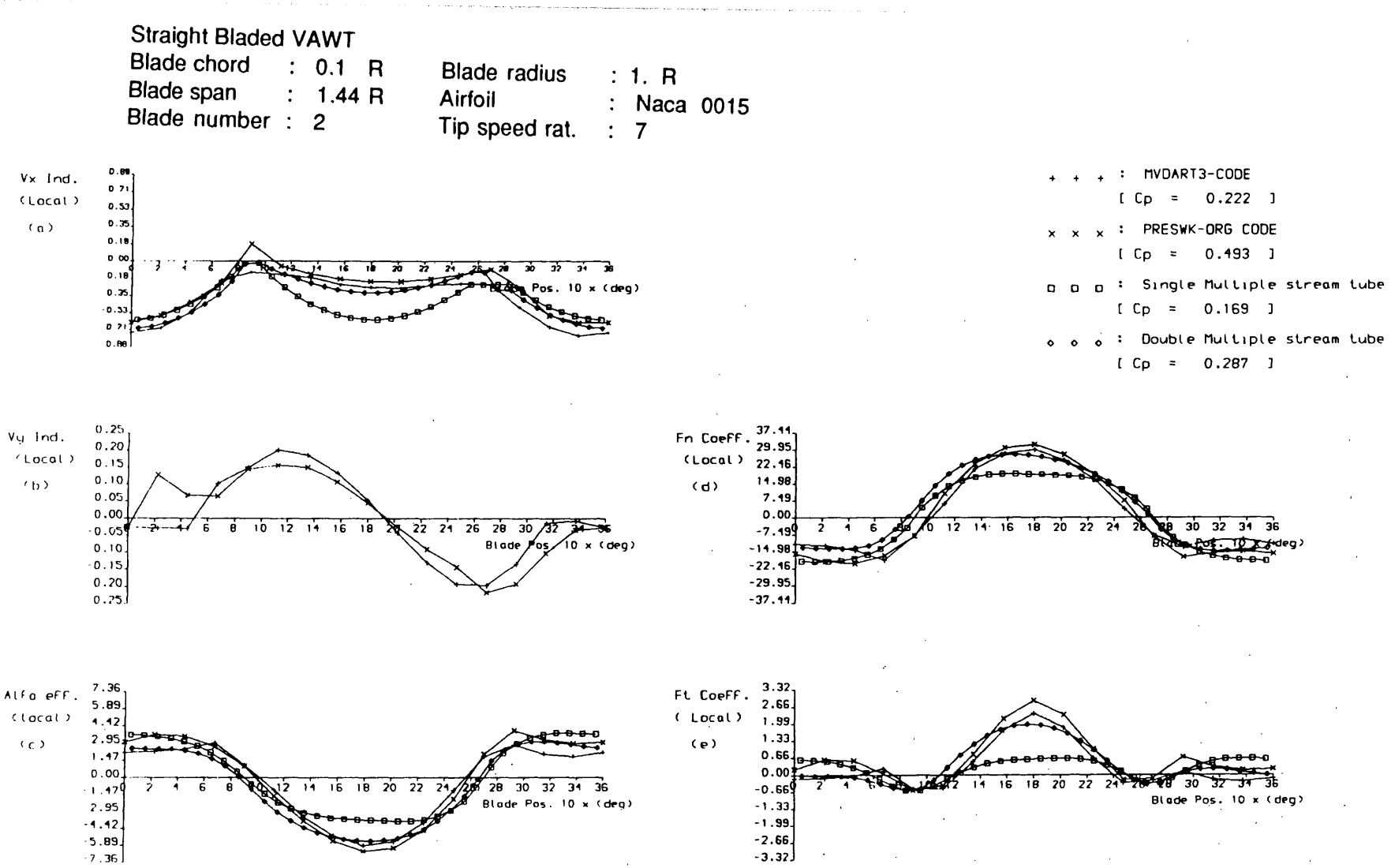

Fig.4.3b A comparison of detailed aerodynamic characteristics near the mid blade against blade azimuth position, between the Free wake method [MVDART3] and PRESWK - Org. for $\lambda = 7$.

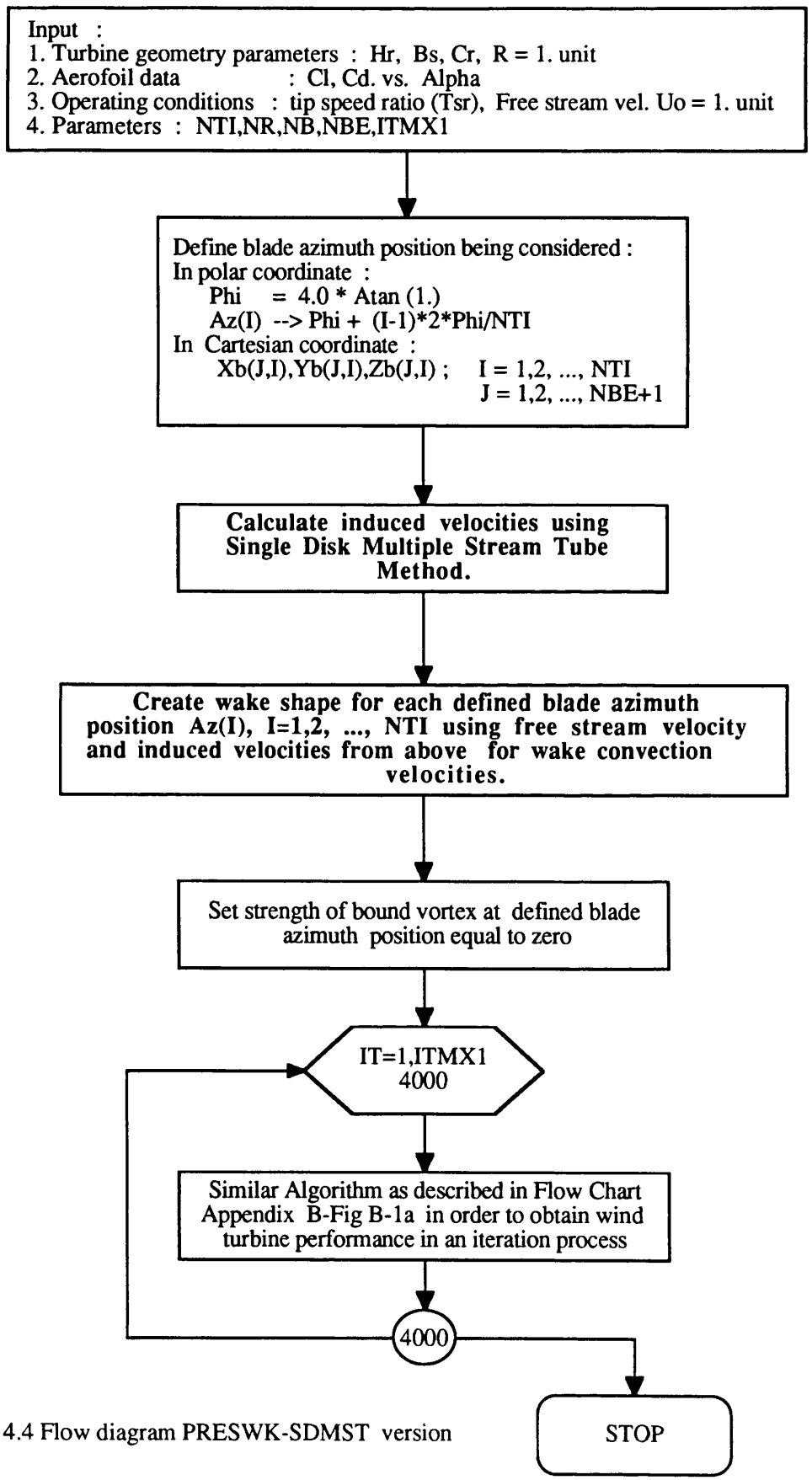

Fig. 4.4 Flow diagram PRESWK-SDMST version

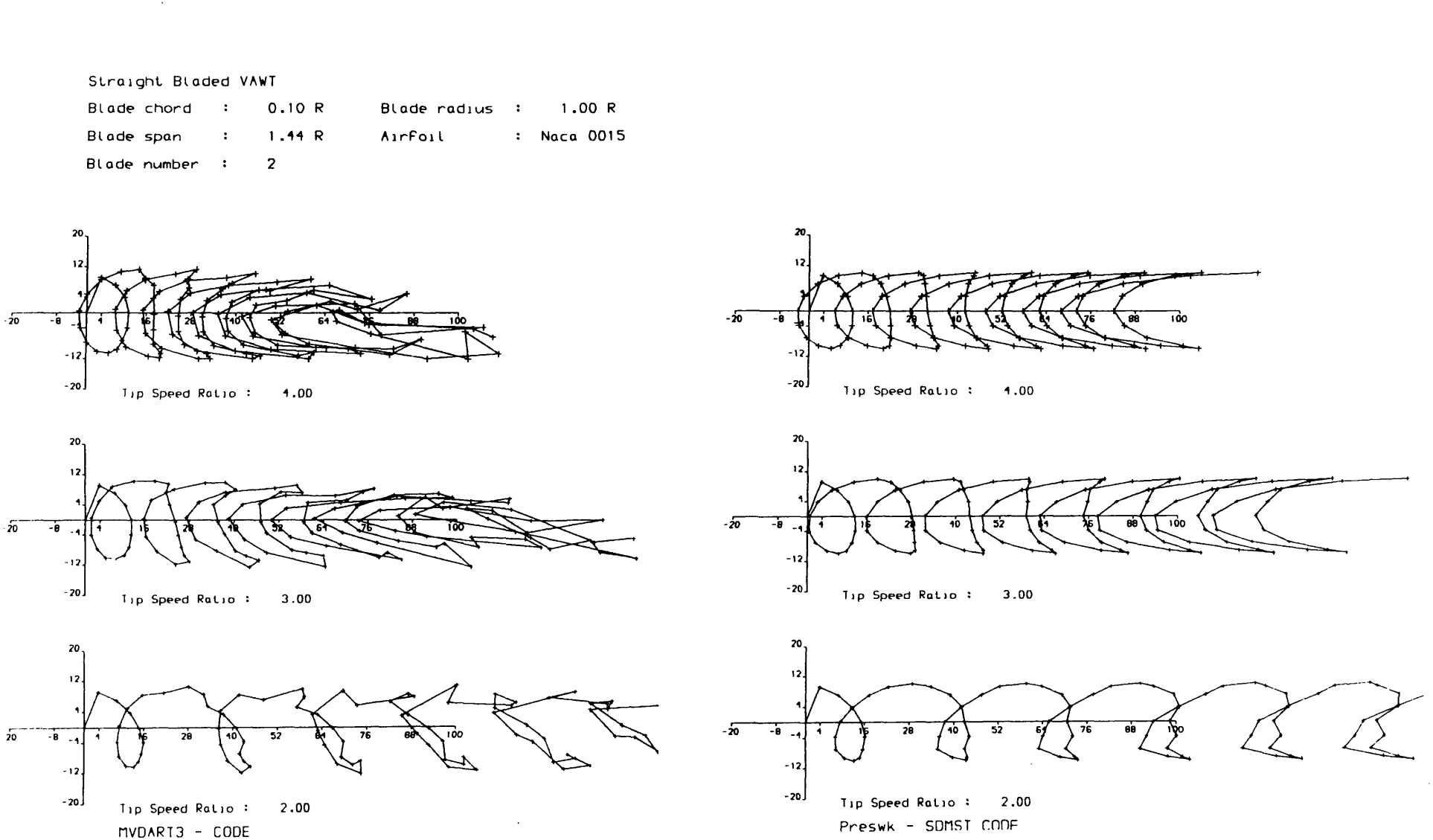

Fig.4.5 A comparison of the wake shapes at the mid blade span between the Free Wake method [MVDART3] and PRESWK-SDMST for different values of tip speed ratio.

Straight Bladed VAWT

Blade chord	: 0.10 R	Blade radius	: 1.00 R
Blade span	: 1.44 R	Airfoil	: Naca 0015
Blade number	: 2		

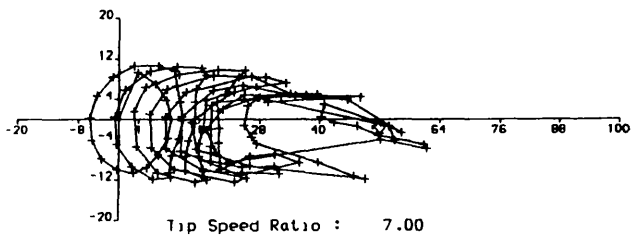

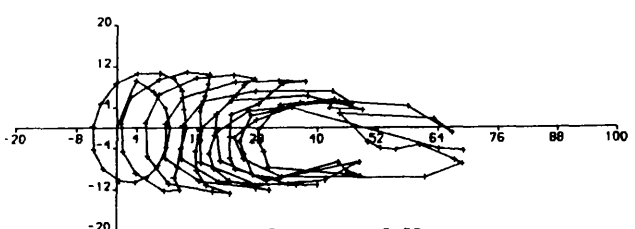

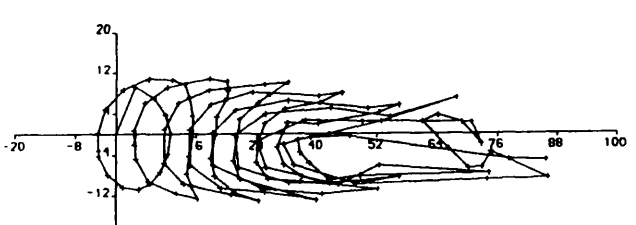

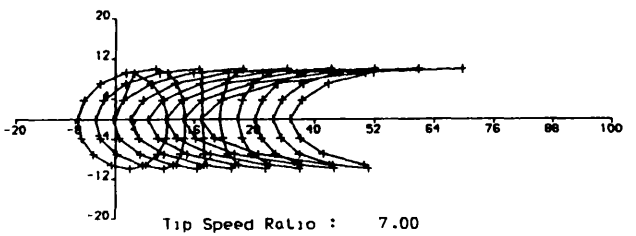

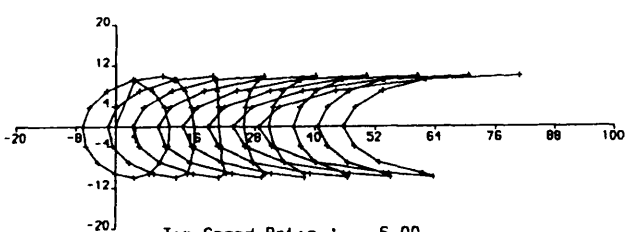

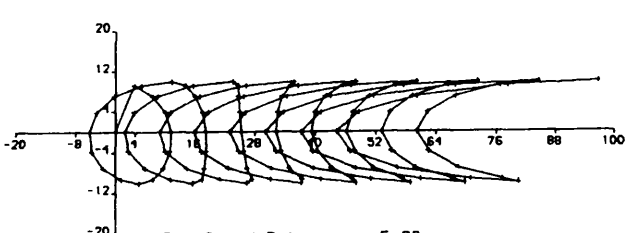

Cont'n from Fig. 4.5

Straight Bladed VAWT

Blade chord	:	0.10 R	Blade radius	:	1.0000 R
Blade span	:	1.44 R	Airfoil	:	Naca 0015
Blade number	:	2	Tip speed rat.	:	2.0000
Span sect.	:	0.63 R			

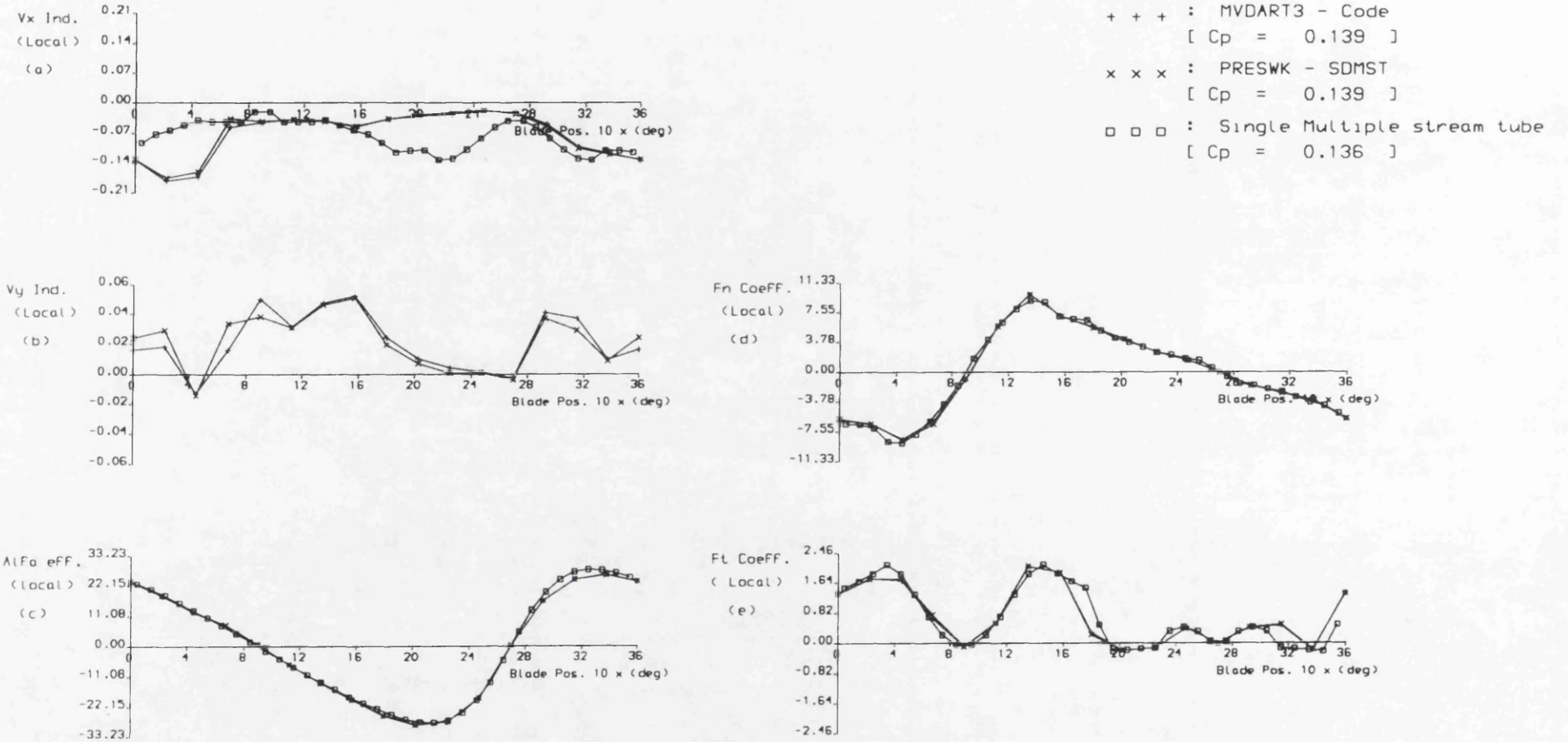

Fig.4.6a A comparison of detailed aerodynamic characteristics near the mid blade against blade azimuth position, between the Free Wake method [MVDART3], PRESWK - SDMST and SDMST for $\lambda = 2$.

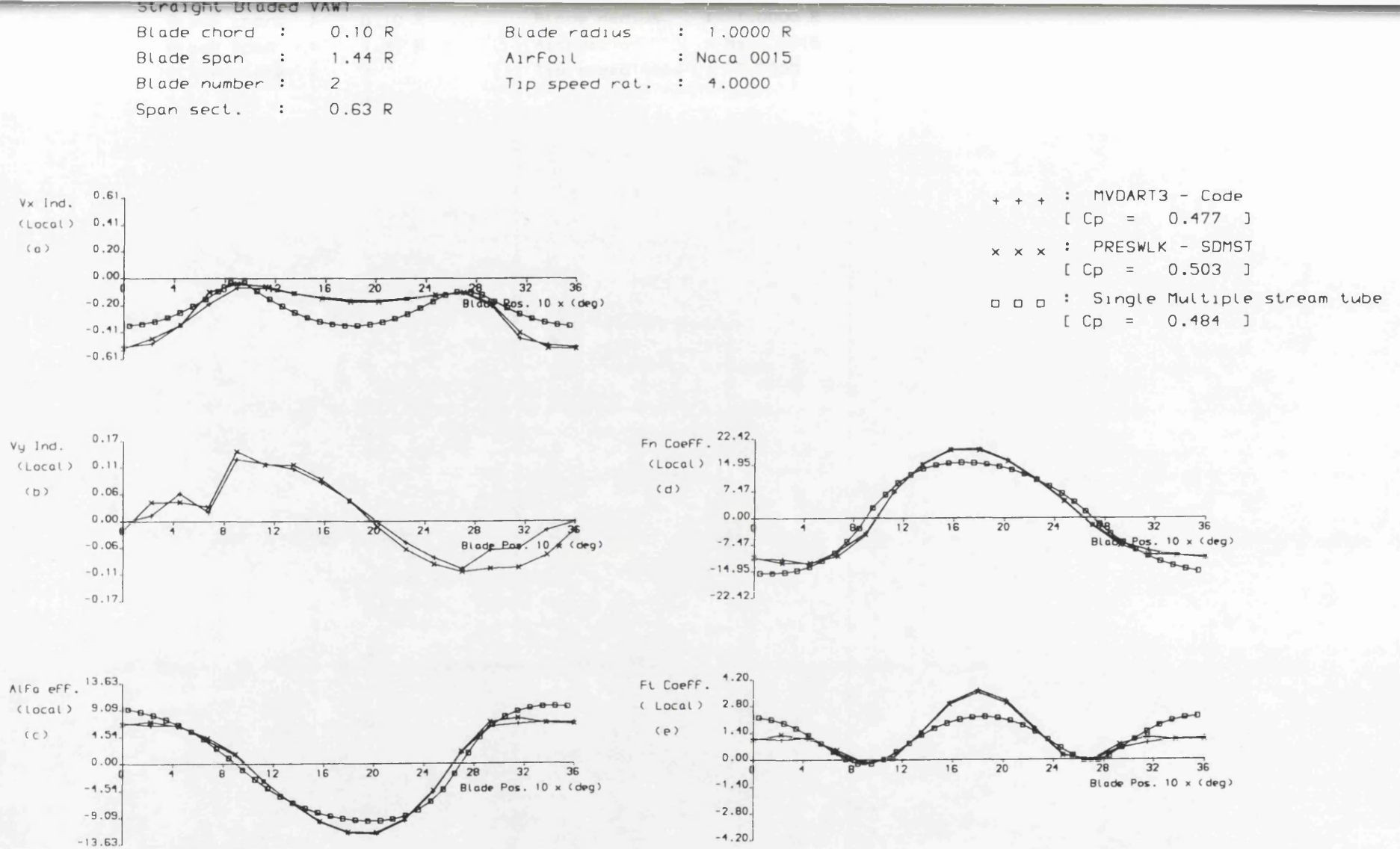

Fig.4.6b A comparison of detailed aerodynamic characteristics near the mid blade against blade azimuth position, between the Free Wake method [MVDART3], PRESWK - SDMST and SDMST for $\lambda = 4$.

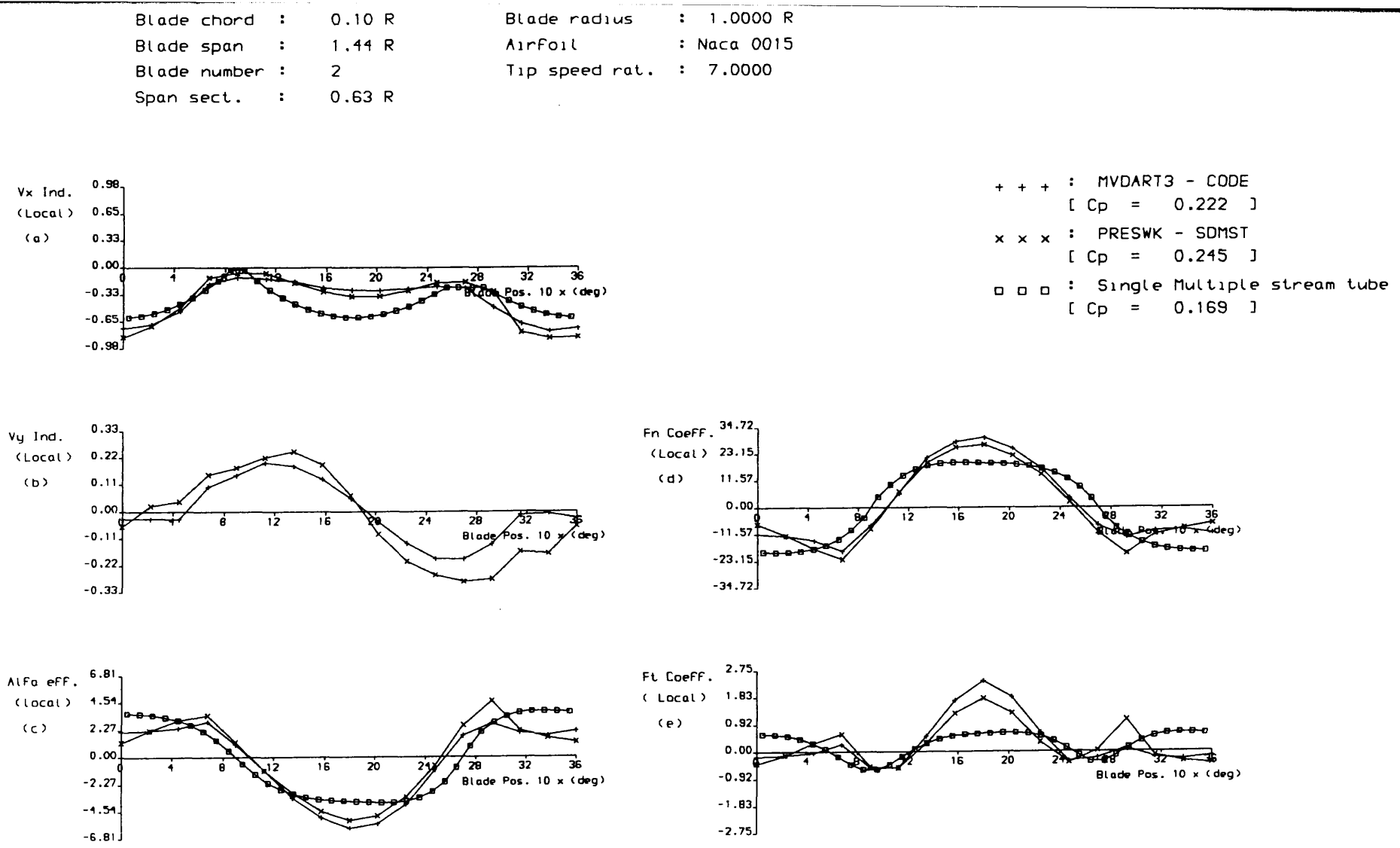

Fig.4.6c A comparison of detailed aerodynamic characteristics near the mid blade against blade azimuth position, between the Free Wake method[MVDART3], PRESWK- SDMST and SDMST for $\lambda = 7$.

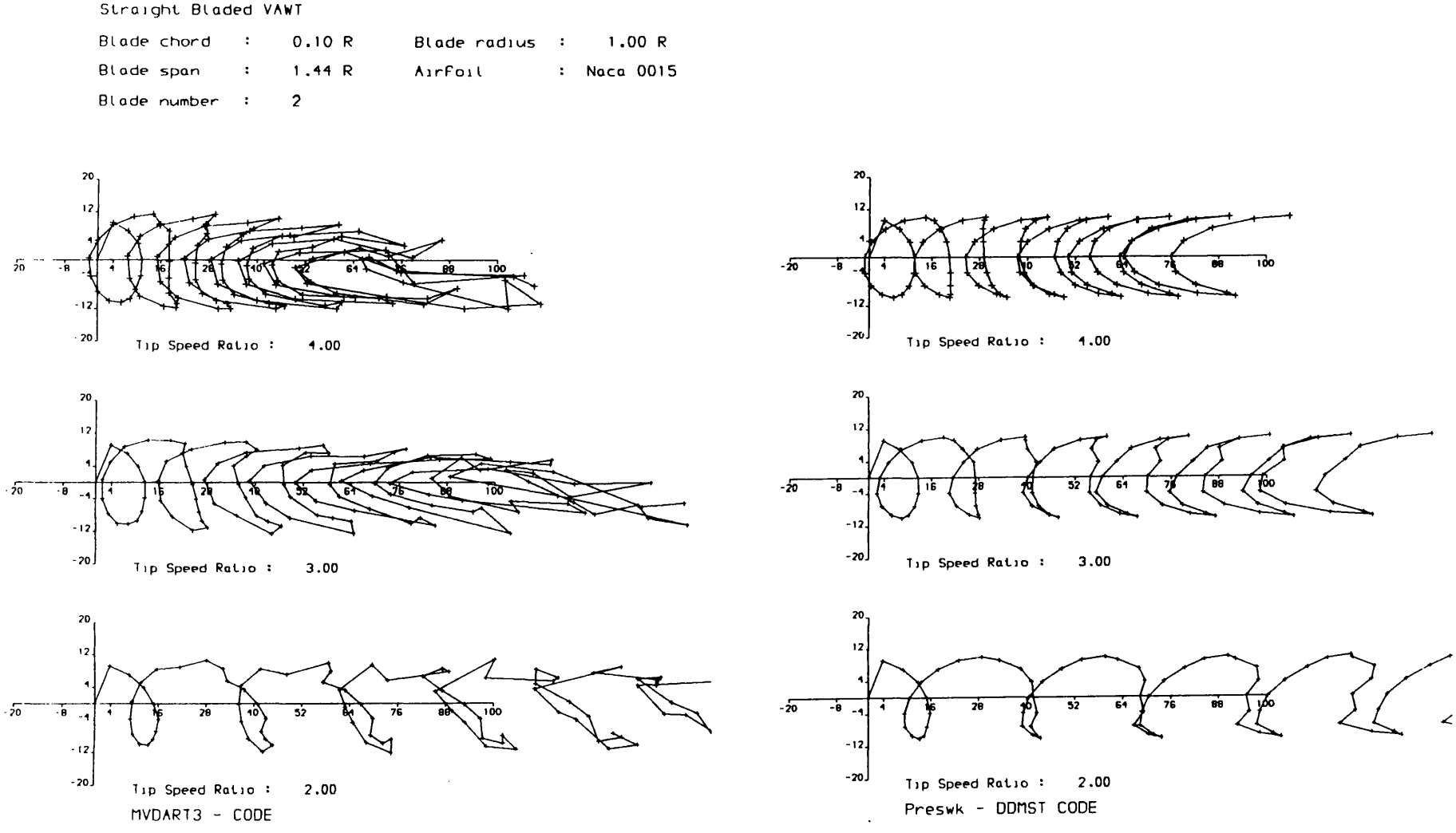

Fig.4.7 A comparison of the wake shapes at the mid blade span between the Free Wake method [MVDART3] and PRESWK-DDMST for different values of tip speed ratio.

Straight Bladed VAWT

Blade chord : 0.10 R Blade radius : 1.00 R

Blade span : 1.44 R Airfoil : Naca 0015

Blade number : 2

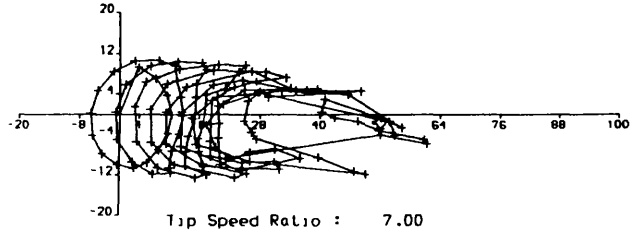

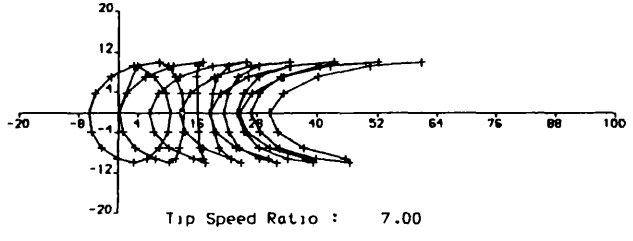

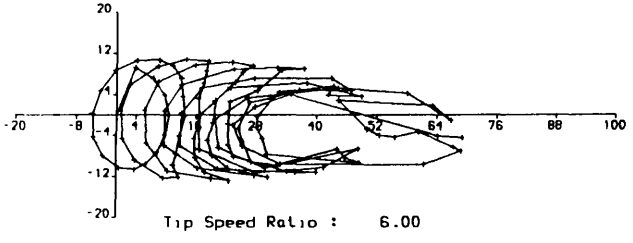

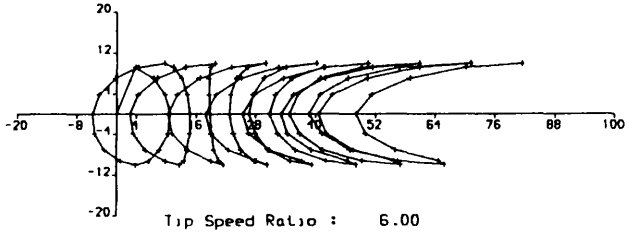

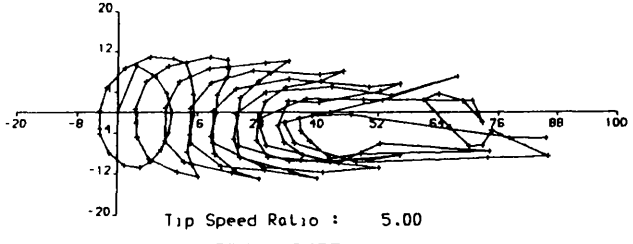

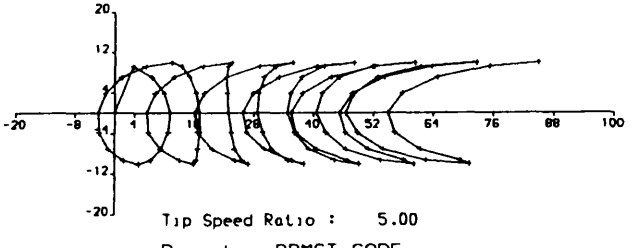

Cont'n from Fig. 4.7

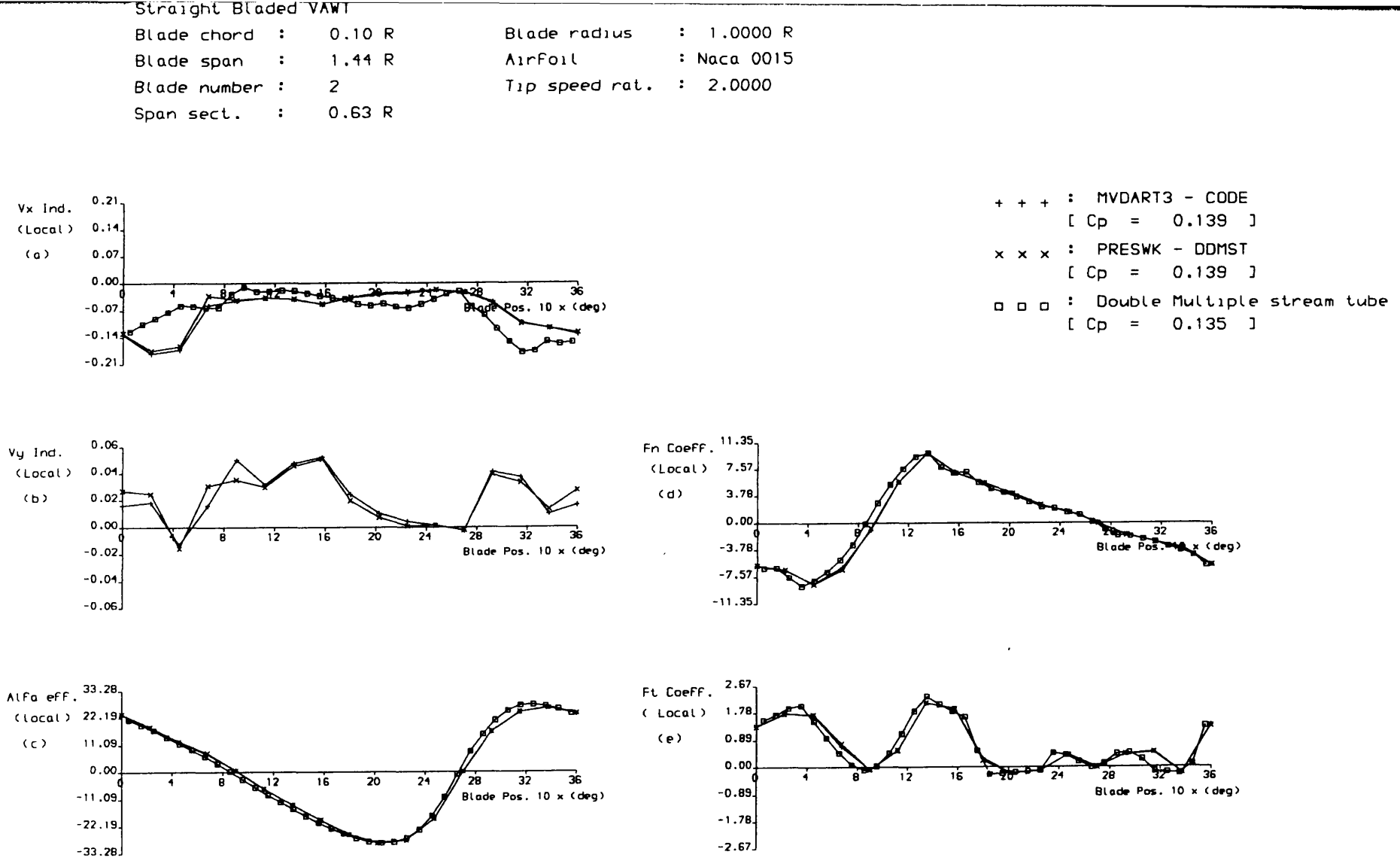

Fig.4.8a A comparison of detailed aerodynamic characteristics near the mid blade against blade azimuth position, between the Free Wake method [MVDART3], PRESWK -DDMST and DDMST for $\lambda = 2$.

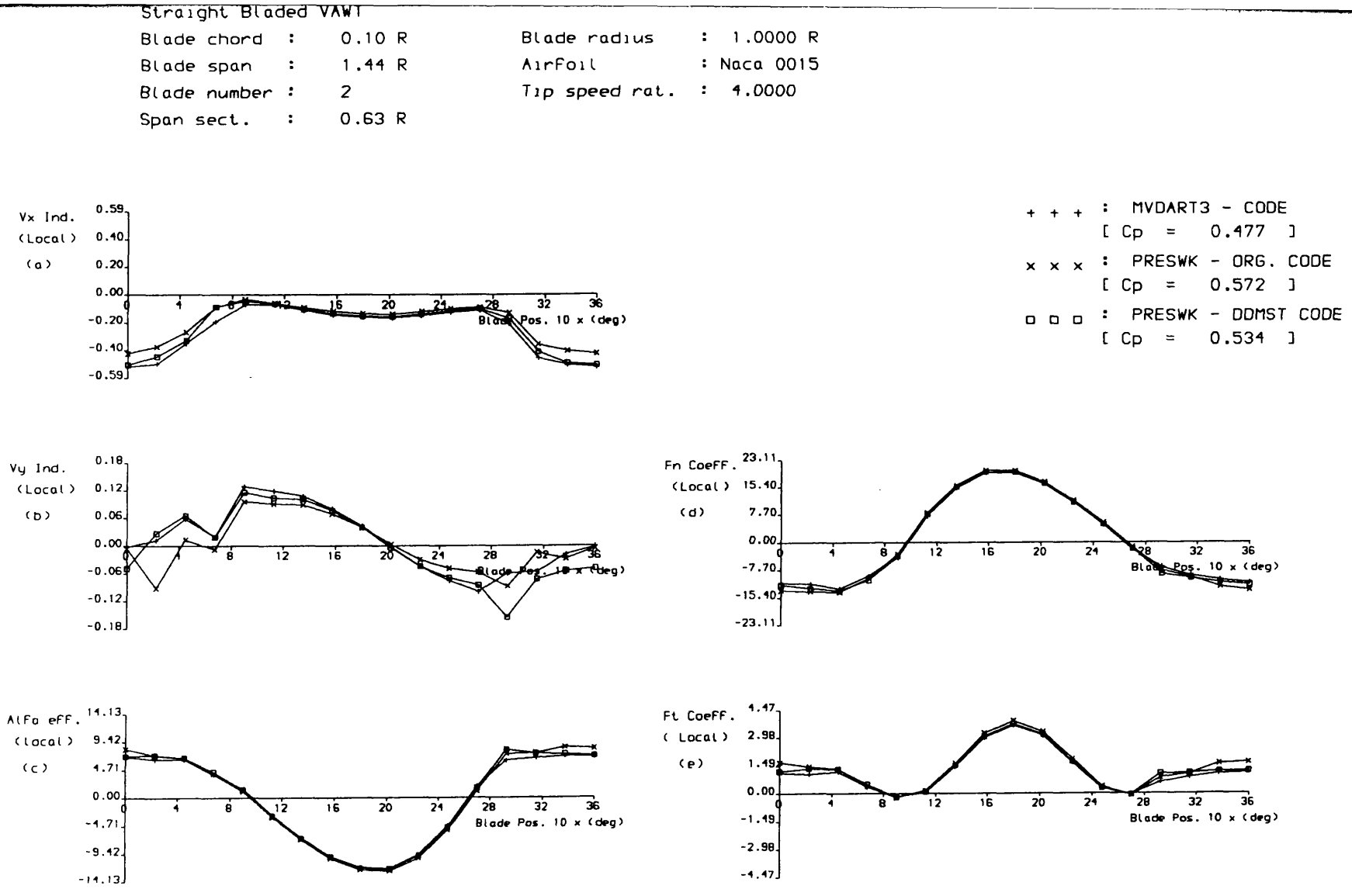

Fig.4.8b A comparison of detailed aerodynamic characteristics near the mid blade against blade azimuth position, between the Free Wake method [MVDART3], PRESWK -Org. and PRESWK- DDMST for $\lambda = 4$.

Blade chord : 0.10 R
Blade span : 1.44 R
Blade number : 2
Span sect. : 0.63 R

Blade radius : 1.0000 R
Airfoil : Naca 0015
Tip speed rat. : 7.0000

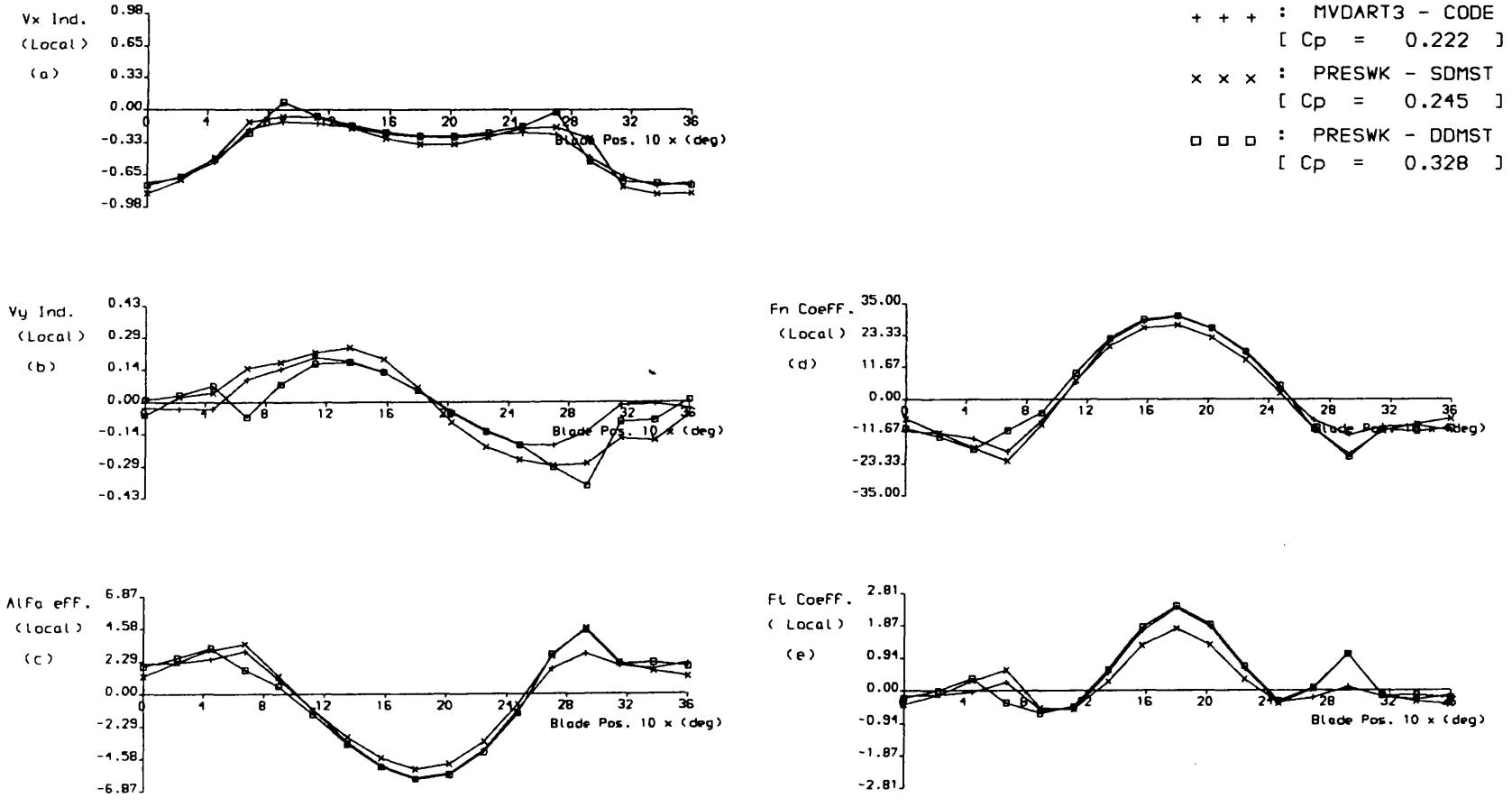

Fig.4.8c A comparison of detailed aerodynamic characteristics near the mid blade against blade azimuth position, between the Free Wake method[MVDART3], PRESWK - SDMST and PRESWK-DDMST for $\lambda = 7$.

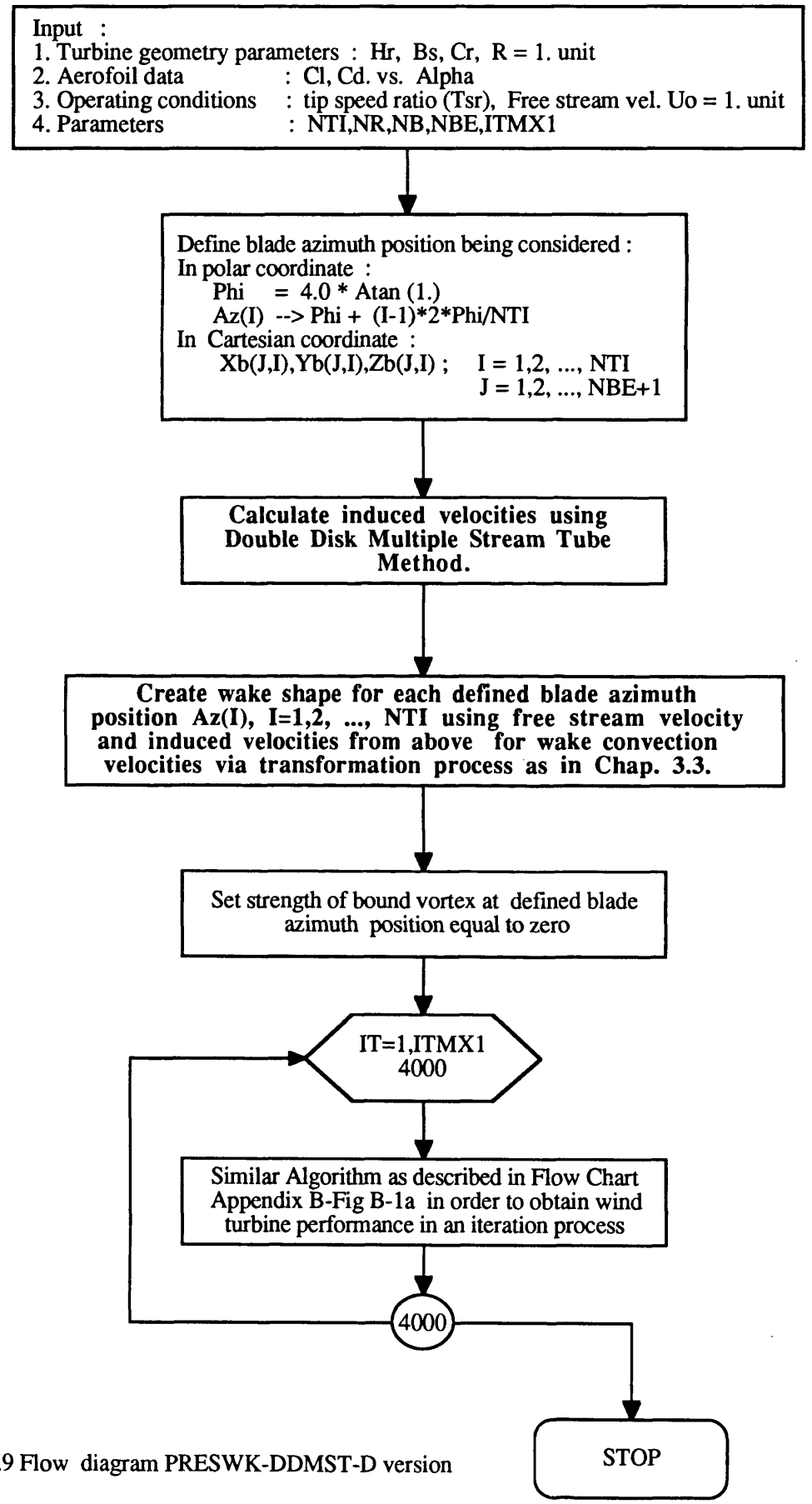

Fig. 4.9 Flow diagram PRESWK-DDMST-D version

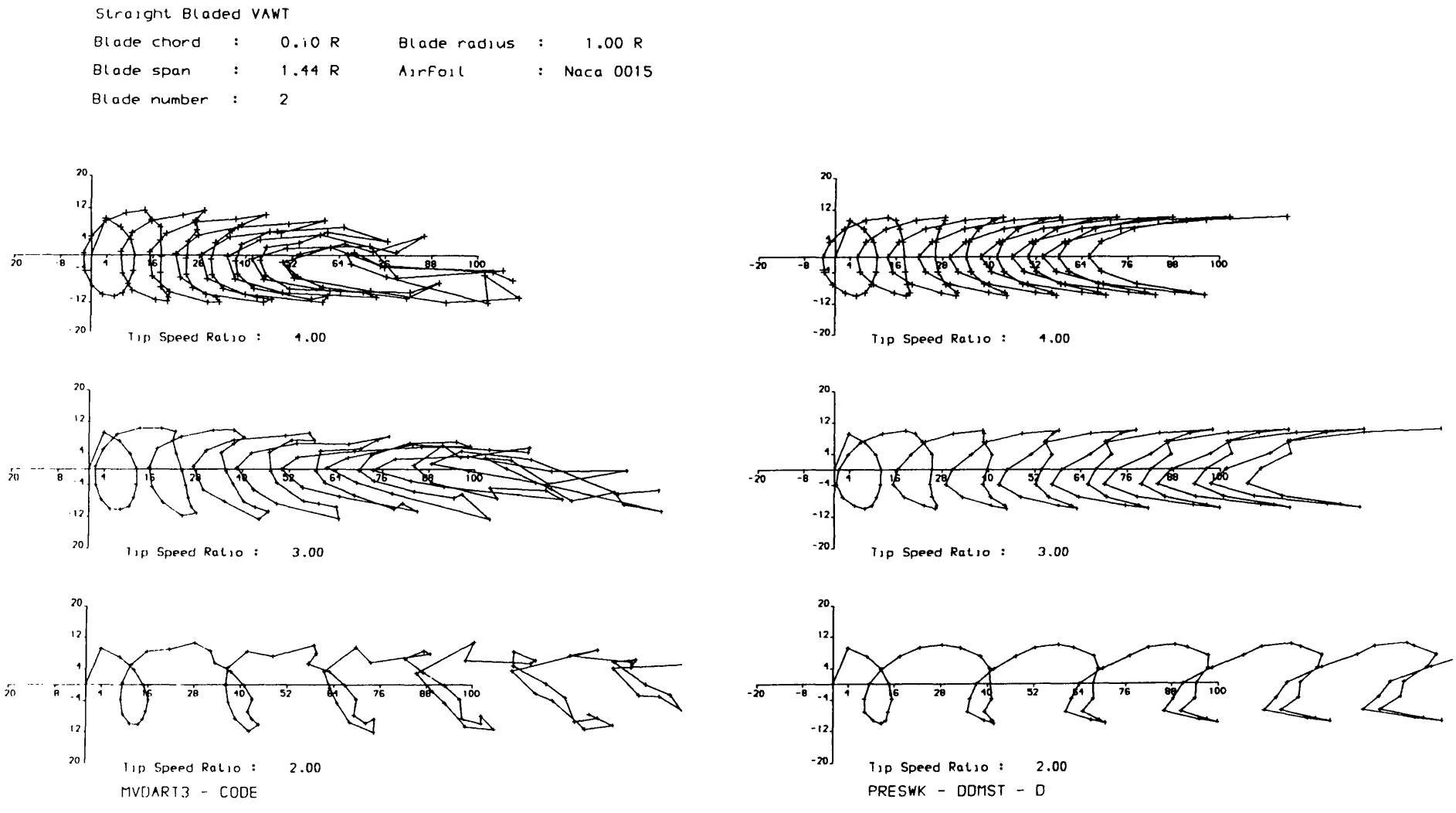

Fig.4.10 A comparison of the wake shapes at the mid blade span between the Free Wake method [MVDART3] and PRESWK-DDMST - D for different values of tip speed ratio.

Straight Bladed VAWT

Blade chord	:	0.10 R	Blade radius	:	1.00 R
Blade span	:	1.44 R	Airfoil	:	Naca 0015
Blade number	:	2			

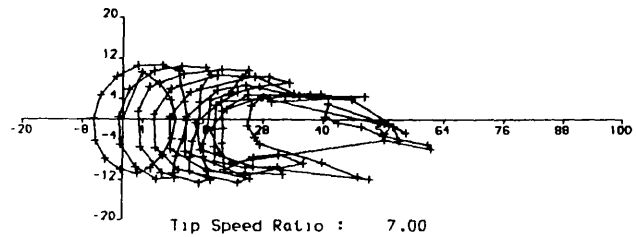

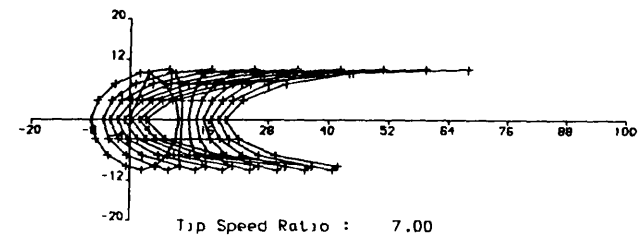

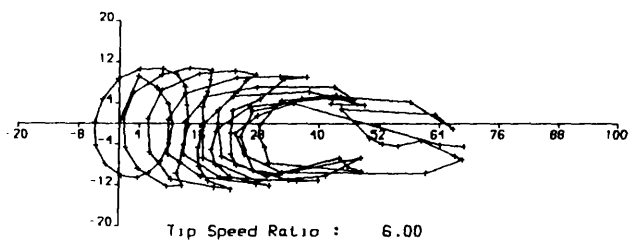

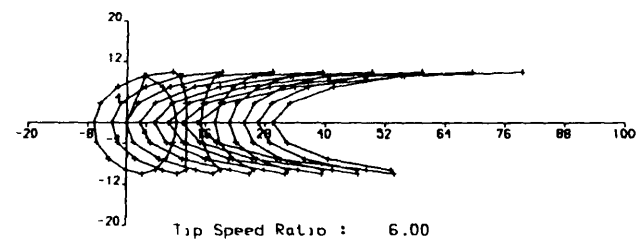

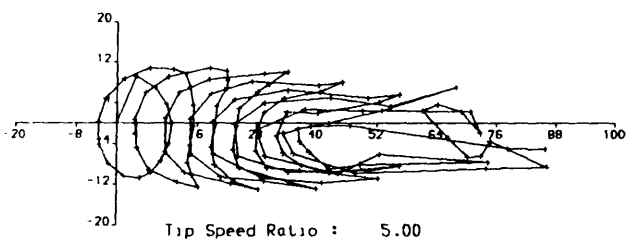

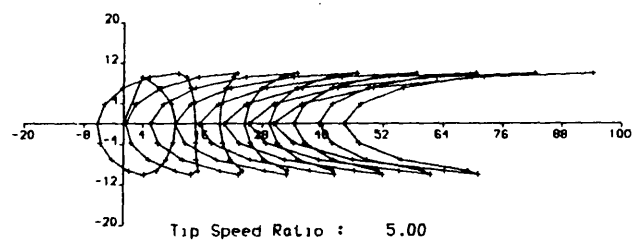

Cont'n from Fig. 4.10

Blade chord	: 0.10 R	Blade radius	: 1.0000 R
Blade span	: 1.44 R	Airfoil	: Naca 0015
Blade number	: 2	Tip speed rat.	: 6.0000
Span sect.	: 0.63 R		

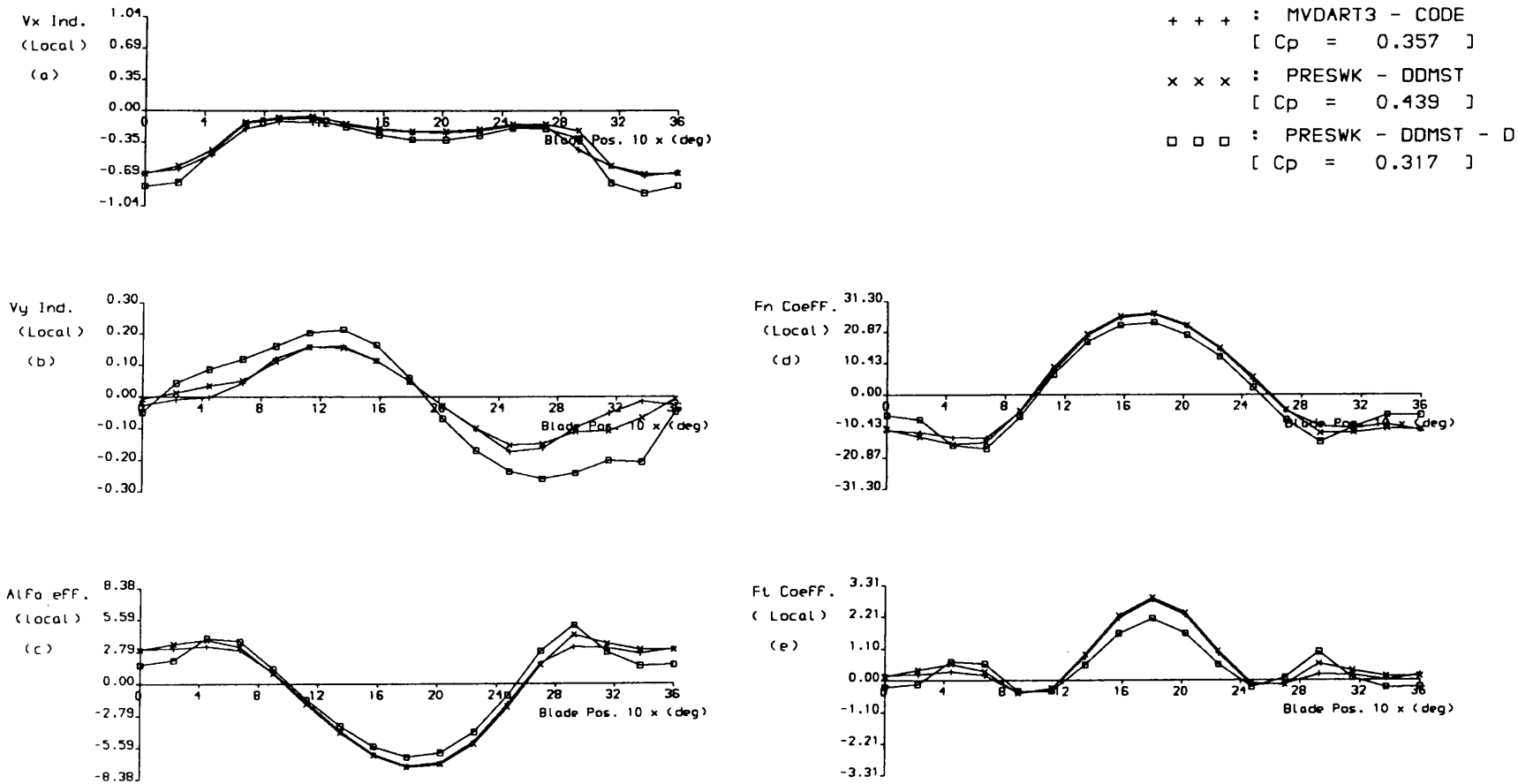

Fig.4.11a A comparison of detailed aerodynamic characteristics near the mid blade against blade azimuth position, between the Free Wake method [MVDART3], PRESWK-DDMST and PRESWK-DDMST-D for $\lambda = 6$.

1-OCT-91

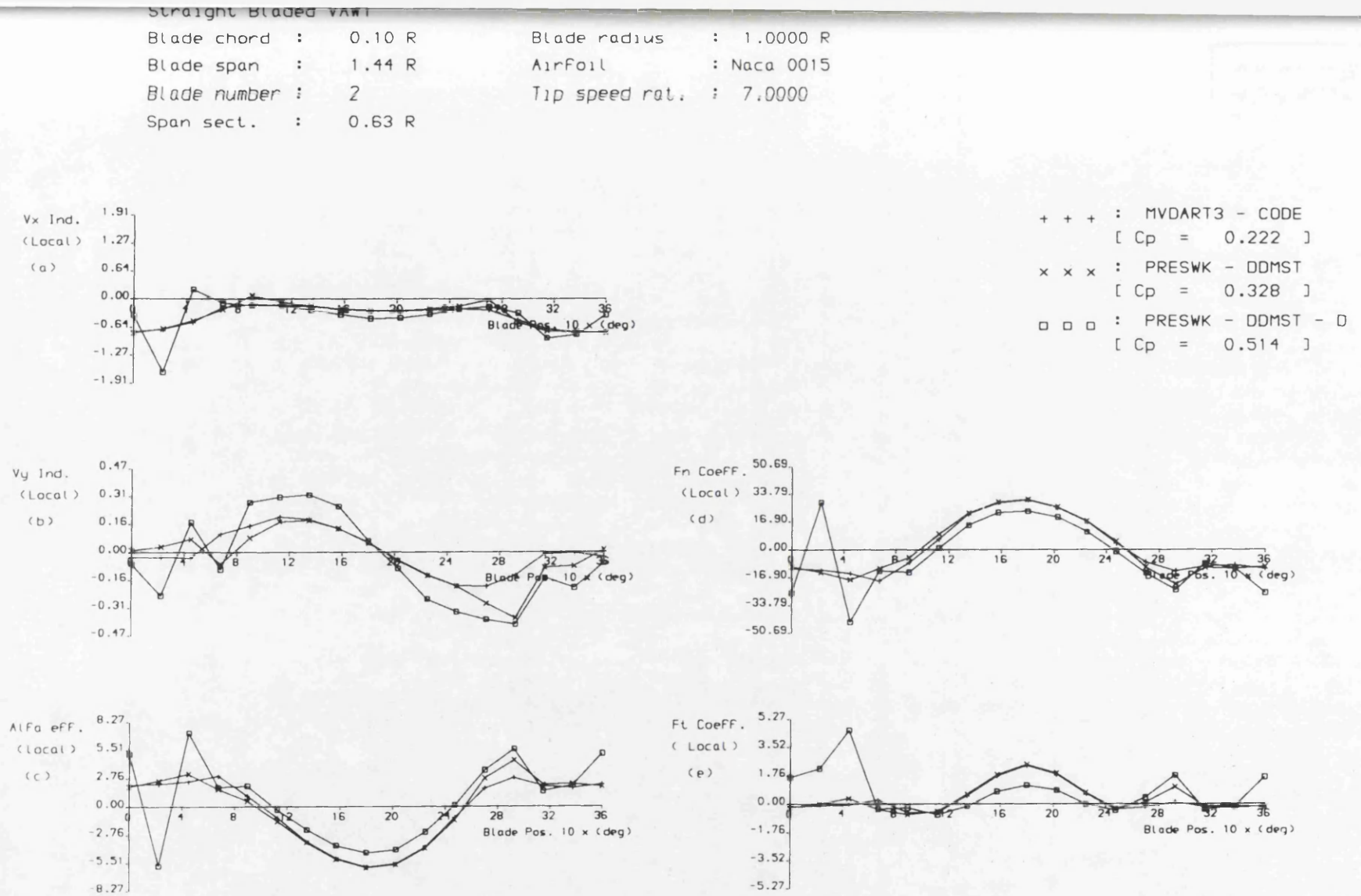

Fig.4.11b A comparison of detailed aerodynamic characteristics near the mid blade against blade azimuth position, between the Free Wake method [MVDART3], PRESWK- DDMST and PRESWK-DDMST-D for $\lambda = 7$.

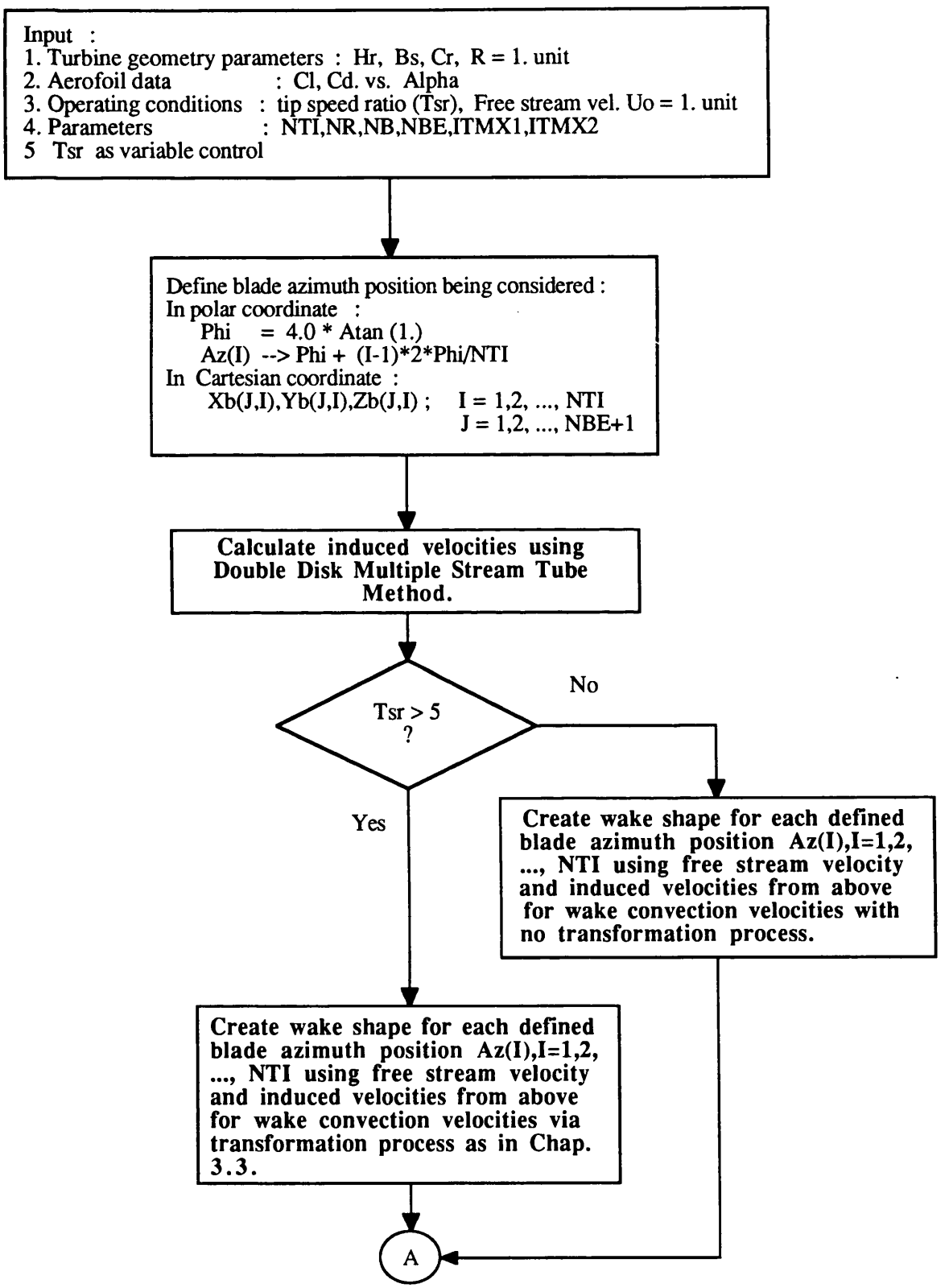

Fig. 4.12 Flow diagram PRESWK-INCON-Y1 version

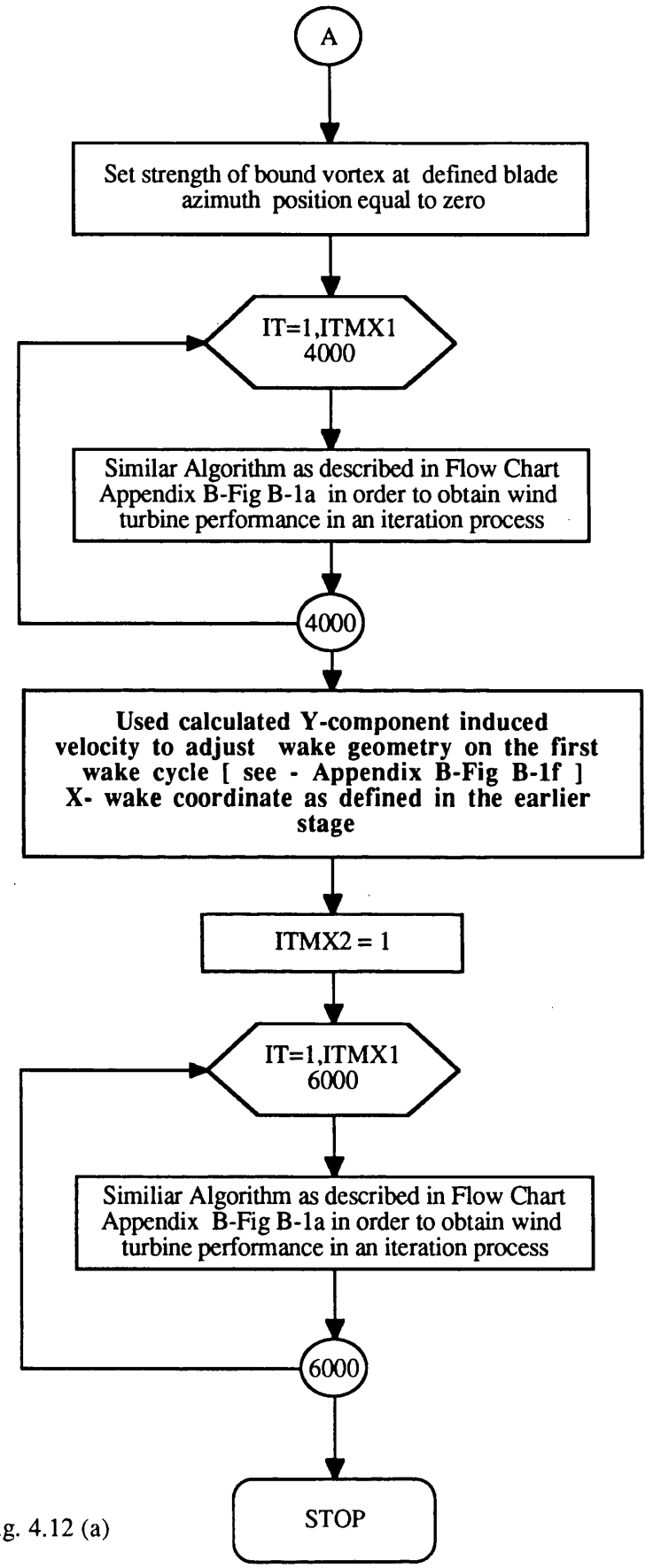

Cont'n from Fig. 4.12 (a)

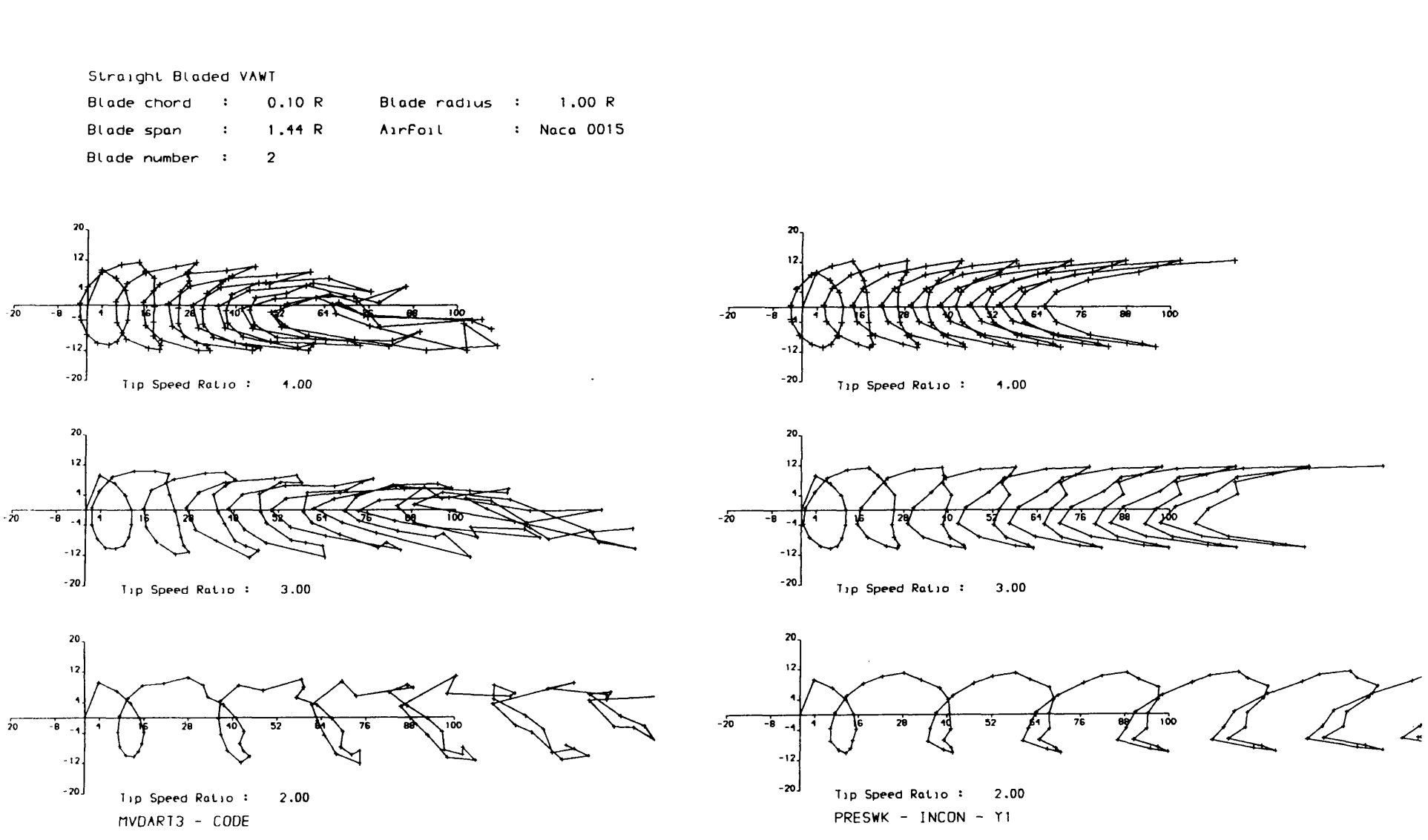

Fig.4.13 A comparison of the wake shapes at the mid blade span between the Free Wake method [MVDART3] and PRESWK-INCON-Y1 for different values of tip speed ratio.

Straight Bladed VAWT

Blade chord : 0.10 R Blade radius : 1.00 R

Blade span : 1.44 R Airfoil : Naca 0015

Blade number : 2

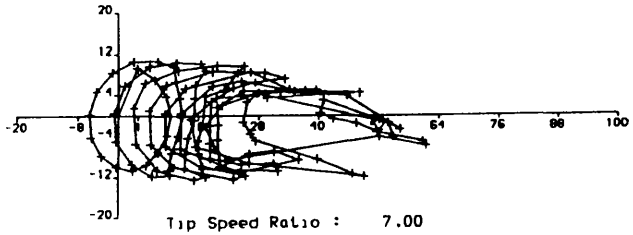

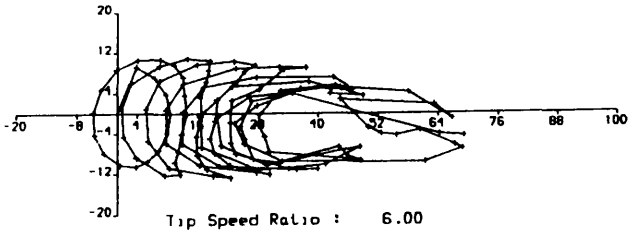

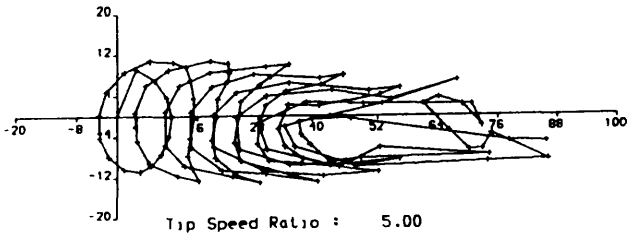

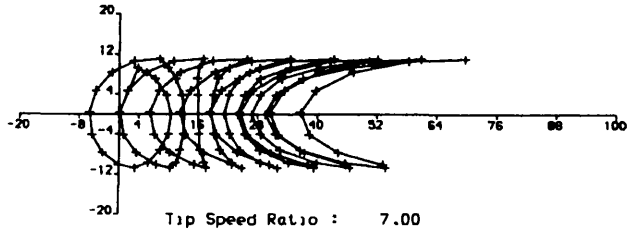

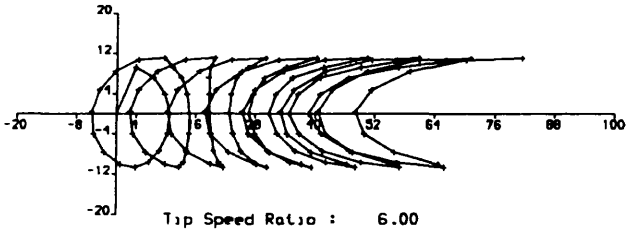

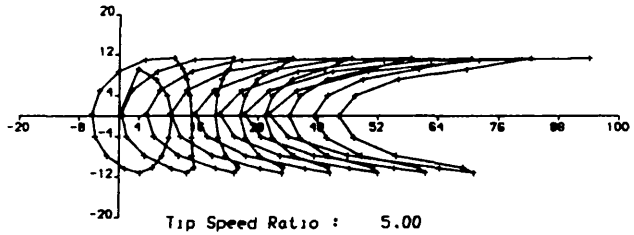

Cont'n from Fig. 4.13

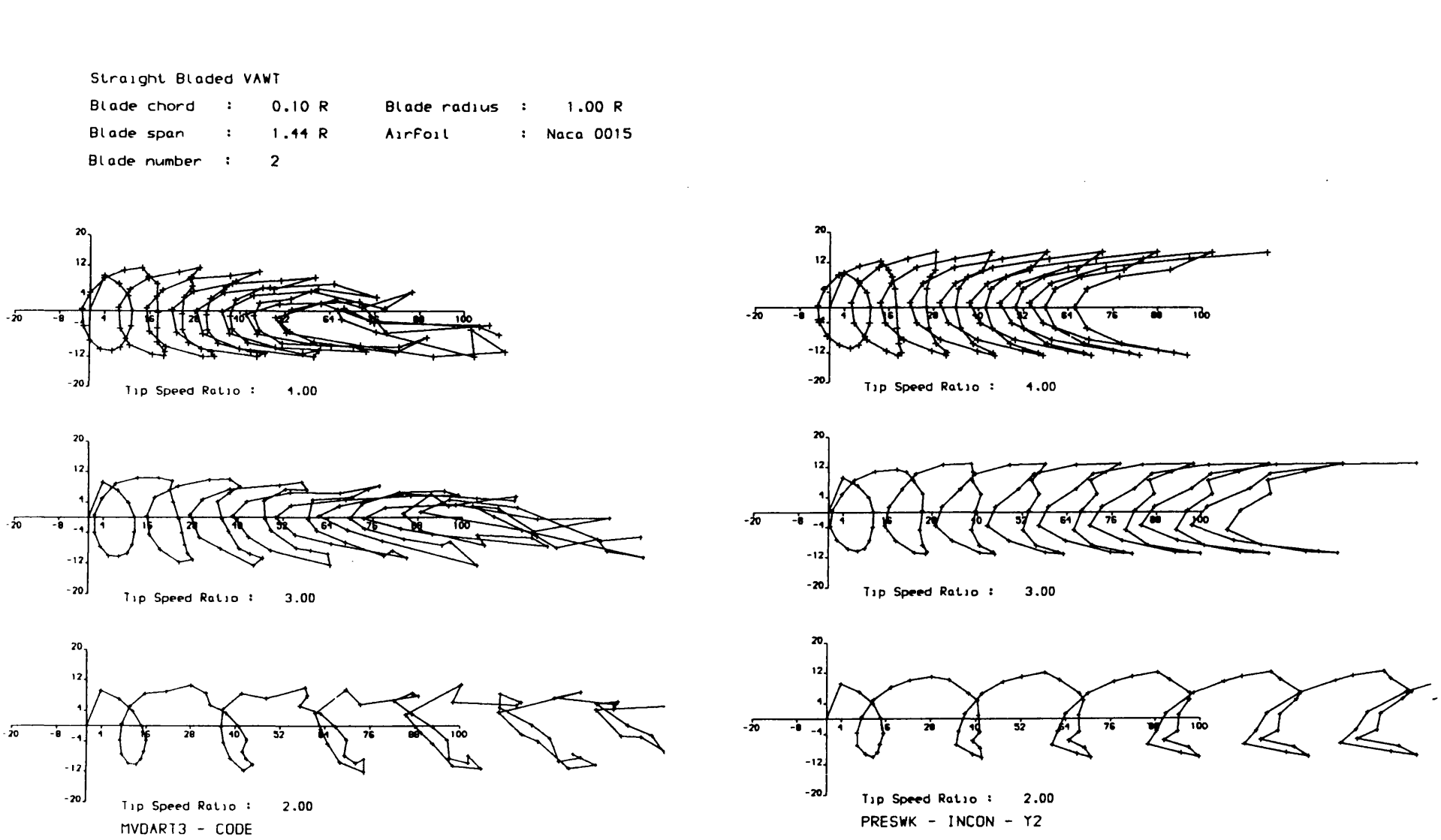

Fig.4.14 A comparison of the wake shapes at the mid blade span between the Free Wake method [MVDART3] and PRESWK-INCON-Y2 for different values of tip speed ratio.

Straight Bladed VAWT

Blade chord	:	0.10 R	Blade radius	:	1.00 R
Blade span	:	1.44 R	Airfoil	:	Naca 0015
Blade number	:	2			

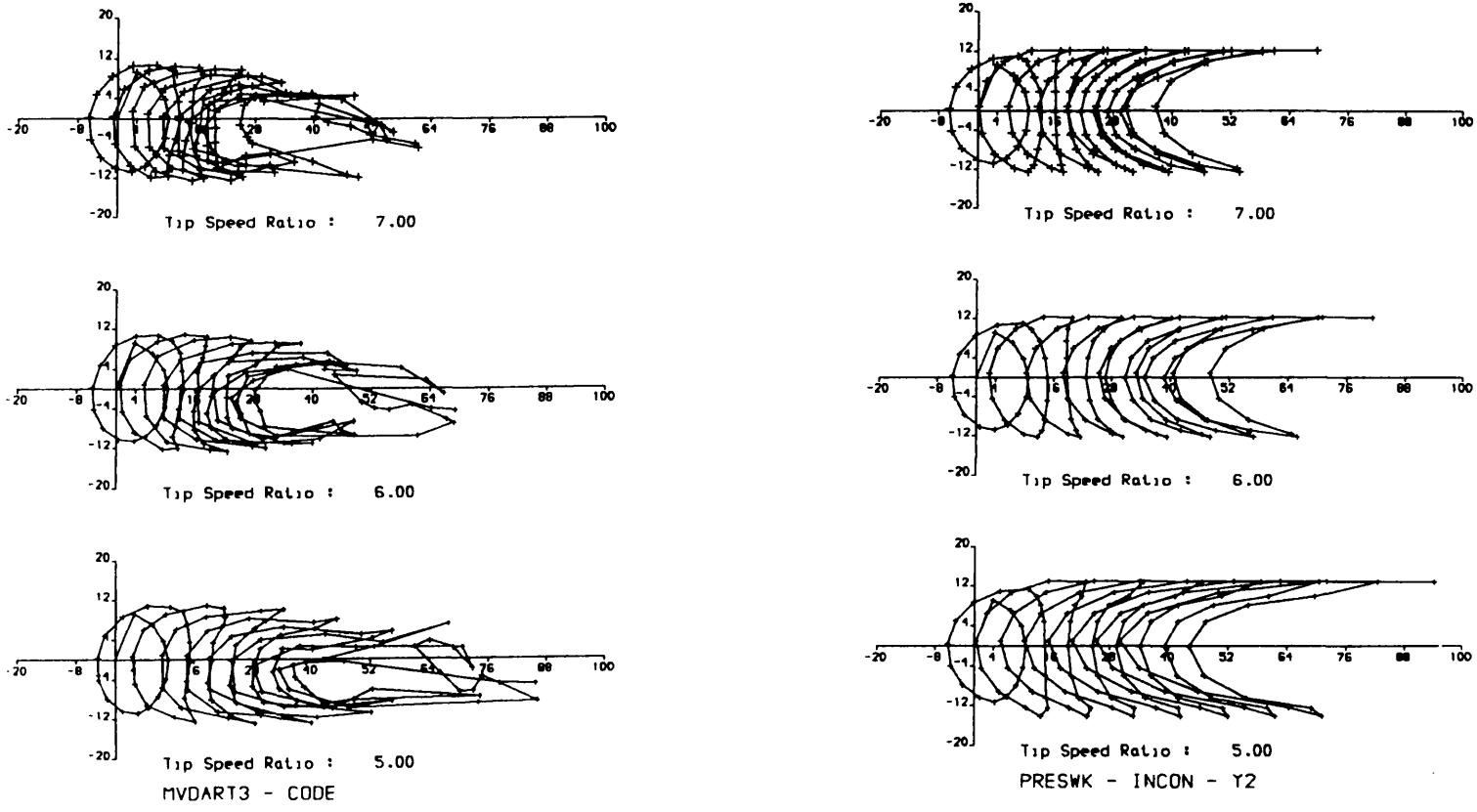

Cont'n from Fig. 4.14

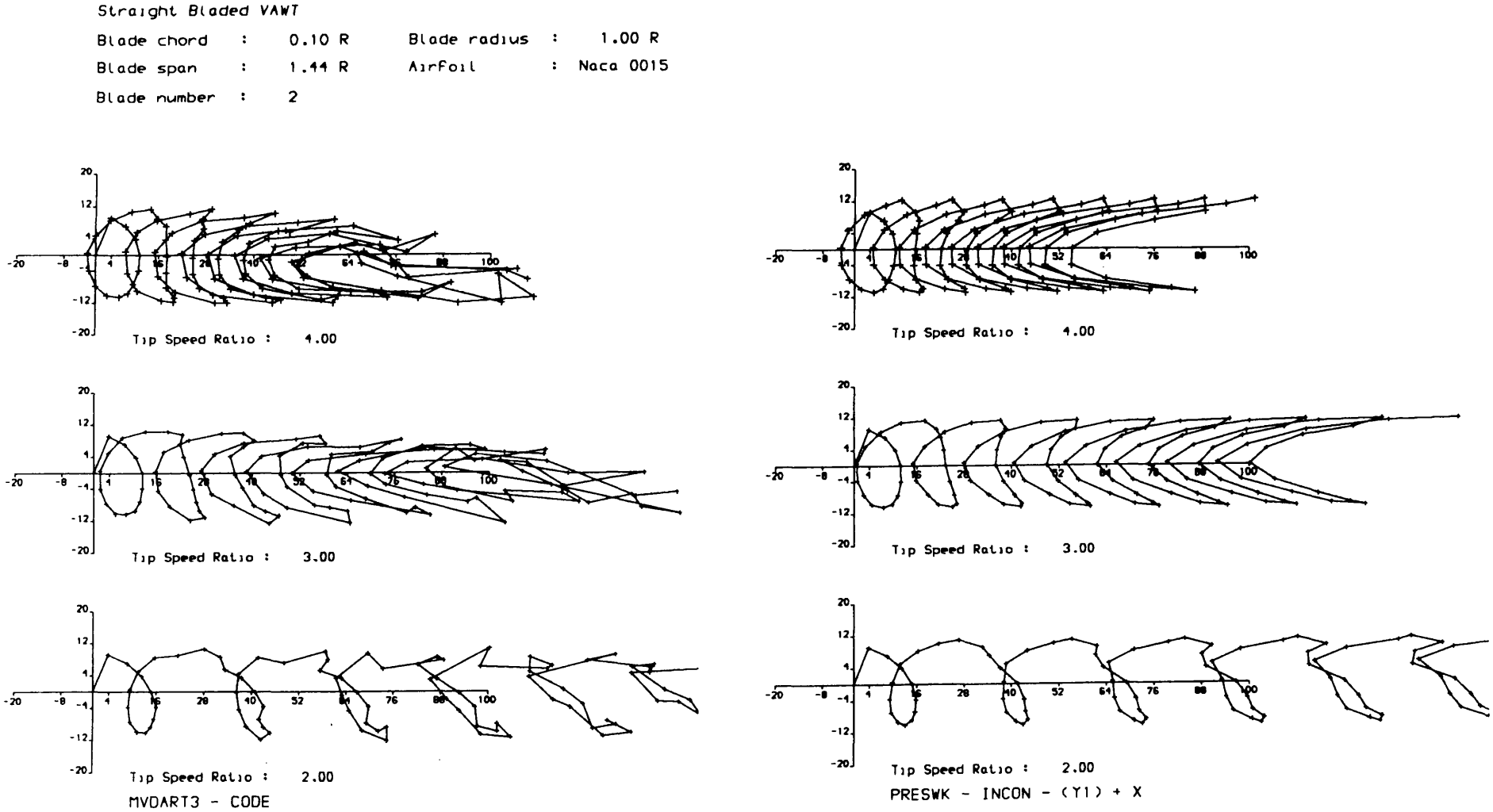

Fig.4.15 A comparison of the wake shapes at the mid blade span between the Free Wake method [MVDART3] and PESWK-INCON-(Y1)+X for different values of tip speed ratio.

Straight Bladed VAWT

Blade chord	: 0.10 R	Blade radius	: 1.00 R
Blade span	: 1.44 R	Airfoil	: Naca 0015
Blade number	: 2		

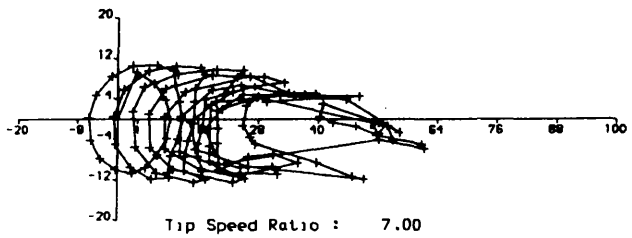

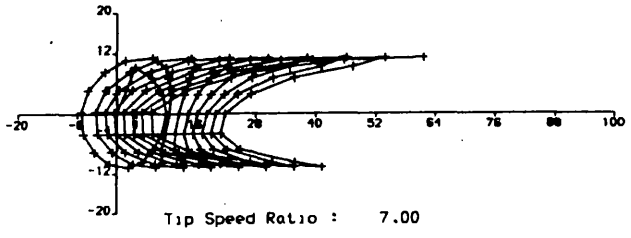

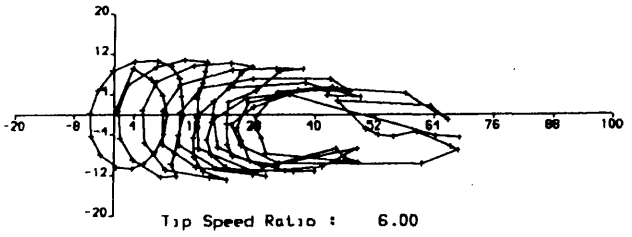

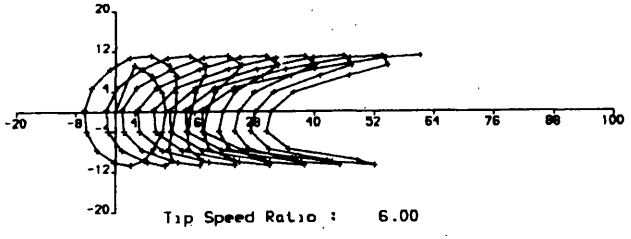

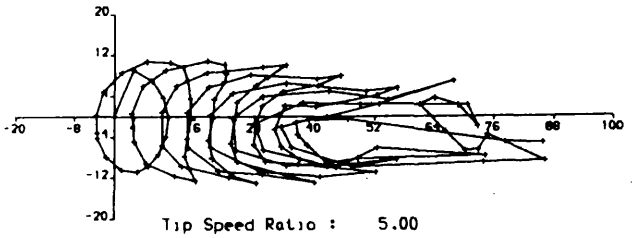

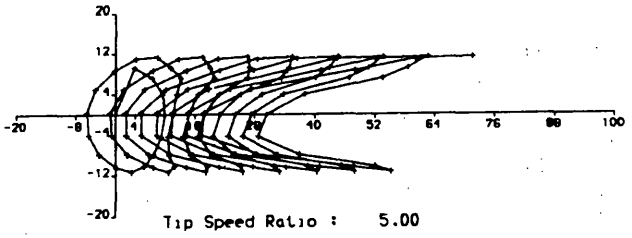

Cont'n from Fig. 4.15

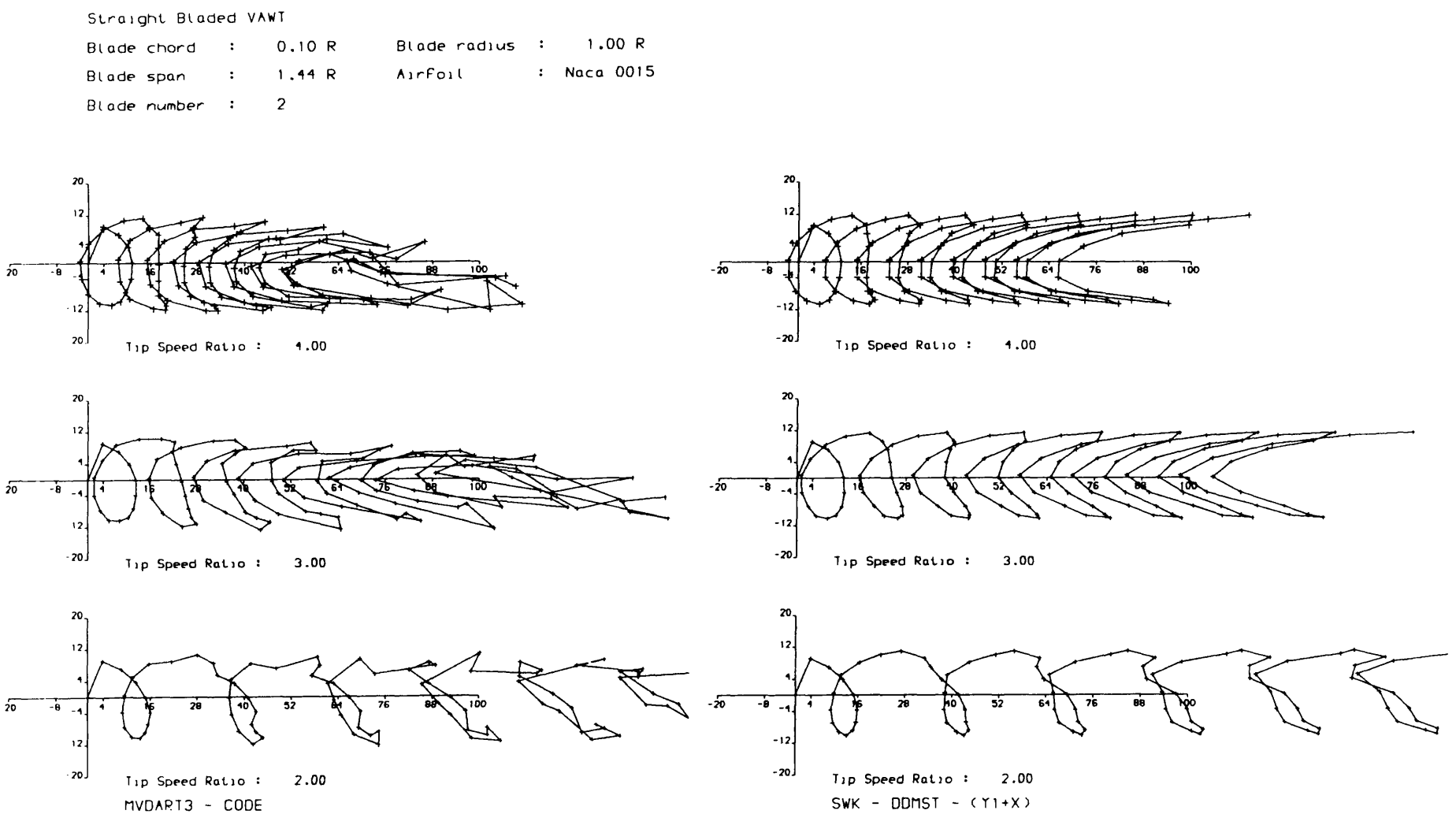

Fig.4.16 A comparison of the wake shapes at the mid blade span between the Free Wake method [MVDART3] and PRESWK-DDMST-(Y1+X) for different values of tip speed ratio.

Straight Bladed VAWT

Blade chord : 0.10 R Blade radius : 1.00 R

Blade span : 1.44 R Airfoil : Naca 0015

Blade number : 2

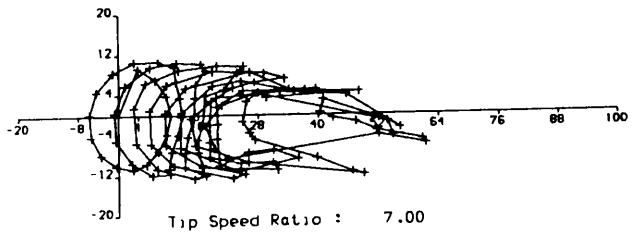

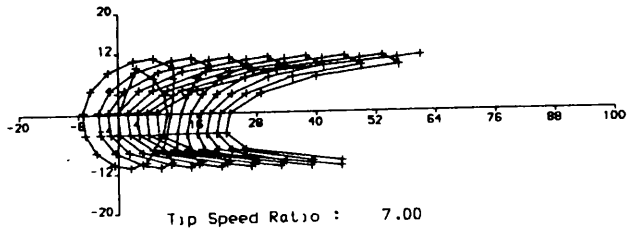

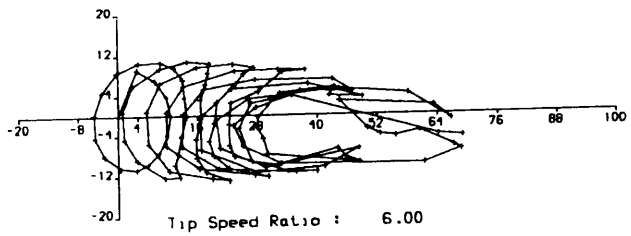

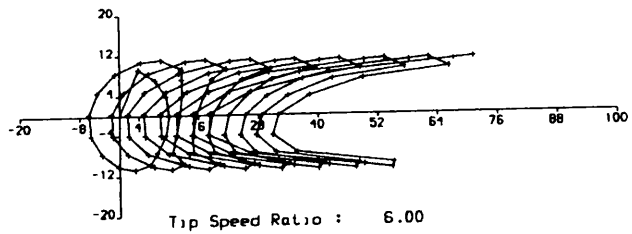

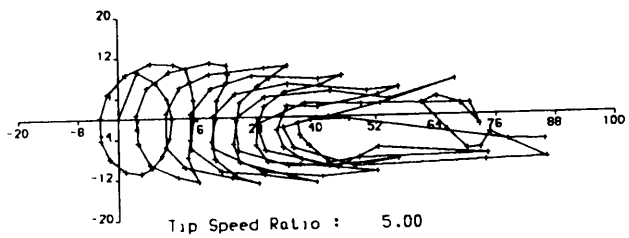

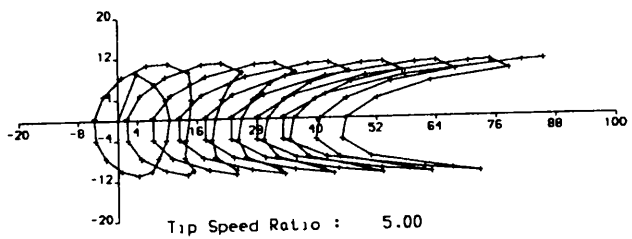

Cont'n from Fig. 4.16

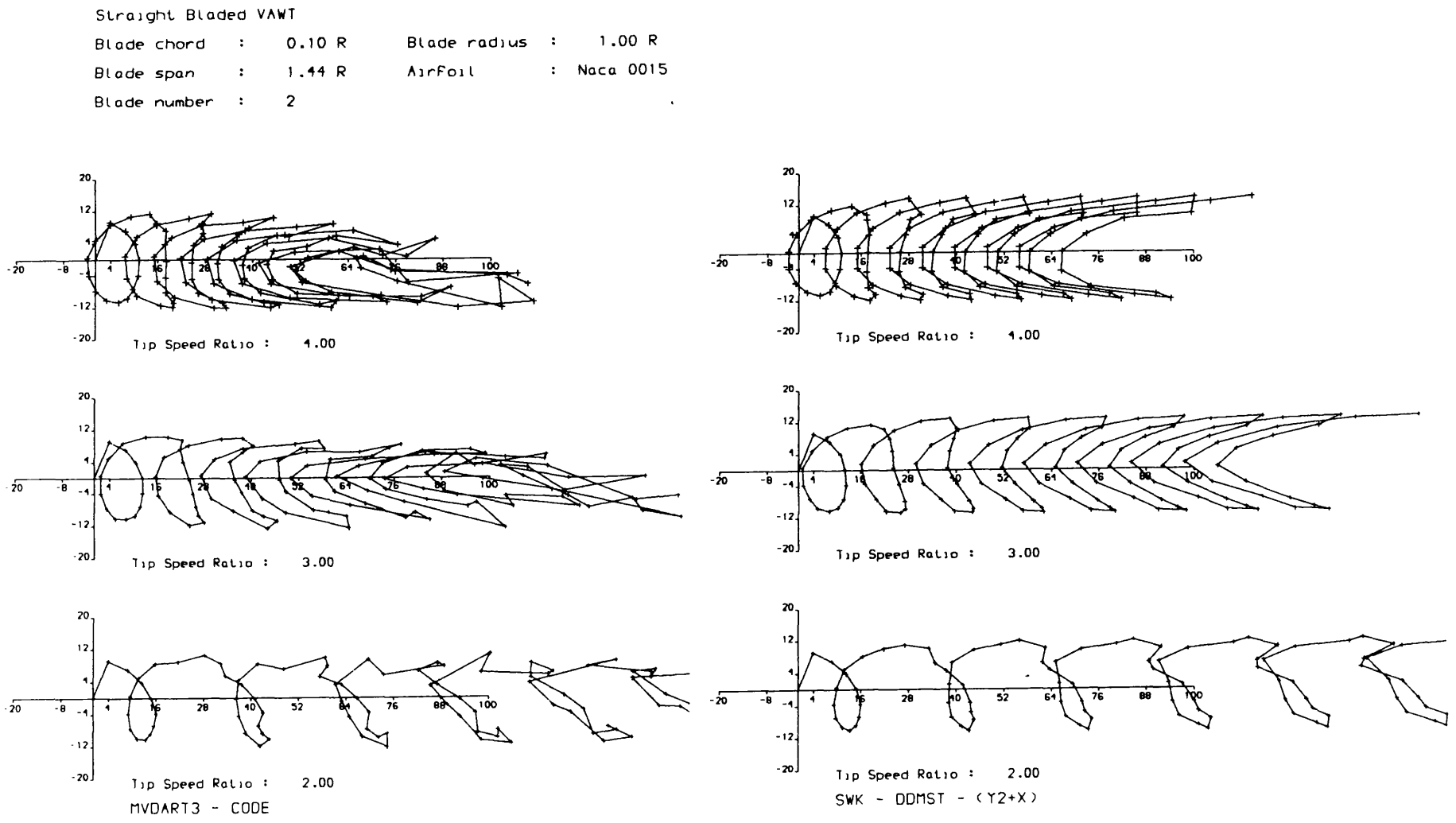

Fig.4.17 A comparison of the wake shapes at the mid blade span between the Free Wake method [MVDART3] and PRESWK-DDMST-(Y2+X) for different values of tip speed ratio.

Straight Bladed VAWT

Blade chord	:	0.10 R	Blade radius	:	1.00 R
Blade span	:	1.44 R	Airfoil	:	Naca 0015
Blade number	:	2			

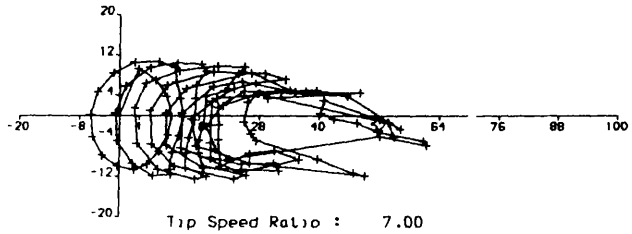

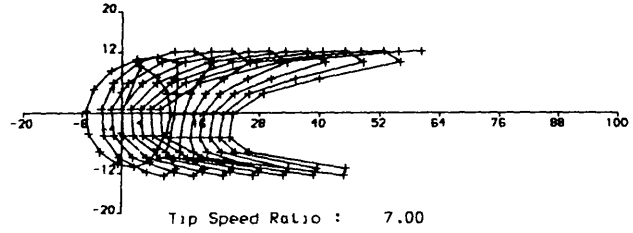

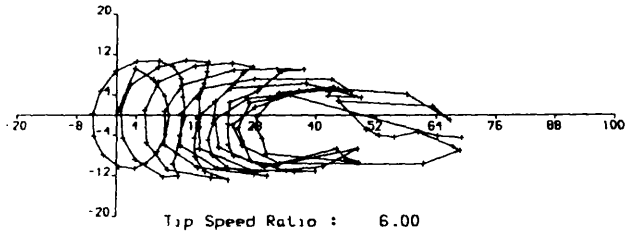

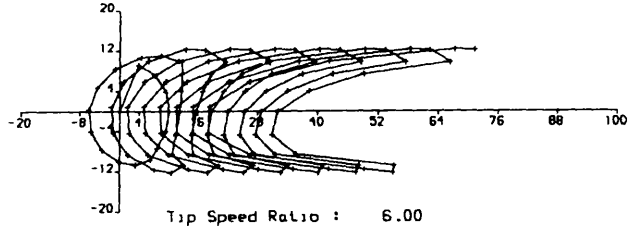

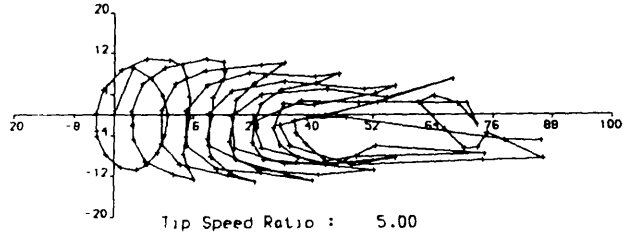

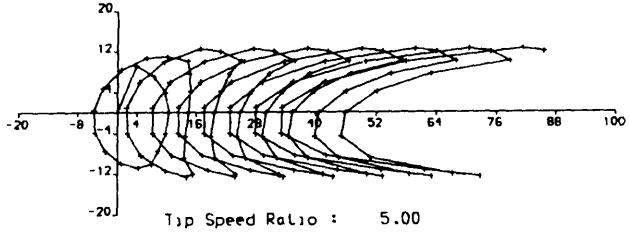

Cont'n from Fig. 4.17

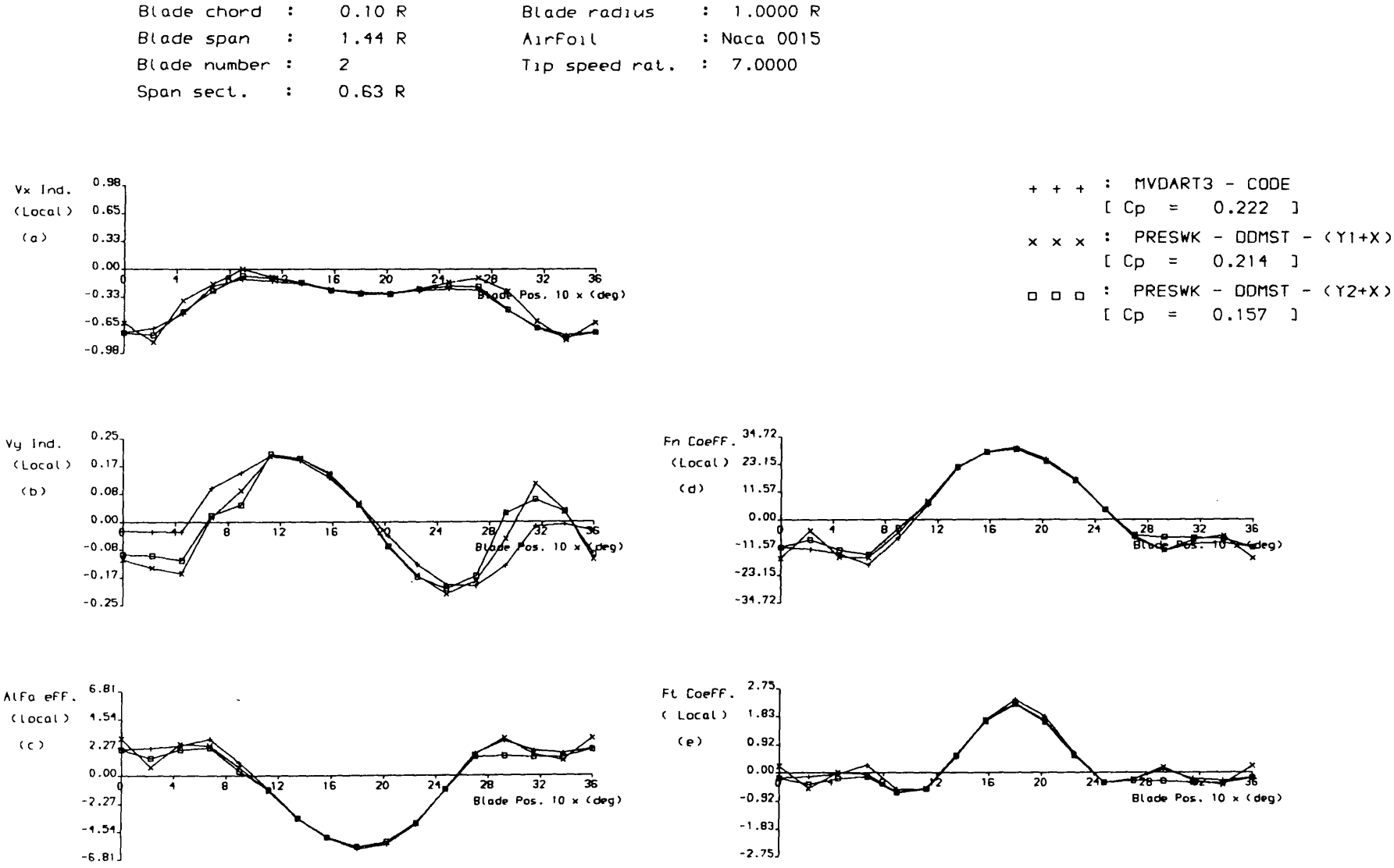

Fig.4.18 A comparison of detailed aerodynamic characteristics near the mid blade against blade azimuth position, between the Free Wake method [MVDART3], PRESWK -DDMST-(Y1+X) and PRESWK-DDMST-(Y2+X) for $\lambda = 7$.

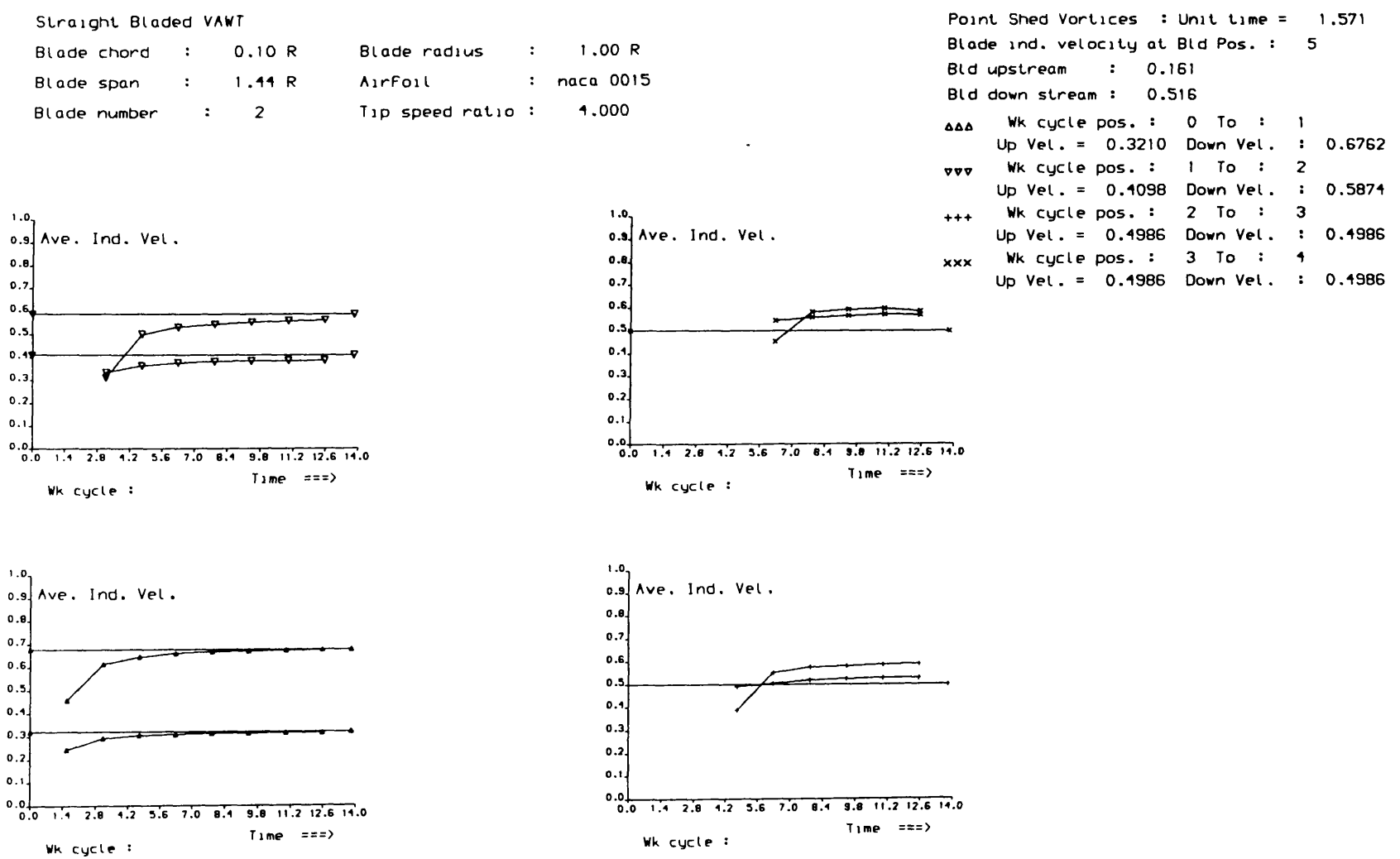

Fig.4.19 The X-component induced velocity in the flow field as function of time for tip speed ratio $\lambda = 4$.

Straight Bladed VAWT

Blade chord	:	0.10 R	Blade radius	:	1.00 R
Blade span	:	1.44 R	Airfoil	:	naca 0015
Blade number	:	2	Tip speed ratio	:	3.000

Point Shed Vortices : Unit time = 2.094
Blade ind. velocity at Bld Pos. : 5
Bld upstream : 0.115
Bld down stream : 0.375

ΔΔΔ Wk cycle pos. : 0 To : 1
Up Vel. = 0.2298 Down Vel. : 0.4894
∇∇∇ Wk cycle pos. : 1 To : 2
Up Vel. = 0.2947 Down Vel. : 0.4245
+++ Wk cycle pos. : 2 To : 3
Up Vel. = 0.3596 Down Vel. : 0.3596
xxx Wk cycle pos. : 3 To : 4
Up Vel. = 0.3596 Down Vel. : 0.3596

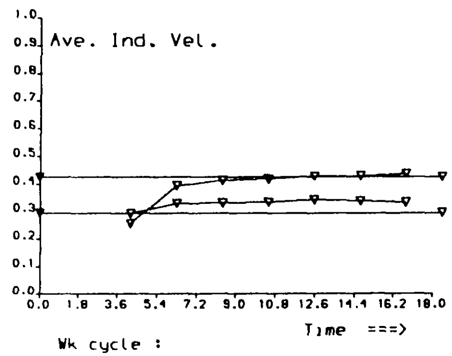

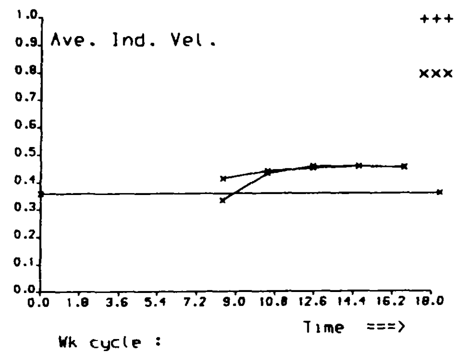

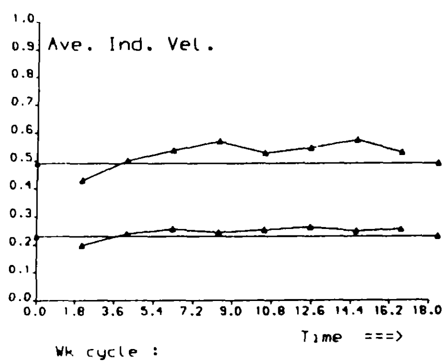

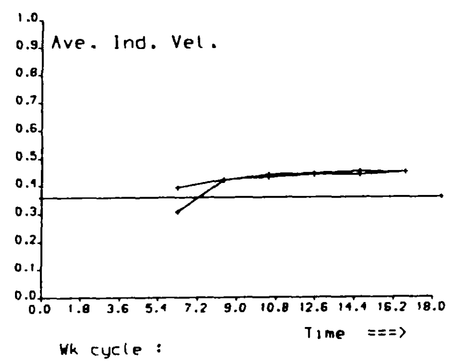

Fig.4.20 The X-component induced velocity in the flow field as function of time for tip speed ratio $\lambda = 3$.

22-NOV-91

Straight Bladed VAWT

Blade chord	: 0.10 R	Blade radius	: 1.00 R
Blade span	: 1.44 R	AirFoil	: naca 0015
Blade number	: 2	Tip speed ratio	: 5.000

Point Shed Vortices : Unit time = 1.257
Blade ind. velocity at Bld Pos. : 5
Bld upstream : 0.200
Bld down stream : 0.625

ΔΔΔ Wk cycle pos. : 0 To : 1
Up Vel. = 0.3991 Down Vel. : 0.8245

▽▽▽ Wk cycle pos. : 1 To : 2
Up Vel. = 0.5054 Down Vel. : 0.7182

+++ Wk cycle pos. : 2 To : 3
Up Vel. = 0.6118 Down Vel. : 0.6118

xxx Wk cycle pos. : 3 To : 4
Up Vel. = 0.6118 Down Vel. : 0.6118

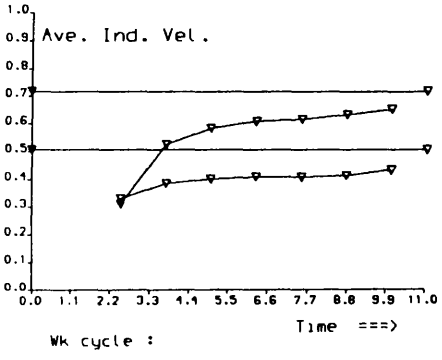

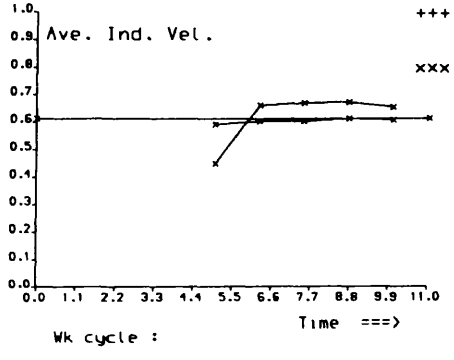

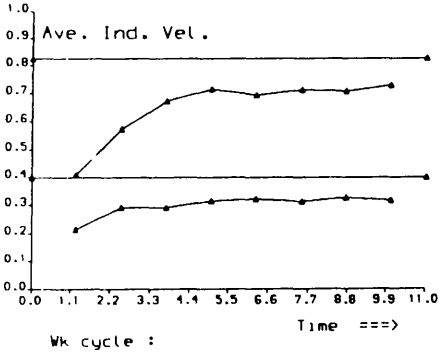

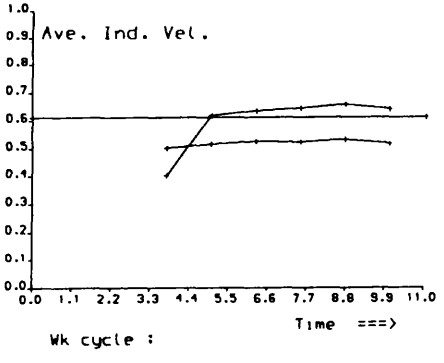

Fig.4.21 The X-component induced velocity in the flow field as function of time for tip speed ratio $\lambda = 5$.

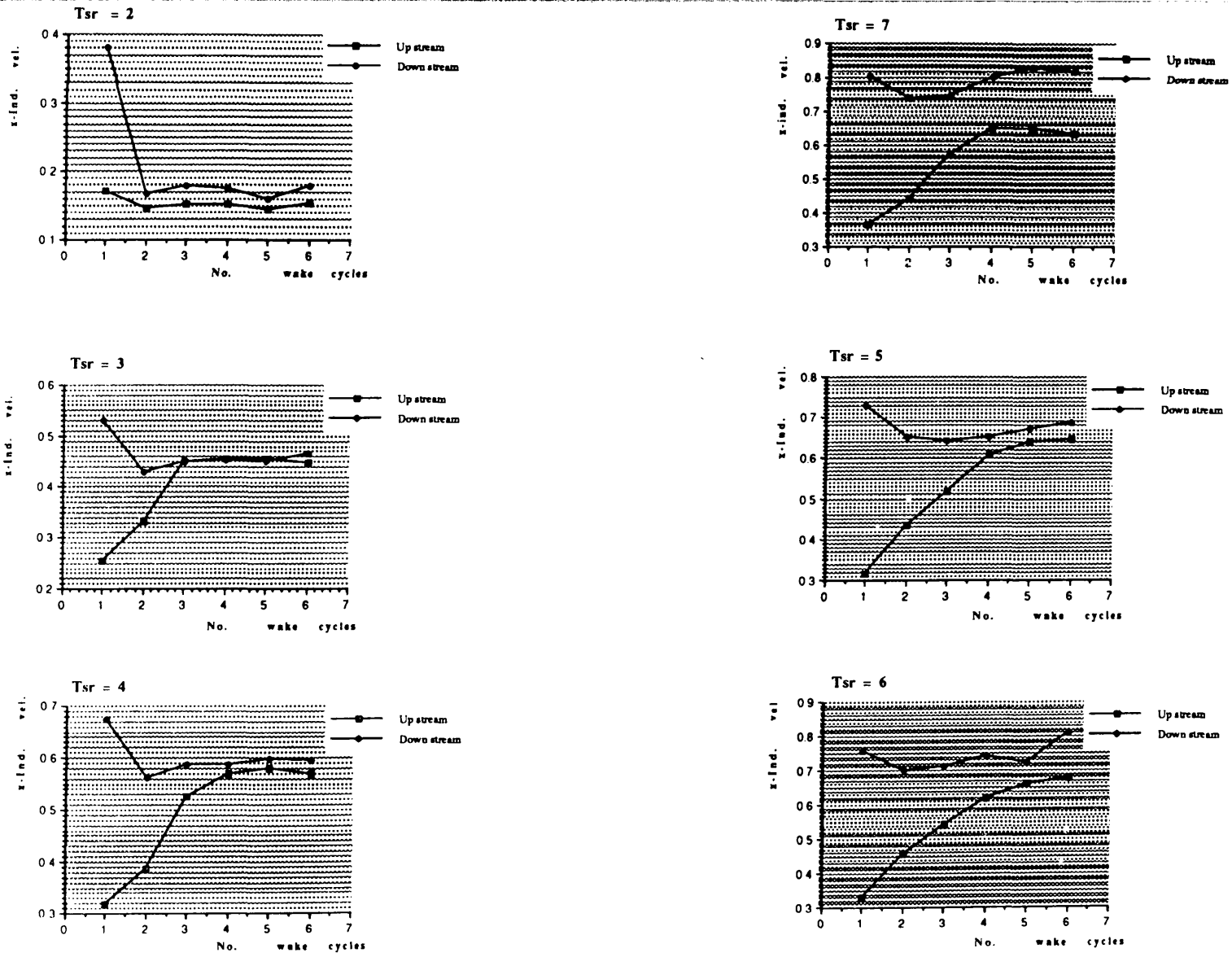

Fig.4.22 The variation of X-component induced velocity based on wake cycle number for the tip speed ratio range $2 \leq \lambda \leq 7$.

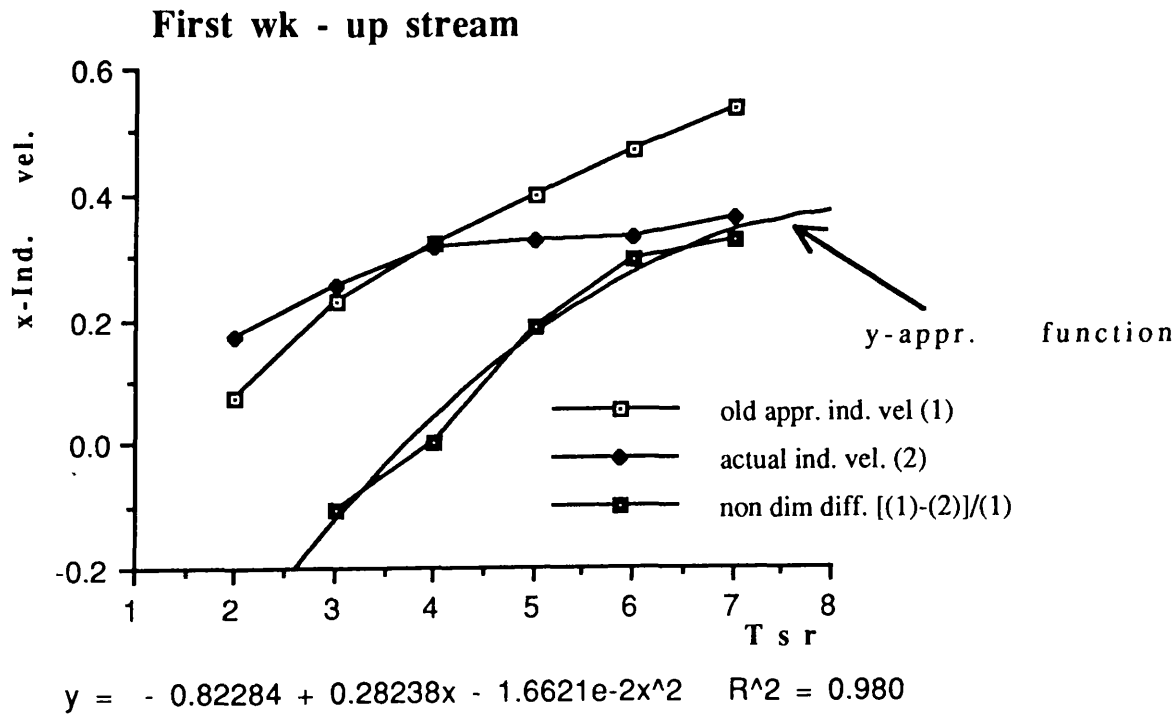

Fig.4.23a The upstream correction factor as function of tip speed ratio λ.

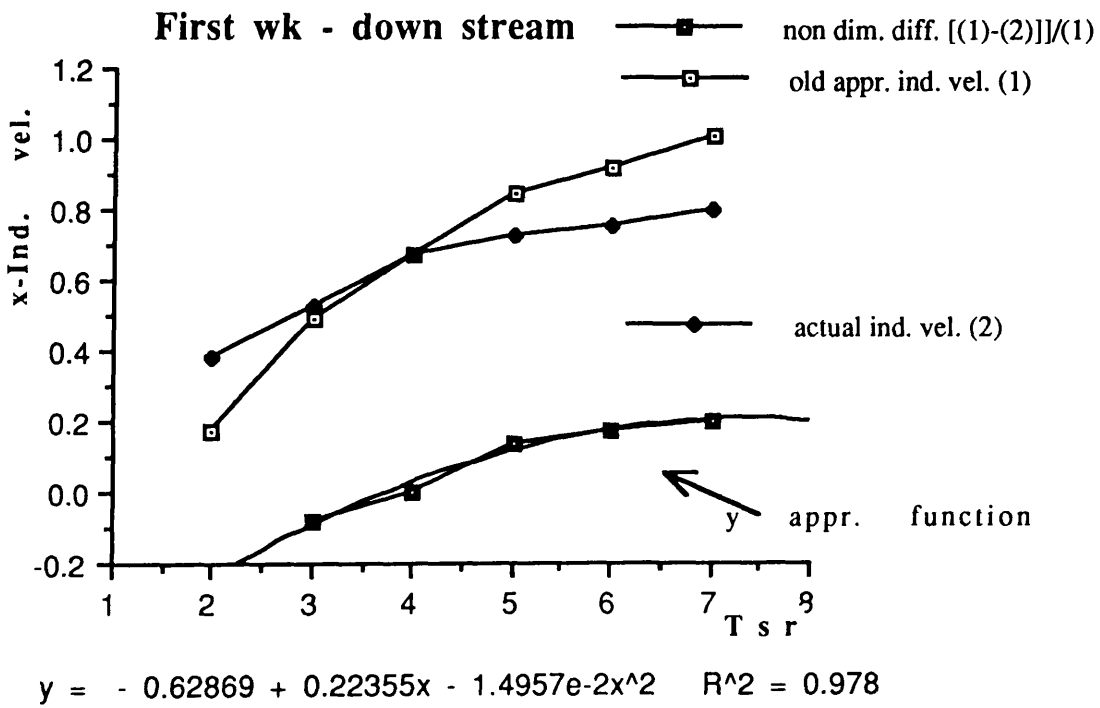

Fig.4.23b The downstream correction factor as function of tip speed ratio λ.

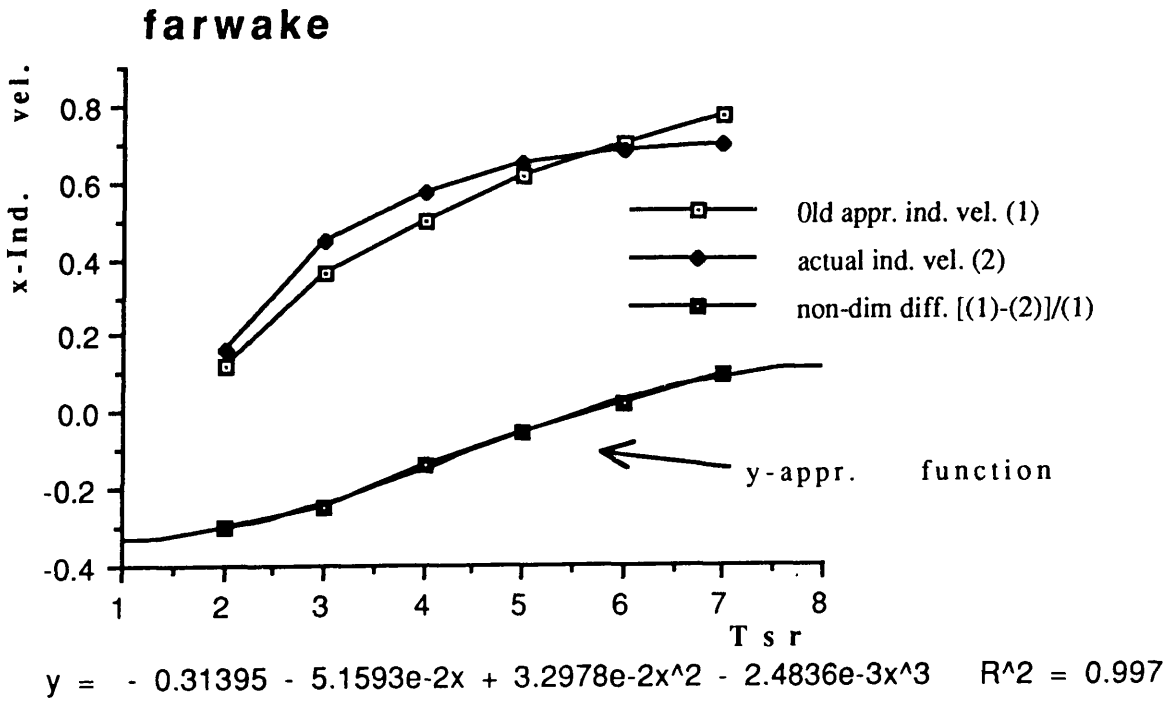

Fig.4.23c The far wake correction factor as function of tip speed ratio λ.

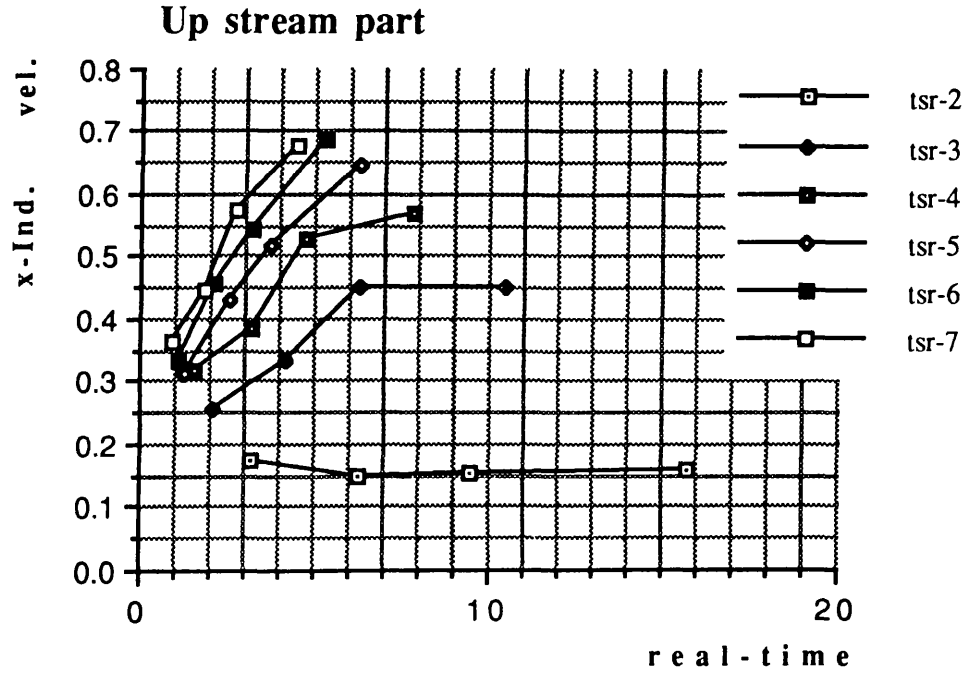

Fig.4.24a The variation of X-component induced velocity on the upstream part of the wake cycle presented as function of real time for the tip speed ratio in the range $2 \leq \lambda \leq 7$.

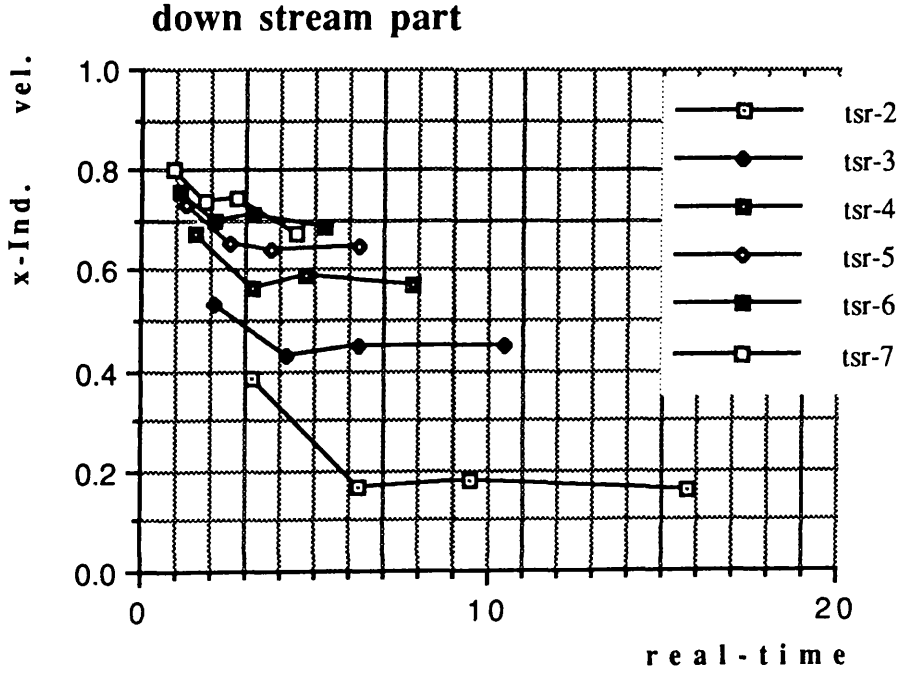

Fig.4.24b The variation of X-component induced velocity on the downstream part of the wake cycle presented as function of real time for the tip speed ratio in the range $2 \leq \lambda \leq 7$.

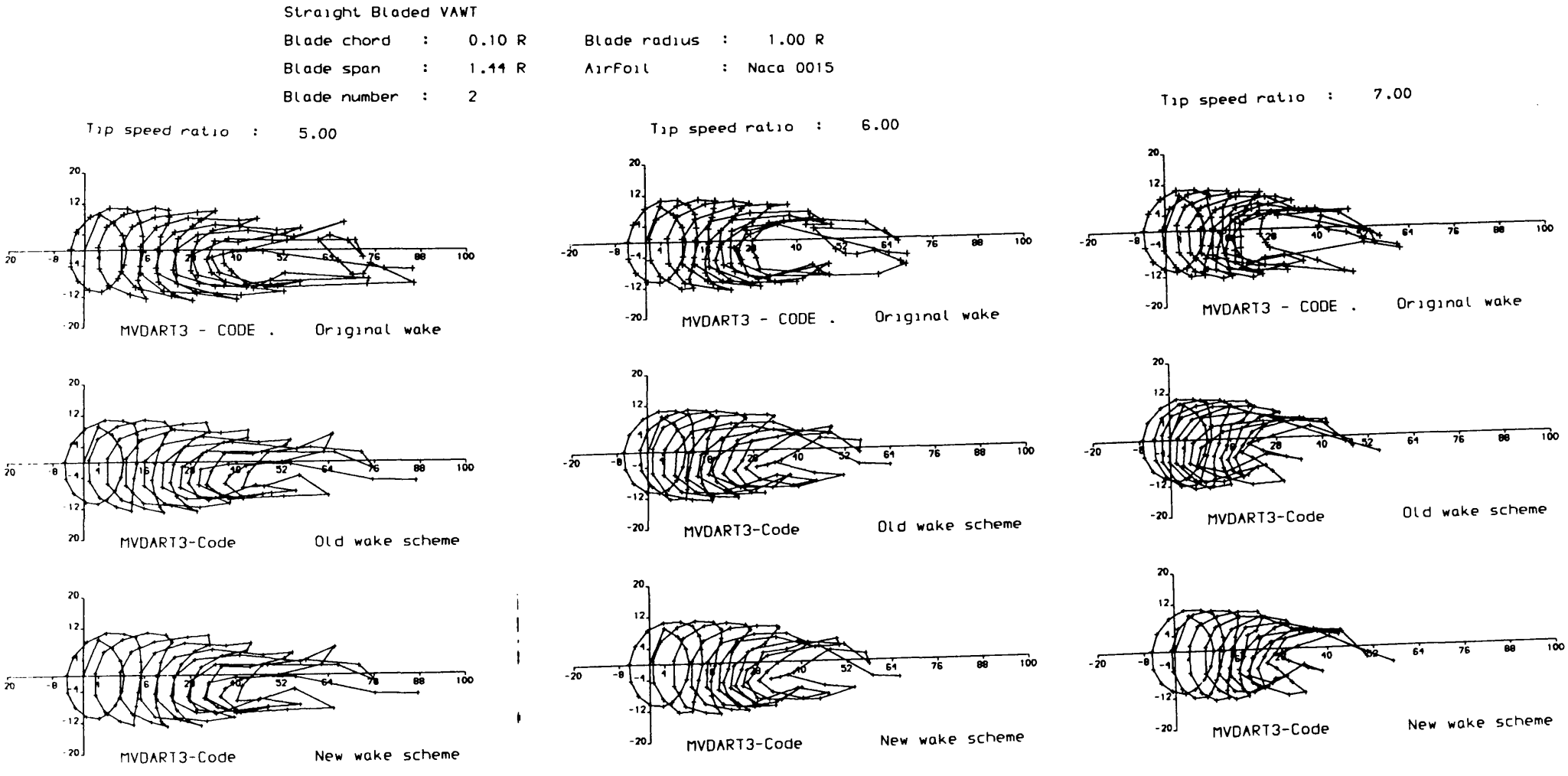

Fig. 4.25 A comparison of wake shapes between the Free wake method, old and new prescribed wake schemes.

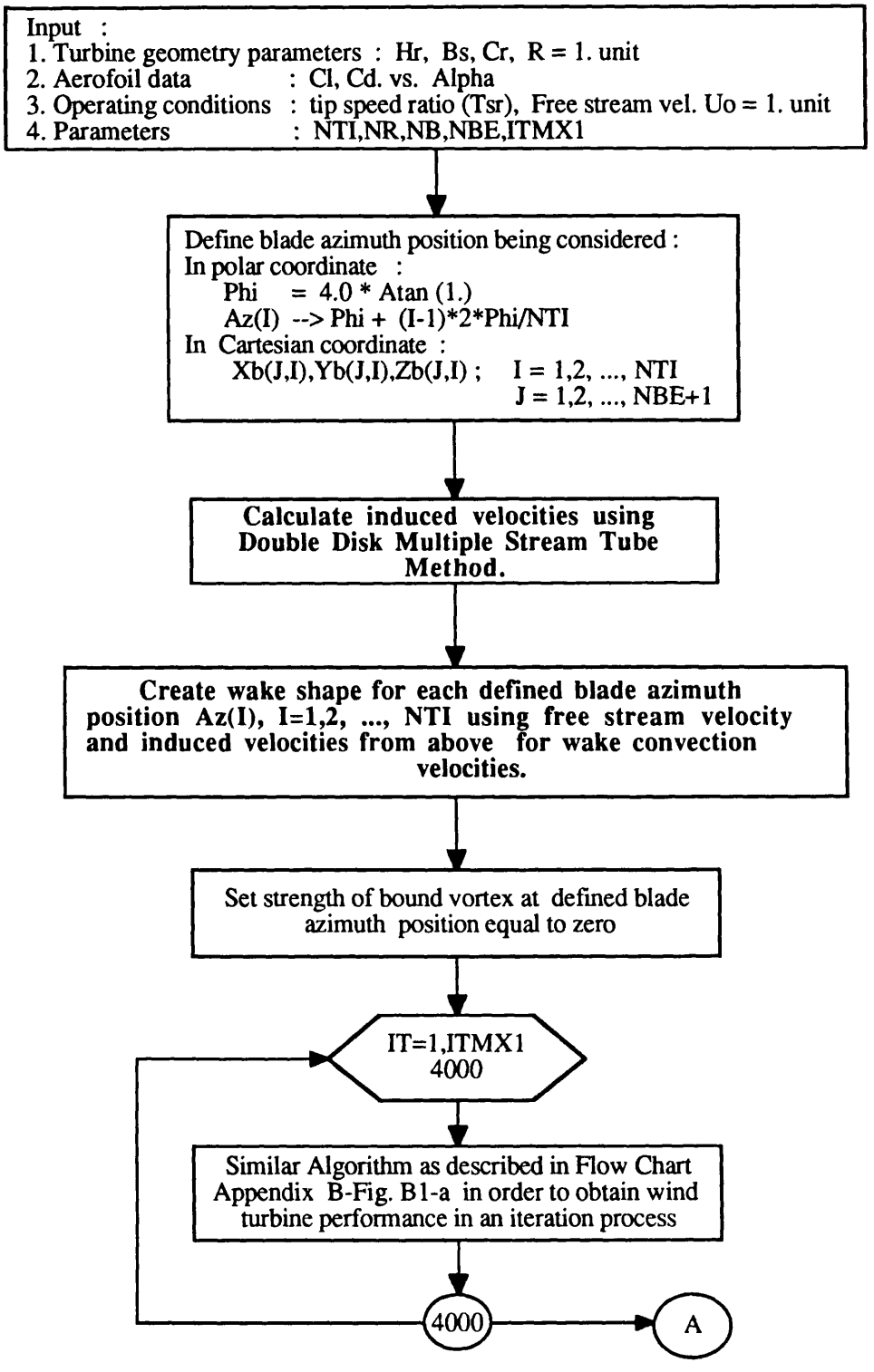

Fig. 4.26 Flow diagram PRESWK-DDMST -(Y2+XN4) version

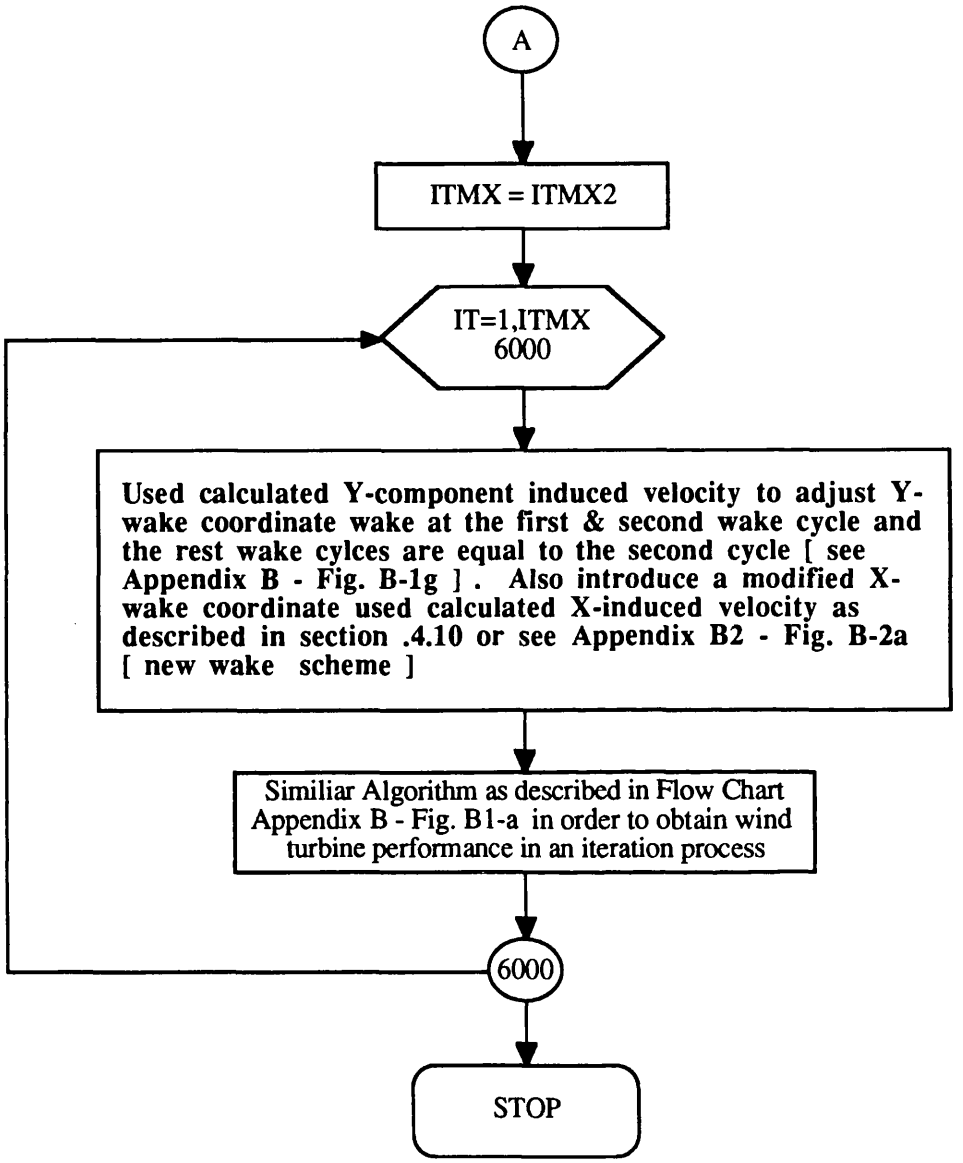

Cont'n from Fig. 4.26 (a)

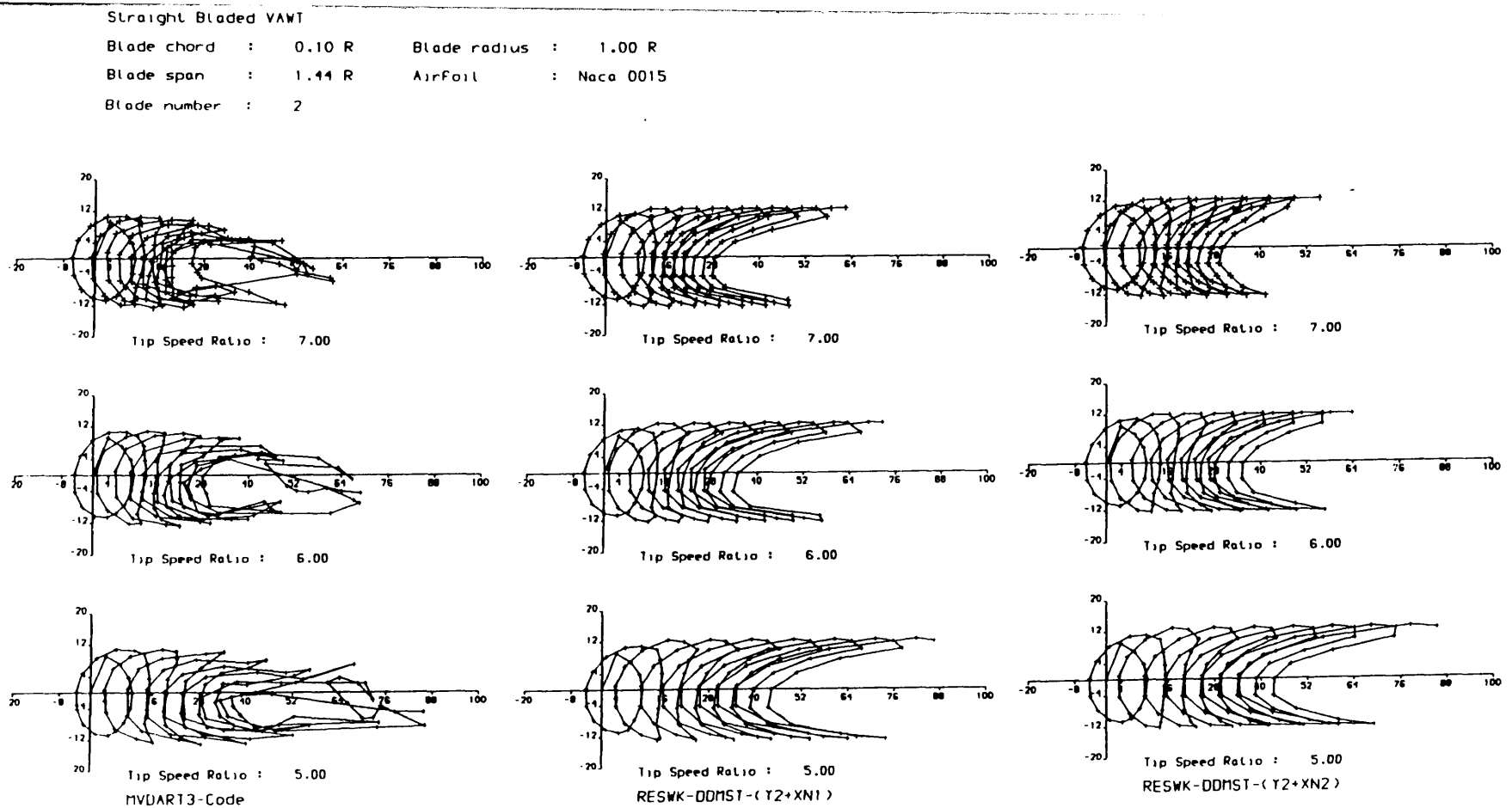

Fig.4.27a A comparison of the wake shapes at the mid blade span between the Free Wake method [MVDART3], PRESWK-DDMST-(Y2+XN1) and PRESWK-DDMST - (Y2+XN2).

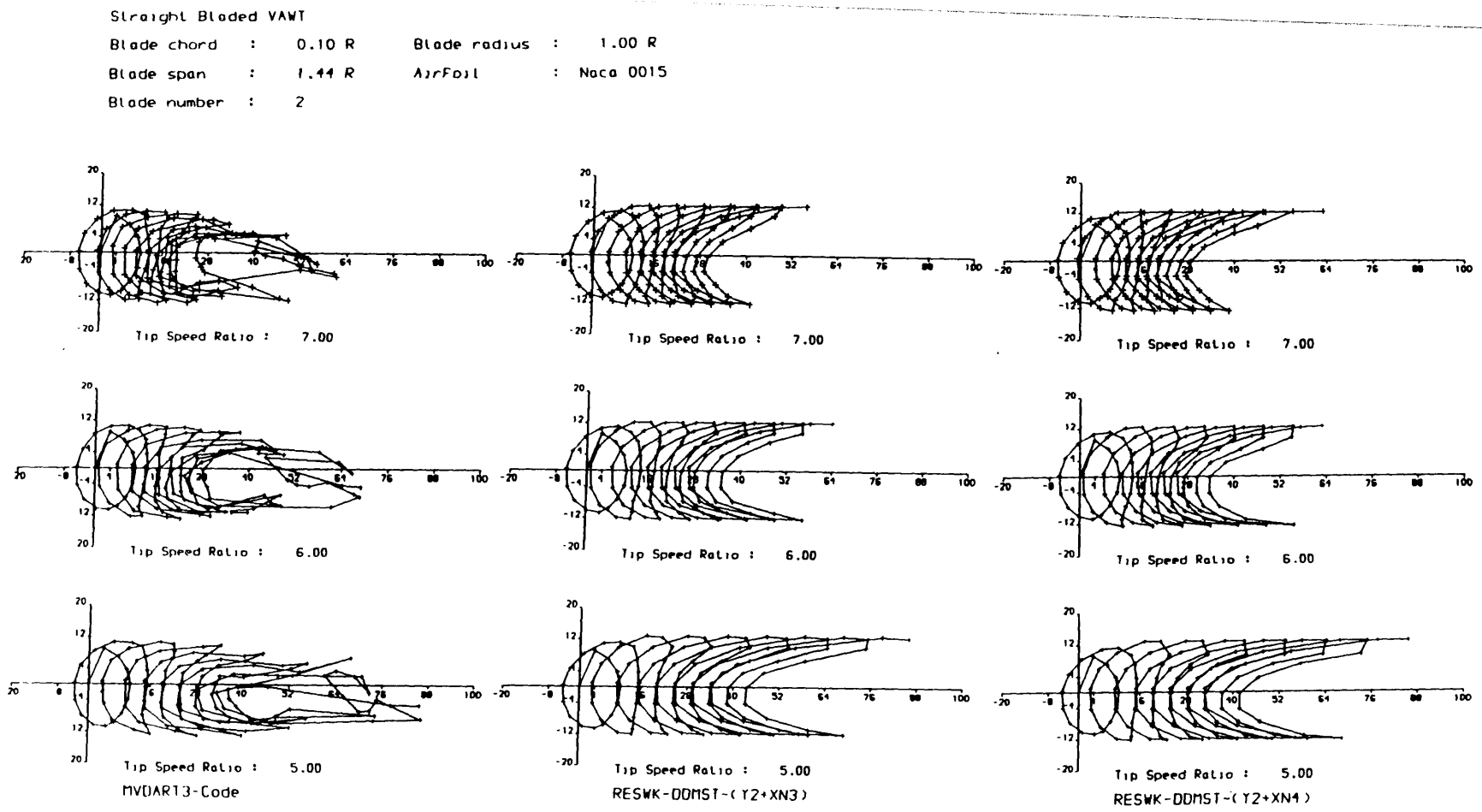

Fig.4.27b A comparison of the wake shapes at the mid blade span between the Free Wake method [MVDART3], PRESWK-DDMST-(Y2+XN3) and PRESWK-DDMST - (Y2+XN4).

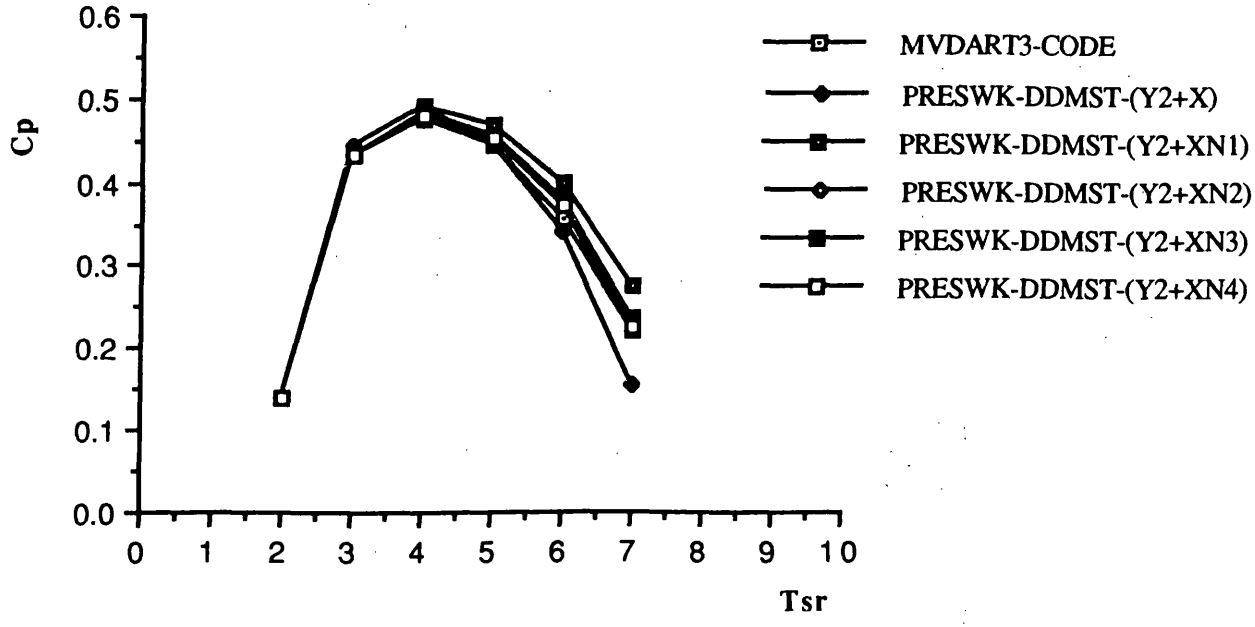

Fig.4.28 A comparison of power coefficients between the Free Wake method [MVDART3] , PRESWK - DDMST-(Y2+XNi); i = 1,2, ..., 4 as a function of tip speed ratio.

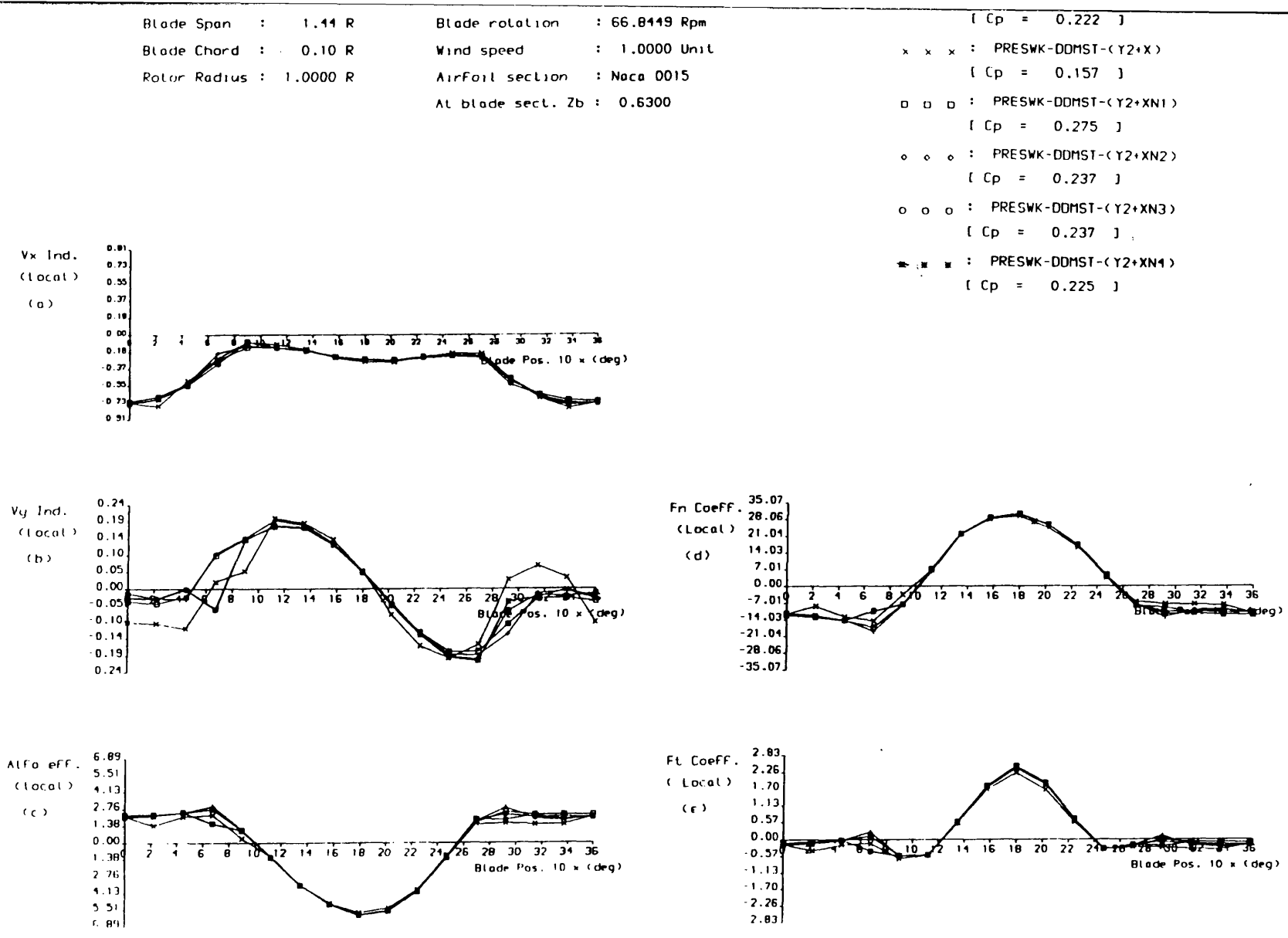

Fig.4.29 A comparison of detailed aerodynamic characteristics near the mid blade against blade azimuth position, between the Free Wake method [MVDART3] and PRESWK -DDMST-(Y2+XNi); i=1,2, ...,4 for $\lambda = 7$.

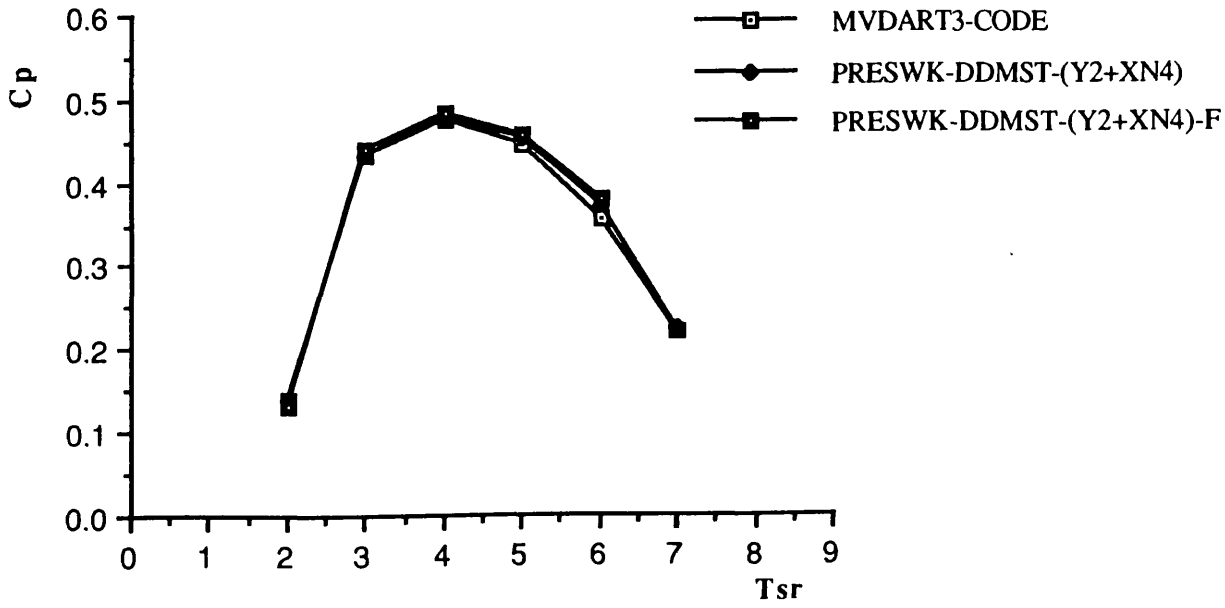

Fig.4.30 A comparison of power coefficients between the Free Wake method [MVDART3] , PRESWK-DDMST-(Y2+XN4) and PRESWK-DDMST- (Y2 + XN4) - F .

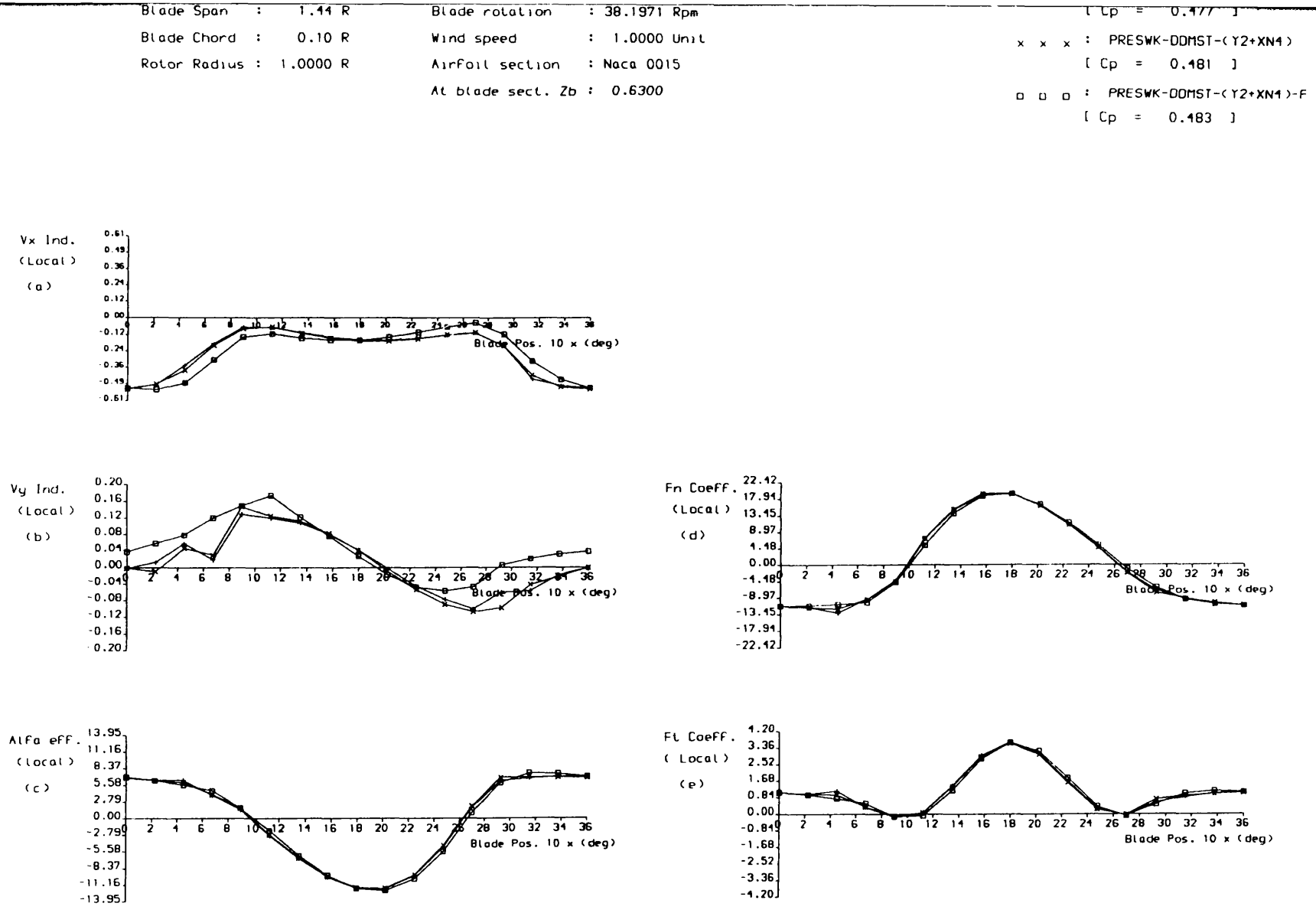

Fig.4.31a A comparison of detailed aerodynamic characteristics near the mid blade against blade azimuth position, between the Free Wake method [MVDART3], PRESWK-DDMST-(Y2+XN4) and PRESWK-DDMST-(Y2+XN)-F for $\lambda = 4$.

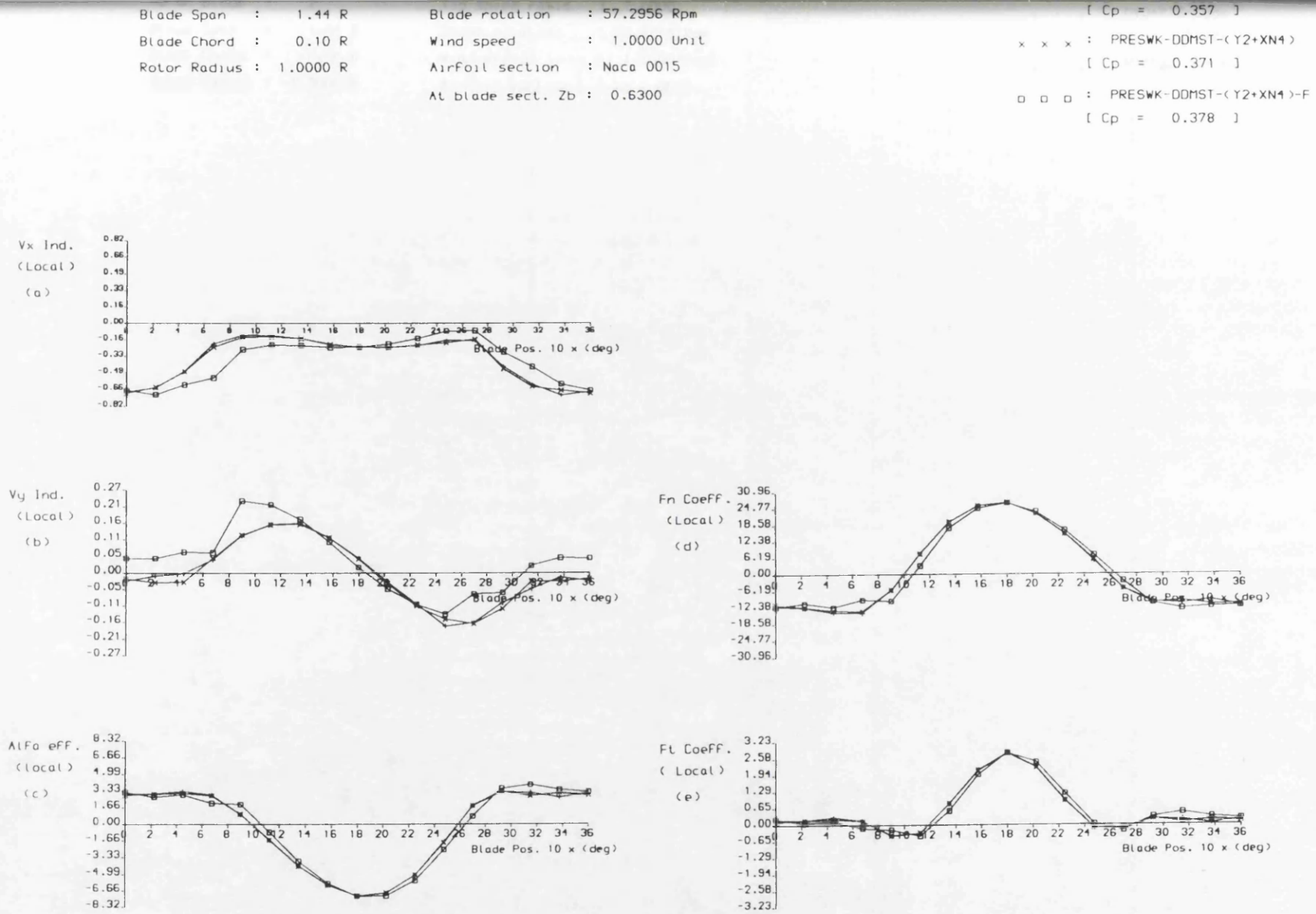

Fig.4.31b A comparison of detailed aerodynamic characteristics near the mid blade against blade azimuth position, between the Free Wake method [MVDART3], PRESWK-DDMST-(Y2+XN4) and PRESWK-DDMST-(Y2+XN)-F for $\lambda = 6$.

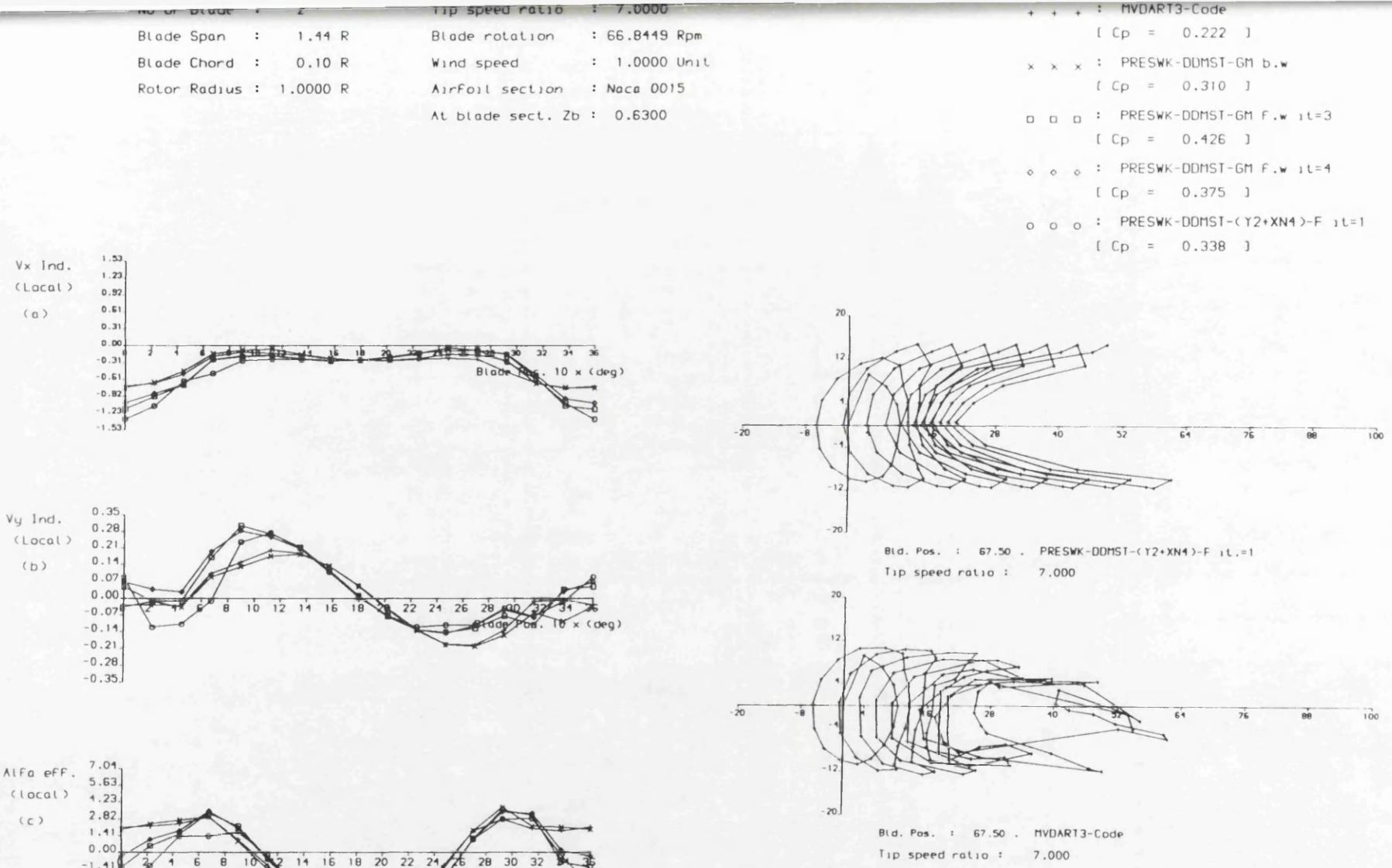

Fig.4.32 The comparison of X & Y-component induced velocities resulting from the first stage iteration for the forward and backward approach and a comparison of the wake shapes at $\lambda = 7$.

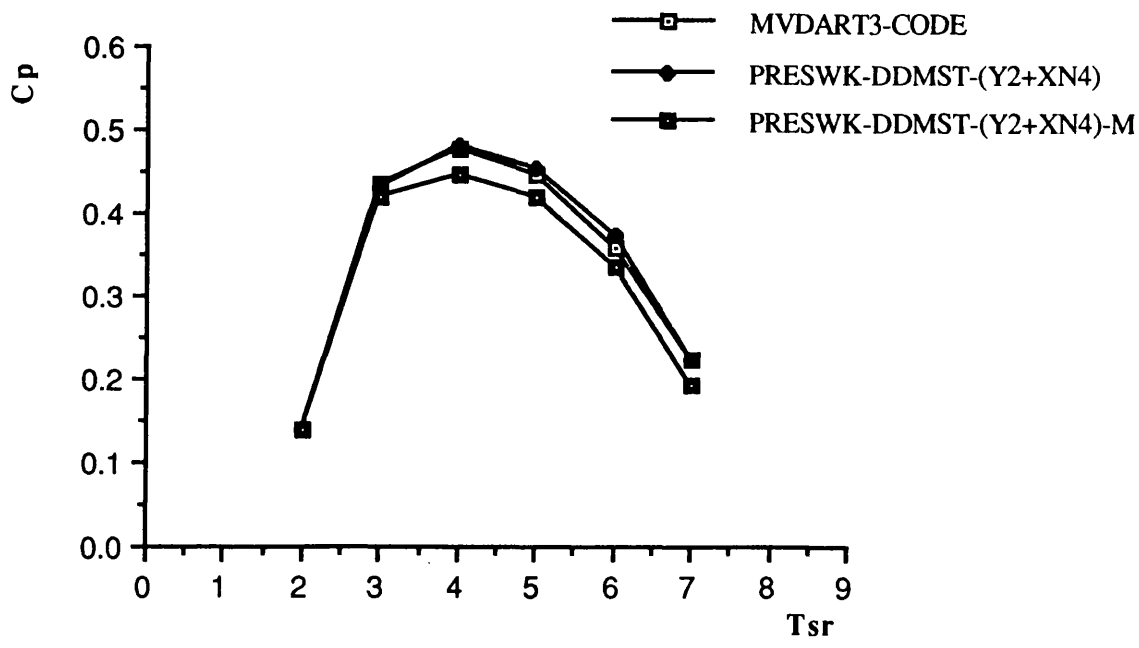

Fig 5.1 A comparison of power coefficients between MVDART3, PRESWK-DDMST - (Y2+XN4) and PRESWK-DDMST-(Y2+XN4) - M.

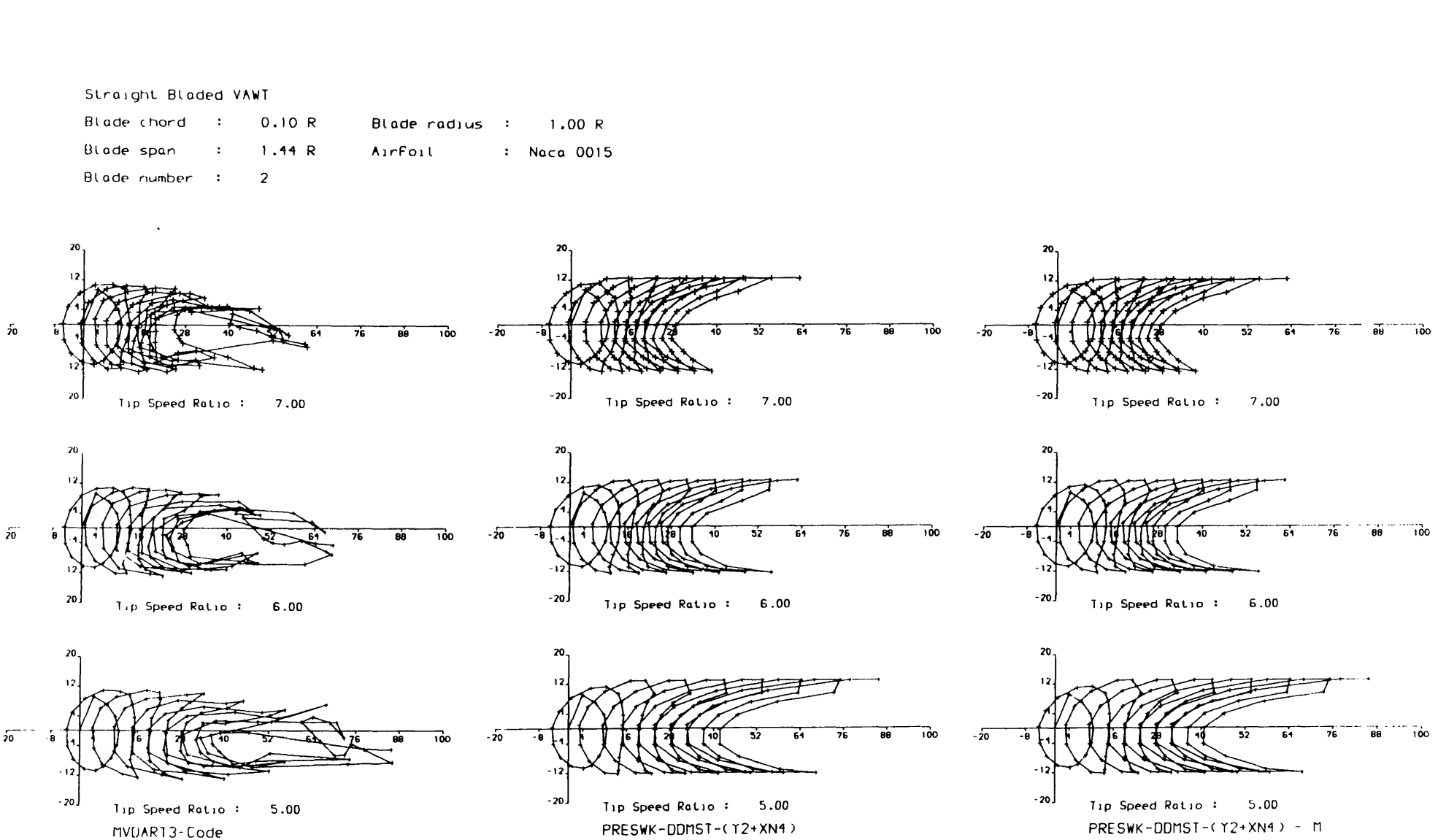

Fig 5.2 A comparison of wake shapes between MVDART3, PRESWK-DDMST -(Y2+XN4) and PRESWK-DDMST-(Y2+XN4)-M.

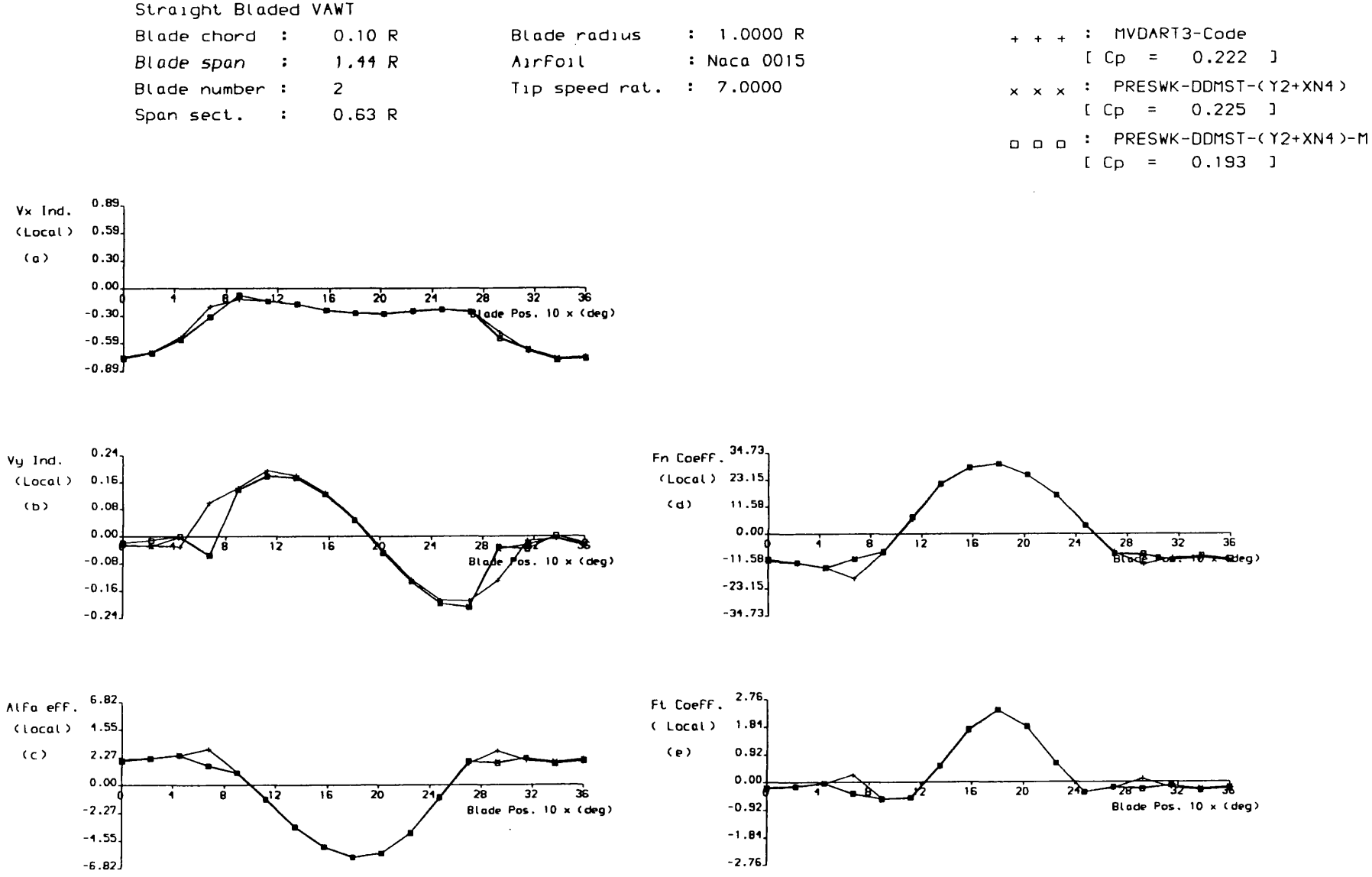

Fig 5.3a A comparison of detailed aerodynamic characteristics near the mid blade span between MVDART3, PRESWK -DDMST-(Y2+XN4) and PRESWK- DDMST -(Y2+XN4)-M at tip speed ratio $\lambda = 7$.

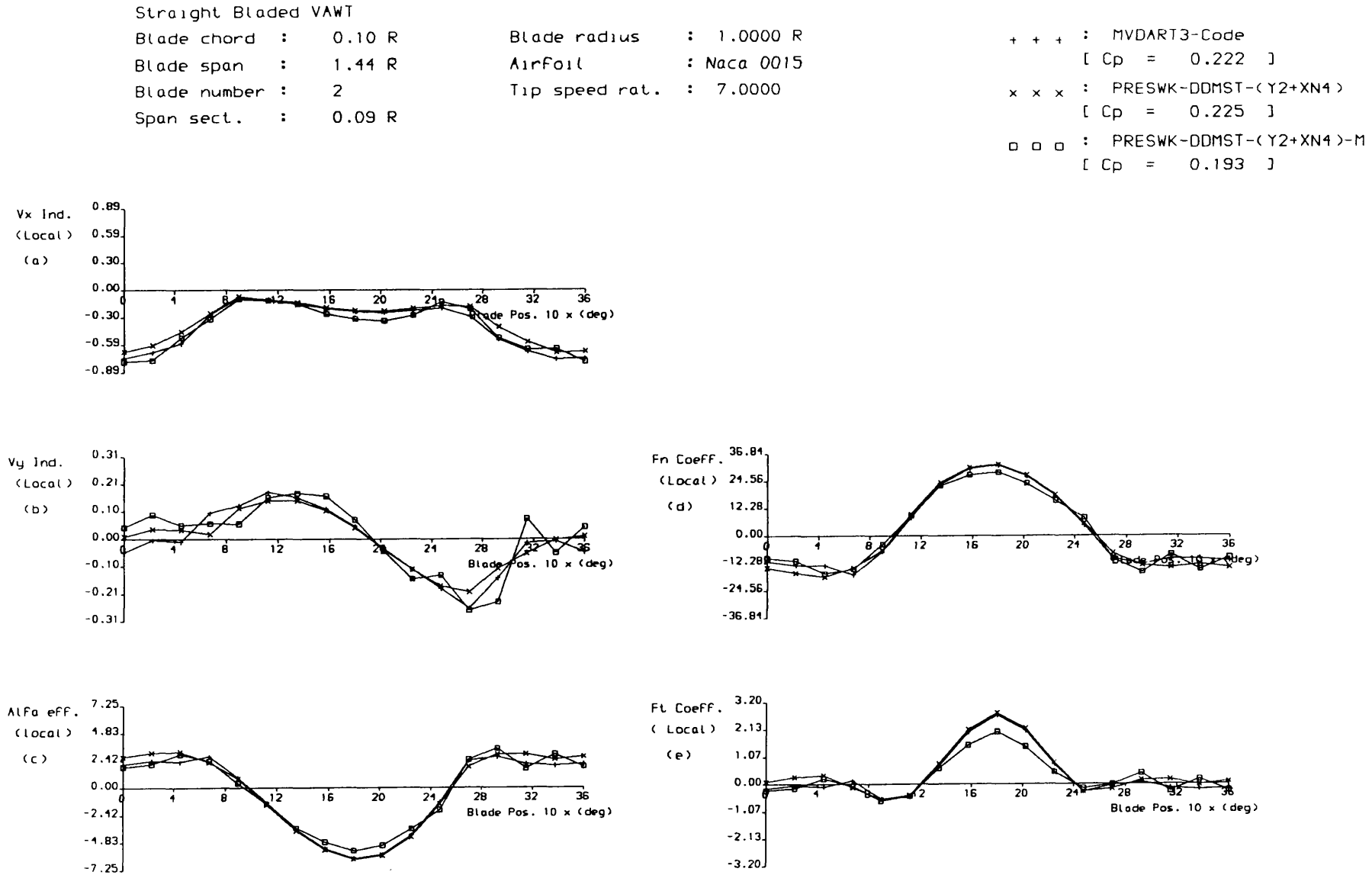

Fig 5.3b A comparison of detailed aerodynamic characteristics near the blade tip between MVDART3, PRESWK -DDMST-(Y2+XN4) and PRESWK-DDMST-(Y2+XN4)-M at tip speed ratio $\lambda = 7$.

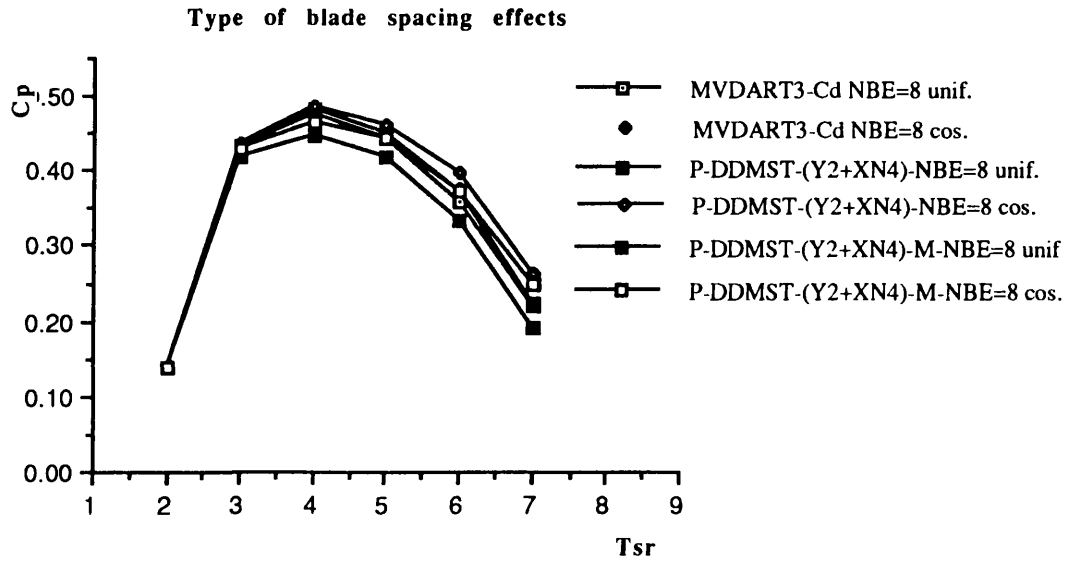

Fig 5.4 A comparison of power coefficients produced by MVDART3, PRESWK-DDMST - (Y2+XN4) and PRESWK-DDMST-(Y2+XN4) - M for two types of blade spacing.

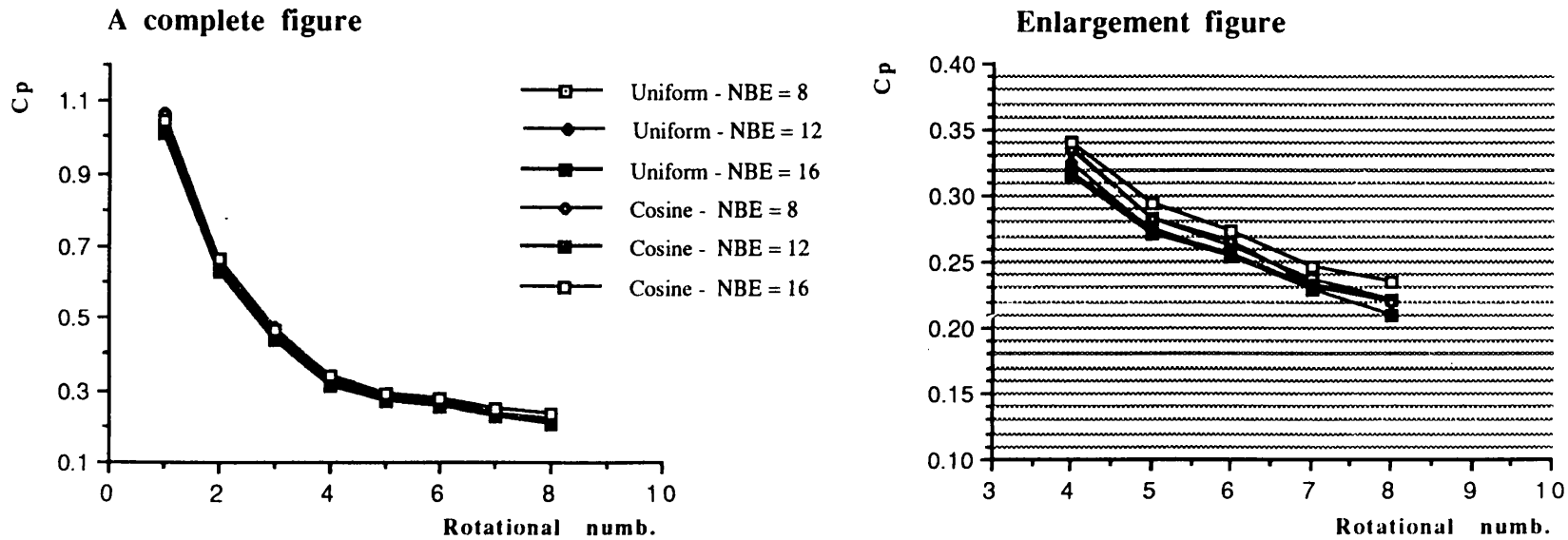

Fig 5.5a The rate of convergence of MVDART3 with respect to the type of blade spacing and the number of blade elements at $\lambda = 7$.

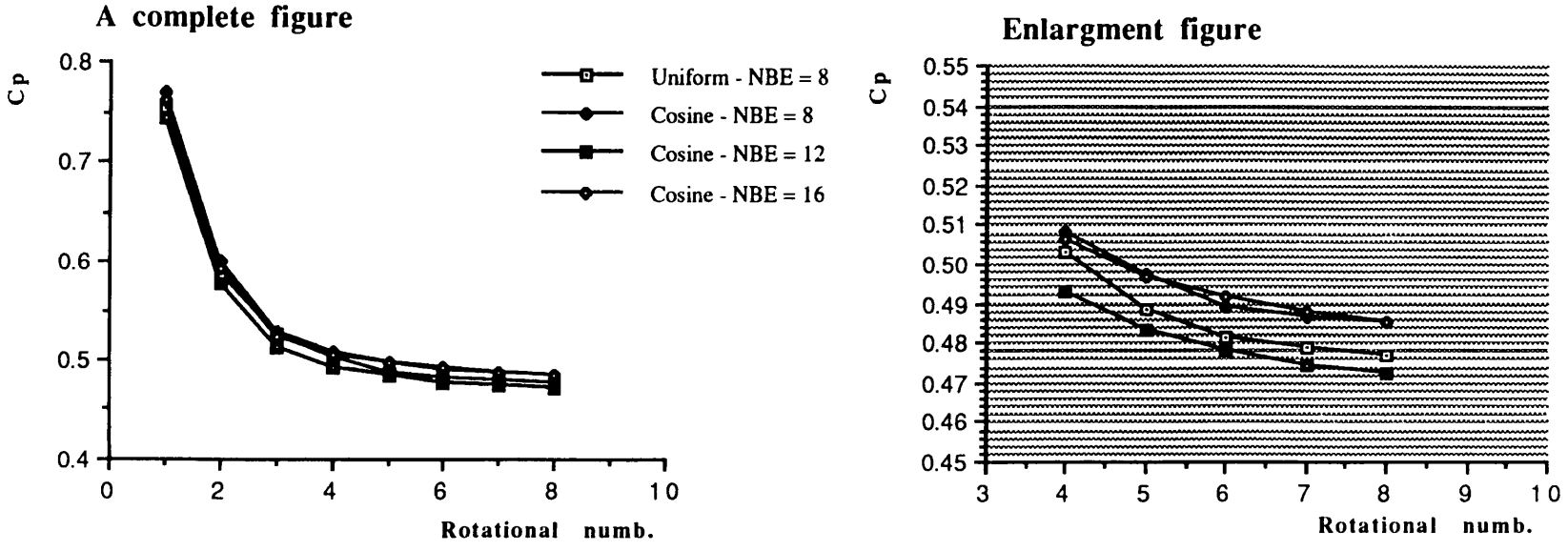

Fig 5.5b The rate of convergence of MVDART3 with respect to the type of blade spacing and the number of blade elements at $\lambda = 4$.

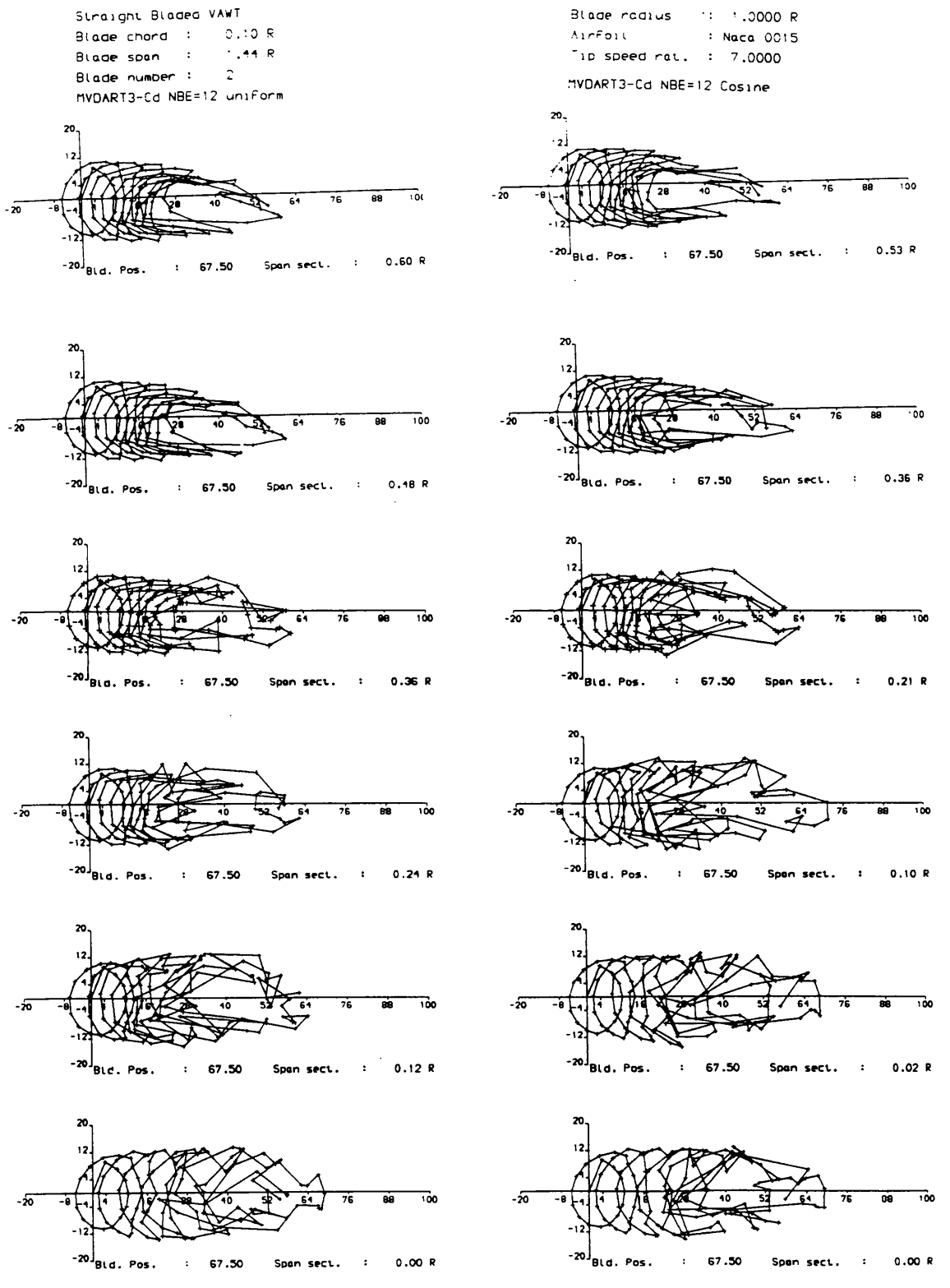

Fig 5.6 The wake shape variation along the half blade span from the MVDART3-Code, with numerical parameters : uniform spacing with NBE=12 and cosine spacing with NBE = 12 at $\lambda = 7$.

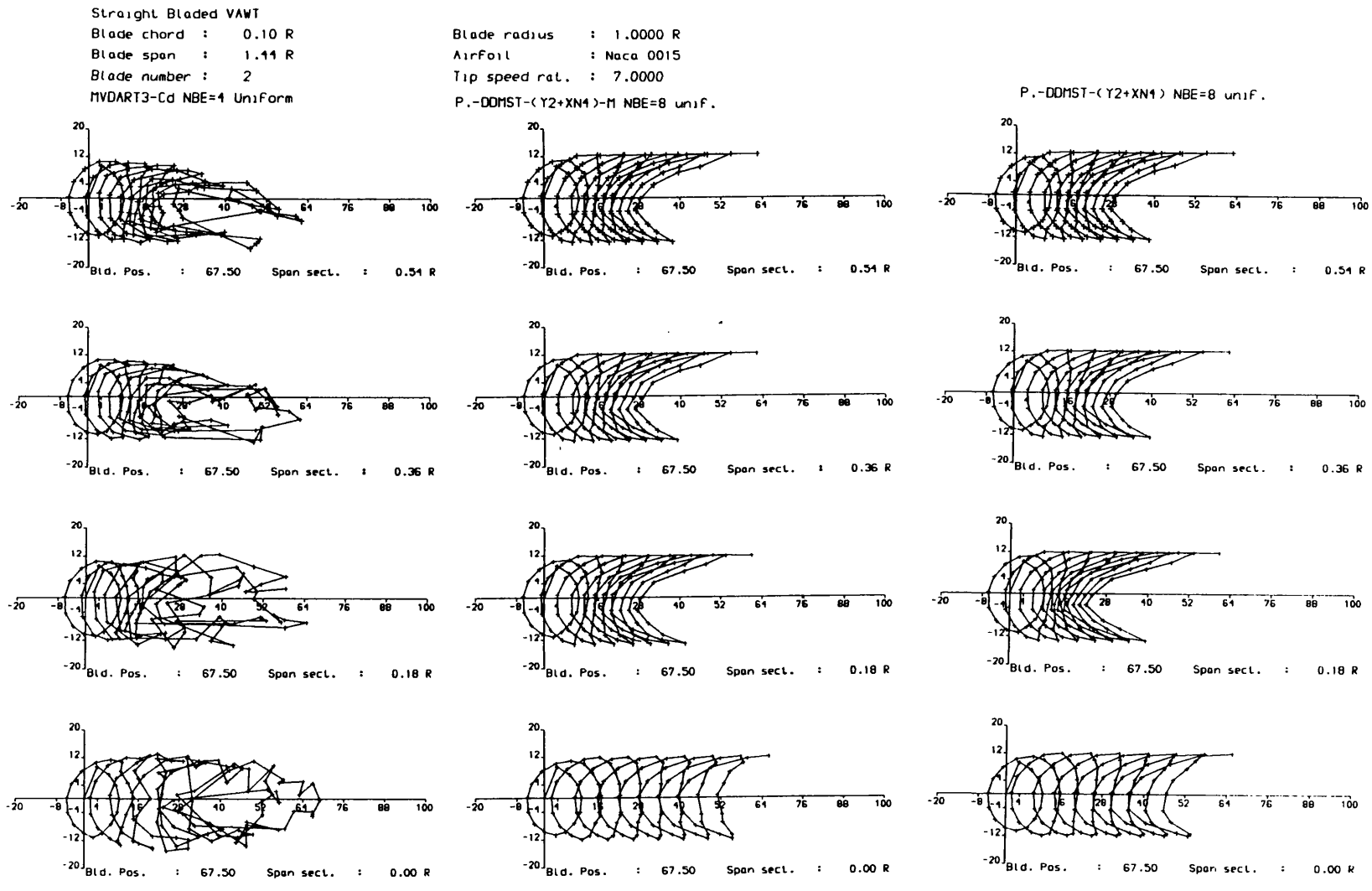

Fig.5.7a A comparison of wake shapes along the half blade span produced by MVDART3, PRESWK-DDMST-(Y2+XN4) and PRESWK-DDMST - (Y2 +XN4) at $\lambda = 7$. Numerical parameters : uniform spacing with NBE=8.

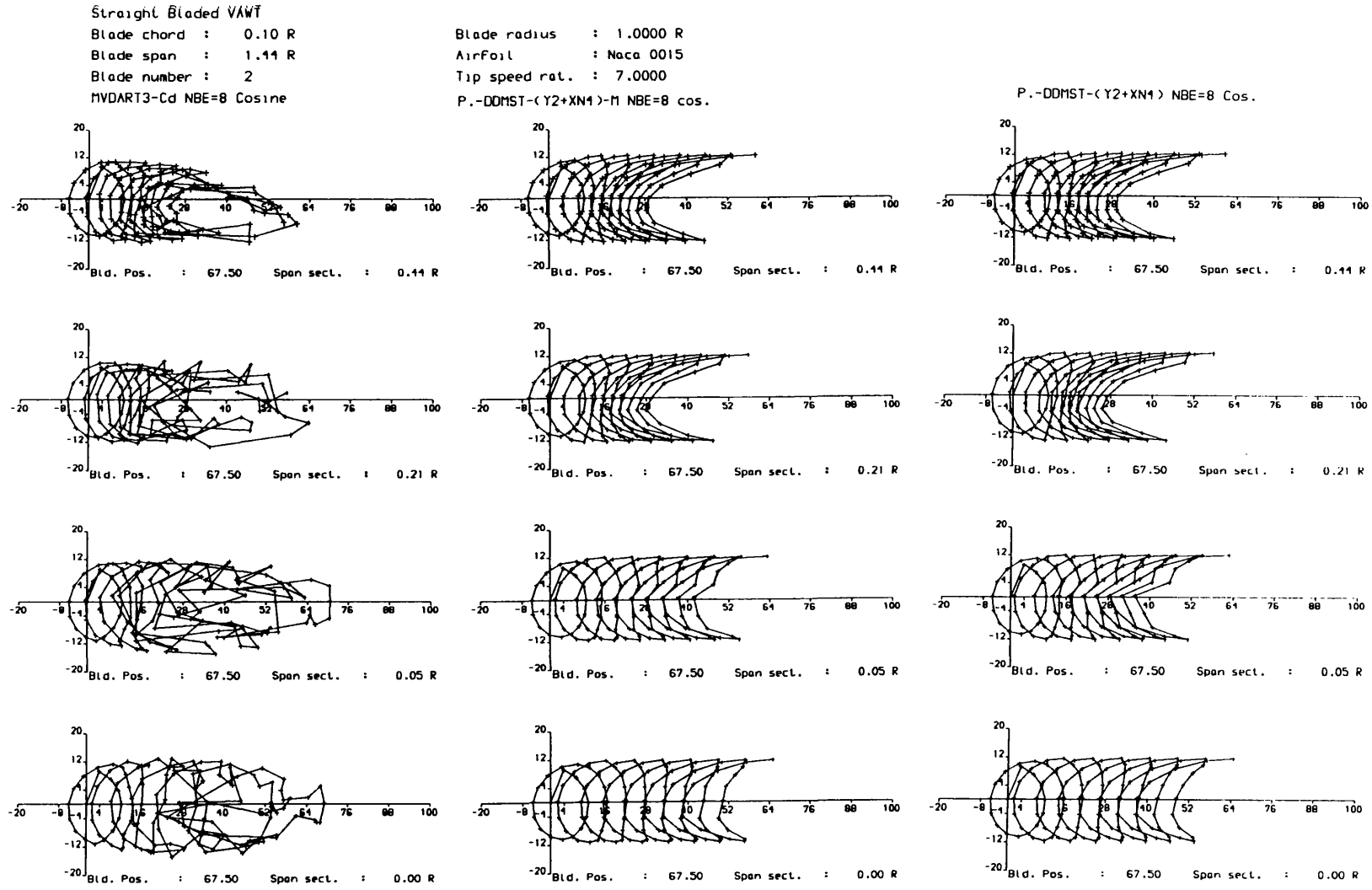

Fig.5.7b A comparison of wake shapes along the half blade span produced by MVDART3, PRESWK-DDMST-(Y2+XN4) and PRESWK-DDMST-(Y2+XN4) at $\lambda = 7$. Numerical parameters : cosine spacing with NBE=8.

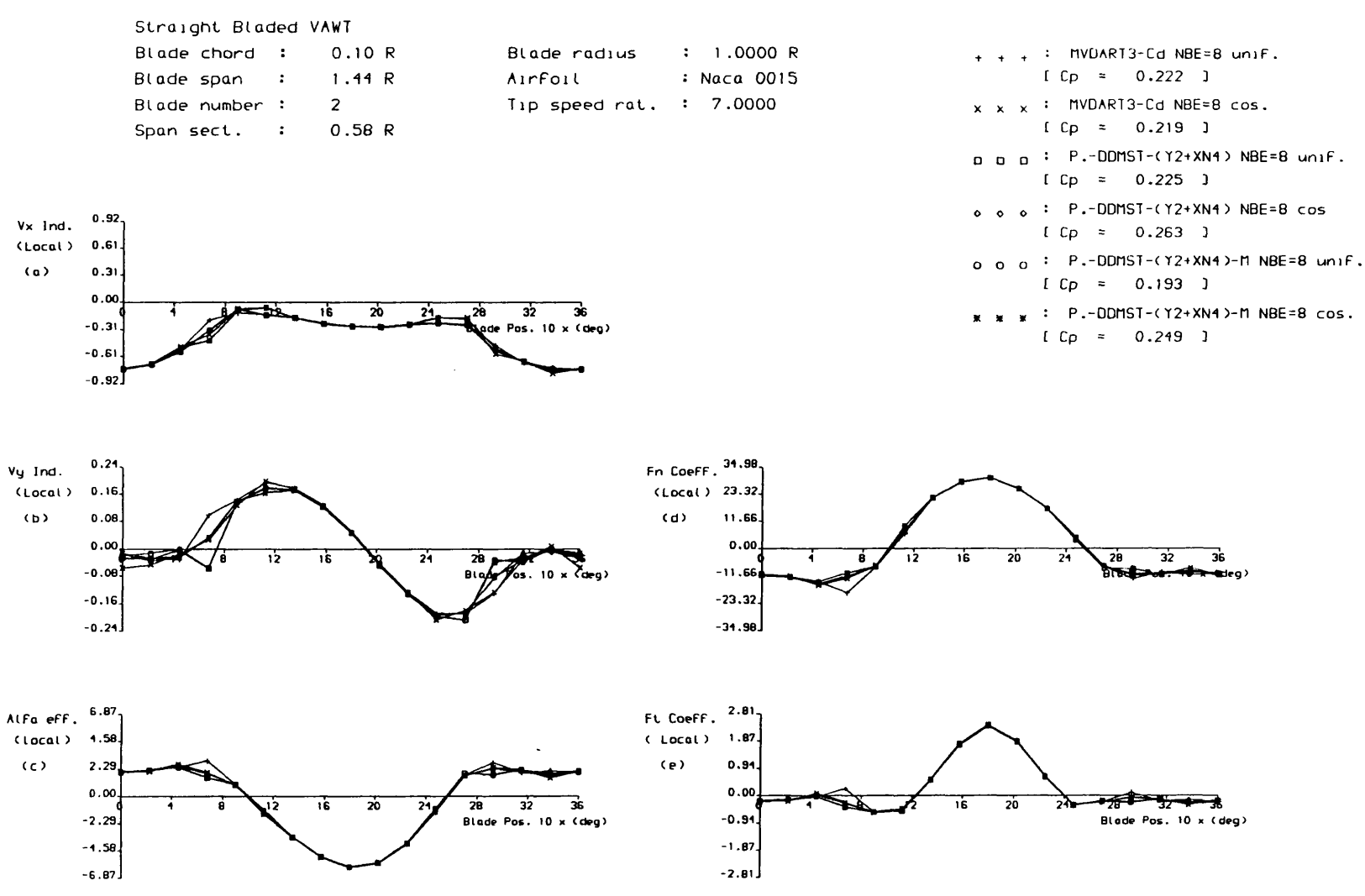

Fig 5.8a A comparison of detailed aerodynamic characteristics near the mid blade span between MVDART3, PRESWK -DDMST-(Y2+XN4) and PRESWK-DDMST-(Y2 + XN4)-M at tip speed ratio λ=7.Uniform spacing at 0.63R; Cosine spacing at 0.58 R.

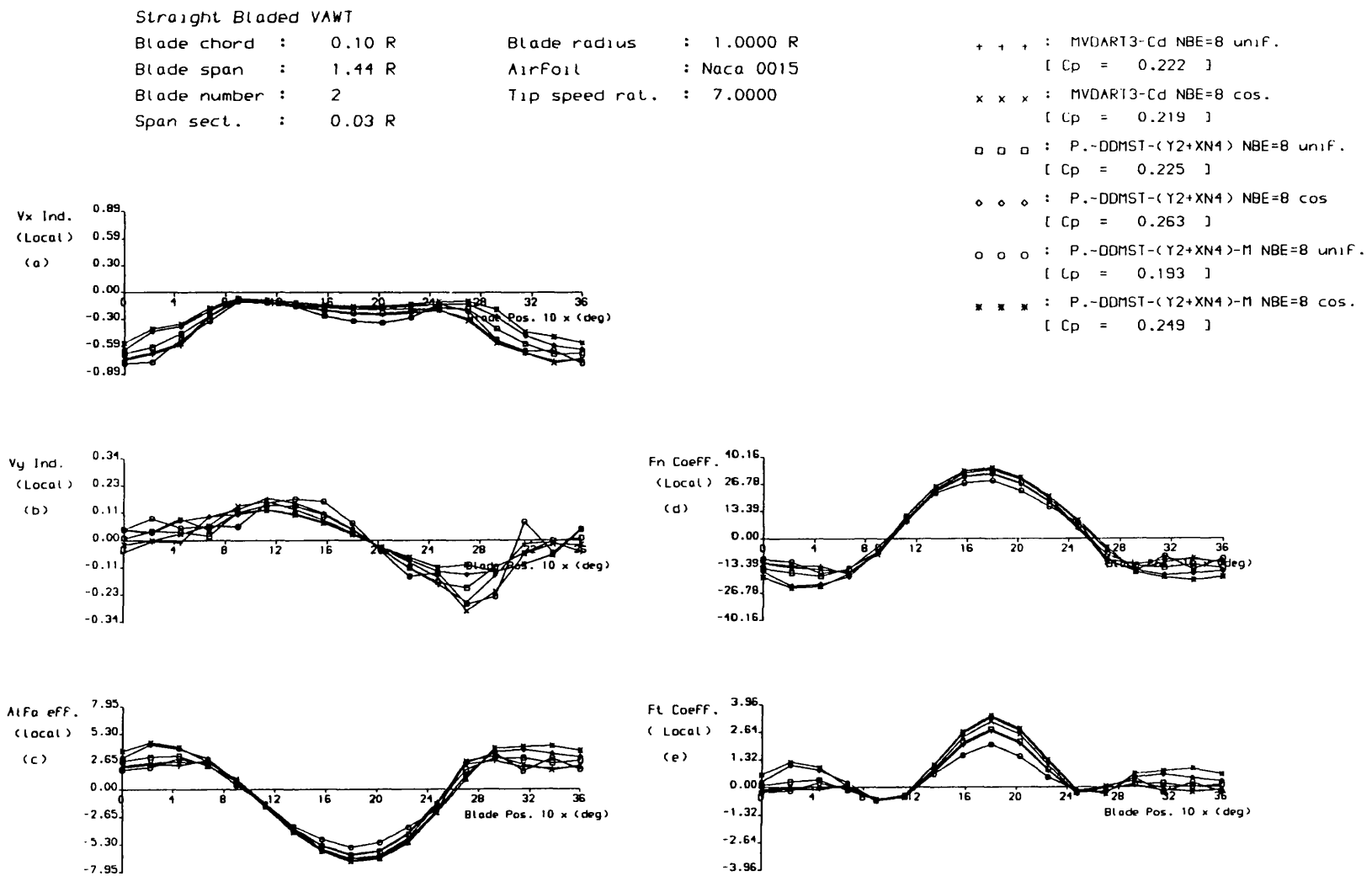

Fig 5.8b A comparison of detailed aerodynamic characteristics near the blade tip between MVDART3, PRESWK -DDMST-(Y2+XN4) and PRESWK-DDMST- (Y2+XN4)-M at tip speed ratio $\lambda = 7$. Uniform spacing at 0.09 R; Cosine spacing at 0.03 R.

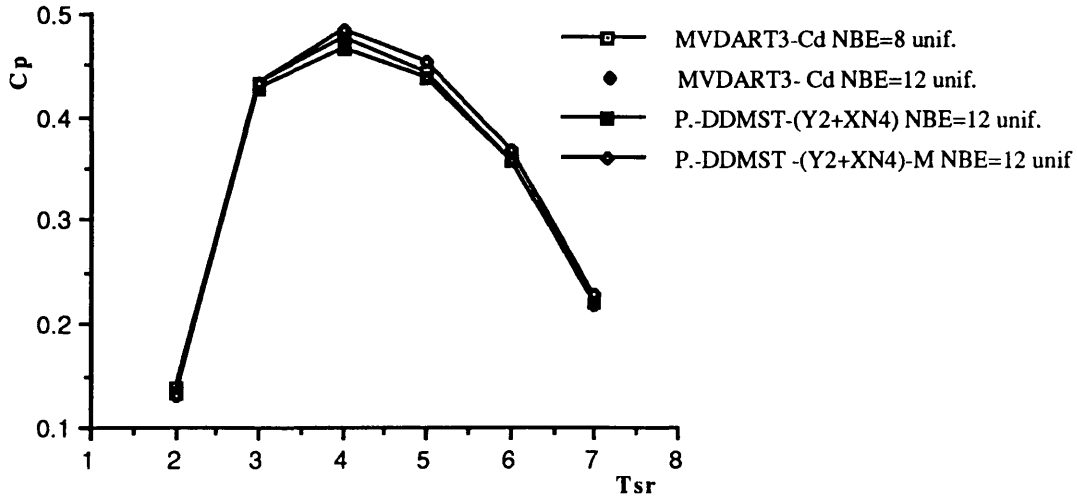

Fig 5.9 The comparison of power coefficient Cp between MVDART3-Code, PRESWK - DDMST -(Y2+XN4) and PRESWK-DDMST-(Y2+XN4) - M with uniform spacing NBE=12.

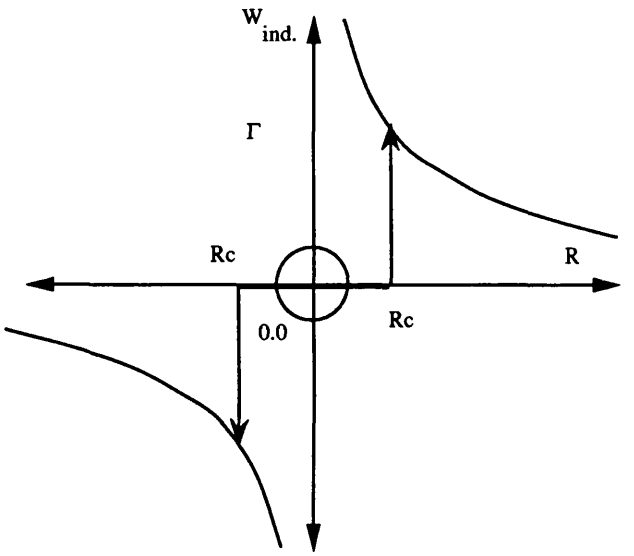

Fig. 5.10a The relationship of induced velocity with respect to the point vortex : A-model

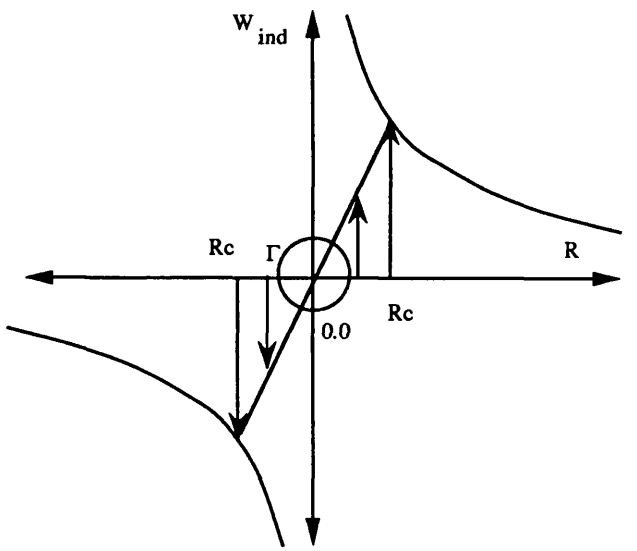

Fig. 5.10b The relationship of induced velocity with respect to the point vortex : B-model

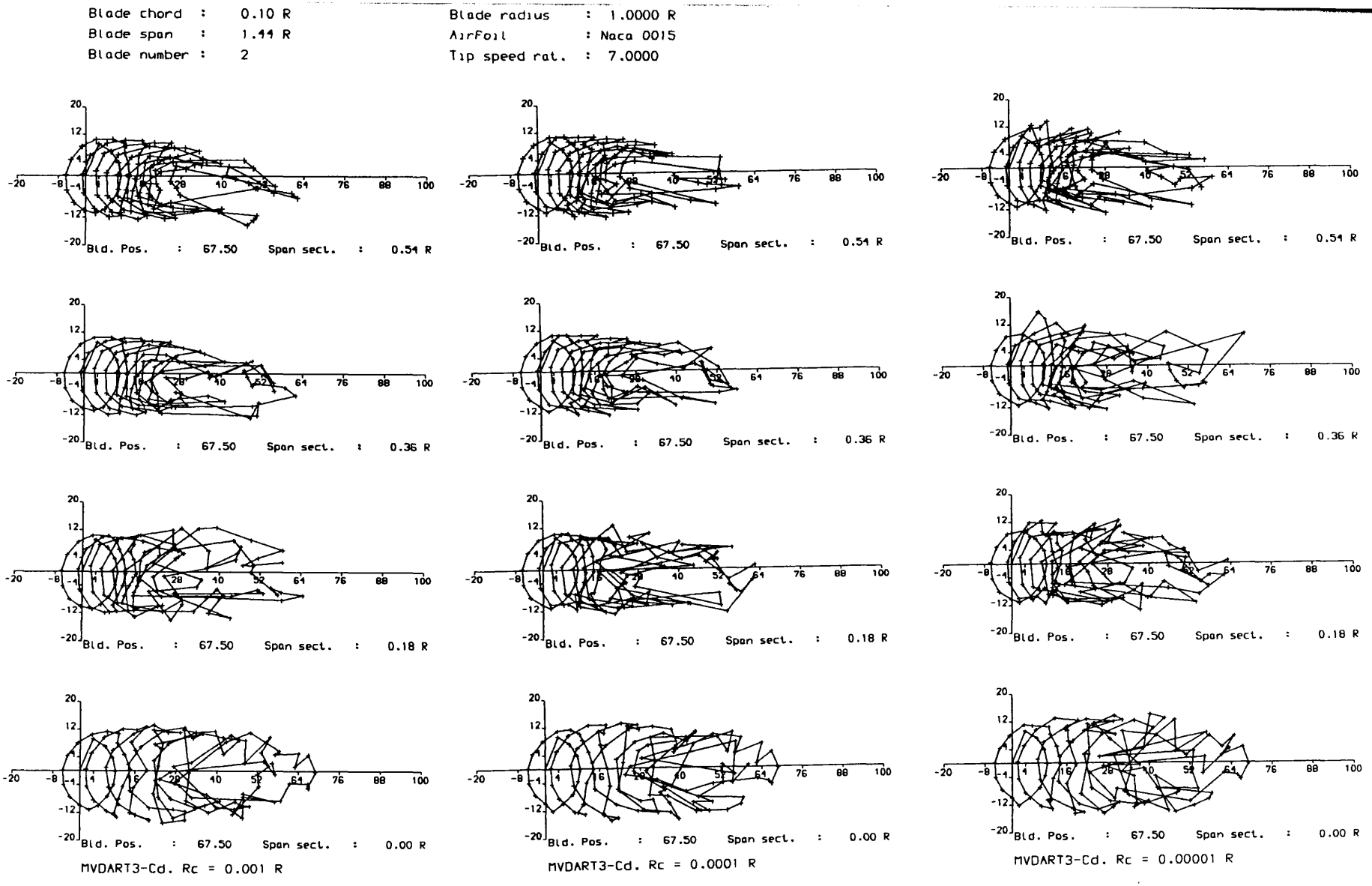

Fig 5.11 The comparison of wake shapes along the half blade span for MVDART3 [Free Wake method] with a variation of R_c at $\lambda = 7$.

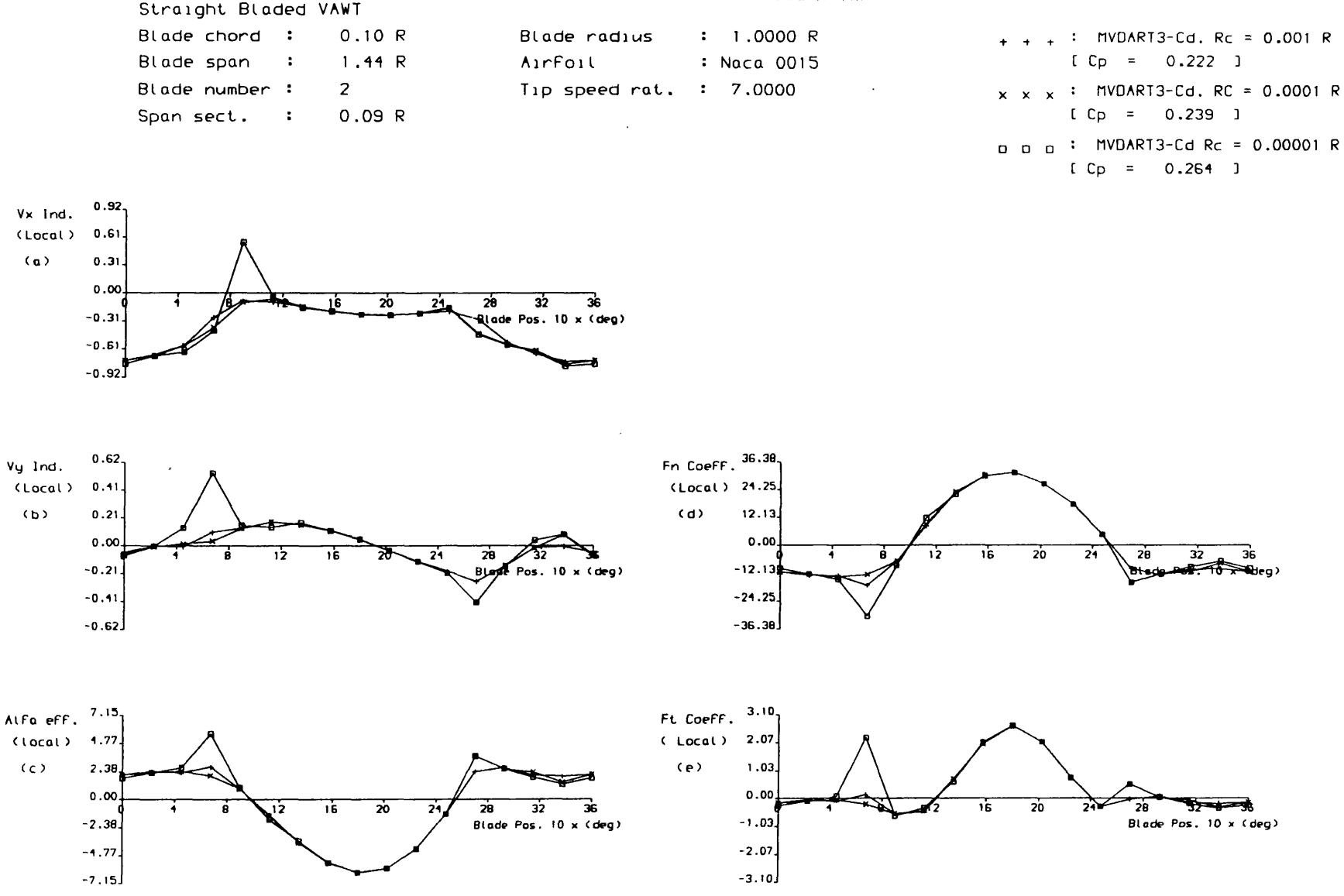

Fig 5.12 A comparison of detailed aerodynamic characteristics near the blade tip for MVDART3 [Free Wake method] with a variation of R_c at $\lambda = 7$.

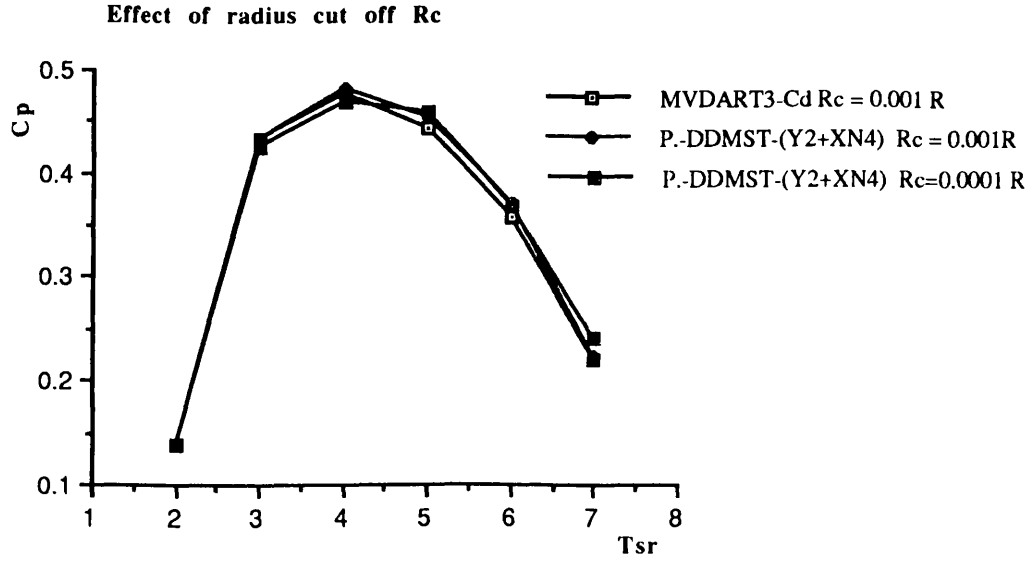

Fig 5.13 A comparison of power coefficients produced by MVDART3 and PRESWK - DDMST -(Y2+XN4) with a variation of R_c.

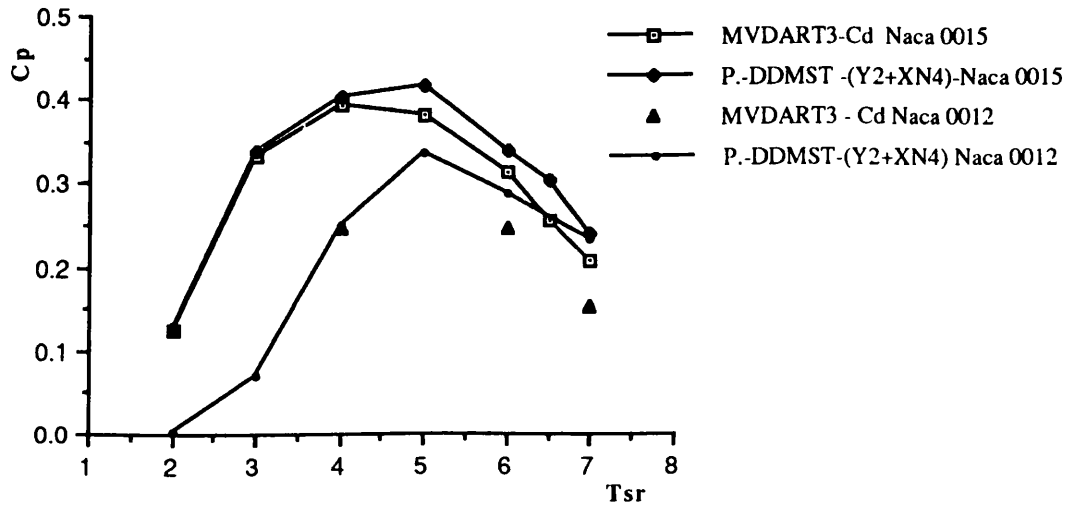

Fig.5.14 The comparison of power coefficients between the MVDART3-Code and PRESWK-DDMST-(Y2+XN4) for the case of a Circular Arc Darrieus wind turbine

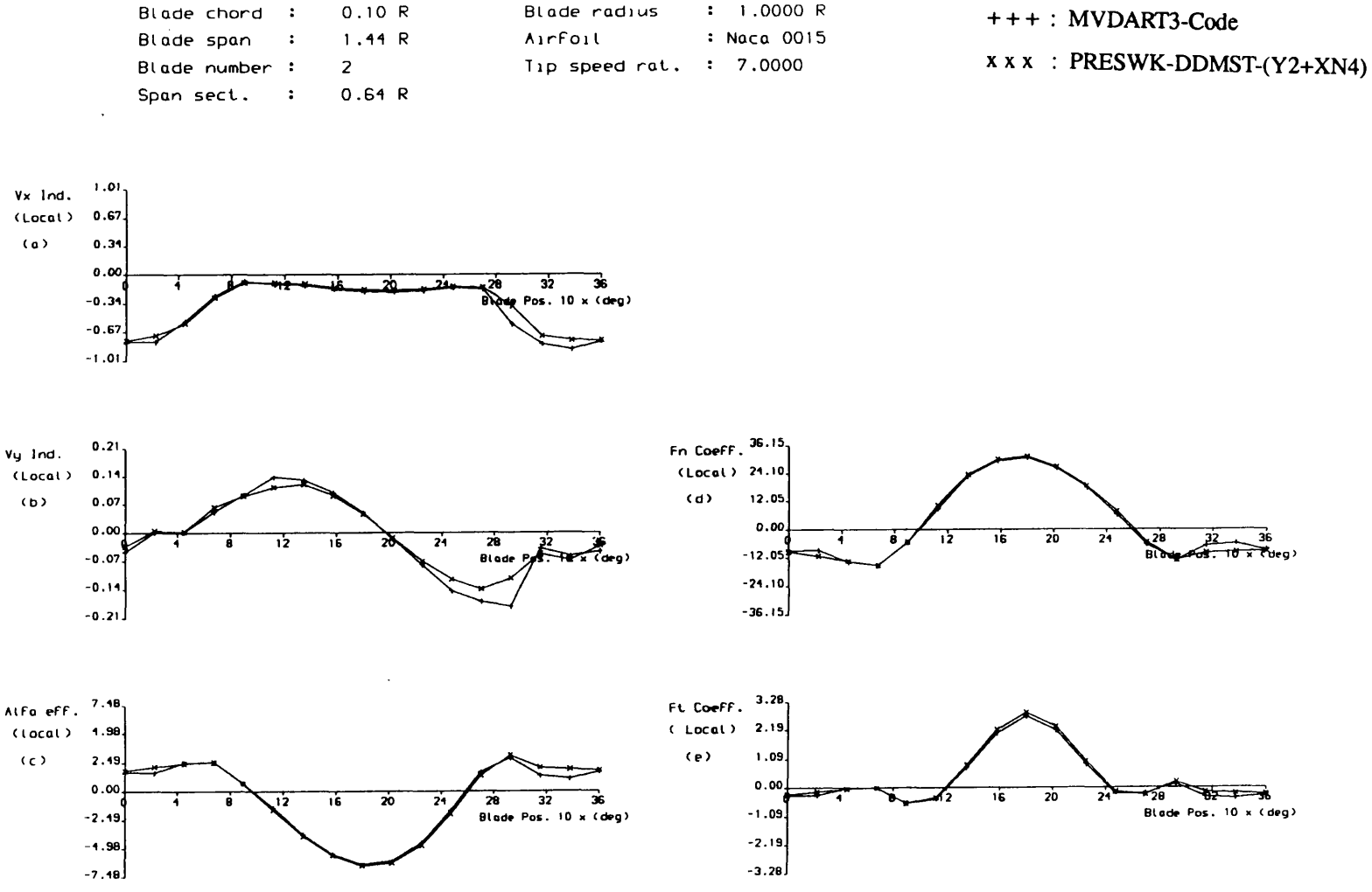

Fig 5.15 The comparison of detailed aerodynamic characteristics along the half blade span between the MVDART3- Code and PRESWK-DDMST - (Y2+XN4) for a Circular Arc Darrieus wind turbine with airfoil Naca 0015 at $\lambda = 7$.

Arc Circle Darrieus WTB

Blade chord	: 0.10 R	Blade radius	: 1.0000 R
Blade span	: 1.44 R	Airfoil	: Naca 0015
Blade number	: 2	Tip speed rat.	: 7.0000
Span sect.	: 0.48 R		

+++ : MVDART3-Code

x x x : PRESWK-DDMST-(Y2+XN4)

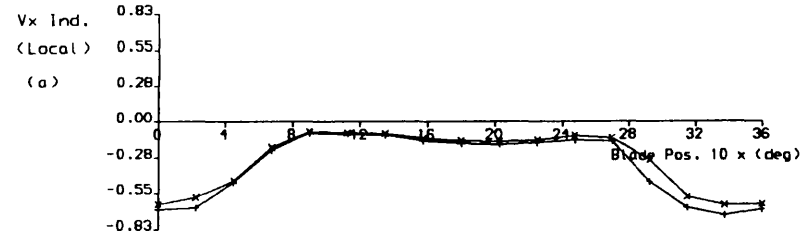

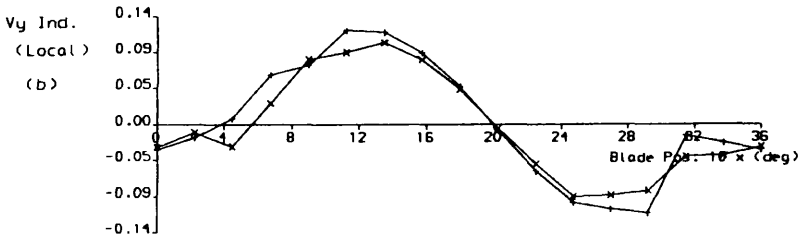

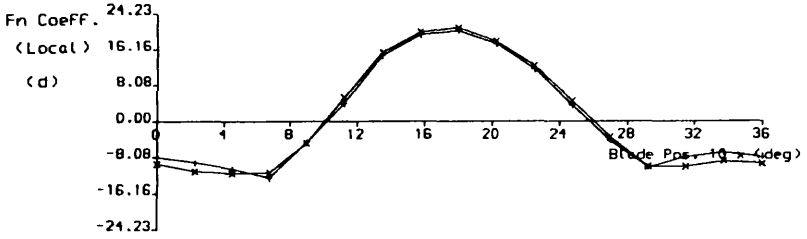

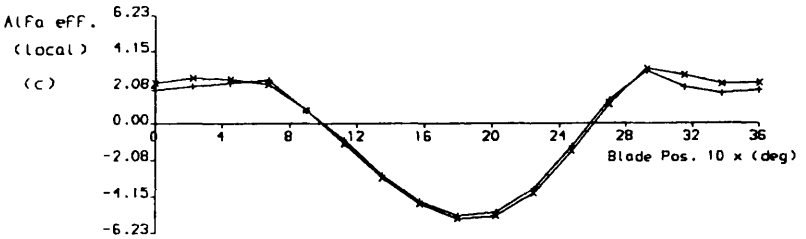

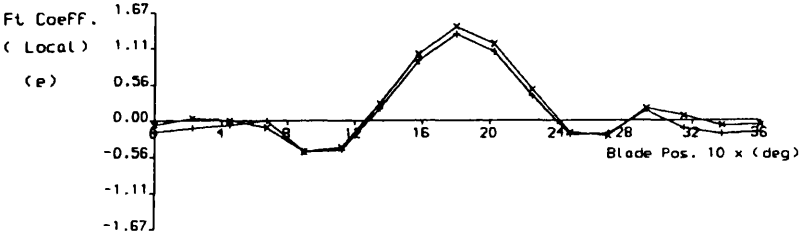

Cont'n from Fig 5.15 (a)

Arc Circle Darrieus WTB

Blade chord	: 0.10 R	Blade radius	: 1.0000 R
Blade span	: 1.44 R	Airfoil	: Naca 0015
Blade number	: 2	Tip speed rat.	: 7.0000
Span sect.	: 0.32 R		

+++ : MVDART3-Code

x x x : PRESWK-DDMST-(Y2+XN4)

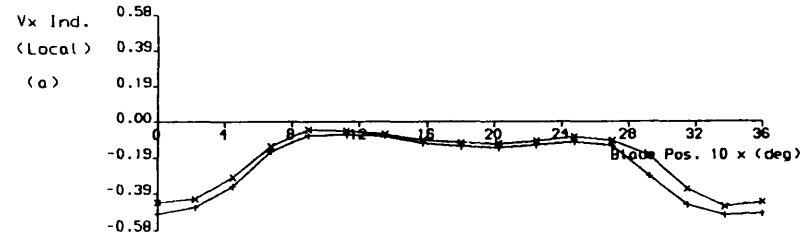

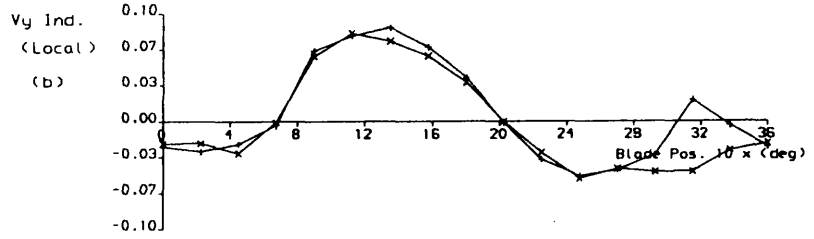

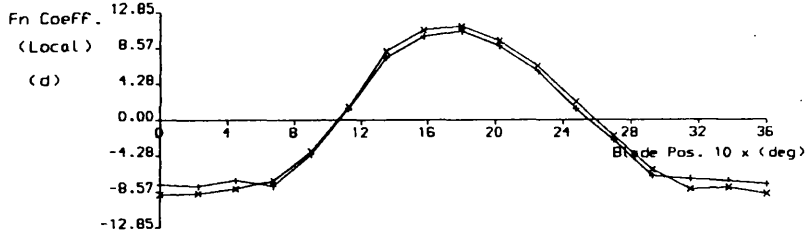

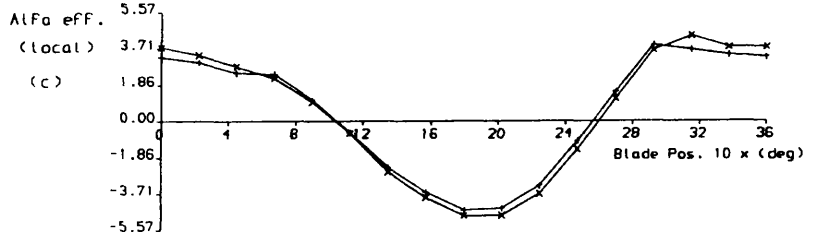

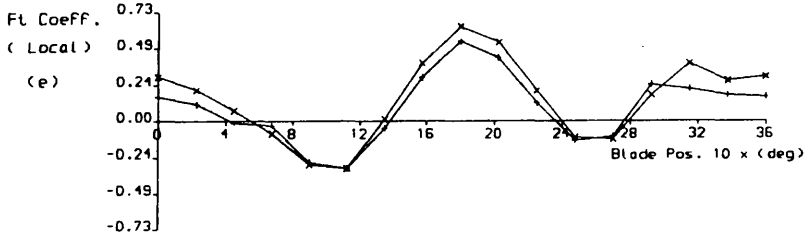

Cont'n from Fig 5.15 (b)

Arc Circle Darrieus WTB

Blade chord	:	0.10 R	Blade radius	:	1.0000 R
Blade span	:	1.44 R	Airfoil	:	Naca 0015
Blade number	:	2	Tip speed rat.	:	7.0000
Span sect.	:	0.15 R			

+++ : MVDART3-Code

x x x : PRESWK-DDMST-(Y2+XN4)

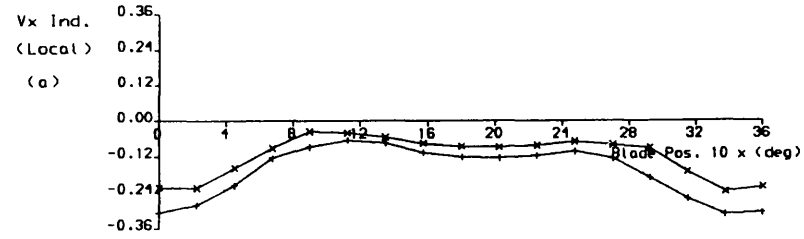

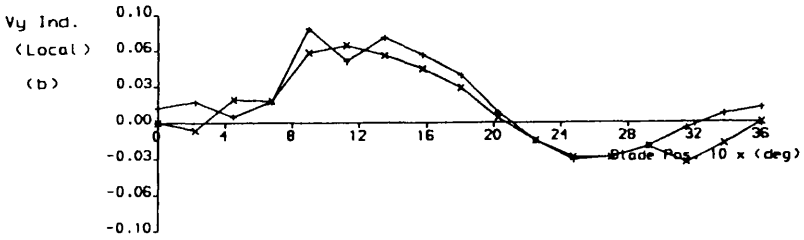

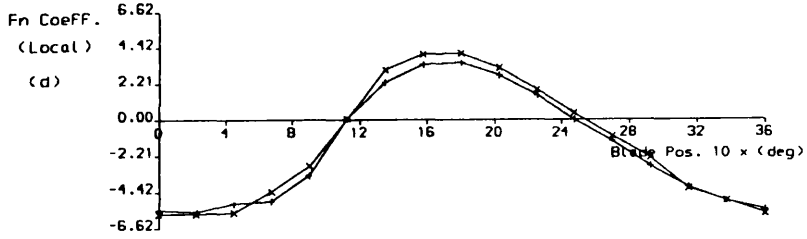

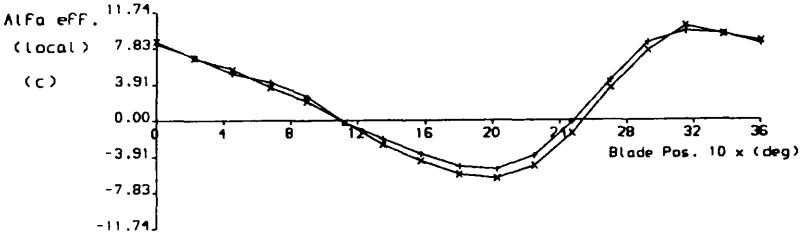

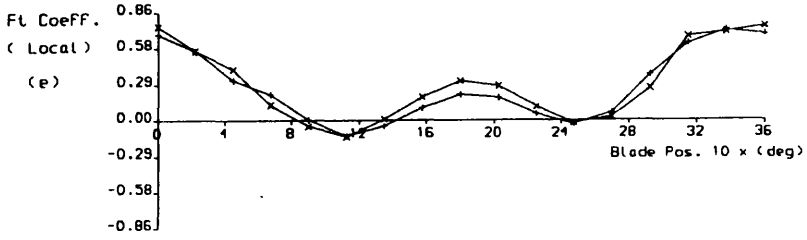

Cont'n from Fig 5.15 (c)

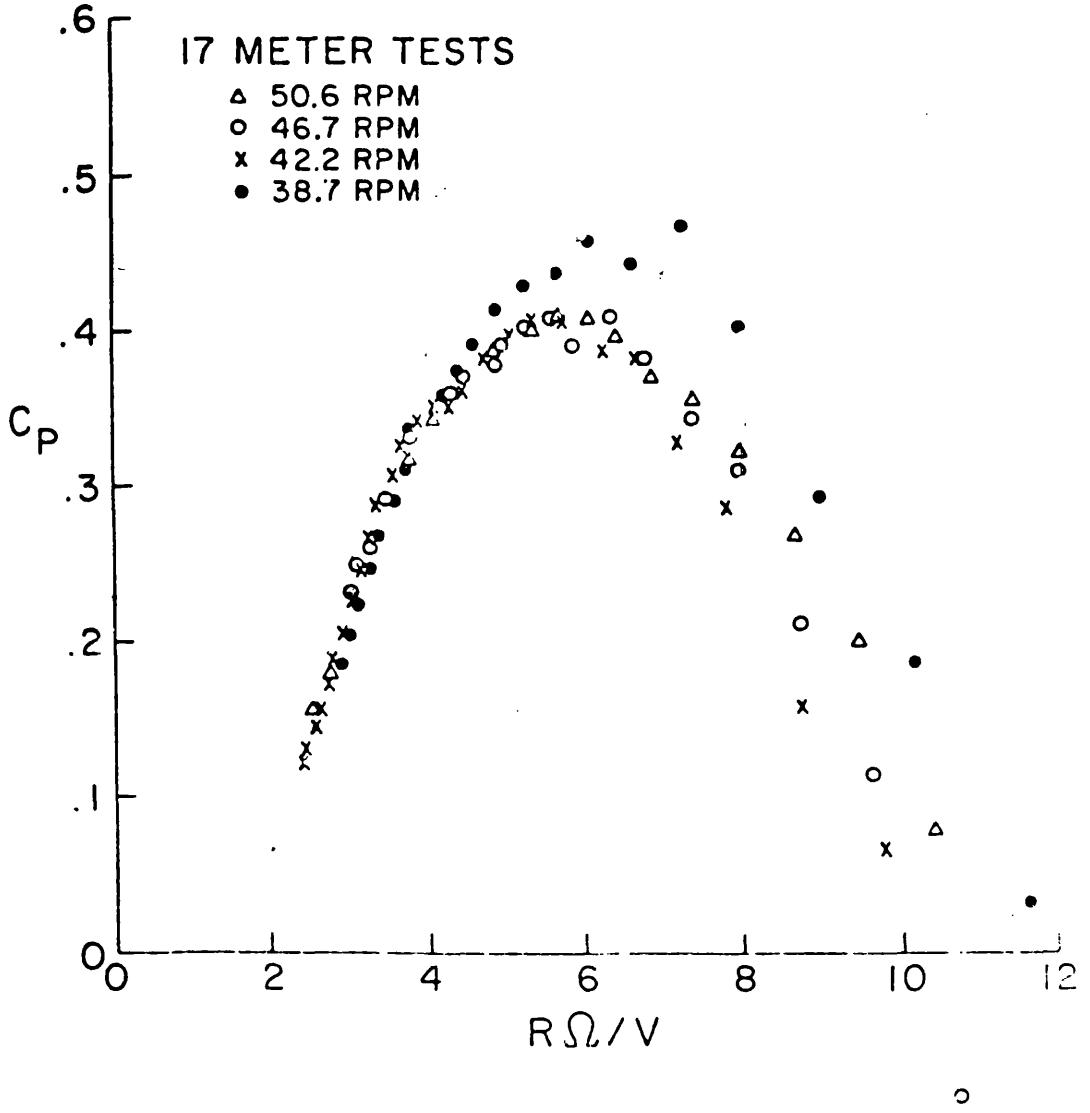

Fig.5.16 The experimental results of power coefficient for the Sandia-17 m wind machine from Ref. 163

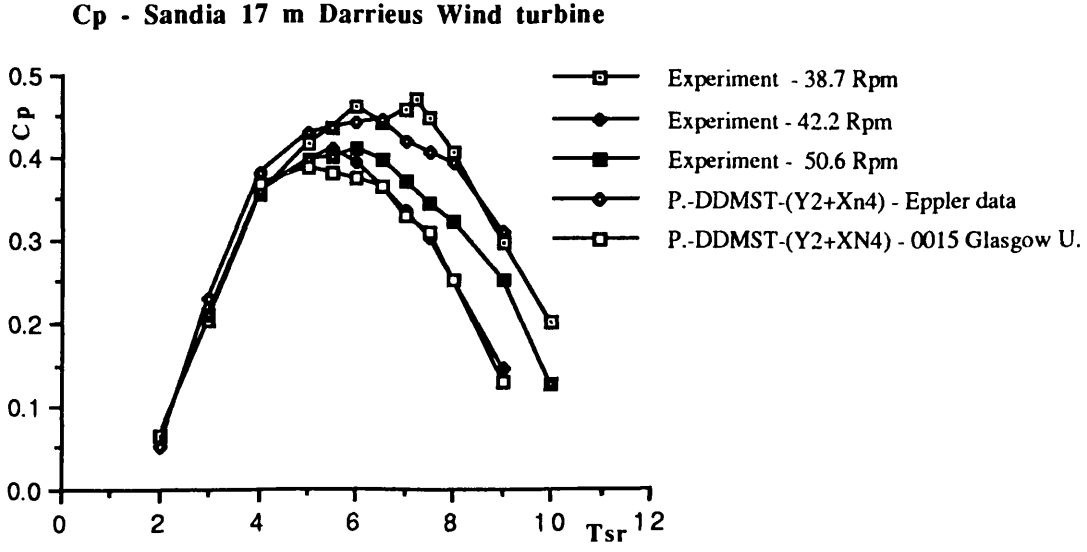

Fig. 5.17 A comparison of power coefficients between the experimental results and PRESWK - DDMST-(Y2+XN4) for the case of the Sandia-17 m Darrieus wind turbine.

APPENDIX - A1

The Application of Blade Element Theory in the Single Disk Single Stream -Tube Method.

Momentum Theory applied in the Single Disk Single Stream Tube Method provides the relationship between the averaged force F, acting normal to the disk actuator, and the disk velocity U as :

$$F = 2\rho A U [U_{\sim} - U] \qquad \text{A1-1}$$

In the above equation $U_{\sim}$ is the free stream velocity and A is the swept area. For the straight bladed vertical axis wind turbine with blade radius R and blade span L, the swept area A is equal to 2RL. In order to obtain the value of disk velocity U, the averaged force F on the left hand side of equation A1-1, needs to be determined. Here one can use Blade Element Theory. In this case, the disk velocity U represents the component of velocity in the direction of the free stream velocity. There is also a rotational velocity due to the blade motion. Hence, on the blade section at any azimuth blade position θ, and assumed pitch angle zero, the diagram of vector velocity acting on the blade as shown in Fig. A1-1. Here the rotational velocity $U_r = \Omega R$ is in the tangential direction parallel to the chord.

At blade azimuth position θ, the disk velocity U can be resolved into tangential [chordwise] and radial [normal to the chord] components. These two component velocities are denoted by V_t and V_n ,respectively and can be written as :

$$V_t = \Omega R + U_{\sim} \sin\theta \qquad \text{A1-2a}$$

$$V_n = U_{\sim} \cos\theta \qquad \text{A1-2b}$$

The resultant velocity V_R and the angle of attack α can be ,simply, defined as :

$$V_R = [\, V_t^2 + V_n^2 \,]^{1/2} \qquad \text{A1-3a}$$

$$\alpha = \text{Arctg}\,[\, V_n/V_t \,] \qquad \text{A1-3b}$$

For a given angle of attack α, the lift L and drag D, for a unit blade span and aerofoil chord c, can be defined, respectively as follows :

$$L = 1/2\, \rho\, U_R^2\, c\, C_l(\alpha) \qquad \text{A1-4a}$$

$$D = 1/2\, \rho\, U_R^2\, c\, C_d(\alpha) \qquad \text{A1-4b}$$

Where C_l and C_d represent the lift and drag coefficients of the blade section. From Fig. A1-1, the lift force L, with respect to blade azimuth position θ, acts at an angle [$\theta+\alpha$], while the drag force D acts at an angle [$\theta - \alpha - 90^o$] . In line with momentum theory, which requires the force in the axial direction, the two forces L and D can be resolved into the axial direction. This provides an instantaneous force , denoted as F_i which can be written as :

$$F_i = L \cos(\theta+\alpha) + D \cos(\theta-\alpha-90^o)$$

$$= 1/2\, \rho\, U_R^2\, c\, [\, C_l(\alpha) \cos(\theta+\alpha) + C_d(\alpha) \sin(\theta-\alpha) \,] \qquad \text{A1-5}$$

If the wind turbine has N_b blades, the instantaneous force F_i is multiplied by N_b to become :

$$F_i = 1/2\, \rho\, U_R^2\, c\, N_b\, [\, C_l(\alpha) \cos(\theta+\alpha) + C_d(\alpha) \sin(\theta-\alpha) \,] \qquad \text{A1-6}$$

Hence the averaged force F can be obtained by integration of equation A1-6 for one complete revolution, i.e. :

$$F_i = 2\rho \int_0^{2\pi} F_i \, d\theta$$

A1-7

Equation A1-7 is too complex to be solved analytically since the angle of attack α, and the resultant velocity V_R are both functions of θ as defined by equation A1-3. However ,the problem in hand can be simplified for high tip speed ratios if the following assumptions are made :

1. $\Omega R >> U_\sim$
2. $C_l(\alpha) = (dC_l/d\alpha) \alpha$; $dC_l/d\alpha$ = constant.
3. α : is a small angle and drag force D can be ignored.

For such imposed conditions the formulae above can be simplified as follows :

$$V_t = \Omega R + U_\sim \sin\theta \cong \Omega R$$

$$V_n = U_\sim \cos\theta$$

$$V_R = [V_t^2 + V_n^2]^{1/2} \cong \Omega R$$

$$\alpha = \text{Arctg}[V_n/V_t] \cong U_\sim \cos\theta / \Omega R$$

$$L = 1/2\, \rho\, U_R^2\, c\, C_l(\alpha) \cong 1/2\, \rho\, (\Omega R)^2\, c\, (dCl/d\alpha)\, \alpha$$

$$D = 1/2\, \rho\, U_R^2\, c\, C_d(\alpha) \cong 0$$

Using the above simplified equations, it is possible to express the instantaneous force F_i as:

$$F_i = 1/2\, \rho\, U_R^2\, c\, N_b [C_l(\alpha) \cos(\theta+\alpha) + C_l(\alpha) \sin(\theta-\alpha)]$$

$$\cong 1/2\,\rho\,(\Omega R)^2\,c\,N_b\,(dCl/d\alpha)\,\alpha\,[\cos(\theta)\,\mathrm{Cos}(\alpha) - \sin(\theta)\,\sin(\alpha)\,]$$

$$\cong 1/2\,\rho\,(\Omega R)^2\,c\,N_b\,(dCl/d\alpha)\,\alpha\,[\cos(\theta)\,\mathrm{Cos}(\alpha) - \alpha\,\sin(\theta)\,]$$

$$\cong 1/2\,\rho\,(\Omega R)^2\,c\,N_b\,(dCl/d\alpha)\,U_{\sim}\,\mathrm{Cos}(\theta)\,[\cos(\theta)\,\mathrm{Cos}(\alpha) -$$

$$- U_{\sim}\,\mathrm{Cos}(\theta)\,\sin(\theta)/(\Omega R)\,] \qquad \text{A1–8}$$

The force F_i given by equation A1-8, when inserted into Eq. A1-7, allows it to be integrated analytically and the result is given by :

$$F = 1/4\,\rho\,(\Omega R)\,c\,N_b\,(dCl/d\alpha)\,U_{\sim} \qquad \text{A1-9}$$

The force F given by equation A1-9 represents the averaged force per unit span, hence, if it is uniform along the blade span L, the right hand side can be simply multiplied by L. Now, equating eq. A1-9 with A1-1, one can obtain the disk velocity U as :

$$1/4\,\rho\,(\Omega R)\,c\,N_b\,(dCl/d\alpha)\,U_{\sim} = 2\,\rho\,2RL\,U\,[U_{\sim} - U]$$

$$U = U_{\sim}\,[1 - 1/8\,(N_b c/2R)\,(\Omega R/U_{\sim})(dCl/d\alpha)\,]$$

$$= U_{\sim}\,[1 - 1/8\,(\sigma\,\lambda\,(dCl/d\alpha))\,] \qquad \text{A1-10}$$

Where $\sigma = N_b c/2R$ is known as the solidity factor and $\lambda = \Omega R/U_{\sim}$ is the tip speed ratio.

Using eq. A1-10, one can define the disk velocity U which, in turn, via eq. A1-1 provides the averaged force F. The average power P of the wind device can then be determined using the relation ship :

$$P = FU. \qquad \text{A1-11}$$

APPENDIX-A2

The Application of Blade Element Theory in the Single Disk Multiple Stream Tube Method

In the single disk multiple stream tube approach, the swept volume of the rotor is divided into a series of adjacent stream tubes. The same basic principle which has been applied to the Single Disk Single Stream Tube model is also valid for each stream tube of this multiple stream tube approach. Implementation of momentum theory in this case will provide the differential averaged axial force dF which, for any given stream tube can be written as :

$$dF = 2\, dm\, (U_{\sim} - U) \qquad \text{A2-1}$$

For the case of a straight bladed vertical axis wind turbine, with blade span L and radius R, the Single Disk Multiple Stream Tube model is as depicted in Fig. A1-1. If the incoming velocity $U_{\sim}$ along the blade span is uniform, the disk velocity U along the blade span is also uniform and the differential rate of mass dm is equal to $\rho L\, dy\, U$, equation A2-1 can be written as :

$$dF = 2\, L\, dy\, \rho U(U_{\sim} - U) \qquad \text{A2-2}$$

In the free stream direction, each stream tube is assumed to have constant width dy. If dF in equation A2-2 can be defined, then the disk velocity U can be obtained. It is known that one possible approach to defining dF is deduced from blade element theory.

Considering a particular stream tube [Fig. A1-1] , located at blade blade azimuth position θ with width dy, the relation between dy and $d\theta$ is given by :

$$dy = R\cos(\theta)\, d\theta \qquad \text{A2-3}$$

Clearly, a given stream tube will experience two blade crossings for every revolution of the turbine. Hence, the stream tube at blade azimuth position θ, will be crossed by the blade when the blade is at azimuth position θ [down stream] and at $\pi-\theta$ [upstream]. In Appendix A1, the formulation for the axial force for any blade azimuth position θ was presented. In this case, the relationship should be considered in a differential form, with the force rewritten as:

$$dF_x = 1/2\rho\, U_R^2\, c\, N_b[\, C_l(\alpha)\, Cos(\theta+\alpha) + C_d(\alpha)\, \sin(\theta-\alpha)\,] \qquad \text{A2-4}$$

Blade element theory can provide information about the force acting on the blade. In order to use such force information in the momentum theory a careful assessment is required. The representation of axial force dF_x, based on Blade element theory, as defined by equation. A2-4, is only valid as long as the blade is in the azimuth interval $d\theta$.

If the angular velocity of the blade is Ω, then the time taken for the blade to cover such an interval will be $d\theta/\Omega$. Since the blade crosses the stream tube twice, the total time a blade interferes with the stream tube is $2\, d\theta/\Omega$. In one revolution , however the blade covers 2π, and the time for one revolution is $2\pi/\Omega$. Hence, the percentage time for which the blade crosses a stream tube $d\theta$ wide will be $d\theta/\pi$. This percentage represents the multiplier to the axial force dF_x when applied to a particular stream tube.

As mentioned above, the blade crosses the stream tube two times, namely when the blade is at θ and $(\pi-\theta)$. Hence, there are two values of axial force, $dF(\theta)$ and $dF(\pi-\theta)$. Here one can introduce an averaging process to these values. The term dF_x, as given by equation A2-4, is already written in terms of the force in the axial x direction, hence the averaged axial force deduced from blade element theory can be

written as :

$$dF_x = 1/2\ [\ dF_x\ (\theta) + dF_x\ (\pi-\theta)\ ]\ (d\theta/\pi) \qquad \text{A2-5}$$

Where $dF_x\ (\theta)$ is as defined by equation A2-4 , and $dF_x\ (\pi-\theta)$ is given by the same equation at $\pi-\theta$. However, since equation A2-4 contains other variables which are also functions of blade azimuth position, $dF_x\ (\pi-\theta)$ becomes :

$$\begin{aligned} dF_x\ (\pi-\theta) &= 1/2\ r\ U_{Ru}\ N_b\ c\ [\ C_l\ (\alpha_u)\ Cos(\pi-\theta+\alpha_u\ ) + C_d(\alpha_u)\ sin(\pi-\theta-\alpha_u\ )] \\ &= 1/2\ r\ U_{Ru}\ N_b\ c\ [\ C_l\ (\alpha_u\ )\{Cos(\pi)Cos(\theta-\alpha_u\ ) + Sin(\pi)sin(\theta-\alpha_u\ ) \\ &+ C_d\ (\alpha_u\ )\{\ sin(\pi)\ cos(\theta+\alpha_u) - cos(\pi)sin(\theta+\alpha_u\ )\}\ ] \\ &= 1/2\ r\ U_{Ru}\ N_b\ c\ [-C_l\ (\alpha_u)\ Cos(\theta - \alpha_u) + C_d\ (\alpha_u)\ sin(\theta+\alpha_u\ )\}\ ] \end{aligned} \qquad \text{A2-6}$$

The index u is introduced into the above equation to distinguish between the corresponding quantity defined in equation A2-4. Equating equation A2-5 with equation A2-2, one can calculate the local disk velocity U; this requires an iteration process.

However , the operating conditions of the vertical axis wind turbine in hand may allow one to introduce the simplifications described in the previous Appendix A1. The axial force according to the Blade element theory for an N_b bladed system, at any blade azimuth position θ, can then be written as :

$$dF_x\ (F) \equiv 1/2\ \rho\ (\Omega R)\ c\ N_b\ (dC/d\alpha)\ U\ \cos^2(\theta)\ [\ 1\ - U\ \sin(\theta)/(\Omega R\ ] \qquad \text{A2-7}$$

Hence, for the blade at azimuth position $(\pi-\theta)$, equation A2-6 becomes :

$$dF_x\ (\pi-\theta) \cong 1/2\ \rho\ (\Omega R)\ c\ N_b\ (dC/d\alpha)\ U\ \cos\ (\pi-\theta)\ [\ Cos(\pi-\theta)\ - U\ Cos(\pi-\theta)$$

$\sin(\pi-\theta)/(\Omega R)\ ]$ A2-8

From trigonometry, one gets :

$$\cos(\pi-\theta) = -\cos(\theta)$$
$$\sin(\pi-\theta) = \sin(\theta) \qquad \text{A2-9}$$

Hence, equation A2-8 can be written as :

$$dF_x(\pi-\theta) \cong 1/2\rho(\Omega R)cN_b(dC_l/d\alpha)\,U(-\cos(\theta))\,[-\mathrm{Cos}(\theta)-(-U\,\mathrm{Cos}(\theta)\sin(\theta)/(\Omega R\,]$$
$$\cong 1/2\,\rho\,(\Omega R)\,c\,N_b\,(dC_l/d\alpha)\,U\cos(\theta)\,[\mathrm{Cos}(\theta)-U\,\mathrm{Cos}(\theta)\sin(\theta)/(\Omega R)]$$
$$\cong 1/2\,\rho\,(\Omega R)\,c\,N_b\,(dC_l/d\alpha)\,U\cos^2(\theta)\,[\,1-\sin(\theta)(U/(\Omega R))] \qquad \text{A2-10}$$

Substituting equation A2-8 and A2-10 into equation A2-5 it follows :

$$dF_x = 1/2\,[\,dF_x\,(\theta) + dF\,(\pi-\theta)\,]\,(d\theta/\pi)$$
$$= \rho\,(\Omega R)\,c\,N_b\,(dC_l/d\alpha)\,U\cos^2(\theta)\,[\,1-\sin(\theta)(U/(\Omega R))]\quad d\theta/\pi \qquad \text{A2-11}$$

If the assumption described in the previous appendix, that $U << (\Omega R)$ is used, the

term $[1-\sin(\theta)(U/(\Omega R))] \cong 1$, and Equation A2-11 becomes :

$$dF_x = \rho\,(\Omega R)\,c\,N_b\,(dC_l/d\alpha)\,U\cos^2(\theta)\quad d\theta/\pi \qquad \text{A2-12}$$

Equating equation A2-12 and equation A2-2, the relation for the local disk velocity U is derived as :

$$\rho\,(\Omega R)\,c\,N_b\,(dC_l/d\alpha)\,U\cos^2(\theta)\quad d\theta/\pi = 2\rho\,dy\,U(U-U)$$

$$\rho\,(\Omega R)\,c\,N_b\,(dC_l/d\alpha)\,U\cos^2(\theta)\,[\,dy\,/(\pi\,R\cos\theta\,)] = 2\rho\,dy\,U(U_\sim - U)$$

or

$$U = U_\sim\left(1. - \frac{\Omega R}{U_\sim}\,\frac{N_b\,c}{2R}\left[\frac{dC_l/d\alpha}{\pi}\right]\cos\theta\right) \qquad \text{A2 - 13}$$

The formula for disk velocity U given by equation A2-13 is slightly different from the formulation given by Ref. 48 [Hunt]. The difference is due to the definition of the system coordinates and also the definition of aerofoil data. Hunt set $C_l = 2\pi\sin\alpha$ and his analysis gave the local disk velocity U as :

$$U = U_\sim\left(1. - \frac{\Omega R}{U_\sim}\,\frac{N_b\,c}{2R}\,|\sin\theta\,|\right) \qquad \text{A2-14}$$

If the formulation of the Force F, via blade element theory, cannot be formulated analytically, the solution to obtain the disk velocity U requires an iteration process. The governing equation is, then, formed by equating equations A2-5 and A2-2 as follows :

$$1/2\,[\,dF_X\,(\theta) + dF_X\,(\pi-\theta)\,]\,(d\theta/\pi) = 2\,L\,dy\,\rho U(U_\sim - U) \qquad \text{A2-14}$$

where $dF_X(\theta)$ and $dF_X(\pi-\theta)$ are as defined by equation. A1-6 [Appendix A1] and A2-6, respectively.

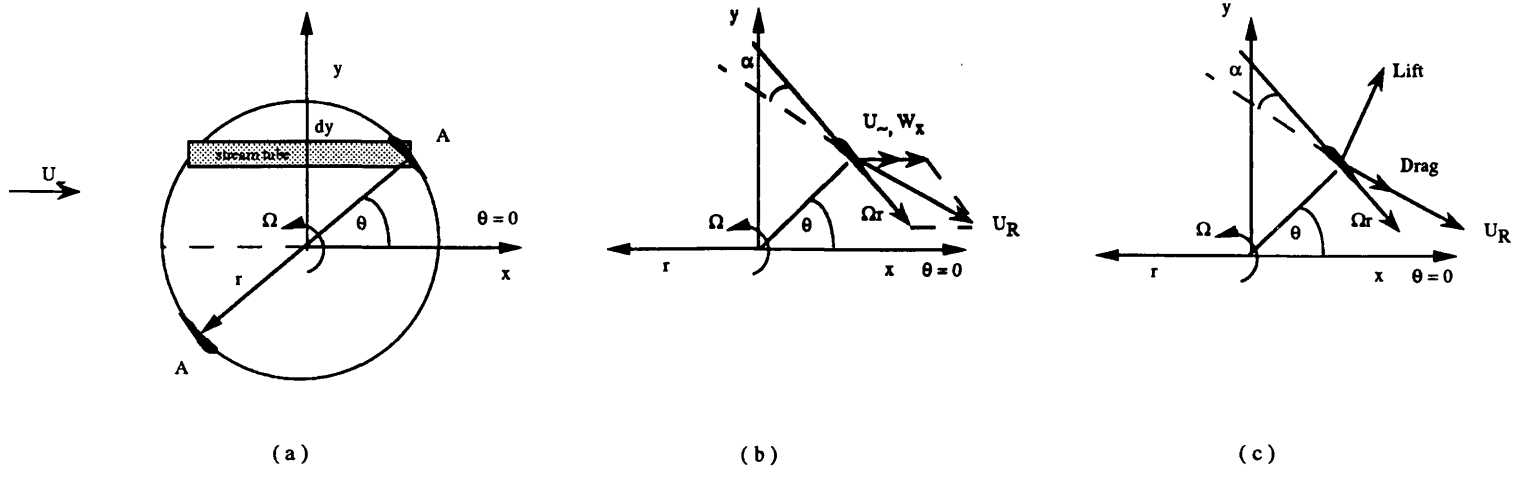

Fig. A1-1 The velocities and forces in a Single Disk Multiple Stream-Tubes model.

APPENDIX - B1

The Flow Chart of the Main Algorithm of the Prescribed Wake Scheme.

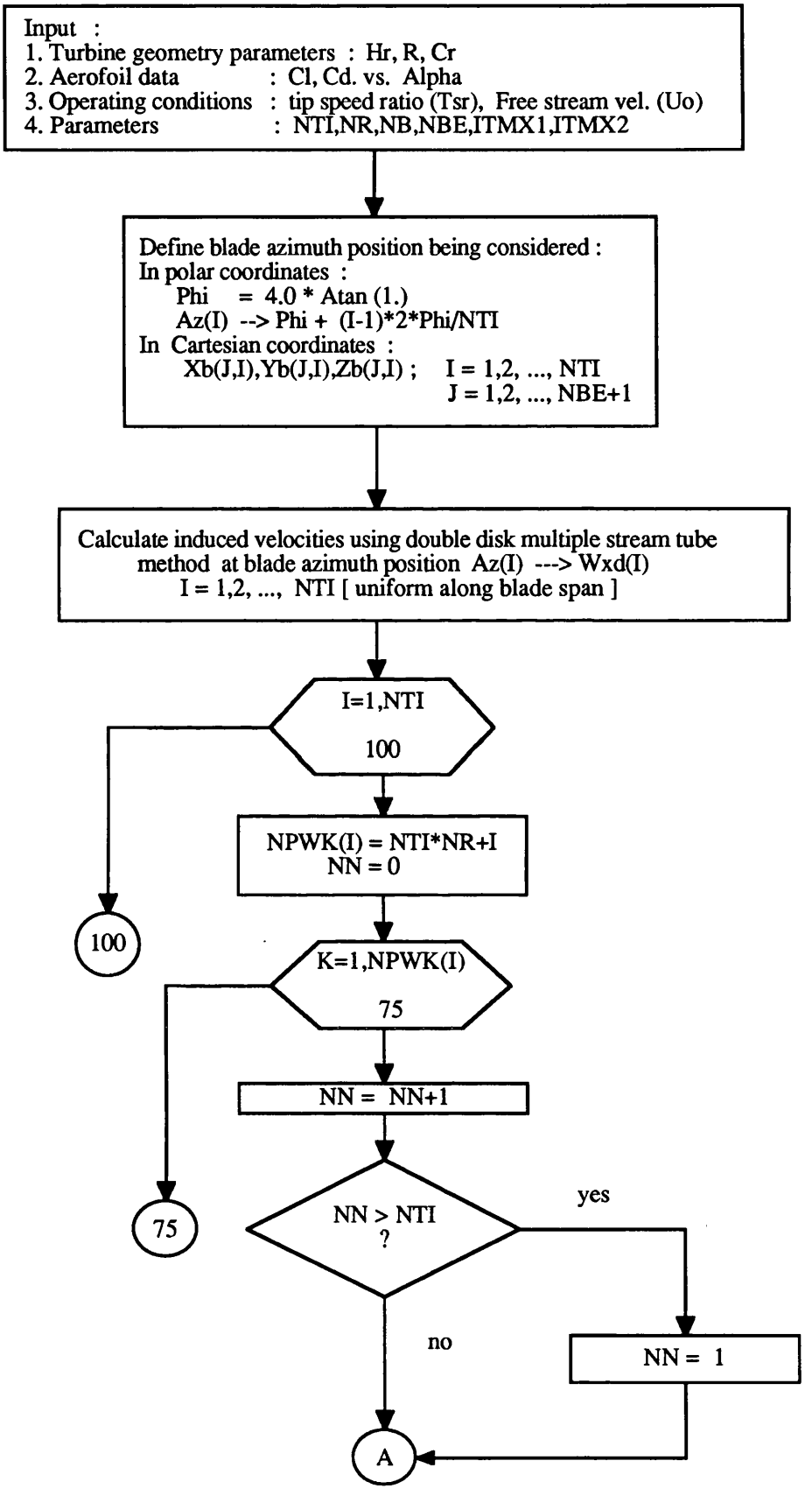

Fig. B-1a : Flow Chart of the main algorithm of the Prescribed Wake scheme

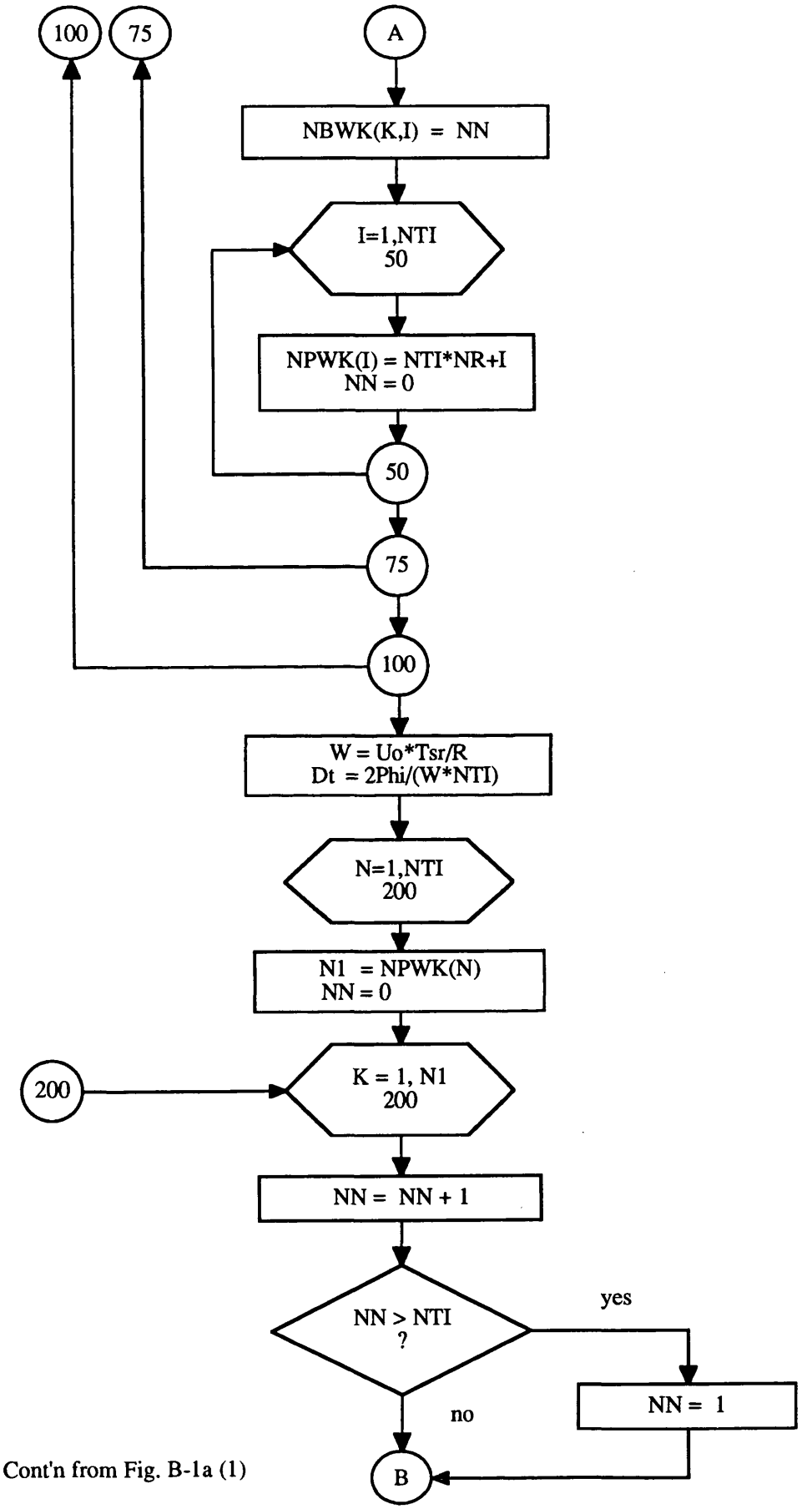

Cont'n from Fig. B-1a (1)

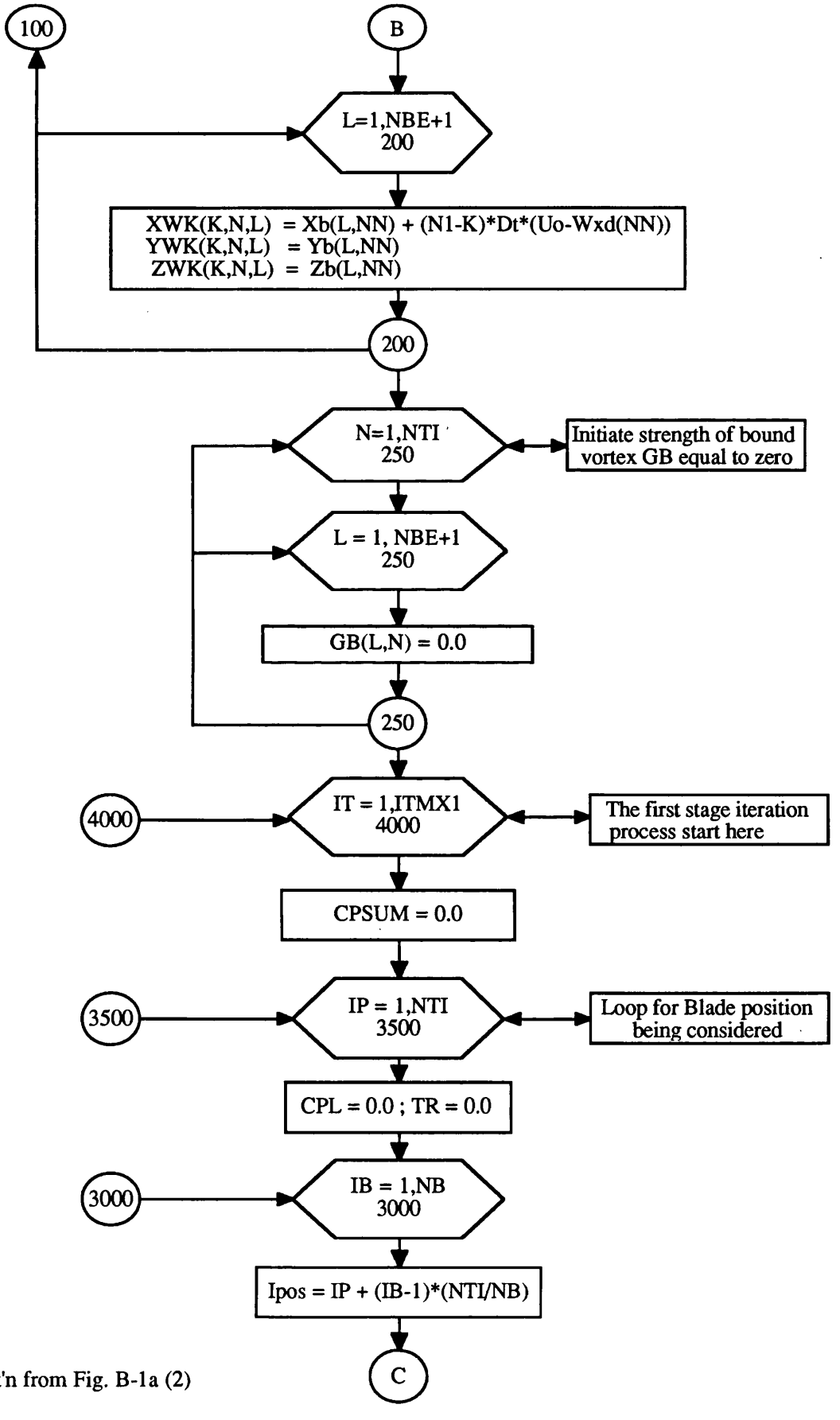

Cont'n from Fig. B-1a (2)

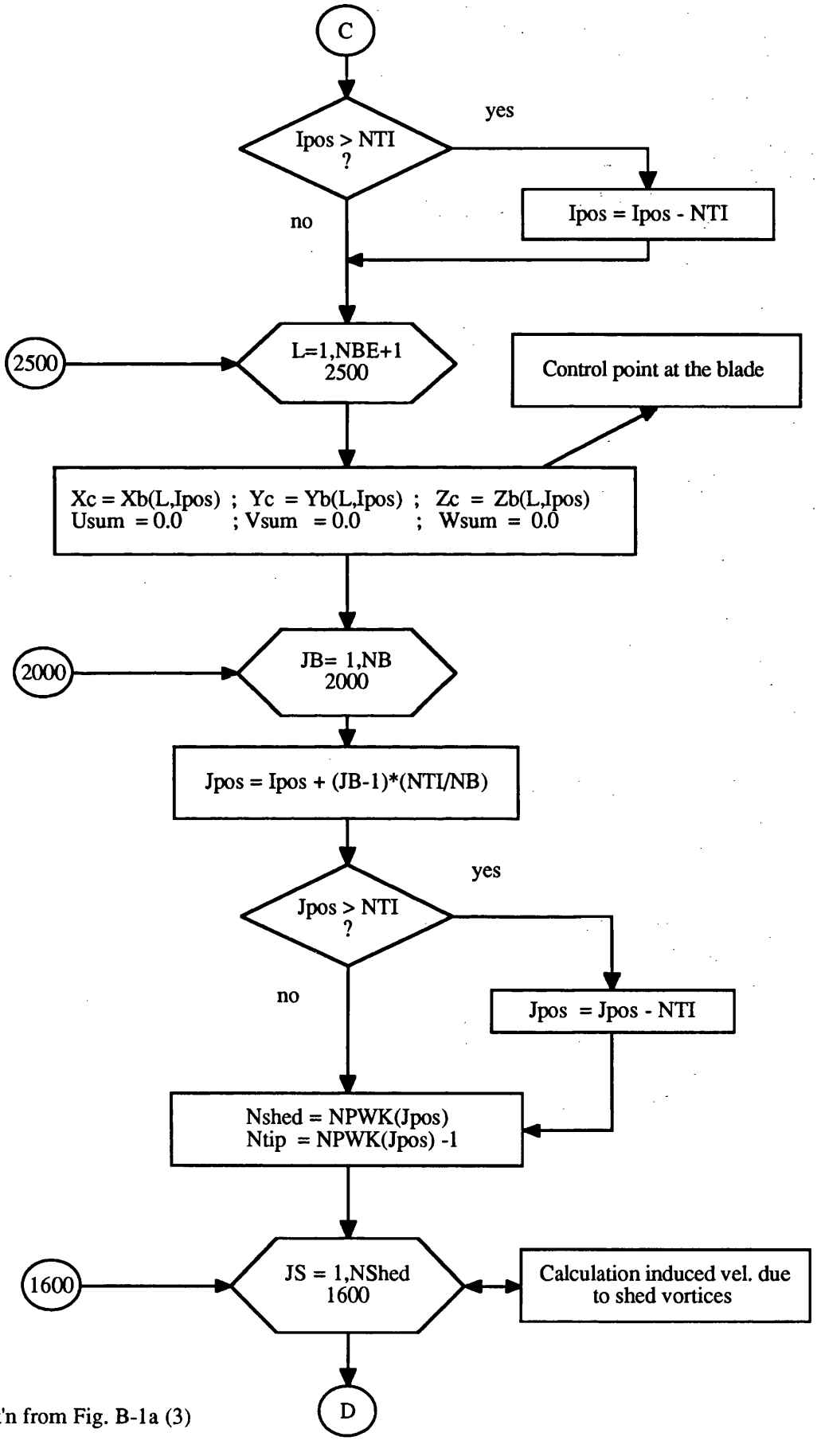

Cont'n from Fig. B-1a (3)

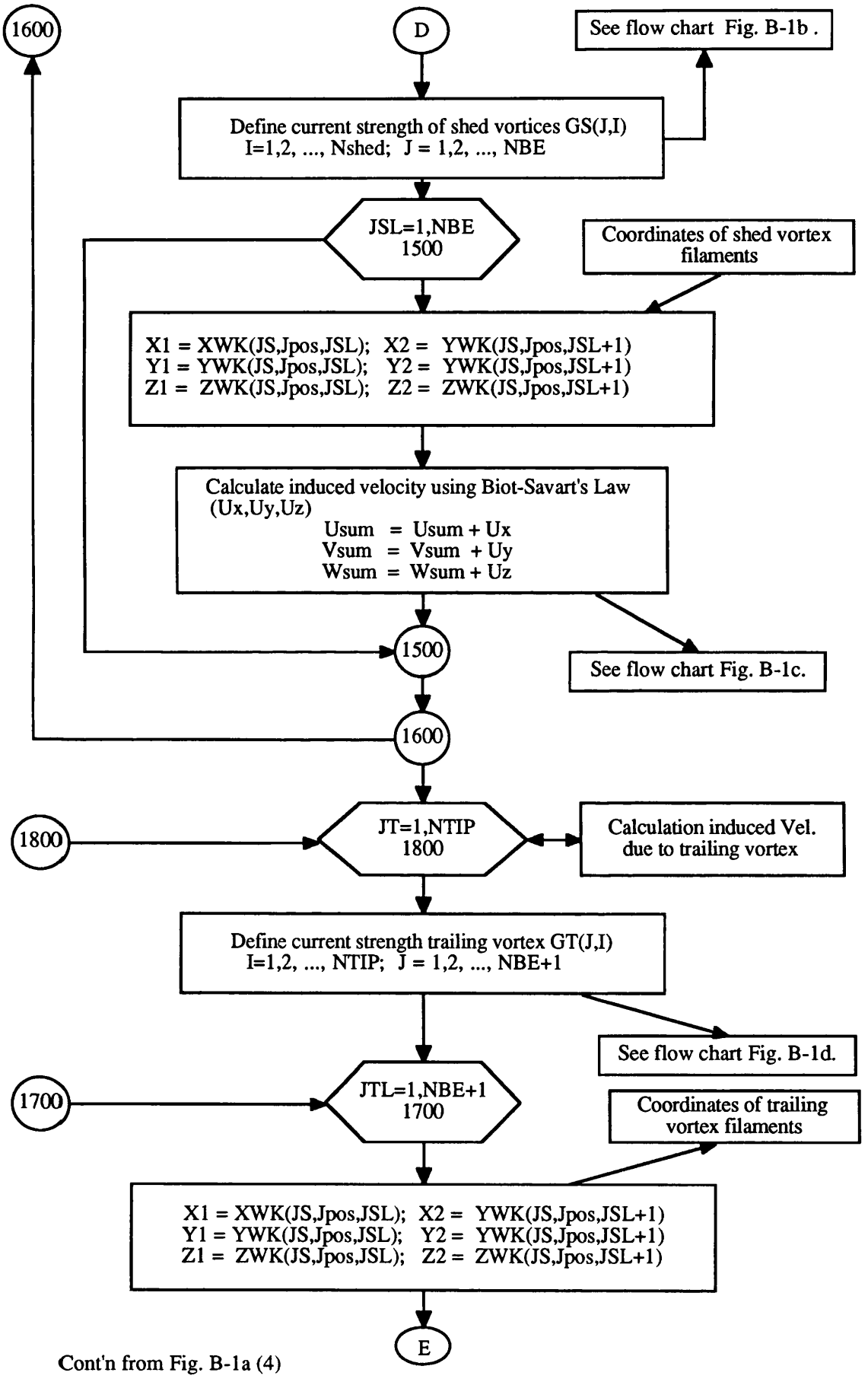

Cont'n from Fig. B-1a (4)

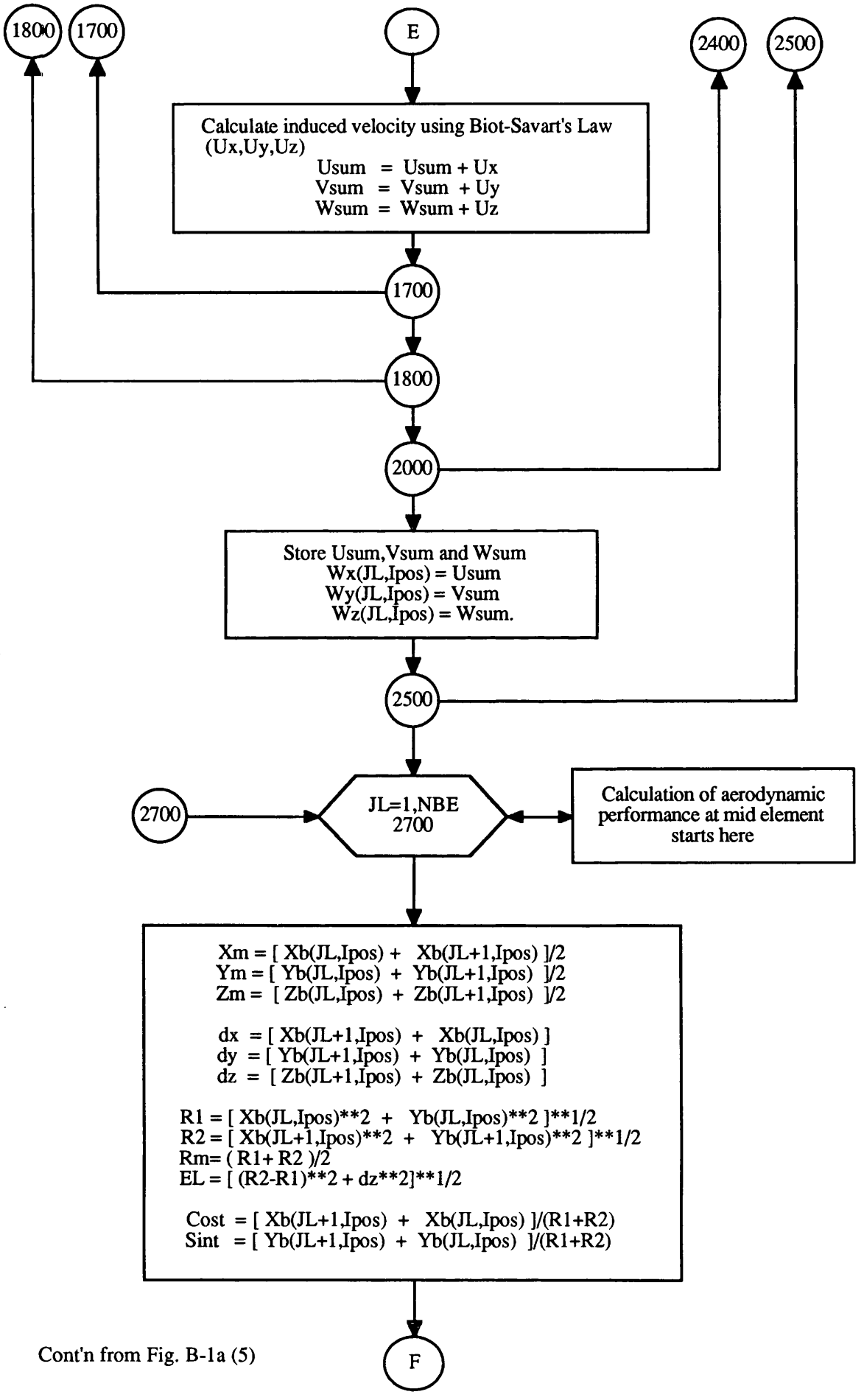

Cont'n from Fig. B-1a (5)

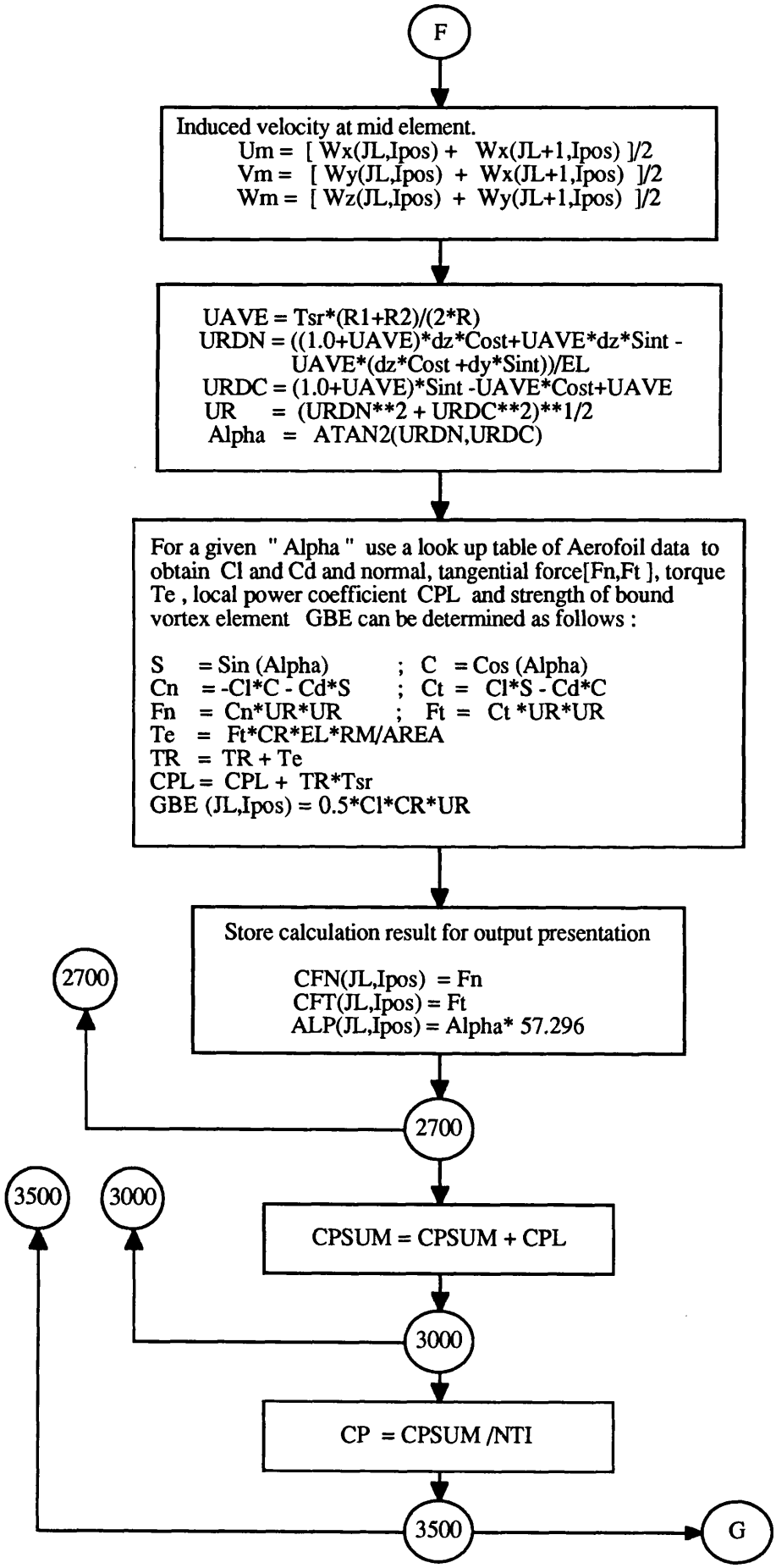

Cont'n from Fig. B-1a (6)

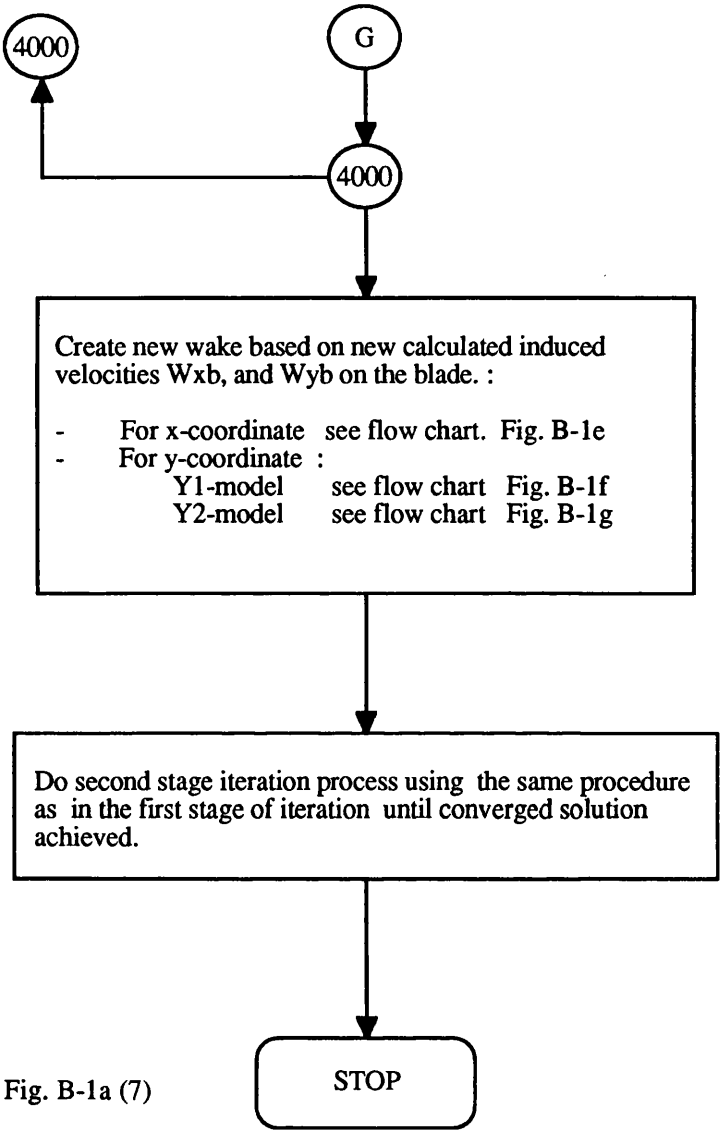

Cont'n from Fig. B-1a (7)

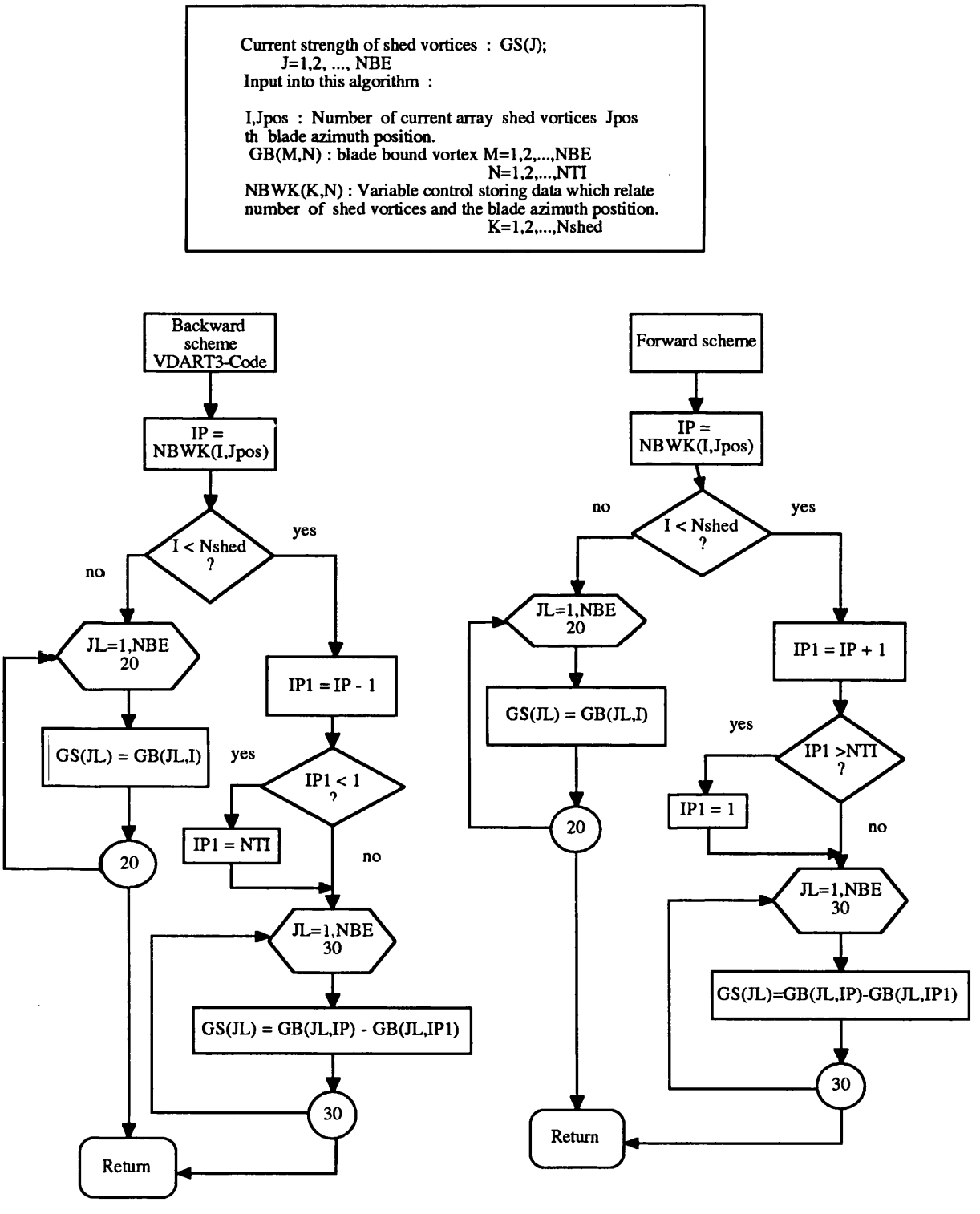

Fig. B-1b Flow chart of the algorithm for defining the strength of shed vortices

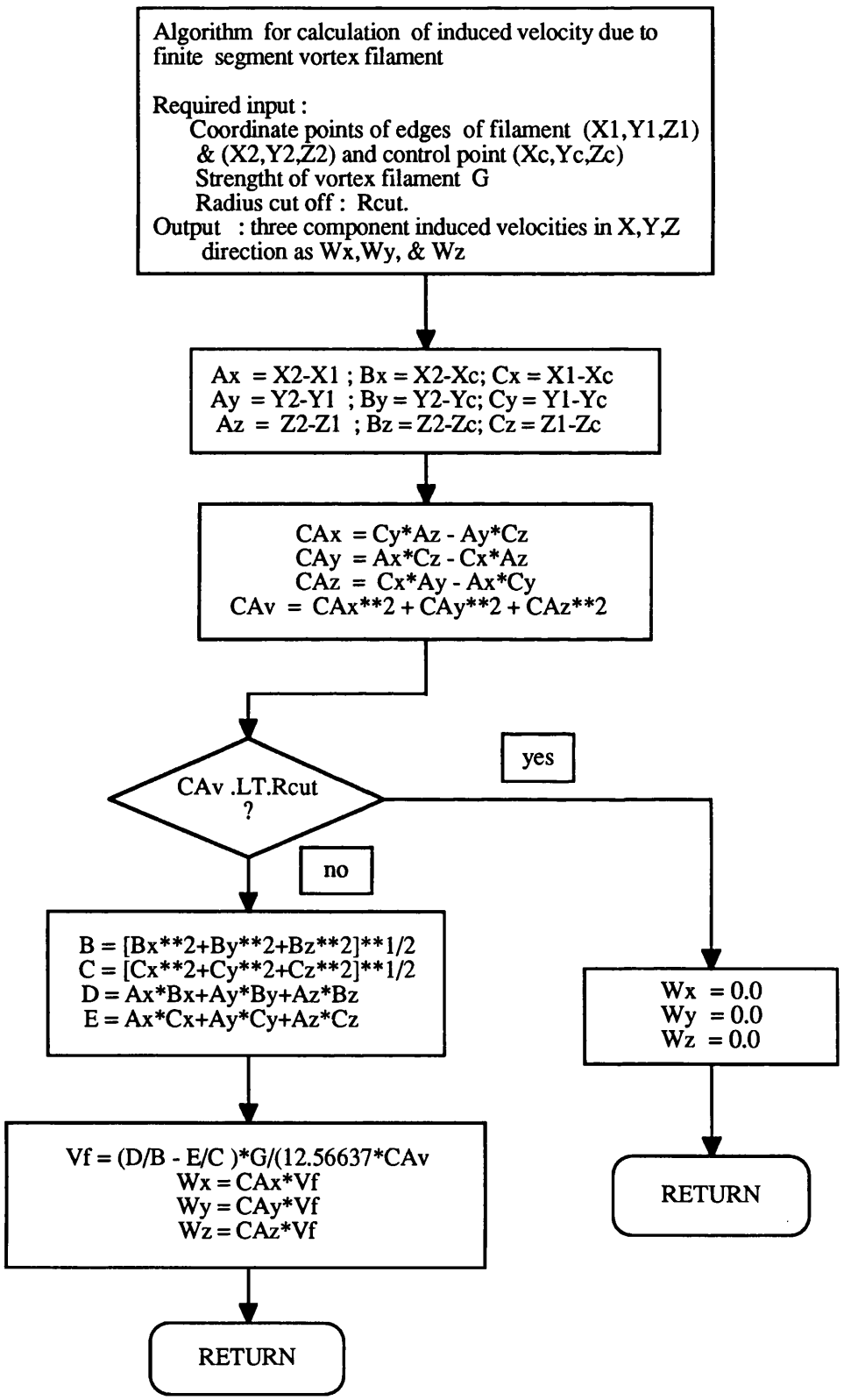

Fig. B-1c. Flow chart of the algorithm for the induced velocity calculation using Biot-Savart's Law

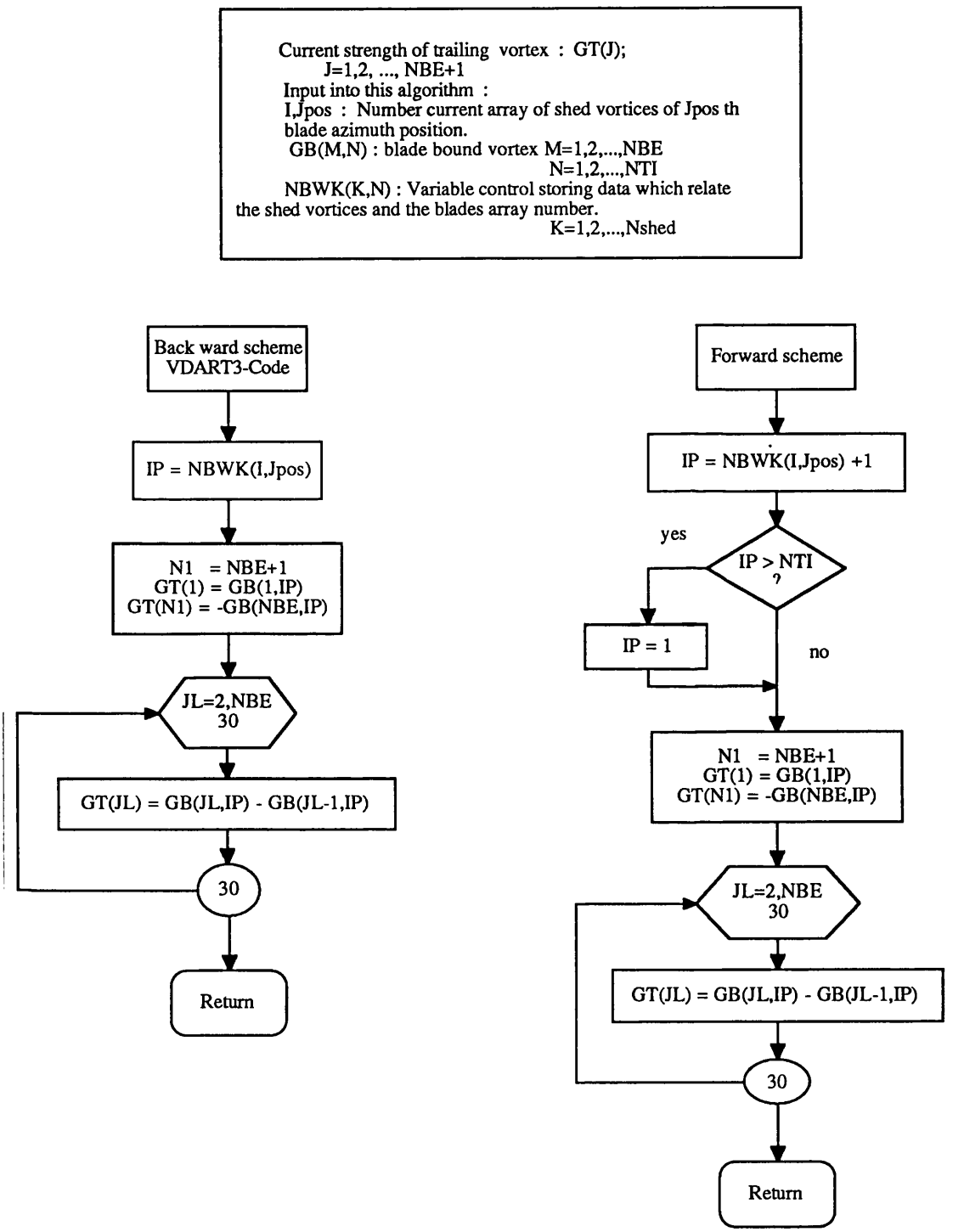

Fig. B-1d Flow chart of the algorithm for defining the strength of trailing vortex

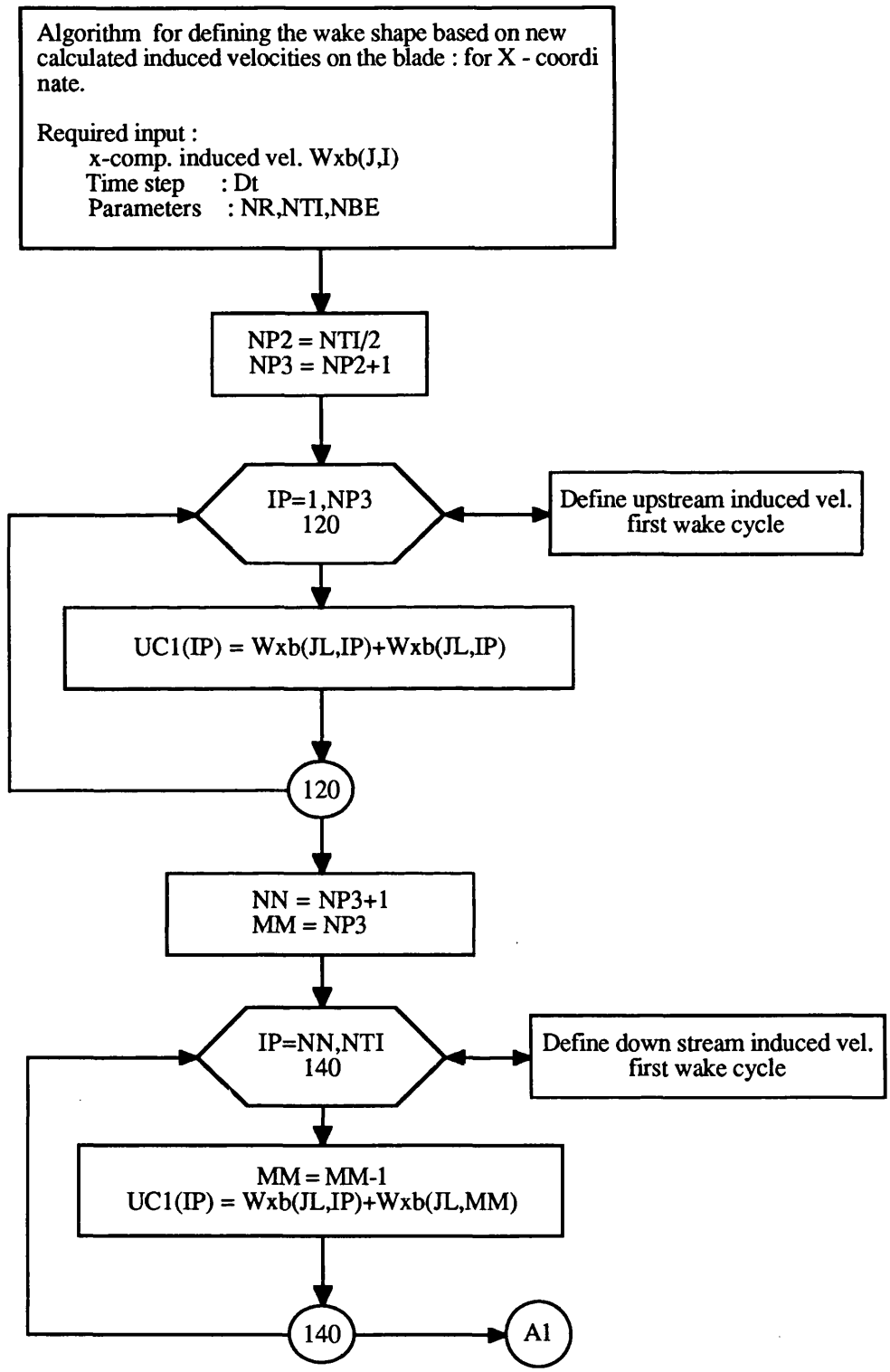

Fig. B-1e Flow chart of the algorithm for the reconstruction of wake shape in X-direction [old wake scheme]

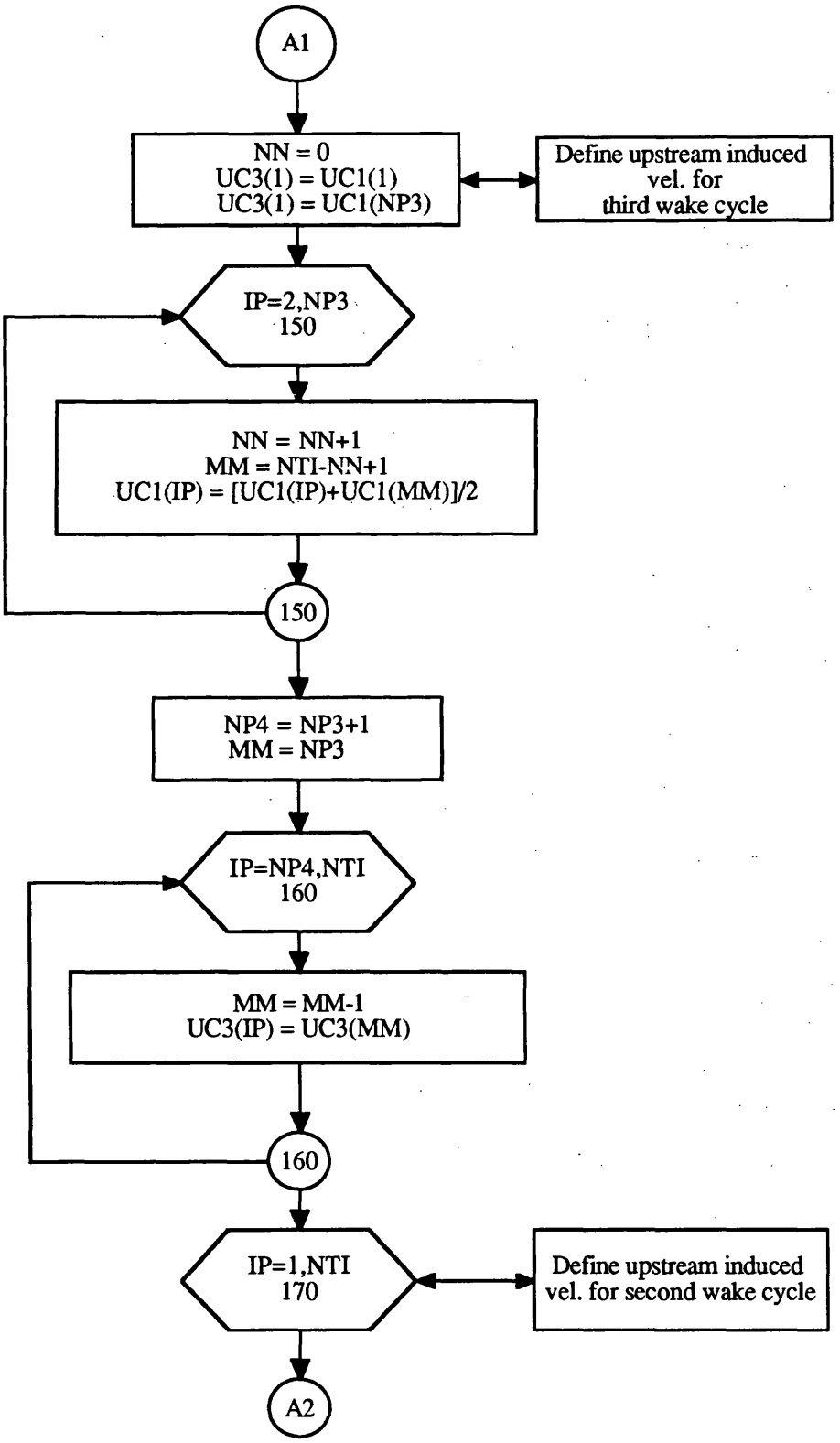

Cont'n from Fig. B-1e (1)

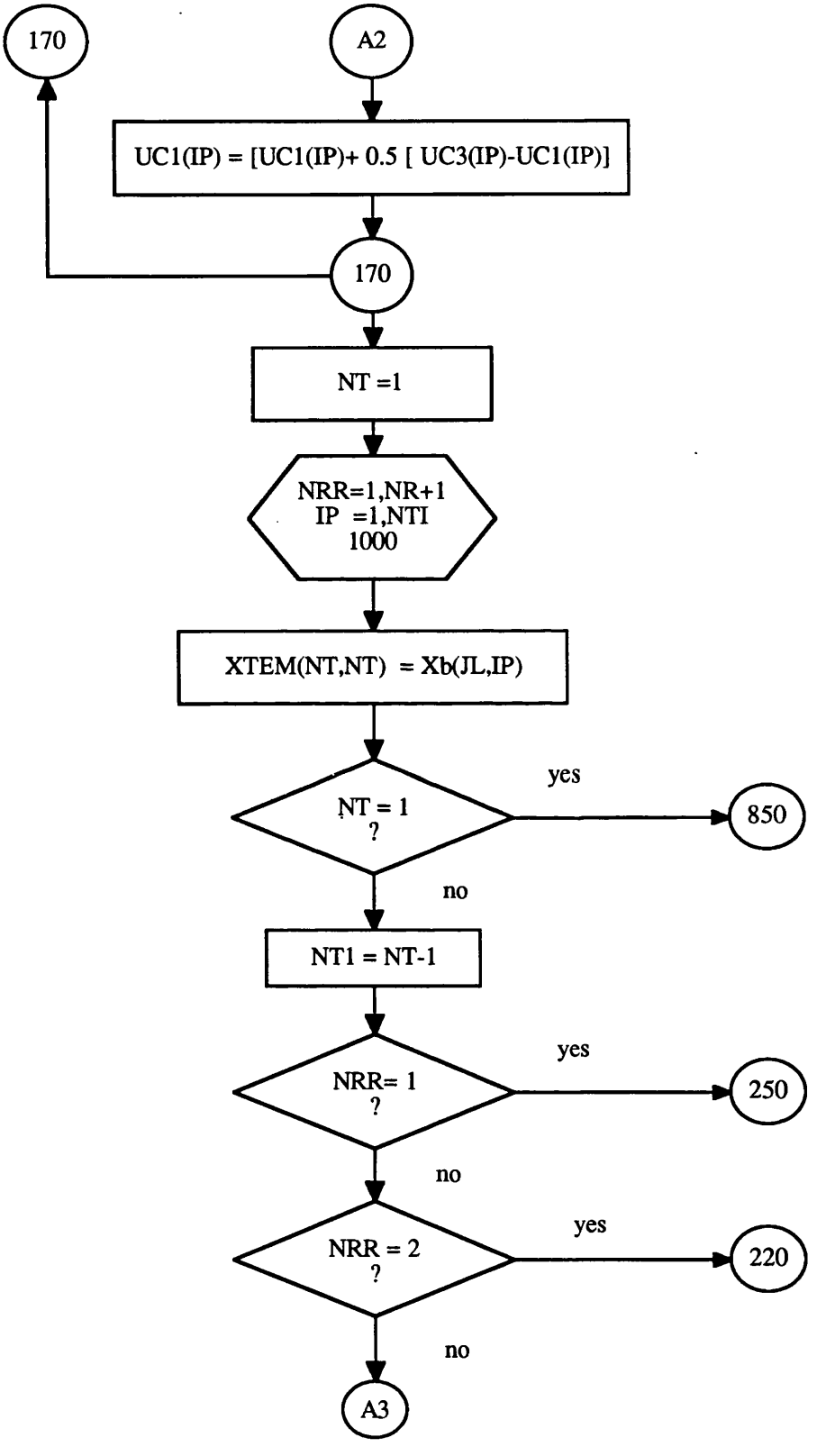

Cont'n from Fig. B-1e (2)

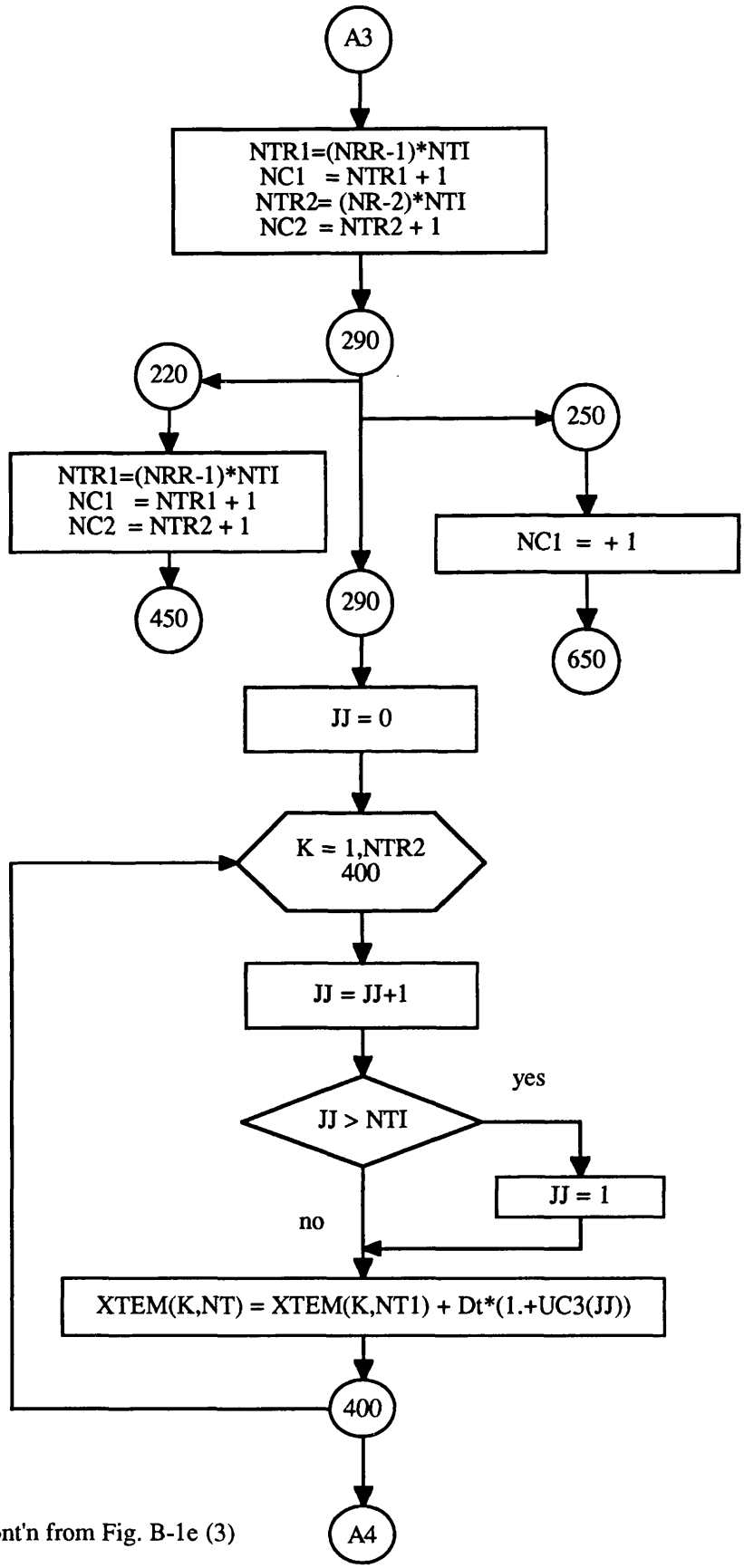

Cont'n from Fig. B-1e (3)

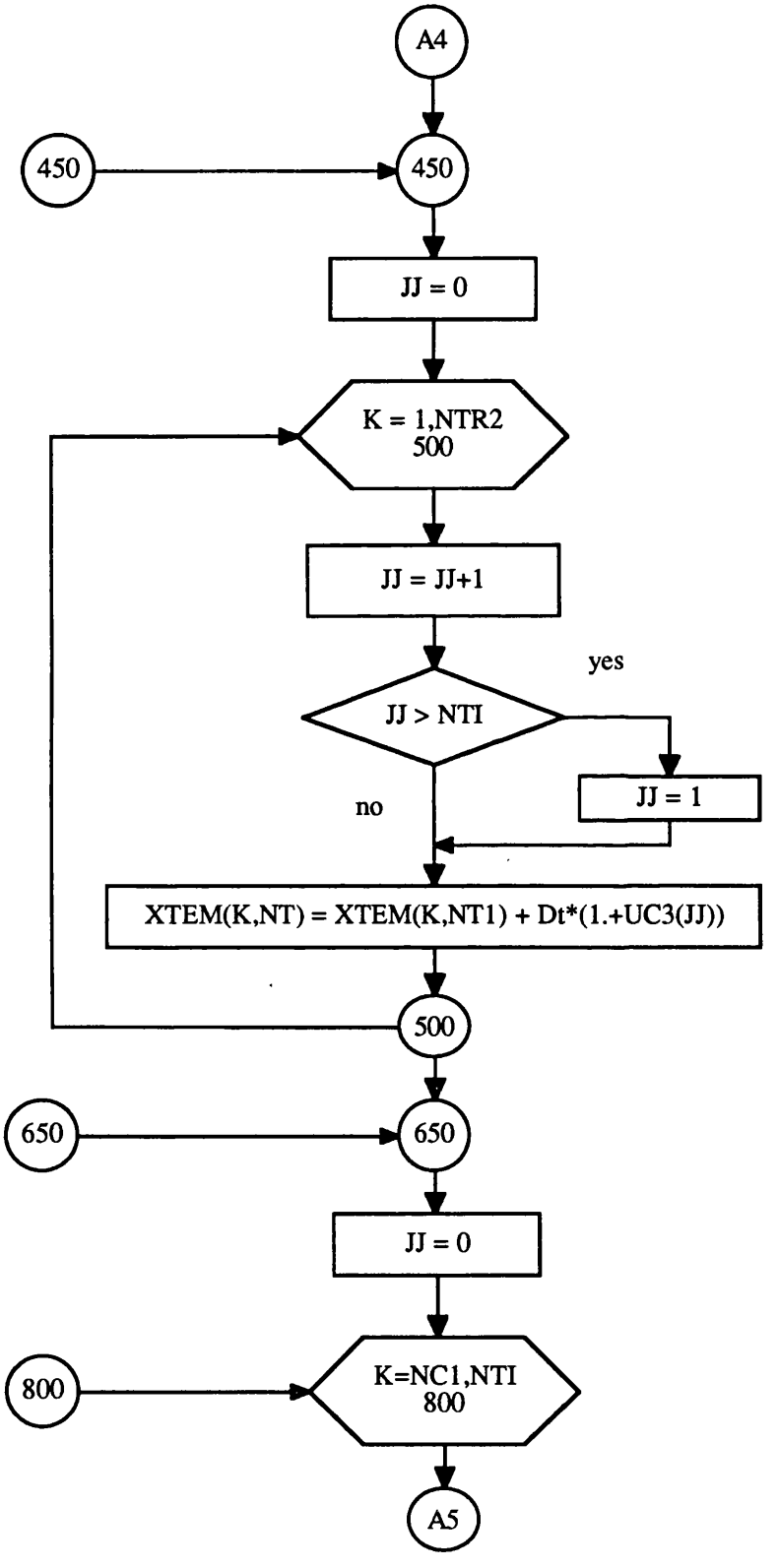

Cont'n from Fig. B-1e (4)

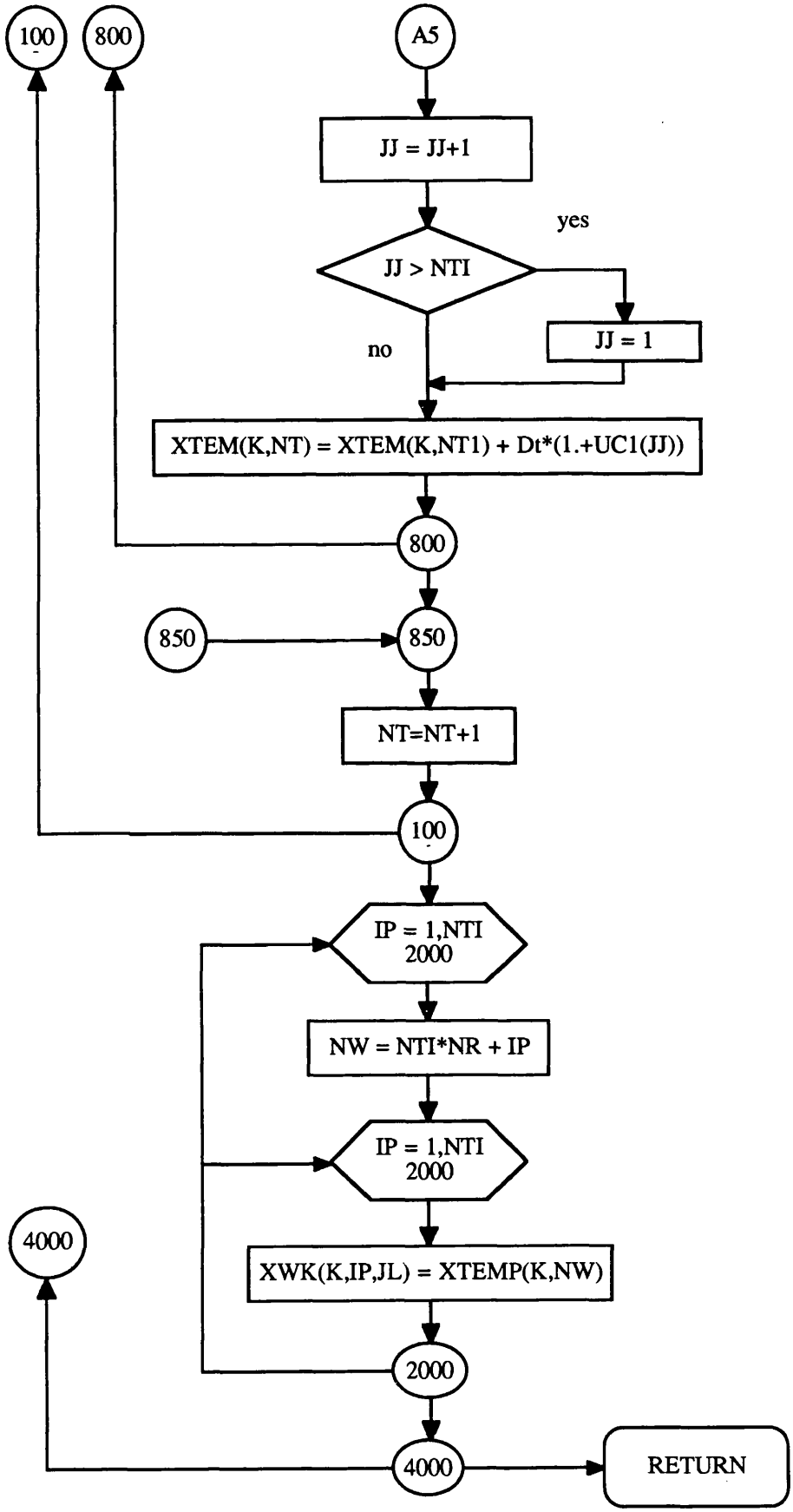

Cont'n from Fig. B-1e (5)

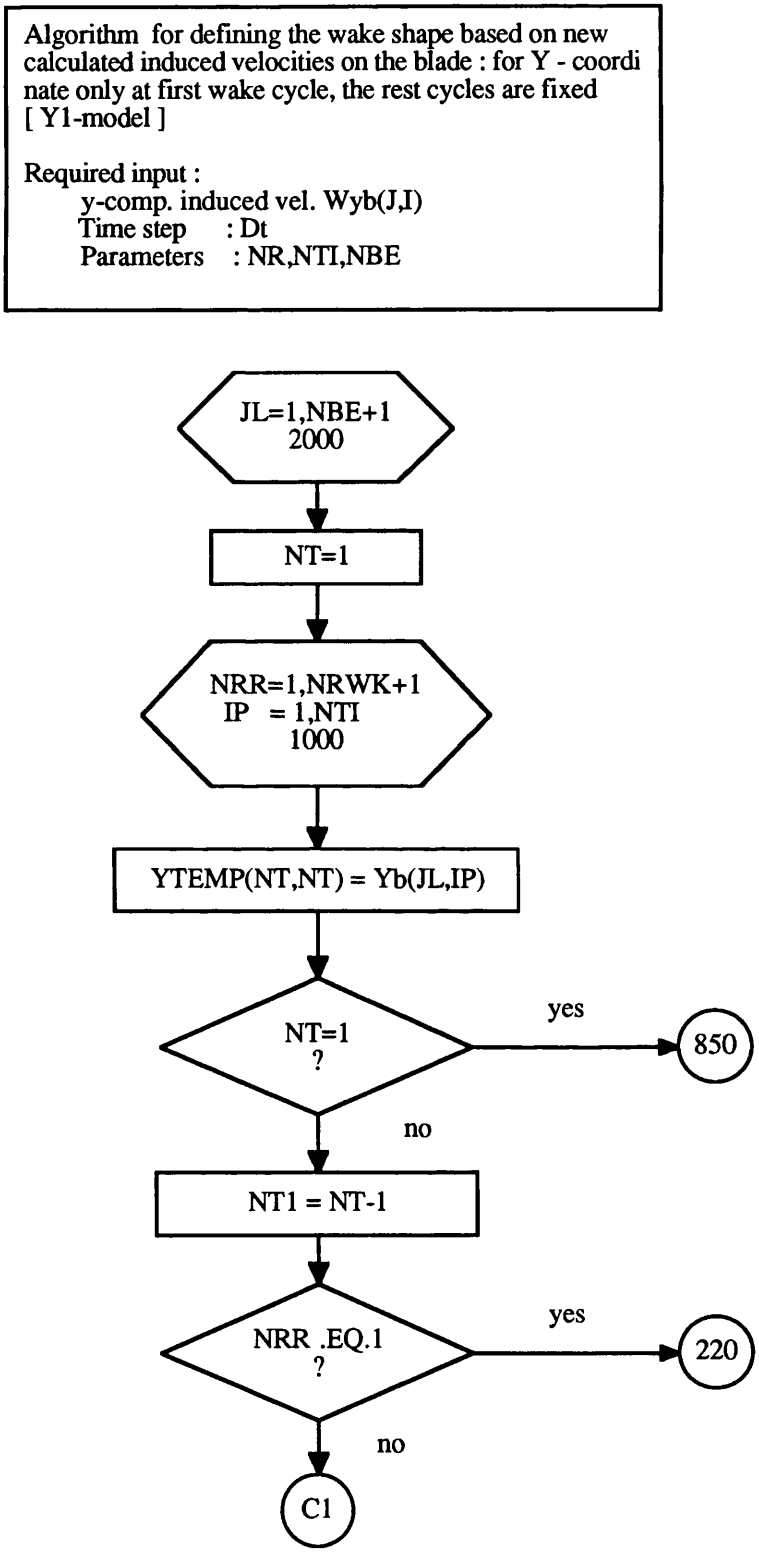

Fig. B-1f Flow chart of the algorithm for the reconstruction of wake shape in Y-direction for the first wake cycle and the rest of wake cycles are kept fixed

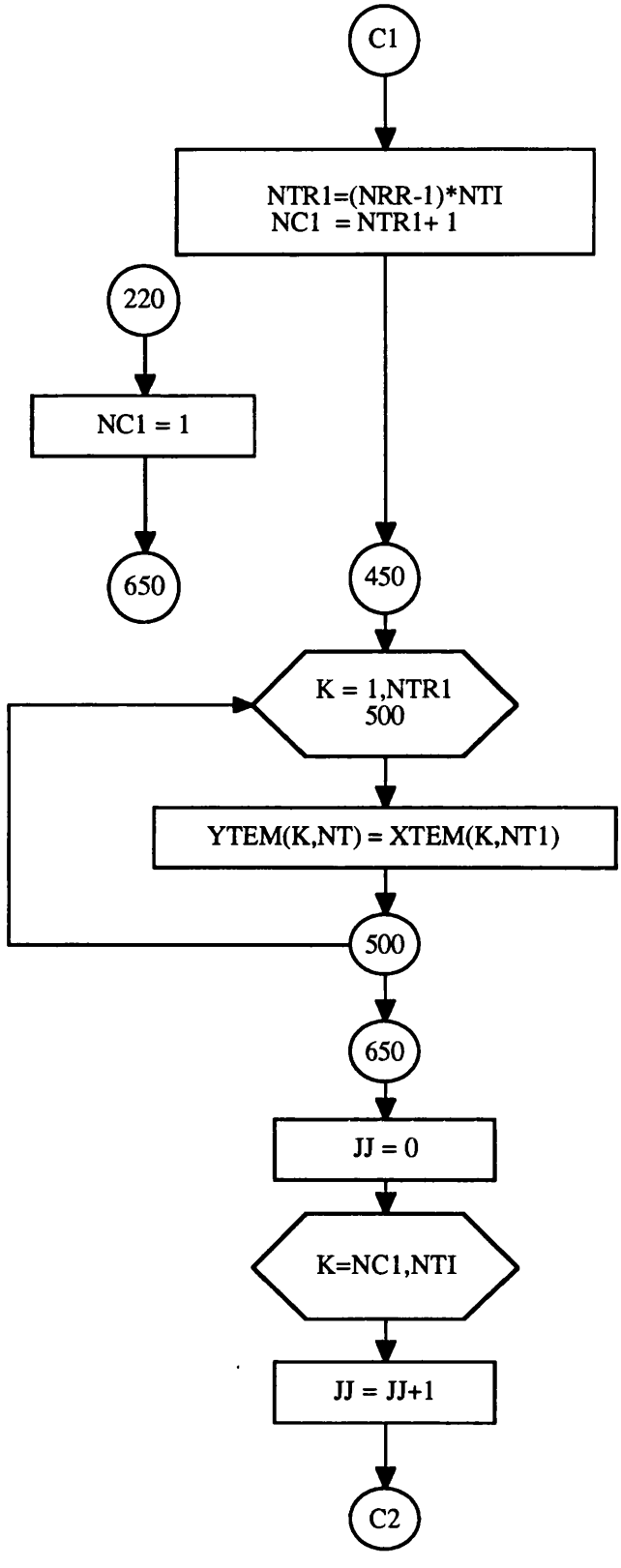

Cont'n from Fig. B-1f (1)

Algorithm for defining the wake shape based on new calculated induced velocities on the blade : for Y- coordi nate until 2nd wake cycle, the rest cycles are fixed
[Y2-model]

Required input :
y-comp. induced vel. Wyb(J,I)
Time step : Dt
Parameters : NR,NTI,NBE

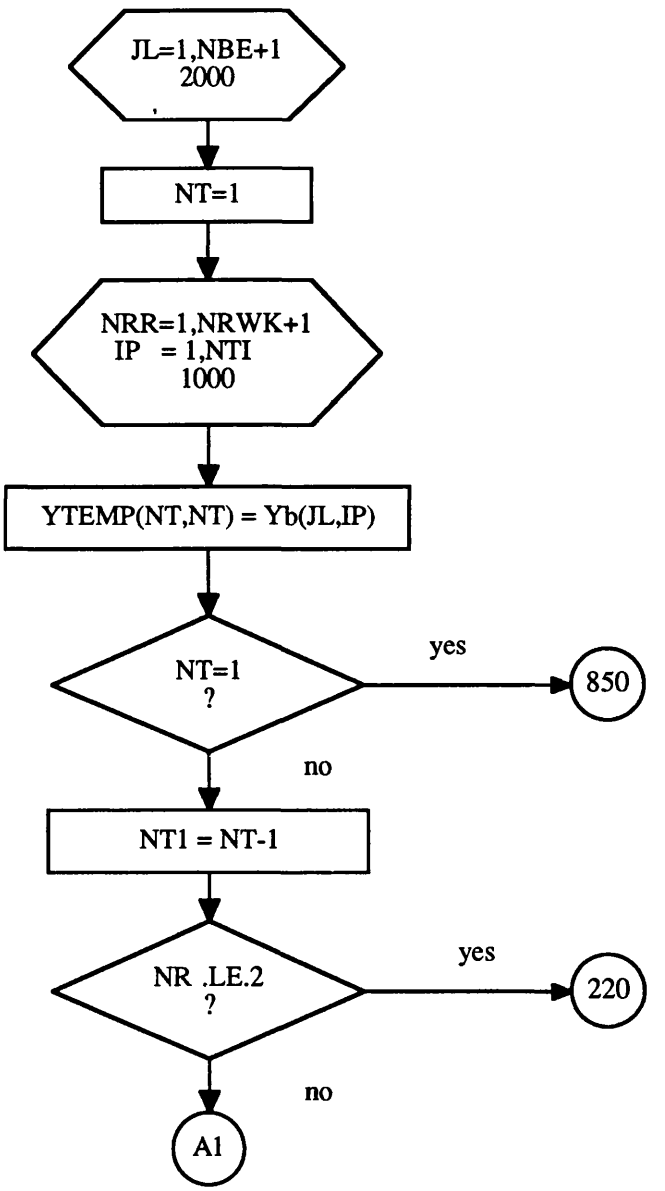

Fig. B-1g Flow chart of the algorithm for the reconstruction of wake shape in Y- direction till the second wake cycle and the rest of wake cycles are kept fixed

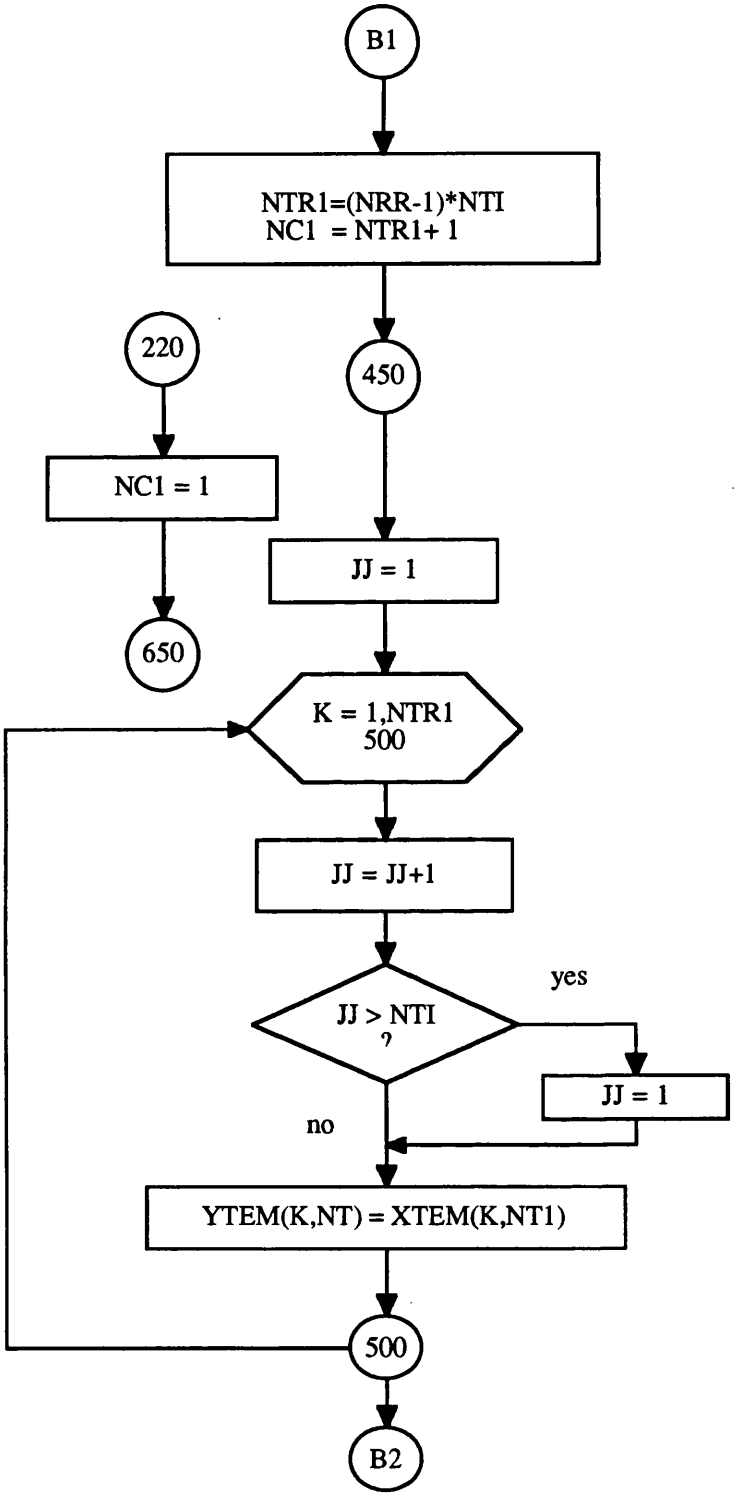

Cont'n from Fig. B-1g (1)

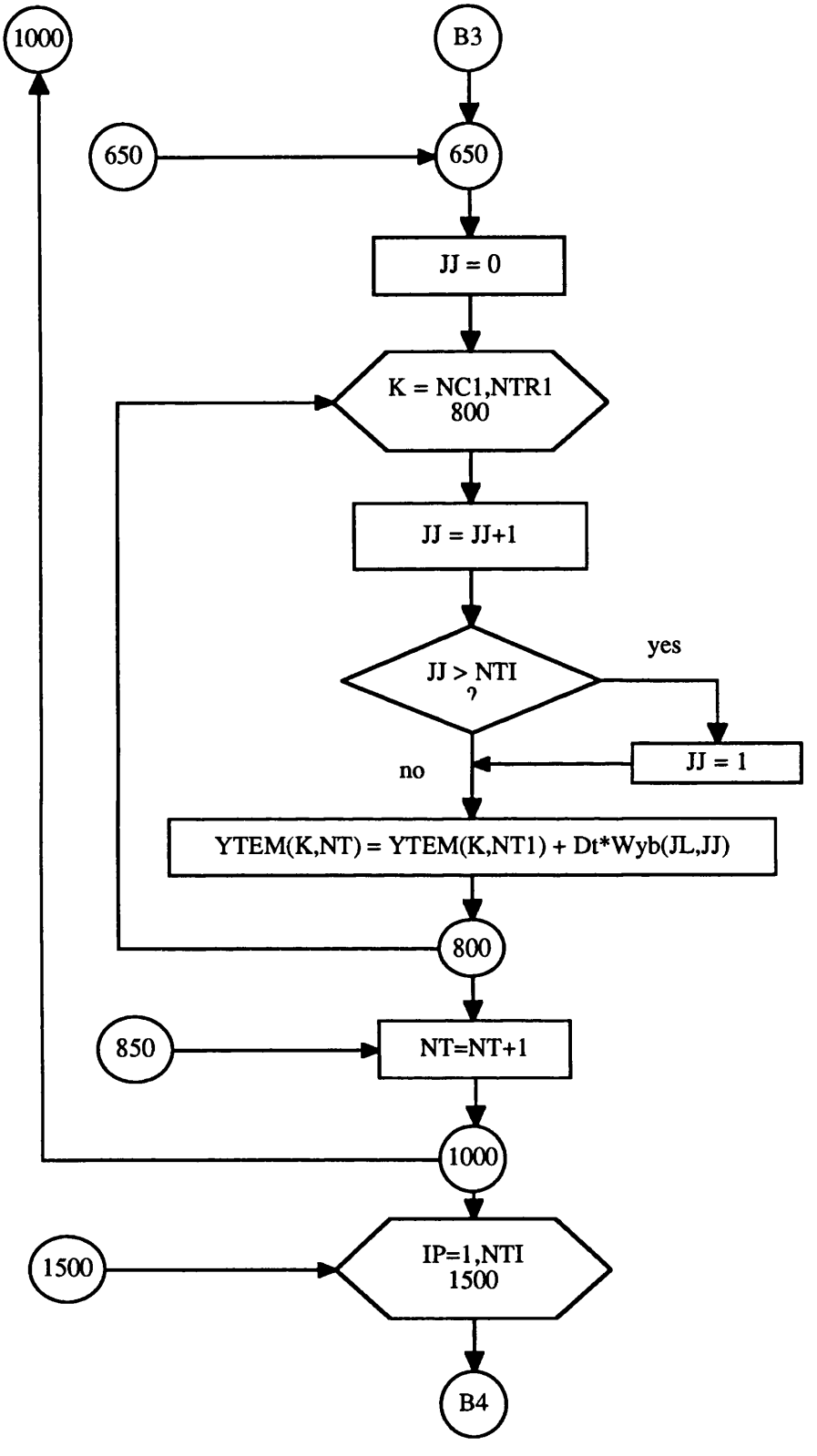

Cont'n from Fig. B-1g (2)

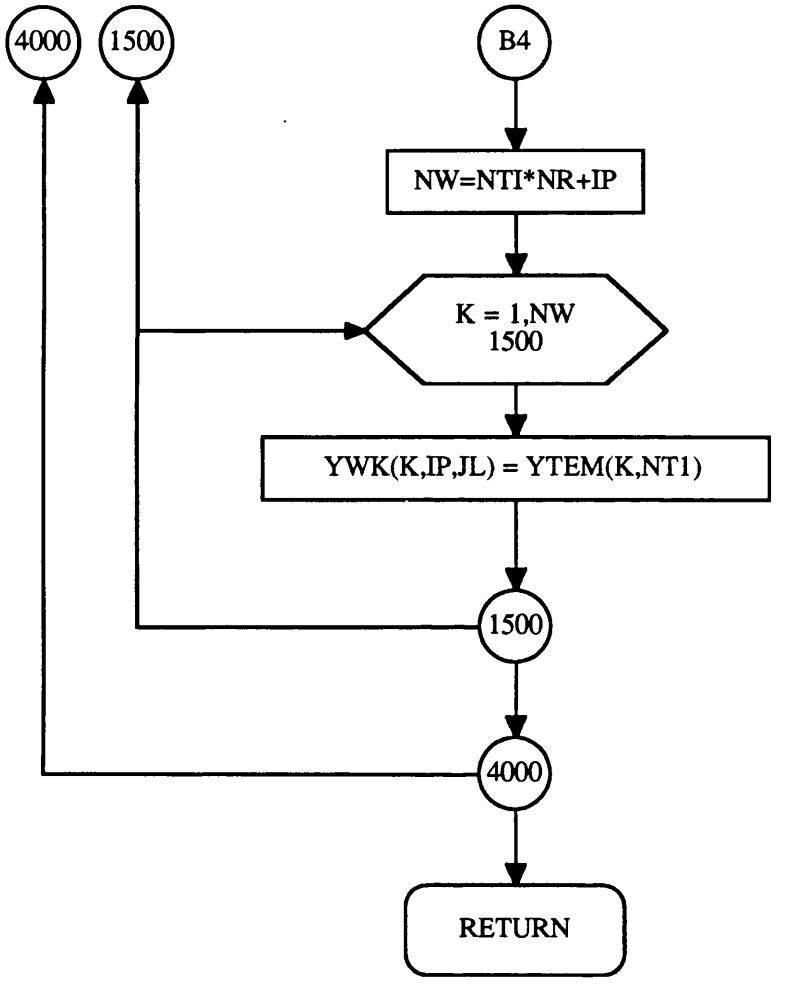

Cont'n from Fig. B-1g (3)

APPENDIX - B2

The Flow Chart of the Algorithm for the Reconstruction of Wake Shape in X-Direction [New Wake Scheme]

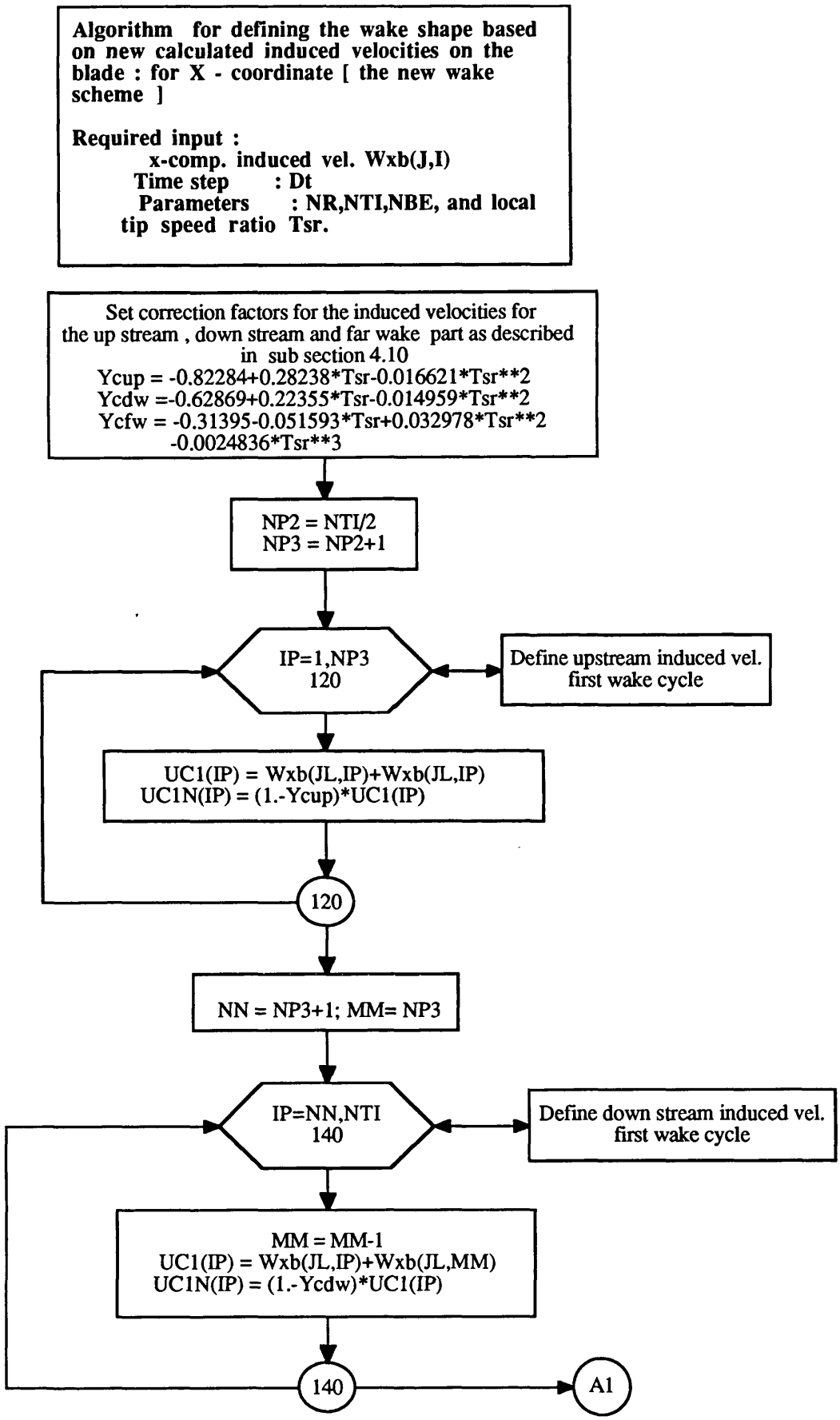

Fig. B-2 Flow chart of the algorithm for the reconstruction of wake shape in X-direction [new wake scheme]

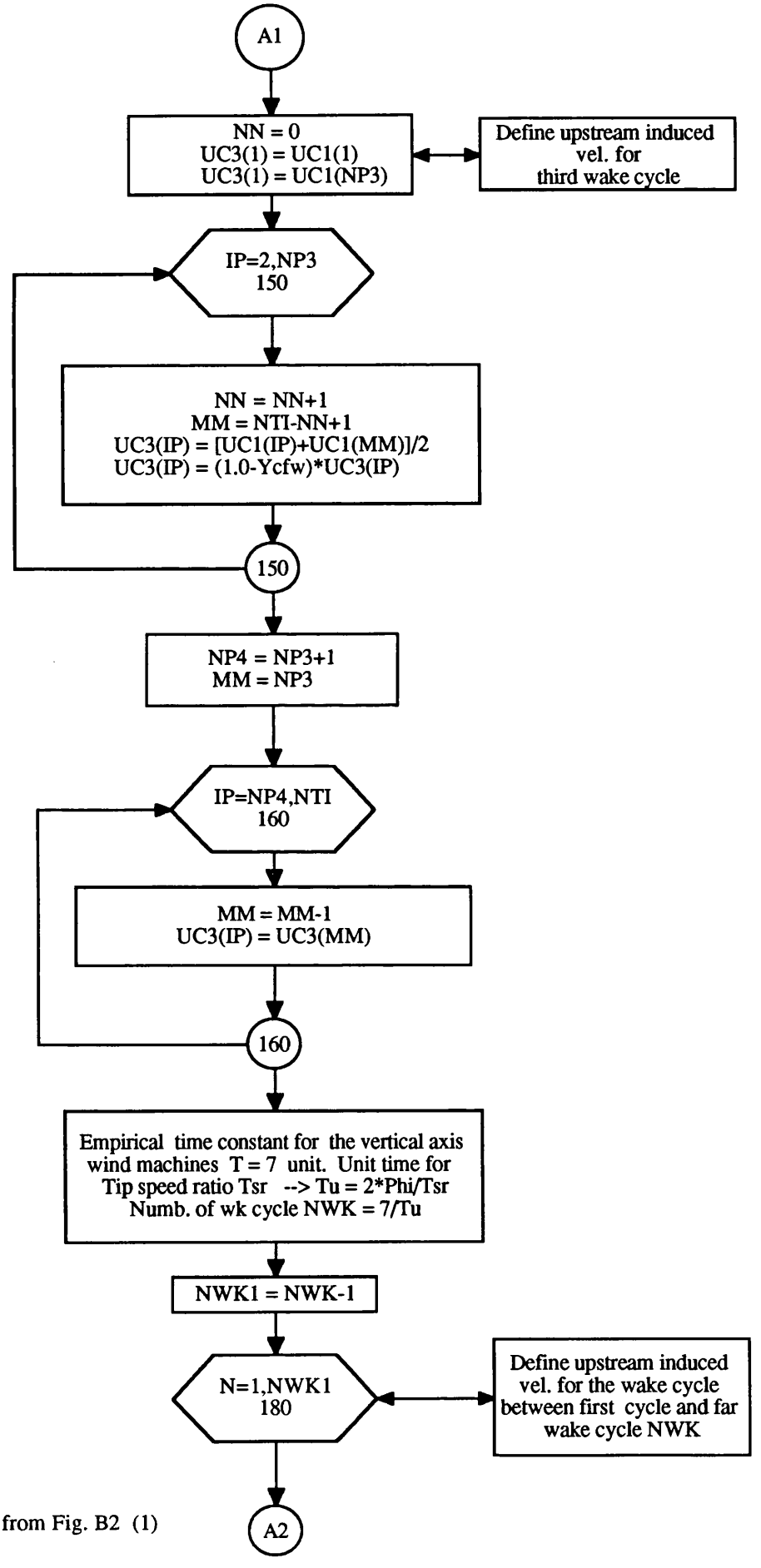

Cont'n from Fig. B2 (1)

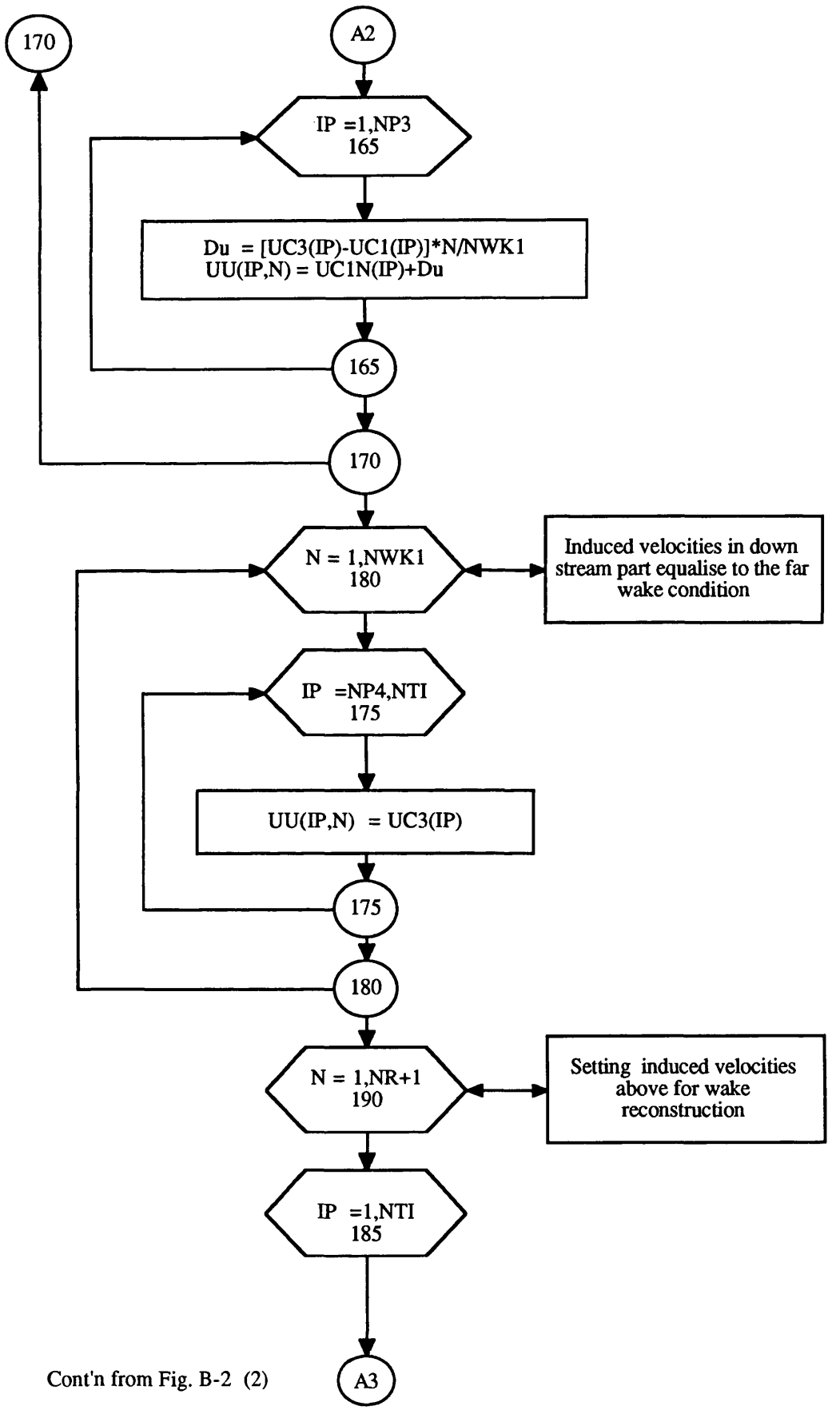

Cont'n from Fig. B-2 (2)

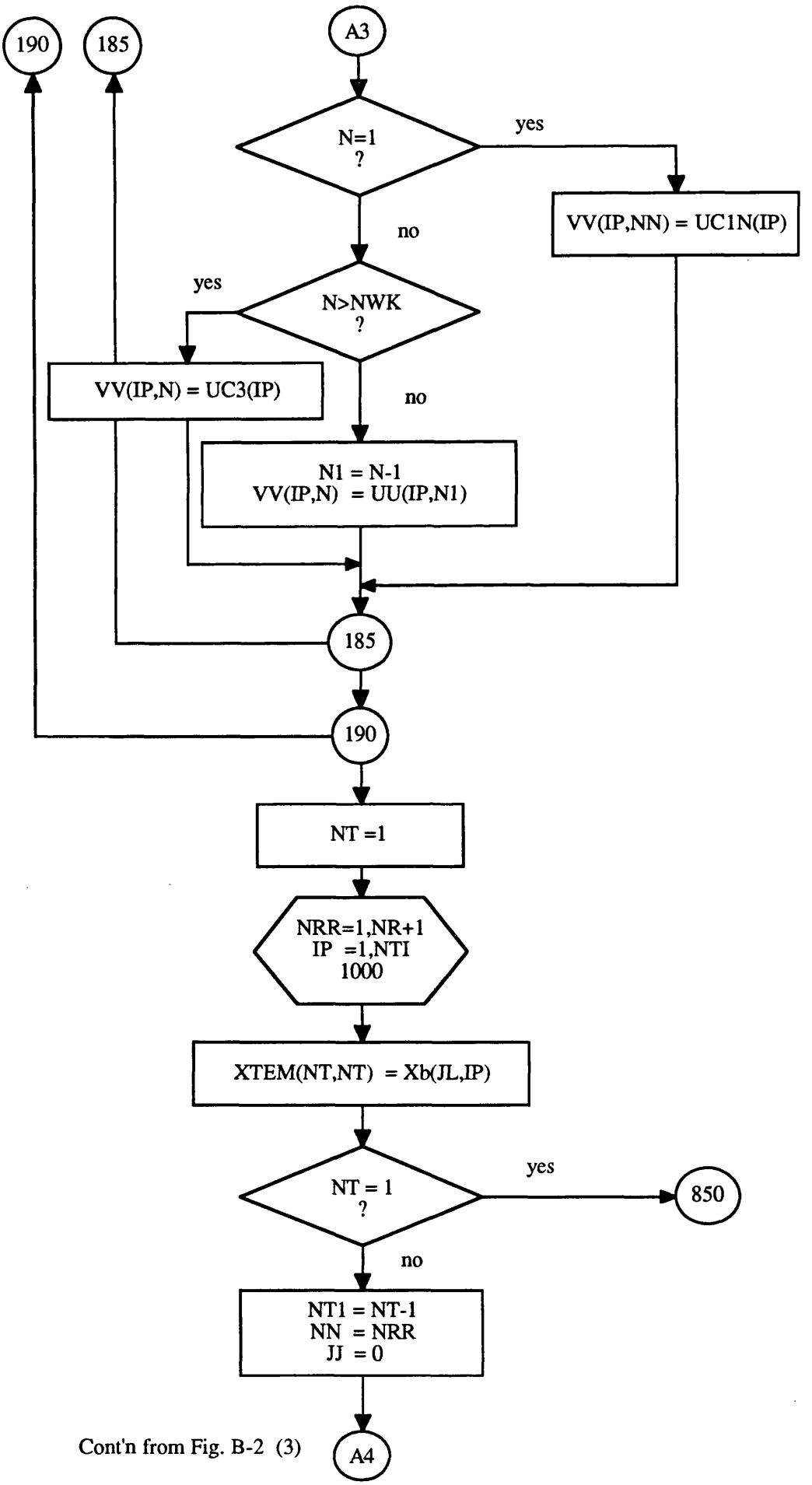

Cont'n from Fig. B-2 (3)

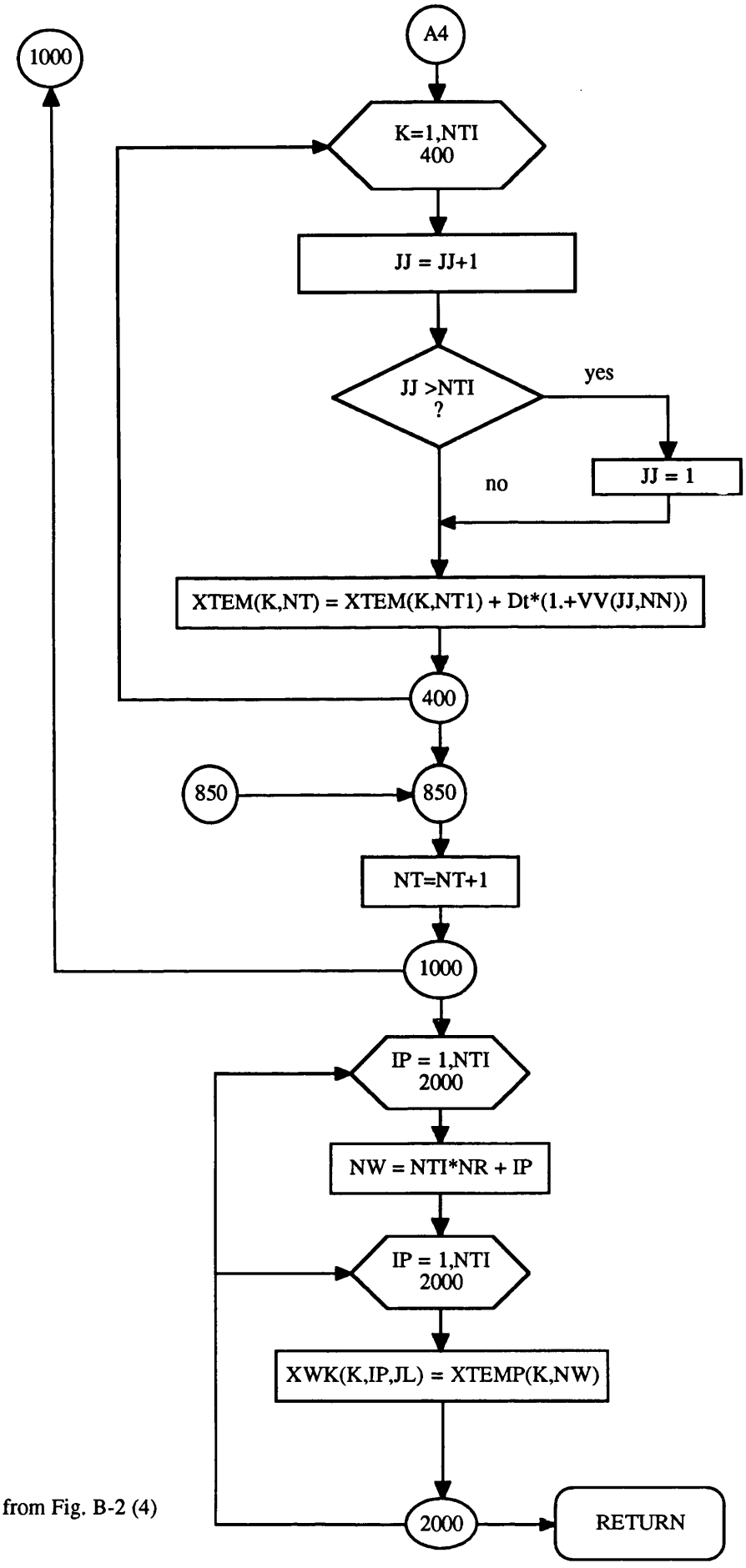

Cont'n from Fig. B-2 (4)